UNIVERSITY
OF TRENTO

Department of Physics
Doctoral School in Physics - XXXVIII cycle

Ph.D. Thesis

Scale Invariance in the Early Universe

Supervisor:
Prof. Massimiliano Rinaldi

Ph.D. Candidate:
Chiara Cecchini

April 2026

Abstract

Scale invariance provides a well-motivated guiding principle for the physics of the early Universe. It emerges as an approximate symmetry in several high-energy regimes and is exactly realized at the fixed points of the renormalization-group flow, where no intrinsic mass or length scale is present. Within this perspective, scale-invariant theories offer a natural setting in which physical mass scales arise dynamically through symmetry breaking. Motivated by these considerations, this thesis investigates the implications of scale-invariant gravity in the context of inflationary cosmology. We study a classically scale-invariant model based on an R^2 modification of the gravitational action coupled to a real scalar field and analyze its inflationary dynamics. We examine the evolution of the background and linear cosmological perturbations, clarifying the role of scale symmetry and the corresponding Noether current. We derive constraints on the model parameters and connect the resulting inflationary dynamics to current observational data. Finally, we explore the implications of scale-invariant inflation for primordial magnetogenesis, investigating a mechanism for breaking electromagnetic conformal invariance during inflation and its phenomenological consequences.

Contents

Introduction

Modern cosmology has entered an unprecedented era of observational precision. Measurements of the cosmic microwave background (CMB), large-scale structure (LSS), baryon acoustic oscillations (BAO), and Type Ia supernovae (SN Ia) have converged into a remarkably consistent description of the Universe on large scales. This concordance picture is commonly referred to as the standard model of cosmology, or ΛCDM, in which the dynamics of the Universe are described by general relativity (GR) and a hot Big Bang cosmological history, with cold dark matter and a cosmological constant responsible for the present phase of accelerated expansion. Despite its empirical success, ΛCDM provides only an effective description of cosmic evolution and leaves the physical origin of its fundamental components – and in particular the physics of the very early Universe – largely unexplained.

When extrapolated to early times, the standard hot Big Bang framework faces a fundamental limitation concerning its predictive power. In the absence of a mechanism governing the initial state of the Universe, the observed level of homogeneity, flatness, and large-scale coherence can be obtained only for highly special and finely tuned initial conditions. Any successful cosmological theory, however, should account for the properties of the observed Universe starting from a generic class of initial configurations, rather than relying on exceptional assumptions.

From the pioneering works of Starobinsky, Guth, and Linde [1–3], **cosmic inflation** has emerged as the leading paradigm for addressing this limitation. Defined as a phase of accelerated expansion preceding the radiation-dominated era, inflation provides a dynamical solution to the initial conditions problem and predicts the generation of primordial perturbations from microscopic quantum fluctuations. During inflation, quantum fluctuations in the energy density are stretched by the accelerated expansion to macroscopic scales, eventually exceeding the physical Hubble horizon. Once a perturbation exits the horizon, causal microphysical processes can no longer affect its evolution, and its amplitude remains effectively frozen until it re-enters the horizon at later times during the standard, non-accelerating Big Bang evolution.

These primordial perturbations act as the seeds for structure formation and leave characteristic imprints in the CMB anisotropies, which have been measured with extraordinary accuracy. The near scale invariance, Gaussianity, adiabatic nature, and phase coherence of the observed primordial power spectrum are among the most compelling pieces of evidence in favor of inflation, establishing it as a unique observational window onto physics at energy scales far beyond those accessible in particle physics experiments.

Despite its phenomenological success, inflation remains conceptually incomplete. In its simplest realizations, it relies on scalar-field dynamics described by effective field theories valid below a cutoff scale, often close to the Planck mass. Questions concerning the naturalness of inflationary potentials, the origin of the inflaton field, and the role of fundamental mass scales remain open. Moreover, inflation typically operates at curvature scales where the classical description of gravity provided by GR is expected to receive significant quantum corrections.

From a theoretical point of view, it is therefore natural to expect the Einstein-Hilbert (EH) action to be modified in the high-curvature regime relevant to the early Universe. In the absence of a complete theory of quantum gravity, these modifications can be systematically described within an effective

field theory framework, in which higher-order curvature invariants arise as quantum corrections to the classical action. When the curvature is small compared to the Planck scale ($R/M_{pl}^2 \ll 1$), such corrections are suppressed, and GR is recovered as an excellent approximation in the regime where it has been experimentally tested. Conversely, when the curvature approaches the Planck scale ($R/M_{pl}^2 \sim 1$), quadratic curvature terms become dynamically relevant, and their impact on the cosmological evolution can no longer be neglected.

A concrete example of the role played by **quadratic gravity** terms is provided by the Starobinsky model, in which the leading modification to the EH action is an R^2 term. Despite its minimal structure, this model yields a successful inflationary phase and shows remarkable agreement with current cosmological observations, making it a widely adopted benchmark for inflation. This empirical success naturally motivates the question of whether the R^2 contribution plays a special role among higher-order curvature terms.

Support for this idea comes from reconstruction approaches to modified gravity, in which the form of the gravitational action is inferred by demanding an inflationary phase consistent with observations. Remarkably, across a wide class of such analyses, an R^2 term systematically emerges as the dominant contribution in the large-curvature regime. This suggests that the appearance of the R^2 term is not accidental, but rather reflects a structural property of gravity in the high-curvature regime.

The R^2 term is further singled out by the fact that it is the only higher-order curvature correction that leads to a ghost-free and one-loop renormalizable gravitational action, and that it enjoys exact **scale invariance**. During the inflationary phase described by the Starobinsky model, the dynamics are dominated by the quadratic term, while the linear EH contribution is subleading. As a result, scale invariance is effectively realized as an approximate symmetry of the inflationary regime.

From this perspective, it is natural to speculate that scale invariance may represent a fundamental symmetry of gravity at high energies, with the EH term emerging only after the symmetry is broken. This observation motivates exploring scale-invariant extensions of gravity and their phenomenological implication in the early Universe, which is the main subject of this thesis.

The rationale behind scale invariance as a fundamental symmetry is not limited to the context of inflation and arises naturally across a wide range of physical systems. At a general level, scale invariance characterizes situations in which no intrinsic mass or length scale is present, so that the underlying dynamics remain unchanged under rescalings of mass or distance. At an intuitive level, the absence of an intrinsic scale implies that absolute notions of size lose meaning, and physical properties can only be characterized through relative comparisons since no preferred reference unit is available. This symmetry is a hallmark of critical phenomena in statistical mechanics, where the divergence of the correlation length at phase transitions renders the system insensitive to rescalings of length. In cosmology, the nearly scale-invariant spectrum of primordial fluctuations provides an observational indication that scale symmetry may have played a role in the very early Universe. Similarly, in particle physics, the Standard Model (SM) is approximately scale invariant at energies well above the electroweak (EW) scale, where particle masses become negligible, an assumption increasingly supported by the absence of new physics at current collider energies.

From a theoretical standpoint, scale invariance emerges whenever the fundamental Lagrangian contains no dimensionful parameters. In four spacetime dimensions, this requirement restricts the allowed operators to those of dimension four, making scale invariance a highly predictive principle. In a broader sense, the idea of scale invariance as a fundamental symmetry of Nature parallels the Copernican principle in cosmology: just as no point in space is privileged, no particular energy or length scale is singled out at the fundamental level. Deviations from exact scale invariance then arise dynamically, through symmetry breaking or quantum effects, giving rise to the characteristic scales observed in Nature.

In particle physics, scale invariance has long been explored as a guiding principle for addressing the origin of mass scales. In this context, masses are not introduced as fundamental parameters

of the theory, but are generated dynamically through symmetry-breaking mechanisms, offering a possible approach to the gauge hierarchy problem. When this idea is extended to gravity and cosmology, it naturally opens the possibility that the Planck scale itself is not fundamental but emerges dynamically from the spontaneous breaking of scale invariance. Within such a framework, all dimensionful quantities acquire physical meaning only after the symmetry is broken, providing a unified perspective on the **dynamical origin of scales** in fundamental physics.

In cosmology, scale invariance offers additional appealing features. Inflationary models based on scale-invariant theories naturally give rise to flat or plateau-like potentials, which are favored by current observations and are robust against radiative corrections. Moreover, the dynamical generation of scales within scale-invariant frameworks provides new perspectives on the cosmological constant problem, as vacuum energy contributions can be tied to symmetry-breaking dynamics rather than to fixed parameters in the fundamental action.

Beyond these phenomenological motivations, scale invariance is also supported by deeper theoretical considerations. Wetterich proposed [4] that scale invariance may provide a unifying effective field theory description that connects early-Universe ultraviolet (UV) physics, the Standard Model (SM), and a late-time infrared (IR) regime, with all physical scales emerging along a single renormalization-group flow. In this framework, scale invariance plays a role that goes beyond conventional renormalizability, acting as an organizing principle for the structure of the theory across widely separated energy scales. These considerations further support the idea that scale invariance may represent a fundamental symmetry of Nature and provide strong motivation for its implementation in gravitational and cosmological frameworks.

In this thesis, we investigate the cosmological implications of a **classically scale-invariant theory** of gravity that includes a quadratic R^2 term and a real scalar field, originally proposed by Rinaldi and Vanzo in [5]. In this setting, scale invariance acquires a genuinely dynamical character, in which the Planck mass naturally emerges from symmetry breaking. The primary goal of this work is to examine how this structure drives inflationary dynamics and shapes the resulting cosmological phenomenology.

A central element of the analysis is the role of scale symmetry and of the associated Noether current during inflation. Exploiting this symmetry, the intrinsically multifield dynamics of the model can be consistently reduced to an effective single-field description, substantially simplifying the analysis of both the background evolution and cosmological perturbations. This symmetry-based reduction also has important implications for stability: while many multifield inflationary scenarios are known to suffer from tachyonic instabilities associated with entropy perturbations, the scale-invariant structure of the theory tightly constrains the perturbation sector and naturally protects the inflationary trajectory from such pathologies. On this basis, a detailed analytical and numerical study of scalar and tensor perturbations is carried out to assess the observational viability of the model and to constrain its parameter space using the latest CMB observations.

Beyond inflation, the scale-invariant framework explored in this work provides a natural setting to address additional cosmological issues. In particular, we investigate the emergence of a residual cosmological constant, which appears generically and unavoidably in all scale-invariant extensions of the model that preserve the same degrees of freedom. We further investigate the phenomenological implications of the theory beyond the scalar sector, with particular emphasis on a mechanism for the inflationary generation of primordial magnetic fields that is naturally embedded within the scale-invariant background dynamics. Taken together, these analyses assess the internal consistency, predictive power, and observational signatures of scale-invariant R^2 gravity models within a unified cosmological framework.

Outline

The first part of the thesis (Chapters 1 and 2) is intended as an overview of the main theoretical foundations and mathematical tools of cosmic inflation and modified gravity.

Chapter 1 introduces the inflationary paradigm in modern cosmology, explaining how inflation addresses the main conceptual issues of the standard hot Big Bang model and analyzing its minimal single-field slow-roll realization. The chapter presents the mathematical tools required to study cosmological perturbations and connects them to the associated power spectra and observational signatures.

Chapter 2 provides an overview of modified theories of gravity, discussing their motivations, theoretical consistency, and phenomenology. Particular attention is devoted to $f(R)$ theories and to Starobinsky inflation as a representative case, as well as to the formulation of these theories in the Jordan and Einstein frames. Section 2.4 introduces the main features of scale invariance, outlining its theoretical motivations in particle physics, cosmology, and quantum field theory.

The second part of the thesis (Chapters 3–5) is devoted to the original contributions of this work.

Chapter 3 investigates the inflationary dynamics of the scale-invariant model introduced in [5], focusing on its homogeneous background evolution. The model is formulated in both the Jordan and Einstein frames, with particular emphasis on the implications of scale symmetry, including the dynamical emergence of the Planck mass through spontaneous symmetry breaking and the conservation of the associated Noether current, which effectively reduces the system to single-field background dynamics. Analytical predictions for single-field slow-roll inflation are then derived under suitable approximations, allowing constraints to be placed on the model parameter space.

Chapter 4 extends the analysis to first-order perturbation theory within a fully multifield analysis. The implications of the underlying symmetry for the stability of the model against entropy perturbations are investigated, and the predictions for non-Gaussianities are evaluated. Section 3.4 presents a numerical analysis aimed at constraining the model using the latest observational data and discusses possible observational signatures that could distinguish it from Starobinsky inflation.

Chapter 5 explores the generation of primordial magnetic fields through a broken-power-law coupling between the inflaton field of the scale-invariant model and the electromagnetic sector, including a Chern-Simons parity-breaking interaction. The evolution of the gauge field in this framework is investigated both analytically and numerically, including an analysis of backreaction effects, gauge-field-sourced tensor perturbations, and possible connections to baryogenesis.

Finally, the Conclusions summarize the main results of the thesis and outline prospects for future research. Each chapter concludes with a brief summary highlighting the main results and findings.

Original contributions

The original content of the thesis is based on the following peer-reviewed publications and conference proceedings.

- [6] M. De Angelis, C. Cecchini, and M. Rinaldi, "Tracing cosmic stretch marks: probing scale invariance in the early Universe", Contribution to: *MG17* (2024), arXiv:2410.05977.
- [7] C. Cecchini, M. De Angelis, W. Giarè, M. Rinaldi, and S. Vagnozzi, "Testing scale-invariant inflation against cosmological data", *JCAP* **07** (2024), arXiv:2403.04316.
- [8] M. Rinaldi, C. Cecchini, A. Ghoshal, and D. Mukherjee, "Scale-invariant inflation", *J. Phys. Conf. Ser.* **2531** (2023), arXiv:2303.16107.
- [9] C. Cecchini and M. Rinaldi, "Inflationary helical magnetic fields with a sawtooth coupling", *Phys. Dark Univ.* **40** (2023), arXiv:2301.07699.

In particular, Chapter 3 is based on and extends the results of [8], Chapter 4 is primarily based on [6, 7], and Chapter 5 critically reviews the results of [9].

Research work carried out during the Ph.D. that is not addressed in this thesis includes

- [10] C. Cecchini, G. Franciolini, and M. Pieroni, "Forecasting constraints on scalar-induced gravitational waves with future pulsar timing array observations", *Phys. Rev. D* **111** (2025), arXiv:2503.10805.

Units and conventions

Unless otherwise stated, we will employ natural units with $\hbar = c = 1$. It is useful to introduce *Planck units*, which are defined as

$$\ell_{pl} = \left(\frac{G\hbar}{c^3}\right)^{1/2} = 1.616 \times 10^{-35}\,\mathrm{m};$$
$$m_{pl} = \left(\frac{\hbar c}{G}\right)^{1/2} = 2.176 \times 10^{-8}\,\mathrm{kg}\,\left(= 1.221 \times 10^{19}\,\mathrm{GeV}/c^2\right);$$
$$t_{pl} = \frac{\ell_{pl}}{c} = 5.391 \times 10^{-44}\,\mathrm{s};$$
$$T_{pl} = \frac{m_{pl}c^2}{k_B} = 1.417 \times 10^{32}\,\mathrm{K}.$$

For a matter of convenience, we will adopt the *reduced Planck mass*,

$$M_{pl} = m_{pl}/\sqrt{8\pi} = 2.436 \times 10^{18}\,\mathrm{GeV}/c^2.$$

The following conventions are adopted:

- Mostly plus metric signature: $(-,+,+,+)$;
- The Greek letters $\alpha, \beta, \ldots$ are used for spacetime indices, whereas the Latin letters $i, j, \ldots$ are used for spatial indices;
- $\sqrt{-g} \equiv \sqrt{-\det(g)}$, where g is the metric tensor with elements $g_{\mu\nu}$;
- Dots stand for derivatives with respect to *physical time* t, primes stand for derivatives with respect to *conformal time* τ or *e-folding time* N, according to the case, whereas "$_{,X}$" denotes partial derivative with respect to variable X, e.g., $f_{,R} \equiv \partial f/\partial R$ and $f_{,RR} \equiv \partial^2 f/\partial R^2$;
- Quantities labeled with subscript 0 are evaluated at the present time; subscript "i" and "f" identify the beginning and the end of inflation, respectively. Finally, subscript "$*$" corresponds to Hubble horizon crossing time, unless otherwise stated;
- The *scale factor* a is considered dimensionless and unitary today, i.e., $a_0 \equiv a(t_0) = 1$.

In Chapter 5, we will adopt units of parsec (pc) for the measures of length and units of gauss (G) for the measures of magnetic field strength.

A parsec is the distance from which an object of size 1 AU (the astronomical unit, AU, is the average distance from Earth to the Sun) is seen under an angle of 1". The following relations hold:

$$1\,\mathrm{pc} = 3.1 \times 10^{16}\,\mathrm{m} = 2.1 \times 10^5\,\mathrm{AU}.$$

It is useful to quote the following conversion:

$$1\,\mathrm{G} = 1.95 \times 10^{-20}\,\mathrm{GeV}^2.$$

Glossary: symbols and acronyms

Symbol	Description
t	Proper time
τ	Conformal time, Eq. (1.2)
N	e-folding time
a	Scale factor
H	Hubble parameter
κ	Curvature parameter
z	Redshift
Λ	Cosmological constant
ϵ, η	Slow-roll parameters, Eqs. (1.20)–(1.21)
$\mathcal{R}$	Comoving curvature perturbation, Eq. (1.37)
$\mathcal{S}$	Isocurvature perturbation, Eq. (4.36)
n_s	Scalar spectral index ($\mathcal{P}_\mathcal{R} \propto k^{n_s-1}$), Eq. (1.44)
n_T	Tensor spectral index ($\mathcal{P}_T \propto k^{n_T}$), Eq. (1.48)
n_B	Magnetic spectral index ($\mathcal{P}_B \propto k^{n_B}$)
BAO	Baryon acoustic oscillations
C.L.	Confidence level
CMB	Cosmic microwave background
EH	Einstein-Hilbert
EF	Einstein frame
EM	Electromagnetic
EW	Electroweak
FLRW	Friedmann-Lemaître-Robertson-Walker
GR	General relativity
IGM	Intergalactic medium
IGMF	Intergalactic magnetic field
IR	Infrared
JF	Jordan frame
LSS	Large-scale structure
MCMC	Markov Chain Monte Carlo
MHD	Magnetohydrodynamics
PMF	Primordial magnetic field
QCD	Quantum chromodynamics
RG	Renormalization group
SM	Standard Model
SN Ia	Supernova Type Ia
SSB	Spontaneous symmetry breaking
UV	Ultraviolet

Chapter 1

The inflationary paradigm

From the pioneering work of Starobinsky, Guth, and Linde [1–3], inflation has now become a milestone of modern cosmology. Defined as a phase of accelerated expansion in the very early Universe, inflation is believed to occur around $\sim 10^{-34} - 10^{-36}$ s after the initial singularity, at energy scales as high as $\sim 10^{15}$ GeV. Besides addressing the major problems of the standard model of cosmology – like the horizon and flatness problem – the inflationary paradigm also predicts the generation of coherent cosmological perturbations, which seed the formation of the large-scale structure (LSS) observed in the Universe today.

1.1 The homogeneous Universe

Cosmology describes the Universe on the largest scales. On such scales ($\gtrsim 100\,\mathrm{Mpc}$), observations of the cosmic microwave background (CMB), the LSS, and galaxy surveys give strong support[1] to the cosmological principle, stating that the Universe is spatially homogeneous (translation invariant, or the same at every point) and isotropic (rotationally invariant, or the same in every direction), and evolving in time. Its evolution can, therefore, be represented as a time-ordered sequence of three-dimensional spacelike hypersurfaces, each homogeneous and isotropic. The most general metric consistent with these assumptions is the Friedmann-Lemaître-Robertson-Walker (FLRW) metric [12–14],

$$\mathrm{d}s^2 = -\mathrm{d}t^2 + a^2(t)\left[\frac{\mathrm{d}r^2}{1-\kappa r^2} + r^2\left(\mathrm{d}\theta^2 + \sin^2\theta\,\mathrm{d}\phi^2\right)\right], \tag{1.1}$$

where $0 < \theta < \pi$ and $0 \leq \phi < 2\pi$ are the comoving coordinates on the sphere of radius r. The *scale factor* $a(t)$ characterizes the relative size of spacelike hypersurfaces Σ at different times. Unless otherwise stated, we will adopt the convention in which the scale factor is dimensionless. Consequently, the comoving coordinate r has dimensions of length, and the curvature parameter[2] κ has dimensions of $(\text{length})^{-2}$. Since current observations suggest that the Universe today is spatially flat with a 1σ accuracy of $0.2\,\%$ [15], we will typically set κ to zero.

The time coordinate t represents the *proper time* measured by a comoving observer at rest with (r, θ, ϕ) constant. It is often convenient to replace the proper time t with the *conformal time* τ, defined via

$$\tau = \int \frac{dt}{a(t)}. \tag{1.2}$$

[1] See, however, the anisotropic anomalies detected in the CMB, which may challenge the standard ΛCDM model [11].

[2] Note that κ can take on any value. Positive, negative, and null values of κ correspond to a closed, open, and flat geometry, respectively.

This is particularly useful for studying light propagation since the radial null geodesics in an FLRW spacetime correspond to $\pm 45°$ straight lines in the (τ, r) plane, as are the light cones in Minkowski spacetime, the only difference being that an FLRW spacetime has a finite age [16].

We further define the *Hubble parameter*

$$H \equiv \frac{\dot{a}}{a}, \tag{1.3}$$

where an overdot denotes derivative with respect to proper time t. The Hubble parameter sets the characteristic scales of the FLRW spacetime: in units of $c = 1$, the Hubble scale $\sim H^{-1}$ sets both the age of the Universe and the size of the observable Universe.

The Einstein equations evaluated on an FLRW metric are the so-called *Friedmann equations*, [3]

$$H^2 = \frac{1}{3}\rho - \frac{\kappa}{a^2}, \tag{1.4}$$

$$\dot{H} + H^2 \equiv \frac{\ddot{a}}{a} = -\frac{1}{6}\left(\rho + 3p\right), \tag{1.5}$$

where $\rho = \rho(t)$ and $p = p(t)$ are the total energy density and pressure of the cosmological fluid filling the Universe, respectively, related through the equation of state $p = w\rho$. If more than one fluid component contributes significantly to the total energy density and pressure, ρ and p are the sum over all contributions

$$\rho = \sum_i \rho_i, \qquad p = \sum_i p_i, \tag{1.6}$$

where each species i satisfies the equation of state $p_i = \omega_i \rho_i$.

Note that Eq. (1.5) implies that a universe filled with ordinary matter (i.e., matter satisfying the strong energy condition: $\rho + 3p \geq 0$) is decelerating, namely $\ddot{a} < 0$. For the same reason, the late-time acceleration the Universe is undergoing is driven by a component that violates the strong energy condition, generally referred to as dark energy.

The Friedmann equations can be integrated to give the evolution of the scale factor a. A radiation-dominated universe ($w = 1/3$) expands as $a \propto t^{1/2}$; when the dominant component is matter ($w = 0$) the scale factor grows as $a \propto t^{2/3}$; finally, for a cosmological constant ($w = -1$) we have $a \propto e^{H_0 t}$, where $H_0 = \sqrt{\Lambda/3}$.

Eq. (1.4) can be also written as

$$1 - \Omega = -\frac{\kappa}{a^2 H^2}, \qquad \text{where} \quad \Omega = \frac{\rho}{\rho_c}, \;\; \rho_c = 3H^2. \tag{1.7}$$

Note that in an expanding universe ($\dot{a} > 0$), a decelerated expansion ($\ddot{a} < 0$) indicates that the scale factor a reaches zero when extrapolated back in time, signaling the occurrence of an initial cosmological singularity, $a(t = 0) = 0$. The existence of this point implies that the cosmology is geodesically incomplete [17]. Formally, the density and temperature diverge, and the geometry shrinks to zero, a sign that the equations used to describe the evolution of the Universe cannot be trusted near this point.

1.2 Big Bang puzzles

The standard model of Big Bang cosmology, which describes an adiabatically expanding radiation-dominated universe, faces a severe issue concerning its predictive power. Indeed, it turns out that only

[3] Unless otherwise stated, in this chapter we adopt reduced Planck units, $M_{pl} = 1$.

very fine-tuned and unnatural initial conditions lead to the Universe as we observe it today. Whether or not the naturalness problem is invoked, the Universe is unique, and a cosmological theory can claim to be a successful physical theory only if it can explain the state of the observed Universe adopting the most generic initial conditions [18].

There are two independent sets of initial conditions that one must fix to determine the evolution of the Universe:

- *Initial spatial distribution* To explain the smoothness of the CMB, the initial Universe must be smooth at a tremendously fine-tuned level. Since this problem comes with the ratio of the homogeneity scale and the causal scale, it can also be formulated as the *horizon problem*;
- *Initial velocities* To ensure that the Universe remains homogeneous at late times, the initial fluid velocities must take very precise values. Since the ratio between the potential energy and the kinetic energy defines the local curvature of a space patch, the initial velocities problem can also be phrased as the *flatness problem*.

Horizon problem

From the definition of conformal time in Eq. (1.2), the maximum distance a light ray can travel from time 0 to time t, corresponding to its entire past light cone, is

$$\chi(\tau) = \tau - \tau_0 = \int_0^t \frac{\mathrm{d}t'}{a(t')} = \int_0^a \mathrm{d}\ln a' \left(\frac{1}{a'H}\right). \tag{1.8}$$

Here, we have expressed the integrand in terms of the *comoving Hubble radius* $(aH)^{-1} = \dot{a}^{-1}$. From Eq. (1.5), it is clear that in a radiation- or matter-dominated universe the comoving Hubble radius increases monotonically in time. As a consequence, the last scattering surface was made up of a large number of causally disconnected patches. Given the smoothness of the CMB, how is it possible that all these regions happened to share the same temperature? The nature of the horizon problem is manifest by looking at the upper part of Figure 1.1: different points that we observe in the CMB have non-intersecting past light cones, meaning that they did not have enough (conformal) time to come into causal contact.

Flatness problem

Another consequence of the comoving Hubble radius growing with time is that, as seen from Eq. (1.7), the quantity $|1-\Omega|$ must diverge with time. Therefore, the value $\Omega = 1$ is an unstable fixed point at $t \to 0$, and the evolution of the Universe at later times tends to bring Ω away from 1. To achieve the observed flatness of the Universe today, $\Omega_0 \sim 1$, the value of Ω has to be unnaturally fine-tuned close to one in the early Universe. To give an example, at the Planck scale [14]

$$|1 - \Omega(a_{pl})| < \mathcal{O}(10^{-61}). \tag{1.9}$$

1.3 Inflation

As emphasized above, the horizon and the flatness problem are related to the fact that the comoving Hubble radius is strictly increasing with time in the standard Big Bang cosmology. Thus, the idea behind inflation: the conclusions above can be circumvented only if the comoving Hubble radius were instead sufficiently *decreasing* at the very early stages of the Universe's expansion. Stated in another way, gravity acted as a repulsive force, thus accelerating the expansion of the Universe.

A stage of accelerated expansion is a necessary condition to address the Big Bang puzzles. Whether it is also sufficient is a matter of the particular model considered.

In the most general way [18]:

> Inflation is a stage of accelerated expansion of the universe when gravity acts as a repulsive force.

Figure 1.1 shows the essence of inflation: if the Universe undergoes a stage of accelerated expansion before recombination – corresponding to adding a span of negative conformal time – all points in the CMB originated from the same, causally connected region of space, where the past light cones at the time of recombination can now overlap.

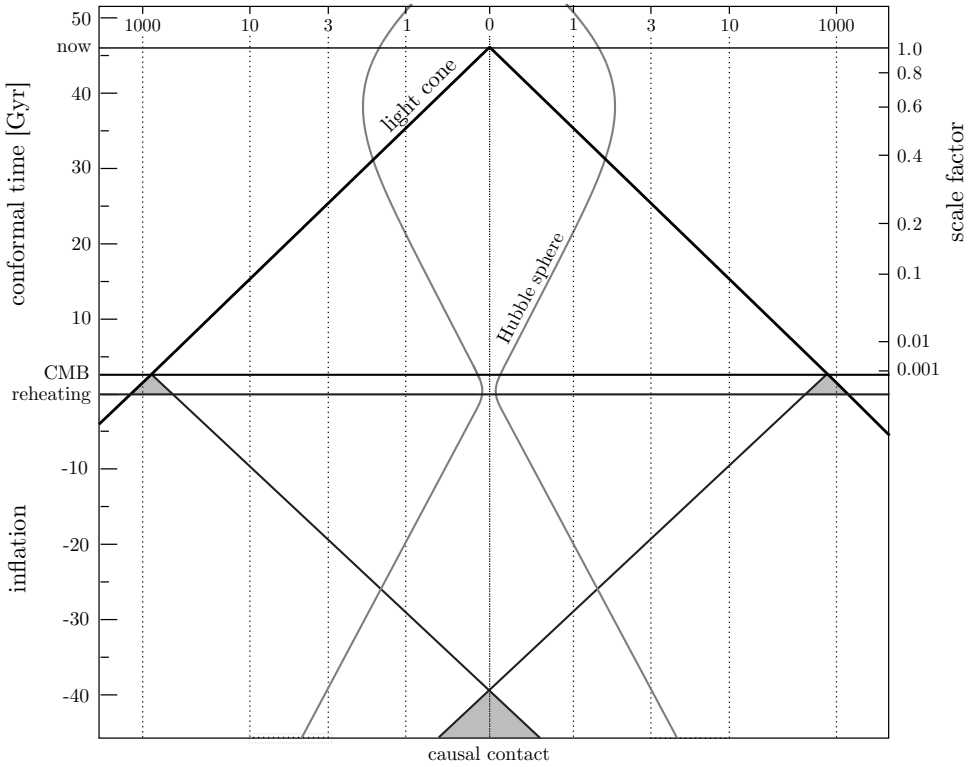

Figure 1.1: From [19]: inflationary solution to the horizon problem. Conformal time τ as a function of comoving distance is represented: we live on the central vertical worldline, while the other dotted vertical lines are worldlines of galaxies receding from us as the Universe expands and are labeled by their redshift (top grid). *Hubble sphere*: the comoving Hubble radius shrinks during inflation and increases during the ordinary Big Bang evolution, until the Universe becomes dark-energy dominated. *Light cones*: all points in the CMB have overlapping past light cones and thus represent causally connected events. The Big Bang singularity at $\tau = 0$ is replaced by the reheating surface and shifted back to large, negative values.

Looking at Eq. (1.7) from this new perspective, it is manifest that if the comoving Hubble radius $(aH)^{-1}$ decreases, the Universe is driven towards flatness instead of away from it. In an accelerating universe, $\Omega = 1$ is a future attractor and the flatness problem is solved.

Solving the horizon problem requires the comoving Hubble radius before inflation to have been larger than the comoving Hubble radius today, H_0^{-1}. A rough estimate [20] shows that this condition is achieved if the scale factor a increases by a factor $10^{27} \sim e^{62}$ during inflation. Introducing the *e-folding time*[4] through the differential relation $\mathrm{d}N \equiv \mathrm{d}\ln a$, this amounts to requiring inflation to last at least $N \sim 62$. The Universe becomes enormously large after inflation, and we see just a tiny part of it. Our

[4]We conventionally define $N \equiv \ln(a/a_i)$. N takes positive values that increase as inflation proceeds.

Universe is almost exactly homogeneous because all the initial inhomogeneities (and other "defects", like magnetic monopoles) were diluted away – or "devalued", hence the name *inflation* –, and for the same reason the Universe looks so flat [21].

As can be seen from Figure 1.2, all scales that are relevant to cosmological observations today were outside the comoving Hubble radius until $a \sim 10^{-5}$, but were instead smaller than it at the beginning of inflation, thus causally connected. For any mode of comoving wavenumber k, we define the *horizon crossing* as the moment when the (comoving) wavelength $\lambda \sim k^{-1}$ becomes comparable to the size of the comoving Hubble radius, that is $k = aH$. We say that a mode *enters the horizon* as it goes from $k \ll aH$ to $k \geq aH$, since it becomes observable for an observer living in the Universe.

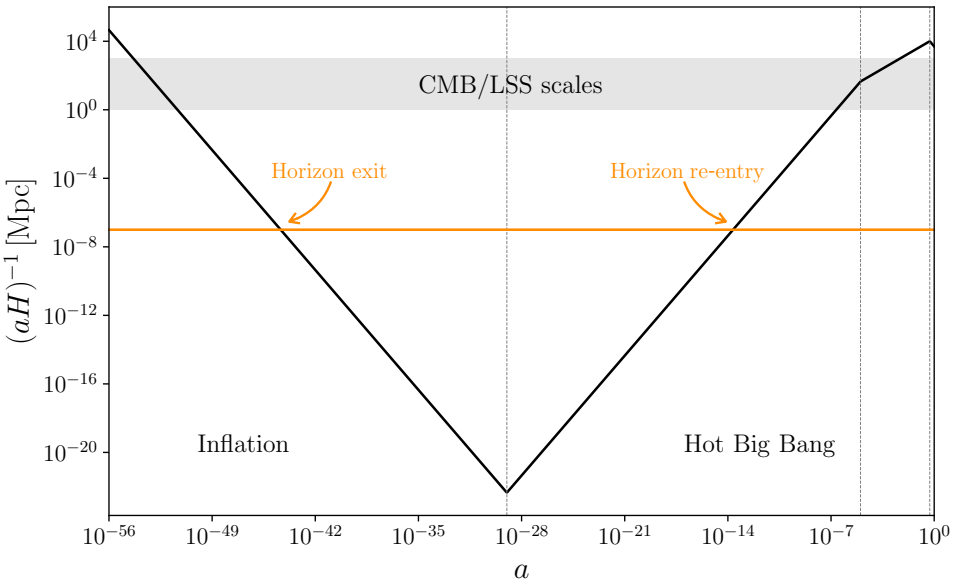

Figure 1.2: Comoving Hubble radius $(aH)^{-1}$ as a function of the scale factor a through different epochs, marked by vertical dotted lines; from left to right: inflation, radiation-domination, matter-domination, and dark-energy domination at the very end. The scales probed by CMB and LSS experiments roughly fall within the horizontal gray band. The horizontal orange line represents a typical mode of a given comoving wavelength λ that was sub-Hubble at the beginning of inflation, crossed the horizon during inflation, and ultimately re-entered during radiation-domination.

In the following paragraphs, we will investigate the conditions for a viable inflation. As already mentioned, the condition $\ddot{a} > 0$ can be realized by a cosmological constant Λ. In that case, the solution to the Friedmann equations is a de Sitter universe, characterized by

$$a(t) \propto e^{H_0 t}. \tag{1.10}$$

However, a pure de Sitter solution corresponds to a cosmological attractor and is thus unsuitable to end inflation with a smooth, graceful exit into the standard hot Big Bang Universe. However, it still offers an excellent approximation at the onset of inflation. As shown in [18], inflation lasts sufficiently long provided the following condition is satisfied

$$\frac{(\rho + p)_i}{\rho_i} \lesssim 10^{-2}. \tag{1.11}$$

At the beginning of inflation, the deviation from the vacuum equation of state $\omega = -1$ must not exceed 1%. However, the vacuum-like energy must still exhibit some time dependence to stop inflation. In the following, we outline the simplest mechanism to satisfy this condition and explain how inflation becomes a physically testable theory through its predictions for perturbations.

1.3.1 The simplest realization of inflation

The simplest candidate to drive inflation is a single scalar field ϕ, the so-called *inflaton*. To show that, let us consider a real scalar field ϕ with Lagrangian density

$$\mathcal{L}_\phi = -\frac{1}{2} g^{\mu\nu} \partial_\mu \phi \partial_\nu \phi - V(\phi). \tag{1.12}$$

The corresponding energy-momentum tensor,

$$T_{\mu\nu} = -\frac{2}{\sqrt{-g}} \frac{\delta(\sqrt{-g}\mathcal{L}_\phi)}{\delta g^{\mu\nu}} = \partial_\mu \phi \partial_\nu \phi + g_{\mu\nu} \mathcal{L}_\phi, \tag{1.13}$$

can be cast in the shape of the energy-momentum tensor for a perfect fluid, namely

$$T_{\mu\nu} = (p + \rho)\, u_\mu u_\nu + p\, g_{\mu\nu}, \tag{1.14}$$

via the following identification

$$\rho = \frac{1}{2}\dot{\phi}^2 + V(\phi), \qquad p = \frac{1}{2}\dot{\phi}^2 - V(\phi), \qquad u_\mu = \frac{\partial_\mu \phi}{\sqrt{-\partial_\alpha \phi \partial^\alpha \phi}}. \tag{1.15}$$

We have neglected the spatial derivatives since we have shown that they become negligible soon after the onset of inflation. The de Sitter limit, $\rho \simeq -p$, is achieved when the potential energy dominates over the kinetic one, $\dot{\phi}^2 \ll V(\phi)$. This is known as *slow-roll limit*. Assuming that there are no other matter fields, the dynamics of the homogeneous field ϕ and the FLRW background can be determined using the first Friedmann equation

$$H^2 = \frac{1}{3}\left(\frac{1}{2}\dot{\phi}^2 + V(\phi)\right), \tag{1.16}$$

and the Klein-Gordon equation for ϕ

$$\ddot{\phi} + 3H\dot{\phi} + V_{,\phi} = 0. \tag{1.17}$$

We further write the second Friedmann equation (1.5), which can be combined with Eq. (1.16) to give

$$\dot{H} = -\frac{1}{2}\dot{\phi}^2. \tag{1.18}$$

Eq. (1.5) can be written as

$$\frac{\ddot{a}}{a} = -\frac{1}{6}(\rho_\phi + 3p_\phi) = H^2(1 - \epsilon), \tag{1.19}$$

where we have defined the *first slow-roll parameter*

$$\epsilon \equiv \frac{3}{2}(w_\phi + 1) = -\frac{\dot{H}}{H^2}. \tag{1.20}$$

Accelerated expansion is achieved when $\epsilon < 1$, and the de Sitter limit corresponds to $\epsilon \to 0$. Therefore, inflation is realized for $\epsilon \ll 1$ and ends by definition when $\epsilon = 1$. As a complementary condition, we require $\ddot{\phi} \ll |3H\dot{\phi}|, |V_{,\phi}|$, so to have a sufficiently long stage of slow-roll. This requires the smallness of a second slow-roll parameter

$$\eta \equiv -\frac{\ddot{\phi}}{H\dot{\phi}} = 2\frac{H_{,\phi\phi}}{H}, \tag{1.21}$$

where the second equality follows from $\dot{\phi} = -2H_{,\phi}$, obtained from Eq. (1.18). In other words, the scalar field ϕ should slowly roll down the potential. The slow-roll conditions $\epsilon \ll 1$ and $|\eta| \ll 1$, translate into

requirements on the shape of the potential. From the slow-roll limit of the equations of motion (1.16) and (1.17), namely $3H^2 \simeq V$ and $3H\dot{\phi} \simeq -V_{,\phi}$, one can express the slow-roll parameters ϵ and η in terms of the potential and its derivatives. We introduce the *potential slow-roll parameters*

$$\epsilon_{\rm v} \equiv \frac{1}{2}\left(\frac{V_{,\phi}}{V}\right)^2, \qquad \eta_{\rm v} \equiv \frac{V_{,\phi\phi}}{V}, \tag{1.22}$$

which satisfy $\epsilon \simeq \epsilon_{\rm v}$, $\eta \simeq \eta_{\rm v} - \epsilon_{\rm v}$ at leading order in the slow-roll approximation. A prolonged inflationary stage therefore requires $\epsilon_{\rm v}, |\eta_{\rm v}| \ll 1$, meaning that the potential must be sufficiently flat: both its slope $V_{,\phi}$ and its curvature $V_{,\phi\phi}$ must remain small relative to V. This naturally favors potentials featuring a plateau-like region, as shown in Figure 1.3. Conversely, steep polynomial potentials $V \propto \phi^p$ generically violate these conditions over a significant field range. As we will see in Sec. 1.5, such models are now strongly disfavored by CMB observations.

The field gains speed as the potential becomes steeper, and the slow-roll condition breaks down. Inflation ends, and the Universe transitions into a phase of decelerated expansion. Eventually, the scalar field oscillates around the minimum of the potential and decays into lighter particles. This process, which marks the transition from the end of inflation to a homogeneous, radiation-dominated universe, is known as *reheating*.

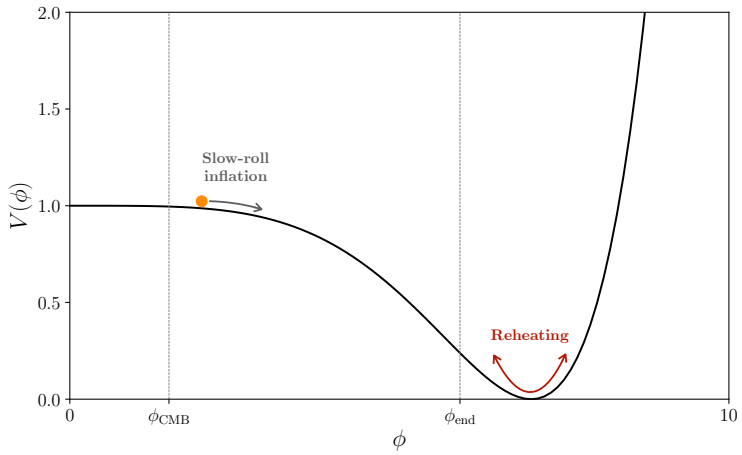

Figure 1.3: Example of inflation driven by a scalar field ϕ with potential $V(\phi) = V_0(1-(\phi/\mu)^4)^2$. Inflation ends at $\phi_{\rm end}$ when $\epsilon = 1$. CMB scales cross the horizon about 60 e-folds before the end of inflation, when the field is at $\phi_{\rm CMB}$. Reheating occurs when the field oscillates about the minimum.

We stress that single-field slow-roll is just one of the many possibilities to describe an inflationary universe. Some generalizations include [22]: multi-field inflation – a well-known example is the classical hybrid inflation model [23] –, theories of modified gravity and non-minimal couplings between the inflaton and gravity – to be discussed in Chapter 2 –, and models with non-standard kinetic terms, like Dirac-Born-Infeld inflation [24] and tachyonic inflation [25]. Even the possibility of having inflation without an inflaton was recently discussed [26].

1.4 Cosmological perturbations

So far, we have described the Universe as perfectly homogeneous and isotropic, which is a good approximation on large scales. On the smallest scales, however, the Universe looks highly inhomogeneous: matter clumps into stars, galaxies, clusters, and filaments, and the cosmological principle can be phrased only in a statistical sense. Here lies the extraordinary power of inflation:

besides addressing the horizon and flatness problems, inflation connects quantum fluctuations generated in the early Universe with the LSS we observe today. During inflation, primordial perturbations in the energy density of the Universe are redshifted at super-horizon scales, ultimately re-entering the horizon and sourcing structure formation via gravitational instability. In this section, we will show how inflation predicts the power spectrum of the generated perturbations, thus gaining the status of a testable theory through observations of the CMB anisotropies.

At recombination, the Universe was nearly homogeneous, the inhomogeneities on the CMB being at the 10^{-5} level. We will therefore split all the quantities of interest into a homogeneous background and a spatially-dependent perturbation

$$X = X^{(0)}(t) + \delta X(t, \mathbf{x}), \tag{1.23}$$

where $\delta X \ll X^{(0)}$. We will consider only perturbations at linear order, since they approximate well the full nonlinear solution.[5] From now on, we will omit the superscript (0) for background quantities, while perturbations will always be written in the form δX.

A crucial aspect of perturbation theory in general relativity (GR) is gauge freedom. If, at the background level, the spacetime symmetries imply the existence of a preferred coordinate system, there are no obvious preferred coordinates for analyzing perturbations. This gauge freedom can lead to misconceptions since one can create fictitious perturbations or remove real perturbations by perturbing the coordinates [18]. To handle the correct physical interpretation of perturbations, it is necessary to have a full set of variables in the matter and metric sectors. This necessity underlines the importance of working with gauge-invariant quantities, which will be highlighted throughout this section by enclosing them in a box. If the goal is merely to compute observables – which are inherently gauge-invariant – an alternative approach is to fix the gauge. In this case, although intermediate steps may depend on the chosen gauge, the final observable results remain physically valid.

Perturbation theory is a cornerstone of modern cosmology, and it is extensively discussed in many books and reviews [14, 18, 20, 28–33]. Nonetheless, we provide the standard derivation, since conventions vary throughout the literature.

A flat FLRW universe with a small perturbation is described by the line element[6]

$$\begin{aligned} \mathrm{d}s^2 &= \left(g_{\mu\nu}(t) + \delta g_{\mu\nu}(t, \mathbf{x})\right) \mathrm{d}x^\mu \mathrm{d}x^\nu \\ &= -\left(1 + 2A\right) \mathrm{d}t^2 + 2aB_i \mathrm{d}x^i \mathrm{d}t + a^2 \left[\left(1 - 2\psi\right) \delta_{ij} + E_{ij}\right] \mathrm{d}x^i \mathrm{d}x^j, \end{aligned} \tag{1.24}$$

where $A(t, \mathbf{x})$ and $\psi(t, \mathbf{x})$ are scalar perturbations, while $B_i(t, \mathbf{x})$ and $E_{ij}(t, \mathbf{x})$ at this stage are generic vector and tensor perturbations, respectively.

The scalar-vector-tensor (SVT) decomposition, which follows from Helmoltz's theorem, can be adopted to split the metric perturbation into scalar, vector, and tensor parts, according to their transformation properties on the spatial hypersurfaces. As a consequence, we can identify

$$B_i \equiv \partial_i B - S_i, \qquad \text{where} \qquad \partial^i S_i = 0, \tag{1.25}$$

$$E_{ij} \equiv 2\partial_{ij} E + 2\partial_{(i} F_{j)} + h_{ij}, \qquad \text{where} \qquad \partial^i F_i = 0, \quad h^i_i = \partial^i h_{ij} = 0. \tag{1.26}$$

The independent functions used to construct $\delta g_{\mu\nu}$ are: four functions for the scalar perturbations, four functions for the vector perturbations (two 3-vectors and two constraints), and two functions for the tensor perturbations (h_{ij} has six independent components, and there are four constraints). Therefore,

[5] We are neglecting all the second-order effects. See, e.g., [27] for a computation of cosmological perturbations up to second order.

[6] Note that in the g_{00} component we use A instead of the commonly adopted Φ to avoid confusion with the scalar field.

there are 10 functions, as the number of independent components of $\delta g_{\mu\nu}$. We will show that the physical components are just six since the other four can be fixed using gauge invariance.

Scalar, vector, and tensor perturbations are decoupled at linear order and can be studied separately.

1.4.1 Scalar perturbations

Scalar perturbations are induced by energy density inhomogeneities; they exhibit gravitational instability and lead to structure formation.

The intrinsic Ricci scalar on constant-time hypersurfaces at first order in perturbations is given by

$$\delta R^{(3)} = \frac{4}{a^2}\nabla^2\psi, \tag{1.27}$$

where $\nabla^2 \equiv \delta^{ij}\partial_{ij}$ is the spatial Laplacian. For this reason, we refer to ψ as the *curvature perturbation*. Let's consider a scalar coordinate transformation

$$t \to t + \delta t, \qquad x^i \to x^i + \delta^{ij}\partial_j \delta x. \tag{1.28}$$

Enforcing the conservation of the line element, one can show that the scalar metric perturbations transform as [29]

$$\begin{aligned} A &\to A - \dot{\delta t}, \\ B &\to B + a^{-1}\delta t - a\,\dot{\delta x}, \\ E &\to E - \delta x, \\ \psi &\to \psi + H\delta t. \end{aligned} \tag{1.29}$$

The simplest gauge-invariant combination of these functions – spanning the two-dimensional space of physical perturbations – are the *Bardeen potentials* [30]

$$\boxed{\Phi \equiv A - \frac{\mathrm{d}}{\mathrm{d}t}\left[a^2\left(\dot{E} - B/a\right)\right]}, \qquad \boxed{\Psi \equiv \psi + a^2 H\left(\dot{E} - B/a\right)}. \tag{1.30}$$

A possibility to exhaust the gauge freedom is to work in the *longitudinal (Newtonian) gauge*, where $B = E = 0$ and the line element – including only scalar perturbations – becomes

$$\mathrm{d}s^2 = -\left(1 + 2\Phi\right)\mathrm{d}t^2 + a^2\left(1 - 2\Psi\right)\delta_{ij}\mathrm{d}x^i\mathrm{d}x^j. \tag{1.31}$$

In the particular case where the spatial part of the energy-momentum tensor is diagonal, i.e. $\delta T^j_i \propto \delta^j_i$, it follows that $\Phi = \Psi$ and we are left with a single metric perturbation variable which plays the role of the Newtonian potential. The physical interpretation of the Bardeen potential becomes clear: they are the amplitudes of the metric perturbations in the longitudinal gauge [32].

Moving to the matter sector, density perturbations transform under (1.28) as

$$\delta\rho \to \delta\rho - \dot{\rho}\,\delta t. \tag{1.32}$$

Analogously, pressure perturbations transform as $\delta p \to \delta p - \dot{p}\,\delta t$. Momentum density perturbation δq, defined through $\partial_i \delta q \equiv (\rho + p)v_i$, transform as

$$\delta q \to \delta q + (\rho + p)\,\delta t, \tag{1.33}$$

from which we can define the *comoving density perturbation*

$$\delta\rho_m \equiv \delta\rho - 3H\delta q. \tag{1.34}$$

Another important gauge-invariant quantity is the *curvature perturbation on uniform-density hypersurfaces* ζ

$$\boxed{-\zeta \equiv \psi + \frac{H}{\dot{\rho}}\delta\rho}, \tag{1.35}$$

measuring the spatial curvature on constant-energy hypersurfaces. Outside the horizon, ζ is constant for *adiabatic matter perturbations*, that is perturbations satisfying

$$\boxed{p_{\rm en} \equiv \delta p - \frac{\dot{p}}{\dot{\rho}}\delta\rho} = 0, \tag{1.36}$$

where we indicate with a subscript 'en' the non-adiabatic part of the pressure perturbation, also known as *entropy perturbation*. Another gauge-invariant scalar is the *comoving curvature perturbation*[7]

$$\boxed{\mathcal{R} \equiv \psi - \frac{H}{\rho + p}\delta q}, \tag{1.37}$$

which can be interpreted as the curvature perturbation on hypersurfaces that are orthogonal to comoving worldlines.

1.4.2 Vector perturbations

Vector perturbations are related to the rotational motions of the fluid. As in Newtonian theory, they decay very quickly and are typically neglected. One exception emerges in the context of magnetic field generation during inflation, a topic we will explore in Chapter 5.

Under a vector coordinate transformation

$$x^i \to x^i + \delta x^i, \tag{1.38}$$

the vector metric perturbations transform as

$$\begin{aligned} S_i &\to S_i + a\,\delta\dot{x}_i, \\ F_i &\to F_i - \delta x_i. \end{aligned} \tag{1.39}$$

The combination $\boxed{V_i \equiv \dot{F}_i + S_i/a}$ is the gauge-invariant shear perturbation and spans the two-dimensional space of physical perturbations.

1.4.3 Tensor perturbations

Tensor perturbations describe gravitational waves, the degrees of freedom of the gravitational field itself. The transverse and traceless perturbation h_{ij} in Eq. (1.26) already describes gravitational waves in a gauge-invariant manner.

1.4.4 Power spectra

Cosmology always deals with statistics, because no known theory predicts the matter overdensity at a given point in space. What inflation predicts is the *statistical distribution* of perturbations, from which one can draw the initial conditions for any subsequent evolution [20].

[7] The two commonly adopted definitions of curvature perturbations ζ and $\mathcal{R}$ are sometimes defined with a different notation, denoting $\mathcal{R}$ by "ζ". Note that $-\zeta = \mathcal{R}$ only when $\delta\rho_m = 0$. This is the case for single-field slow-roll inflation.

In this section, we define the power spectrum of perturbations, a bridge between perturbation theory and observations.

For any function $X(t, \mathbf{x})$ we define its Fourier transform as

$$X_{\mathbf{k}}(t) = \int \mathrm{d}^3\mathbf{x}\, e^{-i\mathbf{k}\cdot\mathbf{x}} X(t, \mathbf{x}). \tag{1.40}$$

Starting from the equal-time two-point correlation function

$$\langle X_{\mathbf{k}}(t) X_{\mathbf{k}'}(t)\rangle \equiv (2\pi)^3 \delta^3(\mathbf{k}+\mathbf{k}') P_X(k), \tag{1.41}$$

where we have assumed statistical homogeneity and isotropy, we define the power spectrum as

$$\mathcal{P}_X(k) \equiv \frac{k^3}{2\pi^2} P_X(k). \tag{1.42}$$

To make contact with other definitions in the literature, note that $P_X(k) \equiv \langle |X(k)|^2\rangle$. The spectrum of scalar curvature perturbations is then defined as

$$\mathcal{P}_{\mathcal{R}} \equiv \frac{k^3}{2\pi^2} \langle |\mathcal{R}|^2\rangle, \tag{1.43}$$

where $\mathcal{R}$ is defined in Eq. (1.37). The scale dependence of the scalar power spectrum is given by the logarithmic derivative of the power spectrum

$$n_s - 1 \equiv \left.\frac{\mathrm{d}\ln \mathcal{P}_{\mathcal{R}}}{\mathrm{d}\ln k}\right|_{k=aH}, \tag{1.44}$$

evaluated at Hubble radius crossing. A scale-invariant power spectrum corresponds to $n_s = 1$. We also introduce the running of the spectral index and the running of the running,

$$\alpha_s \equiv \frac{\mathrm{d}n_s}{\mathrm{d}\ln k}, \qquad \beta_s \equiv \frac{\mathrm{d}\alpha_s}{\mathrm{d}\ln k}. \tag{1.45}$$

The power spectrum is usually approximated as a power law[8]

$$\mathcal{P}_{\mathcal{R}}(k) = A_s(k_*) \left(\frac{k}{k_*}\right)^{n_s(k_*)-1+\frac{1}{2}\alpha_s(k_*)\ln\left(\frac{k}{k_*}\right)+\frac{1}{6}\beta_s(k_*)\left(\ln\left(\frac{k}{k_*}\right)\right)^2}, \tag{1.46}$$

where k_* is some reference pivot scale. It is a conventional scale, often set as the best scale constrained by a given set of observations (e.g., for CMB anisotropies *Planck* sets $k_* = 0.002\,\mathrm{Mpc}^{-1}$) [15].

Similarly, we define the tensor power spectrum as

$$\mathcal{P}_T \equiv 2\frac{k^3}{2\pi^2} \langle |h|^2\rangle, \tag{1.47}$$

where h is the element of the tensor perturbation h_{ij} introduced in Eq. (1.26) and the factor of 2 comes from accounting for the two polarization modes. The scale dependence of the tensor power spectrum is encoded in the tensor spectral index

$$n_T \equiv \left.\frac{\mathrm{d}\ln \mathcal{P}_T}{\mathrm{d}\ln k}\right|_{k=aH}, \tag{1.48}$$

which is defined without -1 for historical reasons.

Another important observational quantity is the *tensor-to-scalar ratio*

$$r \equiv \frac{\mathcal{P}_T}{\mathcal{P}_{\mathcal{R}}}. \tag{1.49}$$

[8]Note that the power-law approximation in Eq. (1.46) is a Taylor expansion of the scalar spectral index n_s. If the primordial perturbations are produced by slow-roll inflation, then generically $(n_s - 1) \sim \mathcal{O}(\epsilon), \alpha_s \sim \mathcal{O}(\epsilon^2), \beta_s \sim \mathcal{O}(\epsilon^3)$ and the Taylor expansion of n_s is valid for cosmological observations, which probe a limited range of scales, $k_*^{\mathrm{CMB}} \in [5\times10^{-3}, 5\times10^{-1}]\ \mathrm{Mpc}^{-1}$ [34]. Caution should be taken when extending this approximation to other scales.

1.4.5 Worked example: single-field inflation

In this section, we present the complete derivation of quantum fluctuations produced during inflation and discuss the associated spectra of cosmological perturbations. We will first focus on scalar perturbations, as they effectively illustrate the overall procedure. We will mainly follow [14].

The starting point is the action of gravity and a scalar field with the general form

$$S = \int \mathrm{d}^4x\sqrt{-g}\left[\frac{1}{2}R - \frac{1}{2}\left(\nabla\phi\right)^2 - V(\phi)\right]. \tag{1.50}$$

We aim to study the perturbations of this action under fluctuations of the scalar field $\phi = \phi(t)+\delta\phi(t,\mathbf{x})$ and the metric. A convenient gauge choice is

$$\delta\phi = 0, \qquad g_{ij} = a^2\left[\left(1-2\mathcal{R}\right)\delta_{ij} + h_{ij}\right], \tag{1.51}$$

where h_{ij} is the transverse and traceless tensor perturbation defined in Eq. (1.26). In this gauge, the scalar field ϕ is unperturbed, and all scalar degrees of freedom are parametrized by $\mathcal{R}$, physically representing the spatial curvature of constant$-\phi$ hypersurfaces.

The action (1.50) can be expanded to second order in $\mathcal{R}$ as [35]

$$S^{(2)} = \frac{1}{2}\int \mathrm{d}^4x\, a^3\frac{\dot{\phi}^2}{H^2}\left[\dot{\mathcal{R}}^2 - a^{-2}\left(\partial_i\mathcal{R}\right)^2\right]. \tag{1.52}$$

By defining the *Mukhanov variable* v as

$$v \equiv z\mathcal{R}, \qquad \text{where} \qquad z \equiv \frac{a\dot{\phi}}{H}, \tag{1.53}$$

and moving to conformal time τ defined in Eq. (1.2), Eq. (1.52) becomes

$$S^{(2)} = \frac{1}{2}\int \mathrm{d}\tau\mathrm{d}^3x\left[\left(v'\right)^2 - \left(\partial_i v\right)^2 + \frac{z''}{z}v^2\right]. \tag{1.54}$$

Since we are working with a linear theory, we can perform a Fourier expansion of the field v

$$v(\tau,\mathbf{x}) = \int \frac{\mathrm{d}^3k}{(2\pi)^3}v_{\mathbf{k}}(\tau)e^{i\mathbf{k}\cdot\mathbf{x}}. \tag{1.55}$$

The corresponding equation of motion is the so-called *Mukhanov equation*[9]

$$v_k'' + \left(k^2 - \frac{z''}{z}\right)v_k = 0. \tag{1.56}$$

Given the dependence of z on the background dynamics, the Mukhanov equation is hard to solve in full generality. We will consider the two limiting cases: sub-horizon, $k \gg aH$, and super-horizon, $k \ll aH$. Quantization is performed by promoting the classical field v to a quantum operator

$$v \longrightarrow \hat{v} = \int \frac{\mathrm{d}^3\mathbf{k}}{(2\pi)^3}\left[v_k(\tau)\hat{a}_{\mathbf{k}}e^{i\mathbf{k}\cdot\mathbf{x}} + v_k^*(\tau)\hat{a}_{\mathbf{k}}^\dagger e^{-i\mathbf{k}\cdot\mathbf{x}}\right]. \tag{1.57}$$

The canonical commutation relations imply the constraint (in units $\hbar = 1$)

$$i\left(v_k^*v_k' - \left(v_k^*\right)'v_k\right) = 1. \tag{1.58}$$

[9] We have dropped the vector notation since the Mukhanov equation only depends on k.

We fix the vacuum state $\hat{a}_{\mathbf{k}}|0\rangle = 0$ as the Minkowski vacuum of a comoving observer in the infinite past $\tau \to -\infty$. In this limit – corresponding to the sub-horizon limit – the Mukhanov equation (1.56) becomes the equation of a harmonic oscillator with a time-independent frequency. The solution providing the minimum energy is

$$\lim_{\tau\to-\infty} v_k = \frac{e^{-ik\tau}}{\sqrt{2k}}. \tag{1.59}$$

Therefore, choosing the vacuum state is equivalent to a boundary condition on the mode function v. Eqs. (1.58) and (1.59) completely fix the mode function at all scales. As discussed in Sec. 1.3, the de Sitter limit is a good approximation to describe inflation, and can therefore be used to find approximate solutions to the Mukhanov equation. In the de Sitter limit, $\tau = -(aH)^{-1}, H \sim \text{const.}, (\dot{\phi}/H)^2 \to 0$, Eq. (1.56) becomes

$$v_k'' + \left(k^2 - \frac{2}{\tau^2}\right) v_k = 0, \tag{1.60}$$

whose exact solution is the so-called *Bunch-Davies function*[10] [36]

$$v_k = \frac{e^{-ik\tau}}{\sqrt{2k}}\left(1 - \frac{i}{k\tau}\right). \tag{1.61}$$

In the super-horizon limit $(-k\tau) \ll 1$, the term k^2 in Eq. (1.60) can be neglected, and the mode function is of the form $v_k = A/\tau + B\tau^2$. As a consequence, $\mathcal{R} \sim v_k/a \sim v_k\tau$ becomes $\mathcal{R} = C + D\tau^3 \to C$ since τ quickly goes to zero during inflation. We have shown that the comoving curvature perturbation is conserved on super-horizon scales in single-field slow-roll inflation.

We conclude by evaluating the power spectrum of curvature perturbations. Employing the relation (1.53) and the de Sitter solution (1.61), we have

$$|\mathcal{R}|^2 = \left(\frac{H}{\dot{\phi}}\right)^2 \frac{|v_k|^2}{a^2} = \left(\frac{H}{\dot{\phi}}\right)^2 \frac{1}{a^2}\frac{1}{2k}\left(1 + \frac{1}{k^2\tau^2}\right) \sim \left(\frac{H}{\dot{\phi}}\right)^2 \frac{H^2}{2k^3}, \tag{1.62}$$

where the last equality is valid in the super-horizon limit. From the definition in Eq. (1.43), we obtain the curvature power spectrum

$$\mathcal{P}_\mathcal{R} = \frac{H_*^2}{(2\pi)^2}\frac{H_*^2}{\dot{\phi}_*^2}, \tag{1.63}$$

which is evaluated at horizon crossing. Since $\mathcal{R}$ is constant on super-horizon scales, Eq. (1.63) is valid also at future times, until a given fluctuation mode re-enters the horizon: this powerful result shows that in single-field inflation, instead of going through the Universe's evolution after inflation, we can equate the curvature power spectrum computed at horizon exit during inflation with the one at horizon re-entry.

Given the k^{-3} dependence in Eq. (1.62), the power spectrum is scale-invariant. Even though this is a good approximation, we stress that this result is related to taking the de-Sitter limit, and deviations from perfect scale invariance are necessary to end inflation. This outcome is clarified in the slow-roll approximation, where, from the slow-roll limit of the equations of motion (1.16)–(1.17), the curvature power spectrum becomes

$$\mathcal{P}_\mathcal{R} \sim \frac{V(\phi)}{24\pi^2\epsilon}. \tag{1.64}$$

Any scale dependence of the spectrum is encoded in the scalar spectral index, which is [14]

$$n_s - 1 = \frac{\mathrm{d}\ln\mathcal{P}_\mathcal{R}}{\mathrm{d}\ln k} = \frac{\mathrm{d}\ln\mathcal{P}_\mathcal{R}}{\mathrm{d}\phi}\frac{\mathrm{d}\phi}{\mathrm{d}N}\frac{\mathrm{d}N}{\mathrm{d}\ln k} = 2\eta - 4\epsilon. \tag{1.65}$$

[10] The solution is uniquely fixed by imposing the boundary conditions (1.58)-(1.59).

We can now briefly outline the corresponding calculation for tensor perturbations. The Einstein-Hilbert action can be expanded to second order in the tensor perturbations as

$$S^{(2)} = \frac{M_{pl}^2}{8} \int \mathrm{d}\tau \mathrm{d}^3x\, a^2 \left[\left(h'_{ij} \right)^2 - \left(\partial_l h_{ij} \right)^2 \right], \tag{1.66}$$

where we have restored M_{pl} to make h_{ij} manifestly dimensionless. Introducing the Fourier expansion

$$h_{ij}(\tau, \mathbf{x}) = \int \frac{\mathrm{d}^3k}{(2\pi)^3} \sum_{p=+,\times} \varepsilon_{ij}^p(k) h_{\mathbf{k},p}(\tau) e^{i\mathbf{k}\cdot\mathbf{x}}, \tag{1.67}$$

where the sum runs over polarizations and the following properties hold: $\varepsilon_{ii} = k^j \varepsilon_{ij} = 0$ and $\varepsilon_{ij}^p \varepsilon_{ij}^{p'} = 2\delta_{pp'}$. By further defining the canonically normalized field

$$v_{\mathbf{k},p} \equiv \frac{a}{2} M_{pl} h_{\mathbf{k},p}, \tag{1.68}$$

the action in Eq. (1.66) becomes

$$S^{(2)} = \sum_{p=+,\times} \frac{1}{2} \int \mathrm{d}\tau \mathrm{d}^3k \left[\left(v'_{\mathbf{k},p} \right)^2 - \left(k^2 - \frac{a''}{a} \right) \left(v_{\mathbf{k},p} \right)^2 \right]. \tag{1.69}$$

The latter expression should be recognized as two copies, one for each polarization state, of the action (1.54). The quantization then follows naturally from the previous results: each gravitational-wave polarization is just a renormalized massless field in de Sitter space,

$$h_{\mathbf{k},p} \equiv \frac{2}{M_{pl}} \psi_{\mathbf{k},p}, \quad \text{with} \quad \psi_{\mathbf{k},p} \equiv \frac{v_{\mathbf{k},p}}{a}. \tag{1.70}$$

Since, from Eqs. (1.62)–(1.63), the power spectrum for $\psi_{\mathbf{k},p}$ is $\mathcal{P}_\psi = (H/2\pi)^2$, we readily obtain the tensor power spectrum

$$\mathcal{P}_T = \frac{2}{\pi^2} \frac{H_*^2}{M_{pl}^2}. \tag{1.71}$$

Following the same procedure as above, one can show that the tensor spectral index in the slow-roll approximation is

$$n_T = -2\epsilon. \tag{1.72}$$

Deviations from exact scale invariance ($n_s = 1, n_T = 0$) are thus quantified by the slow-roll parameters ϵ and η, acting as an indirect probe of the inflationary dynamics.

1.5 Contact with observations

Now that we have seen how cosmological perturbations are generated from quantum fluctuations, we can get to the connection to what we observe. This section does not aim to explain all the details involved in the derivation of the power spectrum of CMB anisotropies. Instead, it provides an overview of the main results that set the basis for the present evidence for inflation.

First, we will connect the CMB temperature and polarization spectra with $\mathcal{P}_\mathcal{R}$ and $\mathcal{P}_T$ as defined in Sec. 1.4. Then, we will outline the current observational status. For the sake of brevity, we will omit the discussion on LSS as a probe of primordial curvature perturbations.

1.5.1 CMB temperature and polarization

The CMB temperature fluctuations relative to the background temperature T_0 can be expanded in spherical harmonics as

$$\Theta(\hat{n}) \equiv \frac{\Delta T(\hat{n})}{T_0} = \sum_{\ell,m} a_{\ell m} Y_{\ell m}(\hat{n}). \tag{1.73}$$

$Y_{\ell m}$ are the standard spherical harmonics on a 2-sphere ($\ell = 0, 1, 2$ for monopole, dipole, and quadrupole, respectively). The multipole moments $a_{\ell m}$ can be combined to form the corresponding angular power spectrum

$$C_\ell^{TT} = \frac{1}{2\ell+1} \sum_m \langle a_{\ell m}^* a_{\ell m} \rangle, \tag{1.74}$$

which can be written in terms of the curvature power spectrum, since temperature fluctuations are dominated by scalar modes [14]

$$C_\ell^{TT} = \frac{2}{\pi} \int \mathrm{d}k\, k^2 \mathcal{P}_\mathcal{R}(k) \Delta_{T\ell}(k) \Delta_{T\ell}(k). \tag{1.75}$$

Here $\Delta_{T\ell}(k)$ is the *transfer function* encoding the linear relation between $\mathcal{R}$ and ΔT. Figure 1.4 shows the observed CMB temperature power spectrum and the theoretical fit to data, which depends on the curvature power spectrum predicted by inflation and the cosmological parameters. Practically, the transfer function $\Delta_{T\ell}$ is usually evaluated numerically using Boltzmann solvers (such as `CAMB` [37, 38] or `CLASS` [39]) and the CMB data is fit simultaneously to the background cosmology and the primordial power spectrum.

Of course, not all the scales had already re-entered the horizon at recombination. Therefore, on large scales (low multipoles), the CMB spectrum arises from projecting the primordial power spectrum from recombination to the present.

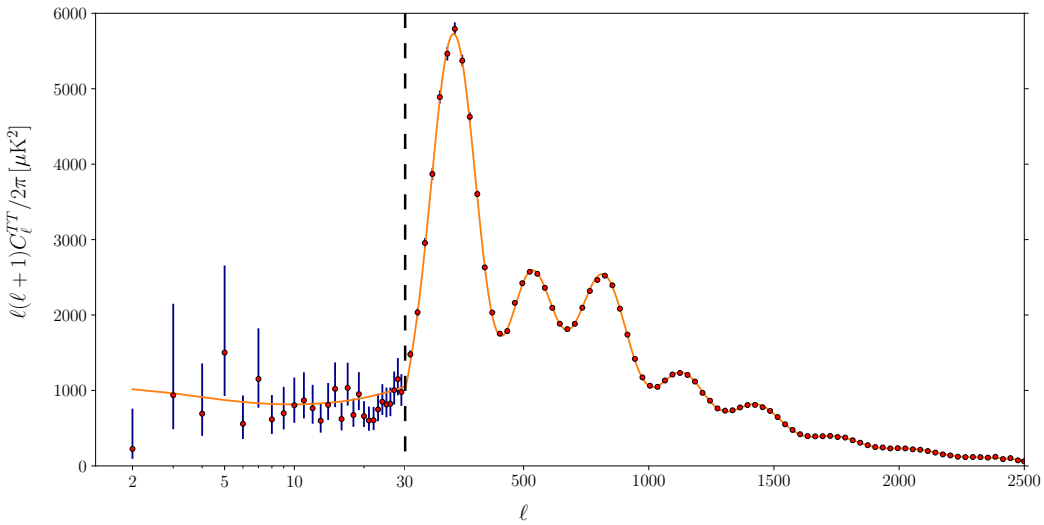

Figure 1.4: *Planck* 2018 temperature power spectrum. The base-ΛCDM theoretical spectrum is also plotted in orange. The theoretical prediction is obtained with `CAMB` fixing the cosmological parameters, including A_s and n_s to the best-fit values to the *Planck* TT,TE,EE+lowE+lensing likelihoods [15]. Note the change from logarithmic to linear scale at $\ell = 30$, marked with a dashed line.

Another crucial probe of inflation resides in the anisotropies in the polarization of the CMB, predicted soon after its discovery [40]. Thomson scattering of unpolarized photons on electrons at last scattering surface generates linear polarization to lowest order in the fine structure constant. If the incoming

radiation field on the electron were isotropic, then the radiation would remain unpolarized. Conversely, if the incident radiation field has a quadrupolar variation in intensity, the result is a linear polarization of the scattered radiation. However, the quadrupole moment is suppressed in the early Universe due to Compton scattering, implying that the amplitude of the polarization spectrum is smaller – and harder to detect – than the temperature one.

The analytical description of the polarization field is more involved as it is described by a tensor, thus requiring a decomposition into tensor spherical harmonics $Y_{\ell m}^{(\pm 2)}$. The best way to describe linearized polarization is to introduce the E and B modes

$$\begin{aligned} E(\hat{n}) &= \sum_{\ell,m} \left(-\frac{1}{2} \left(a_{\ell m}^{(2)} + a_{\ell m}^{(-2)} \right) \right) Y_{\ell m}(\hat{n}) \equiv \sum_{\ell,m} a_{\ell m}^{E} Y_{\ell m}(\hat{n}), \\ B(\hat{n}) &= \sum_{\ell,m} \left(-\frac{1}{2i} \left(a_{\ell m}^{(2)} - a_{\ell m}^{(-2)} \right) \right) Y_{\ell m}(\hat{n}) \equiv \sum_{\ell,m} a_{\ell m}^{B} Y_{\ell m}(\hat{n}). \end{aligned} \tag{1.76}$$

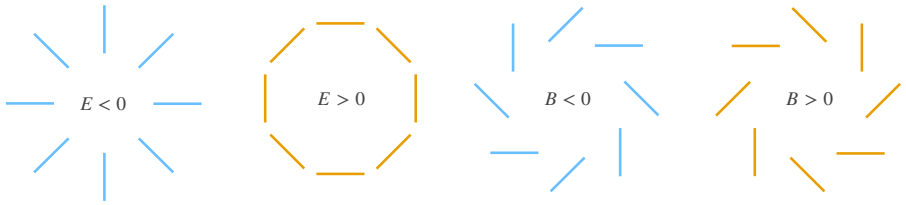

Figure 1.5: Examples of E-modes and B-modes polarization patterns for cold and hot spots in the sky, represented in light-blue and orange, respectively. E (B) is even (odd) under parity transformations. E-mode polarization is curl-free, with polarization vectors that are radial (tangential) around cold (hot) spots in the sky. B-mode polarization is divergence-free but has a curl, and the corresponding polarization vectors form vorticity patterns.

The characteristic polarization pattern of the E and B modes is sketched in Figure 1.5. The advantage of this decomposition is that the E mode is generated by all types of perturbations, whereas the B mode is generated only by vector and tensor perturbations. Since vector perturbations quickly decay during inflation, we can directly relate the B-mode power spectrum to the tensor power spectrum

$$C_\ell^{BB} = (4\pi)^2 \int \mathrm{d}k\, k^2 \mathcal{P}_T(k) \Delta_{B\ell}^2(k). \tag{1.77}$$

Measuring C_ℓ^{BB} is therefore a unique opportunity to access primordial gravitational waves and test inflation.

1.5.2 Current evidence of inflation

So far, CMB observations have provided a remarkable concordance with the predictions of the simplest inflationary models. Below, we discuss the three main pieces of evidence for inflation.

Flatness

As discussed in Sec. 1.2, inflation naturally leads to a flat universe, where $\Omega = 1$ is a future attractor, corresponding to $\Omega_\kappa = 0$. The most precise constraint on the spatial curvature was given by combining baryon acoustic oscillations (BAO) and CMB data [15, 41]

$$\Omega_\kappa = 0.0007 \pm 0.0037 \quad (95\%\,\text{C.L.}), \tag{1.78}$$

showing an almost perfectly flat universe. In a sense, inflation was designed precisely to address the flatness problem, and this observational evidence alone is insufficient to validate inflation.

Power spectrum

As we have seen in Sec. 1.4.5, the simplest single-field slow-roll inflationary model predicts nearly scale-invariant spectra of scalar and tensor perturbations. If, on the one hand, the detection of primordial gravitational waves from inflation is still missing, current CMB observations are in beautiful agreement with the basic inflationary predictions. We report in Table 1.1 the results from *Planck* 2018 data release. Moreover, no deviations from a Gaussian and adiabatic power spectrum have been observed,

Parameter	**TT,TE,EE+lowE+lensing**
$\ln(10^{10}A_s)$	3.044 ± 0.014
n_s	0.9649 ± 0.0042
α_s	-0.0045 ± 0.0067

Table 1.1: *Planck* 2018 68% confidence-level (CL) intervals for the scalar spectrum parameters in the base-ΛCDM model from temperature, polarization, and lensing data combined [42].

which agrees with single-field slow-roll inflation. We will address the discussion of non-Gaussianities and non-adiabatic features in Chapter 4.

Concerning the tensor power spectrum, current observations provide an upper bound on the tensor-to-scalar ratio r (see Eq. (1.49)) at some reference scale k_*. Combining data from *Planck* 2018, BICEP, *Keck Array*, and BICEP3 data up to the 2018 observing season [43] and taking the reference scales $k_1 = 0.005\,\mathrm{Mpc}^{-1}$ and $k_2 = 0.02\,\mathrm{Mpc}^{-1}$, [44] one obtains the bounds

$$\begin{aligned} r_{0.005} &< 0.030 \quad (95\%\,\text{C.L.}), \\ r_{0.02} &< 0.098 \quad (95\%\,\text{C.L.}). \end{aligned} \tag{1.79}$$

Coherence

Perhaps the most convincing observational feature of inflation is the phase coherence necessary to explain the peak/trough structure characterizing the CMB spectrum [45].

Consider a Fourier mode with physical wavelength λ. When sub-horizon-sized, it oscillates with a frequency $k = 2\pi/\lambda$. At horizon crossing, it gets stretched to $\lambda > H^{-1}$. Its amplitude is frozen outside the horizon, and no causal physics can alter its evolution. In this regime, which is unaltered up to horizon re-entry, $\mathcal{R} \sim \text{const.}, \dot{\mathcal{R}} \sim 0$. A generic Fourier mode can be written as a linear combination of sine and cosine, but given that $\dot{\mathcal{R}} \sim 0$ upon horizon re-entry, we conclude that inflation excites cosine modes only (if we set $t = 0$ at horizon re-entry). Once inside the horizon, curvature perturbations source density fluctuations δ, which then evolve under the effect of pressure and gravity,

$$\ddot{\delta} - c_s^2 \nabla^2 \delta = F_g[\mathcal{R}], \tag{1.80}$$

where c_s is the sound speed and F_g is the gravitational source term. In this way, fluctuations in the density field are produced, which, in turn, are tightly coupled to fluctuations in the CMB radiation field. If it were not for the fact that inflation sets coherent initial states way before recombination, the CMB spectrum would appear as the incoherent superposition of random initial phases, and it would be practically indistinguishable from a white noise spectrum. The coherent superposition of Fourier modes generated during inflation, on the other hand, results in the peak/trough structure observed in Figure 1.4: modes with different wavelengths had different phases of the oscillation at recombination, and are therefore captured at maximum, minimum, or zero amplitude.

1.5.3 Constraining single-field inflation

The predictions for a few inflationary models in the (n_s, r) plane are shown in Figure 1.6, compared with the analysis from *Planck* 2018 data alone and in combination with BICEP/*Keck* (BK18) and BAO data.

We have included three classes of single-field inflationary models,

- *Monomial inflation*: $V(\phi) = \lambda M_{pl}^4 \, (\phi/M_{pl})^p$, from *chaotic inflation* originally proposed by Linde [46]. We have varied $p \in \{2/3,\, 1,\, 4/3,\, 2\}$. Generally, models with concave potential ($p < 1$) are favored over those with convex potential. When combined with BK18, *Planck* data strongly disfavors this class of models.

- *Natural inflation*: $V(\phi) = \Lambda^4 \, (1 + \cos(\phi/f))$ [40, 47]. The slow-roll results for n_s and r were derived following [48]. The free parameter f is varied within the colored region. Natural inflation is strongly disfavored by the combined *Planck*+BK18 data.

- *Starobinsky inflation*: $V(\phi) = \Lambda^4 \left(1 - e^{-\sqrt{2/3}\phi/M_{pl}}\right)^2$ [1]. The lowest-order prediction, to be explicitly derived in Sec. 2.3.4, $n_s = 1 - 2/N$, $r = 12/N^2$, is in excellent agreement with current data.

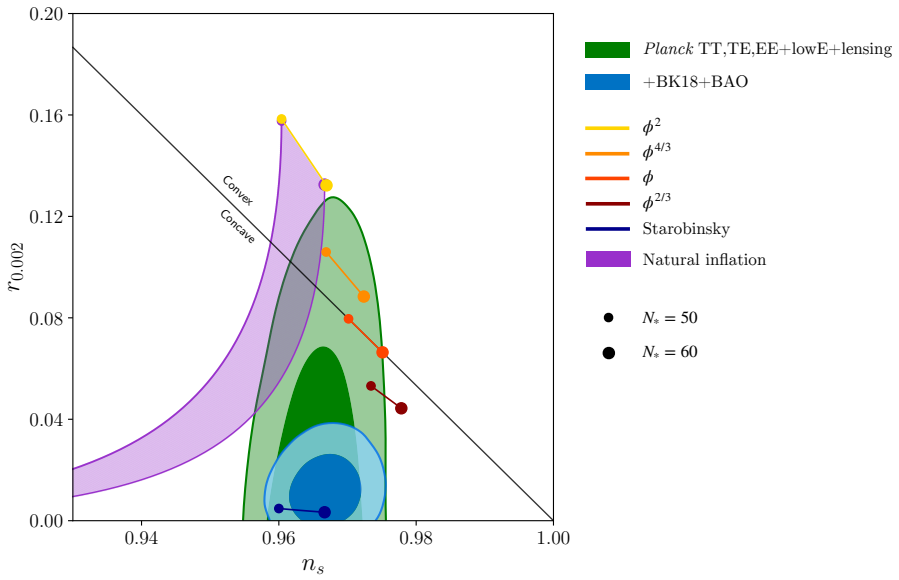

Figure 1.6: Marginalized joint 68% and 95% confidence level (CL) regions for n_s and r at $k = 0.002\,\mathrm{Mpc}^{-1}$ from the *Planck* 2018 baseline analysis (green contours) and in combination with BICEP/*Keck* data at the end of the 2018 season and BAO data (blue contours), obtained assuming $\alpha_s = 0$ [43]. The predictions of selected inflationary models are also reported.

Present data disfavor most of the simplest inflationary models, whose prediction for r is too large. An exception arises with Starobinsky's model. For this reason, we will analyze it in detail in Chapter 2.

After *Planck*, a wealth of ongoing and future experiments offers unprecedentedly sensitive CMB measurements. The most crucial evidence for inflation would probably be a detection of CMB B-modes, since this would be a smoking gun for inflationary gravitational waves. Moreover, detecting $\alpha_s \neq 0$, non-Gaussianities, or isocurvature fluctuations would rule out single-field inflation.

Recently, the ground-based Atacama Cosmology Telescope (ACT) and the South Pole Telescope (SPT) released their latest temperature and polarization anisotropies data, providing an almost fully

independent set of measurements, and pushing temperature measurements to smaller angular scales (higher multipoles ℓ). So far, there is no evidence for a deviation from near-scale-invariance and adiabaticity of the primordial perturbations, and no statistically significant preference for a departure from the baseline ΛCDM model has been reported [49, 50].

Concerning future observations, the upcoming generation of CMB experiments, including the ground-based Simons Observatory (SO) [51, 52] and CMB-S4 [53, 54], and the LiteBIRD satellite [55, 56], will significantly improve our ability to constrain the tensor amplitude, hopefully leading to a detection of primordial tensor modes. Citing some reference values reported by the collaborations, it is expected that SO will achieve a sensitivity $\sigma(r) \sim 0.003$, along with an improvement in the constraining power on the scalar spectral index to $\sigma(n_s) \sim 0.003$. CMB-S4 should reach $\sigma(r) \sim 0.001 - 0.007$ and $\sigma(n_s) \sim 0.002$. LiteBIRD is also expected to have a similar sensitivity of $\sigma(r) \leq 0.001$.

1.6 Challenges for inflationary cosmology

Unarguably, the inflationary paradigm was the first convincing description of the Universe at the earliest times. Besides addressing the Big Bang puzzles, inflation turned out to be a theory with predictive power, providing a causal mechanism for generating small-scale cosmological fluctuations that evolved into the perturbations observed in the CMB anisotropies and the Universe's LSS. However, some conceptual criticalities are rooted in the formulation of inflation and in its scalar-field implementation. In this section, we review the three main challenges for inflation: the initial singularity problem, the initial conditions problem, and the cosmological constant problem.

Initial singularity problem

The Hawking-Penrose theorem [57] states that the standard Big Bang cosmology is incomplete since it has an initial singularity. As anticipated in Sec. 1.1, inflation does not address this issue. Even though many inflating spacetimes violate the weak energy condition – a key assumption in singularity theorems – it was shown [17] that they are incomplete in null and timelike past directions. This implies that to describe the past boundary of the inflating region of spacetime, new physics must be invoked.

Initial conditions problem

Inflation was devised precisely to avoid finely tuned initial conditions to explain the Universe's degree of homogeneity and flatness. To be considered a success, inflation should arise without imposing very special initial conditions on the inflaton's position and velocity. In models of small field inflation – when the scalar field moves over a range $\Delta\phi \lesssim M_{pl}$ – it was shown [58] that to obtain a sufficiently long period of inflation, the initial scalar field's velocity has to be fine-tuned, a condition that seems unnatural for many potentials. This is not the case for large field inflation, where the inflationary slow-roll is a local attractor in initial condition space [59].

At a more profound level, the problem of initial fluctuations has also been pointed out [60]. In some models, inflation typically lasts longer than the minimum span required to solve the horizon problem (see Sec. 1.3). This implies that the physical wavelength of comoving modes corresponding to today's CMB scales was smaller than ℓ_{pl} at the onset of inflation. In other words, inflation began at $t_i \ll t_{pl}$ in these cases. The issue is that the evolution of fluctuations depends on the choice of the vacuum state at time t_i. The choice of the Bunch-Davies initial condition (see Eq. (1.61)) might not be adequate at sub-Planckian scales, where the validity of GR and the use of semiclassical fields to model matter break down.

Cosmological constant problem

In the slow-roll regime, the scalar field moves in an almost constant potential. There is, in principle, another form of constant energy, the quantum vacuum energy, which should not gravitate to solve the famous cosmological constant problem. The mechanism by which this is made possible is yet unknown. The first issue is understanding how this mechanism does not render the constant part of the potential gravitationally inert [60]. Even so, a successful inflationary mechanism should dynamically drive $V(\phi)$ to negligible values at the end of inflation, which could result in an additional fine-tuning problem.

These conceptual drawbacks of inflation led to the development of other early-universe models. Some broad classes include bouncing cosmologies (see, e.g., [61] for a review), string gas cosmologies [62], and emergent Universe models [63]. None of them, however, is entirely free from criticalities. We will therefore stick to inflationary cosmology in the following chapters.

1.7 Summary

In this chapter, we have introduced the inflationary paradigm as a cornerstone of modern cosmology, providing a coherent description of the very early Universe and addressing the main shortcomings of the standard Big Bang scenario. We started in Sec. 1.1 by reviewing the homogeneous and isotropic FLRW background and the corresponding Friedmann equations, which govern the dynamics of the cosmic expansion. Within this framework, we discussed in Sec. 1.2 the horizon and flatness problems, showing that a decelerating radiation- or matter-dominated Universe requires extremely fine-tuned initial conditions to reproduce the observed large-scale homogeneity and near spatial flatness.

In Sec. 1.3, we introduced inflation as a phase of accelerated expansion during which the comoving Hubble radius decreases. This mechanism naturally resolves the Big Bang puzzles by allowing all observable scales today to originate from a single causally connected region and by dynamically driving the Universe toward spatial flatness. We emphasized that a viable inflationary phase corresponds to a quasi-de Sitter expansion, characterized by an approximately constant Hubble parameter and a slowly varying equation of state close to $w \simeq -1$. As a simple realization of inflation, we derived the background dynamics of a slowly rolling scalar field in a flat potential. In the slow-roll regime, the potential energy dominates over the kinetic term, leading to a quasi-de Sitter evolution controlled by small slow-roll parameters, ϵ and η, defined in Eqs. (1.20)–(1.21). We clarified how inflation eventually ends when slow-roll conditions break down, smoothly connecting to the subsequent hot Big Bang evolution.

A central part of the chapter was devoted to cosmological perturbations. In Sec. 1.4, we developed the analytical framework required to study linear perturbations (scalar, vector, and tensor) around an FLRW background, carefully addressing the issue of gauge freedom. We introduced key gauge-invariant quantities, such as the comoving curvature perturbation $\mathcal{R}$, see Eq. 1.37, and linked them to the associated power spectra and spectral indices. We then derived the generation of primordial perturbations from quantum fluctuations, focusing on single-field slow-roll inflation as a worked example. By quantizing the Mukhanov variable, we showed that comoving curvature perturbations are conserved on super-horizon scales, with a prediction for a nearly scale-invariant spectrum.

In Sec. 1.5, we connected the primordial power spectra to cosmological observations, illustrating how CMB temperature and polarization anisotropies translate into quantitative constraints on inflationary models. We also provided a concise overview of the current status of CMB observations and their implications for inflation.

Finally, in Sec. 1.6, we discussed some of the main conceptual issues and open questions underlying the formulation of the inflationary paradigm.

Chapter 2

Modified gravity

The Big Bang puzzles outlined in Sec. 1.2 – and the role of inflation as a viable solution – emphasize how the standard cosmological model based on GR and the Standard Model (SM) of particle physics is inadequate to describe the Universe at extreme regimes. At the same time, GR is formulated as a classical theory that breaks down when a full quantum description of spacetime and gravity is sought. These challenges have long motivated extensions of Einstein's theory, with attempts to go beyond GR and incorporate it in a unified theory beginning shortly after its original formulation. Notable examples are: Eddington's theory of connections [64], Weyl's scale-independent theory [65], and the higher-dimensional theories of Kaluza and Klein [66, 67]. In recent decades, and particularly following the discovery in 1998 of the late-time accelerated expansion of the Universe, modified theories of gravity have gained renewed attention as viable extensions of the gravitational sector.

2.1 Motivations

In the broad context of modifications of GR, we refer to *modified gravity* as any theory in which the Einstein equations

$$G_{\mu\nu} = \frac{1}{M_{pl}^2} T_{\mu\nu}, \tag{2.1}$$

are modified on the geometric sector on the left-hand side, including, e.g., adding higher-order invariants of the curvature tensor such as $R^2, R_{\mu\nu}R^{\mu\nu}, R_{\mu\nu\alpha\beta}R^{\mu\nu\alpha\beta}$, or non-minimally coupled terms between matter fields and geometry. Such deviations from GR are expected to become significant at cosmological scales (large scales) or in the strong-field regime (small scales). GR has been extensively tested at intermediate scales and in the weak-field regime, such as within the Solar System, where it remains the paradigm theory of gravity. In the following, we outline the primary motivations behind the modified gravity approach.

2.1.1 Astrophysical and cosmological challenges

From the observational data of Supernova Type Ia (SN Ia) accumulated by the year 1998, two independent works [68, 69] reported the evidence that the present Universe is undergoing acceleration. Since then, a wealth of observations point towards the existence of some form of *dark energy*, which makes up roughly the 70% of the present Universe and behaves as a fluid with negative pressure. The Pantheon+ analysis of SN Ia data, combined with *Planck* CMB and BAO measurements, constrains the present-day dark energy equation of state parameter as [70]

$$w_0 = -0.978^{+0.024}_{-0.031}, \tag{2.2}$$

suggesting that the simplest candidate for dark energy is the cosmological constant Λ ($w_\Lambda = -1$), whose energy density remains constant, ultimately dominating the total energy content of the Universe. Initially introduced by Einstein in 1917 to obtain a static universe in the framework of GR [71], the cosmological constant was temporarily abandoned after the discovery of the Universe's expansion by Hubble and restored after 1998 as a fundamental part of the standard model of cosmology (ΛCDM). However, besides failing to explain why the inferred value of Λ is so tiny compared to the typical vacuum energy density predicted by particle physics – the famous cosmological constant problem already mentioned in Sec. 1.6 –, the ΛCDM model leaves us with another controversy: the *coincidence problem*. If dark energy is in the form of Λ, then we happen to live in a very special moment, since Λ has started dominating the Universe's energy content extremely close to the present day on cosmological scales. This is best represented as a spike in the variation of Ω_Λ, located close to a_0, as represented in Figure 2.1.

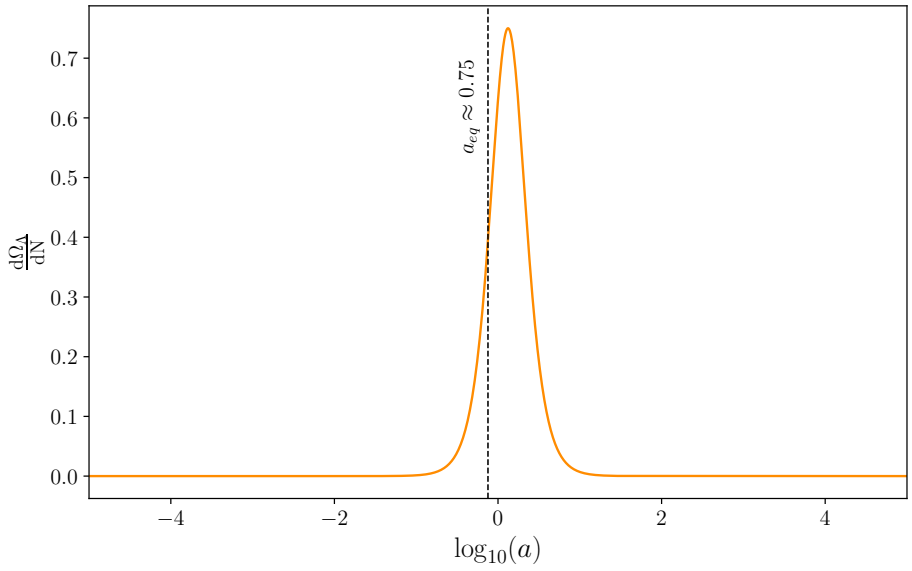

Figure 2.1: Graphical representation of the coincidence problem. The derivative of Ω_Λ with respect to e-folding time N peaks very close to the present epoch ($\log_{10}(a_0) = 0$). We have fixed the present-day density parameter to $\Omega_\Lambda = 0.7, \Omega_m = 0.3$. In this framework, the matter-dark energy equality occurs at $a_{eq} \approx 0.75$.

These shortcomings of the ΛCDM model are clear indications that we are still missing something and motivate us to seek alternative models to explain the Universe's acceleration. A first approach is to modify the Einstein equations through modifications in the matter sector, introducing specific forms of the energy-momentum tensor $T_{\mu\nu}$ with negative pressure. This is the case for the so-called cosmon or quintessence, k-essence, and perfect fluid models. See, e.g., [72] for a comprehensive review. A second approach is to modify the gravity sector, hence the name "modified gravity". It should be pointed out that the two approaches are not fundamentally different, as long as we neglect their quantum field implications, since, in the spirit of GR, one can always cast the matter sector into the gravity sector by defining a suitable energy-momentum tensor that equals the Einstein tensor.

On the observational side, it is worth mentioning that the most recent DESI BAO data from the second year of observations, combined with CMB data from *Planck* and SN Ia data, provide moderate to strong evidence for a time-evolving dark energy component [73, 74]. Even though these findings warrant additional tests to carefully assess potential systematics before drawing definitive conclusions (see, e.g., [11] for a critical review), it seems that the role of the cosmological constant is further weakened by the most recent measurements.

Modified gravity theories have attracted significant interest in cosmology because they naturally provide a mechanism to drive inflation. According to Lovelock's theorem, the Einstein-Hilbert (EH)

action gives the only second-order metric field equations in 4D. Any modification of GR, involving, e.g., higher-order or non-minimally coupled terms, introduces higher-derivative contributions. It was shown [75, 76] that by means of conformal transformations these terms always correspond to one or more scalar field(s) minimally coupled to the curvature. A scalar condensate, the simplest ingredient to drive inflation, as shown in Sec. 1.3.1, can thus be entirely imitated within gravity, with no need to invoke exotic matter components. This outcome further motivates modified gravity, especially in the context of inflation, and will be discussed in detail in the following.

2.1.2 Fundamental issues of GR

The need for a quantum theory of gravity was recognized in the late 50s, when physicists began seeking a unified way to describe all interactions at a fundamental level using quantum field theory. The primary difficulty with GR lies in its structure: the gravitational field both defines the gravitational degrees of freedom and the background metric in which they evolve.

With a prospect of including quantum effects in the gravitational sector, it is assumed that the spacetime geometry directly interacts with the quantum matter fields, which backreact on it. This interaction unavoidably introduces corrections to the standard EH action, laying the first fundamental motivation for modified gravity [77].

To give a glance at the explicit calculation, we report the Lorentzian one-loop effective action for a scalar field in a curved background. We follow the derivation presented in [78]. We consider a minimally coupled scalar field, namely a scalar field with no explicit coupling to the curvature scalar or other curvature invariants, and set its potential term to zero, $V(\phi) = 0$, such that the field is massless. Adopting the heat kernel method [79, 80], one finds

$$\Gamma_{\rm L}[g_{\mu\nu}] = \int \frac{\mathrm{d}^4x\sqrt{-g}}{32\pi^2}\left[-A(\tau_0) + \frac{B(\tau_0)}{6}R - C(\tau_0)\left(\frac{R^2}{120} + \frac{R_{\mu\nu}R^{\mu\nu}}{60}\right) + (\text{finite terms})\right], \tag{2.3}$$

where τ_0 is the proper time cutoff parameter. The functions $A(\tau_0), B(\tau_0)$, and $C(\tau_0)$ all diverge for $\tau_0 \to 0$.[1]

The total gravitational action is given by the sum of the free gravitational action – the usual EH action – and the effective action (2.3) induced by quantum fields. Since the cosmological constant term Λ and the curvature term R in the EH action are similar to the first two divergent terms in (2.3), the renormalization procedure is implemented as follows. We *assume* that the free gravitational action also contains the terms quadratic in the curvature,[2]

$$S^{\rm grav}_{\rm bare}[g_{\mu\nu}] = \int \mathrm{d}^4x\sqrt{-g}\left[\frac{R - 2\Lambda_B}{16\pi G_B} + \alpha_B\left(\frac{R^2}{120} + \frac{R_{\mu\nu}R^{\mu\nu}}{60}\right)\right], \tag{2.4}$$

where G_B, Λ_B, α_B are the *bare coupling constants*.

The modified action for gravity is thus the sum of the free action (2.4) and the effective action (2.3),

$$\begin{aligned} S^{\rm grav}[g_{\mu\nu}] = \int \mathrm{d}^4x\sqrt{-g}\Bigg[&\left(\frac{1}{16\pi G_B} + \frac{B(\tau_0)}{192\pi^2}\right)R - \left(\frac{\Lambda_B}{8\pi G_B} + \frac{A(\tau_0)}{32\pi^2}\right) + \\ &+ \left(\alpha_B - \frac{C(\tau_0)}{32\pi^2}\right)\left(\frac{R^2}{120} + \frac{R_{\mu\nu}R^{\mu\nu}}{60}\right) + (\text{finite terms})\Bigg]. \end{aligned} \tag{2.5}$$

[1] Since small proper times correspond to small distances $(x-y) \sim \tau^{1/2}$ or equivalently to large momenta $k \sim \tau^{-1/2}$, these divergences are referred to as *ultraviolet (UV) divergences*.

[2] We are recovering the factor $16\pi G$ to clarify the role of the coupling constant.

The renormalization procedure consists of assuming that the bare constants are functions of τ_0 such that they cancel the divergences of $A(\tau_0), B(\tau_0)$, and $C(\tau_0)$ when $\tau_0 \to 0$. We can therefore identify

$$\begin{aligned} \frac{\Lambda}{8\pi G} &= \frac{\Lambda_B}{8\pi G_B} + \frac{A(\tau_0)}{32\pi^2}, \\ \frac{1}{16\pi G} &= \frac{1}{16\pi G_B} + \frac{B(\tau_0)}{192\pi^2}, \\ \alpha &= \alpha_B - \frac{C(\tau_0)}{32\pi^2}. \end{aligned} \tag{2.6}$$

The renormalized constants Λ, G, and α are equal to the observed values of the cosmological constant, Newton's constant, and the constant α. The EH action is recovered only for $\alpha = 0$. However, in general (i.e., without fine-tuning), the gravitational action also contains the two quadratic terms $\propto R^2, R_{\mu\nu}R^{\mu\nu}$ that are necessary to renormalize the backreaction of matter fields on gravity.

It was Stelle who, in 1977, first demonstrated [81] that introducing the above quadratic terms in the EH action makes the theory renormalizable. The physical implication of such additional terms is that they introduce new degrees of freedom in addition to the familiar massless spin-2 gravitons, associated with additional poles in the propagator. These include massive spin-2 and spin-0 particles. However, the massive spin-2 excitations are *ghost* particles, a common drawback of higher-derivative models, as we will show in Sec. 2.2. Ghost particles are associated with negative kinetic energy, leading to instabilities, since the energy of the system is unbounded from below. In quantum theory, ghosts are negative-norm states that violate unitarity. For these reasons, a theory with ghosts should be discarded. It is worth mentioning, however, that given the great interest of quadratic gravity as a perturbatively renormalizable theory – at variance with GR –, there have been many attempts to deal with or avoid ghosts, see, e.g., [82–84].

It is then manifest that the EH action gets modified by higher-order terms as soon as we move to a quantum gravity regime. In the absence of a satisfactory theory of quantum gravity, one can regard the extra terms from an effective field theory perspective. If the curvature is small compared to the Planck scale ($R/M_{pl}^2 \ll 1$), the extra terms are subdominant and the linear one of the standard EH action is recovered. Then GR is recovered and holds as a good approximation in the regime in which it has been tested so far. Conversely, if the curvature approaches the Planck scale ($R/M_{pl}^2 \sim 1$), the quadratic terms become important [78]. For this reason, it makes perfect sense to take their impact on cosmology seriously. This was the leading motivation for Starobinsky's model, to be discussed in Sec. 2.3.4.

Quadratic models are also an active field of research in the context of static solutions, i.e., black holes [85–90].

2.2 Caveats

There exist many possible ways to modify GR, and indeed a plethora of alternative or extended theories of gravity have been proposed over the years. These include, e.g., additional scalar, vector, or tensor degrees of freedom, higher order curvature theories, nonlocal theories, and extra-dimensional theories. See [91] for a schematic representation of the landscape of modified gravity theories. However, in practice, one must carefully consider several caveats when dealing with such modifications.

In this section, we outline some of the mathematical conditions that modified gravity models should satisfy to be viable for cosmology, i.e., the ones regarding mathematical instabilities.

2.2.1 Ostrogradsky instabilities

Back to 1850, Ostrogradsky proved that higher-than-second order equations of motion are unstable [92]. In this sense, Newton was right to assume that the laws of physics take the form of second-order

differential equations when expressed in terms of fundamental dynamical variables [93].

To outline Ostrogradsky's theorem, let's consider for simplicity the case of a Lagrangian depending on second-order time derivatives of the fields, $\mathcal{L} = \mathcal{L}(t, \phi^I, \dot{\phi}^I, \ddot{\phi}^I)$. The generalization to N-times derivatives can be found, e.g., in [93, 94]. Ostrogradsky's theorem applies to any *non-degenerate* Lagrangian, that is, to Lagrangians whose Hessian has non-vanishing determinant. In the second-order case, the Lagrangian is non-degenerate if

$$\det\left(\frac{\partial^2 \mathcal{L}}{\partial \ddot{\phi}^I \partial \ddot{\phi}^J}\right) \neq 0. \tag{2.7}$$

Degeneracy is associated with the fact that some of the highest-order derivatives can be eliminated, for instance, after integration by parts or by redefining the fields appropriately [94].

By making use of Ostrogradsky's procedure, we define the canonical variables as

$$q_1^I \equiv \phi^I, \qquad q_2^I \equiv \dot{\phi}^I, \qquad \pi_{1,I} \equiv \frac{\partial \mathcal{L}}{\partial \dot{\phi}^I} - \frac{\mathrm{d}}{\mathrm{d}t}\frac{\partial \mathcal{L}}{\partial \ddot{\phi}^I}, \qquad \pi_{2,I} \equiv \frac{\partial \mathcal{L}}{\partial \ddot{\phi}^I}, \tag{2.8}$$

where $\pi_{i,I}$ are the conjugate momenta. It can be shown (see Appendix A for the full derivation) that the Hamiltonian reads

$$\mathcal{H} = \pi_{1,I} q_2^I + \mathcal{F}\left(t, q_1^I, q_2^I, \pi_{2,I}\right) \pi_{2,I} - \mathcal{L}\left(t, q_1^I, q_2^I, \mathcal{F}\left(t, q_1^I, q_2^I, \pi_{2,I}\right)\right). \tag{2.9}$$

Ostrogradsky's proof shows that the Hamiltonian $\mathcal{H}$ in Eq. (2.9) is manifestly linear in the momentum π_1, and it is therefore unbounded from below in the direction of the phase space given by π_1. As a consequence, any dynamical variable experiencing the Ostrogradsky instability will carry both positive and negative creation and annihilation operators. Since energy conservation holds just as it would in a lower-derivative theory, if the system is non-interacting, the instability will not manifest. If instead the system is interacting, there will be interactions between particles with positive and negative energy, and the vacuum state could decay into a collection of positive and negative excitations. If, in addition, we are dealing with an interacting and continuous field theory, the decay will be instantaneous: there will be just one possibility for the system to stay empty, but infinitely many possible ways for it to decay into arbitrarily large positive and negative energy states, making this condition entropically favored [95].

The main assumption beneath Ostrogradsky's theorem is the non-degeneracy of the Lagrangian. To avoid the instability, one can thus break this assumption and construct a degenerate theory. Some examples, see [94, 95], include:

- Write a second-order Lagrangian as a first-order one plus a total time derivative. After integration by parts and neglecting the surface term, one can obtain a Lagrangian that contains only first-order time derivatives. Degeneracy is trivially realized. This is the case for Lovelock theories [96], which have the same spectrum as GR (a massless graviton).

- All theories featuring a continuous symmetry are degenerate. The symmetry-induced degeneracy is cured by fixing the gauge. However, this is not sufficient to avoid Ostrograsky instabilities, in general. To do so, the number of gauge constraints must be equal to or greater than the number of unstable directions in canonical phase space.

- A remarkable example of degenerate Lagrangians is $f(R)$ theories, which are equivalent to GR plus a propagating healthy scalar, as we will discuss in Sec. 2.3. Analogously, Lagrangians consisting of an arbitrary function of the Gauss-Bonnet invariant, known as $f(\mathcal{G})$ theories [97, 98], are free from instabilities.

It is important to stress that a system fulfilling Ostrogradsky's conditions can still develop instabilities, but this does not directly imply that all solutions of such a system are unstable. Examples of systems featuring bounded motions are: quadratic gravity expanded at linear order around the flat or de Sitter spacetime [99, 100] and the Pais-Uhlenbeck model [101, 102].

2.2.2 Tachyonic, gradient, and ghost instabilities

Ostrogradsky instabilities arise at the background level. In this section, we instead outline the types of instabilities arising with perturbations. Let's consider, for simplicity, linear perturbations of a scalar field propagating in an isotropic background. The associated quadratic action reads[3]

$$S^{(2)}_{\delta\phi} = \frac{1}{2}\int \mathrm{d}^4x \left(a\,\dot{\delta\phi}^2 - b(\partial_i\delta\phi)^2 - \mu^2\delta\phi^2\right), \tag{2.10}$$

where the coefficients a, b, and μ^2 carry information about the background. In general, such coefficients depend on spacetime coordinates, but they vary on the time/length scales T, L characteristic of the background on which the perturbation $\delta\phi$ evolves. Since we are interested in describing the dynamics of the perturbations on much smaller time/length scales, we will assume a, b, and μ^2 to be constant at leading order. Moving to the Fourier domain, the field equations are[4]

$$a\,\ddot{\delta\phi}_k + \left(bk^2 + \mu^2\right)\delta\phi_k \simeq 0, \tag{2.11}$$

where $\simeq$ clarifies that the terms on the right-hand side are suppressed as $\mathcal{O}(T^{-1}, L^{-1})$. The solution to Eq. (2.11) is

$$\delta\phi_k \simeq A_k e^{-i\left(\sqrt{\frac{b}{a}}\,\mathbf{k}\cdot\mathbf{x}-\omega t\right)} + A_k^* e^{i\left(\sqrt{\frac{b}{a}}\,\mathbf{k}\cdot\mathbf{x}-\omega t\right)}, \qquad \text{where} \qquad \omega = \sqrt{\frac{b}{a}k^2 + \frac{\mu^2}{a}}, \tag{2.12}$$

and $|A_k|$ are set by appropriate initial conditions and must be small to keep the validity of linear perturbation theory. According to the relative sign of the background-dependent coefficients, the perturbation can be stable or grow unboundedly. In the latter case, the perturbation will backreact on the background, and its evolution will no longer be decoupled from the background typical scales T and L. In this case, we say that the background is unstable for perturbations $\delta\phi$.

In the following, we summarize the different cases and their physical interpretation [94, 103].

Stable case: $a > 0$, $b > 0$, $\mu^2 \geq 0$

The field equations reduce to the usual wave equations, thus $\delta\phi_k$ have oscillatory behavior and are therefore bounded at all times and throughout space. The frequency ω is real, and the energy density is always positive. For $b < a$ the ϕ-perturbations propagate at subluminal speed, for $b = a$ at the speed of light, and for $b > a$ at superluminal speed, so that we may require $a > b > 0$.

[3] The derivation follows in complete analogy to the one performed in Sec. 1.4. From the definition of comoving curvature perturbations in Eq. (1.37) and using the single-field result $\delta q = -\dot{\phi}\delta\phi$, the Mukhanov variable introduced in Eq. (1.53) reduces to $v = a\,\psi(\dot{\phi}/H) + a\,\delta\phi$, hence $v = a\,\delta\phi$ in a unperturbed background. The resulting action then follows from Eq. (1.54)

[4] See, for analogy, the Mukhanov equation (1.56).

Tachyonic instability: $a > 0$, $b > 0$, $\mu^2 \leq 0$

The frequency ω becomes imaginary for modes with sufficiently low momenta, i.e., $k < k_{\rm low} = \sqrt{|\mu^2|/b}$, thus we also speak about infrared (IR) instability. In such cases, the solutions in Eq. (2.12) become

$$\delta\phi_k^{\rm IR} \simeq A_k e^{-i\sqrt{\frac{b}{a}}\,\mathbf{k}\cdot\mathbf{x}} e^{-|\omega|t} + A_k^* e^{i\sqrt{\frac{b}{a}}\,\mathbf{k}\cdot\mathbf{x}} e^{|\omega|t}, \tag{2.13}$$

displaying an exponential growth. These are called tachyonic modes. This is indeed a problem if the time scale at which the tachyonic instability kicks in, $t_c = |\omega|^{-1}$, is much shorter than the time scale characteristic of the background, T. In the opposite case, $t_c \gg T$, the exponential growth of the IR modes shows up only when the background has evolved significantly, but in this regime the approximation of slowly varying $a(t), b(t)$, and $\mu^2(t)$ no longer holds. In this case, to assess the system's stability properties, one must conduct a full background dynamical analysis.

Gradient/Laplacian instability: $(a > 0, b < 0) \vee (a < 0, b > 0)$

The frequency ω becomes imaginary for the UV modes, which display an exponential growth. Unlike tachyonic instabilities, gradient/Laplacian instabilities grow arbitrarily fast; the background is always unstable.

Ghost instability: $a < 0, b < 0$

In this case, UV modes are always stable, and IR modes develop a tachyonic instability if $\mu^2 > 0$. However, independently of the sign of μ^2, the Hamiltonian of the system is unbounded from below in the direction of increasing momenta: if the theory is interacting, then it will display a ghost instability as Ostrogradsky's ones. In a classical interacting theory, the field could decay to arbitrarily low (negative) energy states by exciting other fields to high (positive) energy states. In a quantum interacting theory, the state $|0\rangle$ identified with the vacuum state of the theory is unstable, since the process $|0\rangle \to \delta\phi\delta\phi + A\bar{A}$ – with A any particle the field ϕ is interacting with – is always allowed by energy conservation for arbitrarily high momenta of the outgoing particles up to the UV scale below which we can trust the theory.

2.3 *f(R)* theories

One of the simplest generalizations of GR are $f(R)$ gravity theories, where the EH Lagrangian density, $f_{\rm EH} = R - 2\Lambda$ is replaced with a generic function $f(R)$ of the Ricci scalar,

$$S_J = \frac{M_{pl}^2}{2}\int \mathrm{d}^4x\sqrt{-g}f(R) + \int \mathrm{d}^4x\mathcal{L}_M(g_{\mu\nu}, \Psi_M), \tag{2.14}$$

where $\mathcal{L}_M$ is a matter Lagrangian that depends on $g_{\mu\nu}$ and matter fields Ψ_M. Subscript J refers to the Jordan frame (JF), as opposed to the Einstein frame (EF) that will be introduced later.

Despite its apparent simplicity, $f(R)$ gravity exhibits a rich phenomenology. In particular, it is free from Ostrogradsky instabilities and can account for both early- and late-time cosmic acceleration. Since our focus is on the inflationary epoch, we do not discuss the implications of $f(R)$ theories for dark energy in this section; for a comprehensive review, see [72]. The analysis presented here is primarily based on [72, 104, 105].

It is known [106, 12] that there are two variational principles to derive Einstein's equations from the EH action: in the *metric formalism* the field equations are derived by varying the action with respect to the metric tensor $g_{\mu\nu}$, while in the *Palatini formalism* the metric tensor and the connection are treated as independent variables and one varies the action with respect to both of them. Even

though the two approaches lead to the same field equations for Lagrangians that are linear in R, this is no longer true for nonlinear Lagrangians. Therefore, in the context of $f(R)$ gravity, we will consider two distinct versions according to the adopted variational principle.

Metric formalism

The field equations can be derived by varying the action (2.14) with respect to $g_{\mu\nu}$,

$$F(R)R_{\mu\nu} - \frac{1}{2}f(R)g_{\mu\nu} - \nabla_\mu\nabla_\nu F(R) + g_{\mu\nu}\Box F(R) = M_{pl}^{-2}T^M_{\mu\nu}, \tag{2.15}$$

where $F(R) \equiv \partial f/\partial R$ and $\Box F = (1/\sqrt{-g})\partial_\mu(\sqrt{-g}g^{\mu\nu}\partial_\nu F)$. $T^M_{\mu\nu}$ is the energy-momentum tensor defined from the matter Lagrangian

$$T^M_{\mu\nu} \equiv -\frac{2}{\sqrt{-g}}\frac{\delta\mathcal{L}_M}{\delta g^{\mu\nu}}, \tag{2.16}$$

which satisfies the continuity equations, $\nabla^\mu T^M_{\mu\nu} = 0$. The trace of Eq. (2.15) is

$$3\Box F(R) + F(R)R - 2f(R) = M_{pl}^{-2}T^M, \tag{2.17}$$

where $T^M \equiv g^{\mu\nu}T^M_{\mu\nu}$. The field equations (2.15) are fourth-order partial differential equations in the metric, since R already includes second derivatives of $g_{\mu\nu}$. If $f(R)$ is linear in R, the last two terms on the right-hand side vanish, and the equations reduce to the second-order ones of GR.

Palatini formalism

The action is formally the same as in the metric formalism, but now the Riemann tensor and the Ricci tensor are constructed with the connection $\Gamma^\alpha_{\beta\gamma}$, which is independent of the metric. To further stress that these are not equivalent in general, we will adopt the notational convention of [105], denoting the Ricci tensor defined in terms of the connection as $\bar{R}_{\mu\nu}$ and the corresponding Ricci scalar as $\bar{R} \equiv g^{\mu\nu}\bar{R}_{\mu\nu}$. The action is thus the one in Eq. (2.14), with $f(\bar{R})$. We stress that in the Palatini formalism the matter Lagrangian $\mathcal{L}_M$ is assumed to depend on the metric and the matter fields, but not on the independent connection. This assumption is relaxed in metric-affine $f(R)$ gravity [107], where the Palatini variational principle is considered but taking the matter action as a function of the connection, too: $\mathcal{L}_M = \mathcal{L}_M(g_{\mu\nu}, \Gamma^\lambda_{\mu\nu}, \Psi_M)$. We will not treat metric-affine gravity here. Variation of the action with respect to the metric gives

$$F(\bar{R})\bar{R}_{\mu\nu} - \frac{1}{2}f(\bar{R})g_{\mu\nu} = M_{pl}^{-2}T^M_{\mu\nu}, \tag{2.18}$$

whose trace is

$$F(\bar{R})\bar{R} - 2f(\bar{R}) = M_{pl}^{-2}T^M. \tag{2.19}$$

Varying the action with respect to the connection and rearranging terms gives[5]

$$\bar{\nabla}_\lambda\left(\sqrt{-g}F(\bar{R})g^{\mu\nu}\right) = 0, \tag{2.20}$$

where we denote with an overline the covariant derivative defined with the independent connection $\Gamma^\alpha_{\beta\gamma}$.

[5]Using the result [13] $\delta\bar{R}_{\mu\nu} = \bar{\nabla}_\lambda\delta\Gamma^\lambda_{\mu\nu} - \bar{\nabla}_\nu\delta\Gamma^\lambda_{\mu\lambda}$, one obtains the equation $-\bar{\nabla}_\lambda(\sqrt{-g}F(\bar{R})g^{\mu\nu}) + \bar{\nabla}_\sigma(\sqrt{-g}F(\bar{R})g^{\sigma\mu})\delta^\nu_\lambda = 0$. The second term cancels out after taking the trace.

In GR, $F(\bar{R}) = 1$, and Eq. (2.20) becomes the definition of the Levi-Civita connection for the (initially independent) $\Gamma^{\lambda}_{\mu\nu}$. We can thus identify $\bar{R}_{\mu\nu} = R_{\mu\nu}$ and $\bar{R} = R$. The Einstein equations (2.15) and (2.18) coincide for GR. This is not the case when $f(R)$ is a nonlinear function of R: the term $\Box F(R)$ in the metric formalism does not vanish, indicating that there is a propagating scalar degree of freedom $\varphi \equiv F(R)$, called *scalaron*. Its dynamics are governed by the trace equation (2.17). In the Palatini formalism, on the other hand, this scalar field is not propagating: from the trace equation (2.19) we can see that $\bar{R}$ – hence $F(\bar{R})$ – is algebraically related to the matter fields and therefore carries no dynamical content on its own.

The propagating scalar degree of freedom makes metric $f(R)$ theories particularly appealing for inflation. As will be clearer in the following, these theories can support a phase of accelerated expansion driven by the scalaron field, thereby realizing inflation entirely within the gravity sector, rather than introducing a scalar field by hand. For this reason, from now on, we will consider $f(R)$ theories in the metric formalism only.

Before describing the dynamical evolution of such theories, let's consider their maximally symmetric solutions. Imposing $R = \text{const.}$ and $T_{\mu\nu} = 0$, the trace equations (2.17) and (2.19) reduce to

$$F(R)R - 2f(R) = 0. \tag{2.21}$$

We have two classes of maximally symmetric spacetimes

- If $R = 0$ is a root of Eq. (2.21), taking this root the Einstein equations (2.15) reduce to $R_{\mu\nu} = 0$, corresponding to *Minkowski spacetime*;
- If the root of Eq. (2.21) is $R = C$, with C a generic constant, the Einstein equations (2.15) reduce to $R_{\mu\nu} = g_{\mu\nu}C/4$, corresponding to *de Sitter* or *anti-de Sitter* according to the sign of C.

The model $f(R) = \alpha R^2$ satisfies the condition (2.21), so it possesses an exact de Sitter solution [1].

Taking the (0,0) and (i,i) components of the Einstein equations (2.15) in a spatially flat FLRW background, one gets the Friedmann equations of $f(R)$ gravity

$$\begin{aligned} 3FH^2 &= (FR - f)/2 - 3H\dot{F} + M_{pl}^{-2}\rho_M, \\ -2F\dot{H} &= \ddot{F} - H\dot{F} + M_{pl}^{-2}\left(\rho_M + p_M\right), \end{aligned} \tag{2.22}$$

where the energy-momentum tensor for matter fields has been taken as that of a perfect fluid $T^{\mu}_{\nu} = \text{diag}\left(-\rho_M, p_M, p_M, p_M\right)$.

2.3.1 Equivalence to Brans-Dicke theories

By introducing an auxiliary field χ, the action (2.14) can be written as

$$S_{\text{BD}} = \frac{M_{pl}^2}{2}\int \mathrm{d}^4x\sqrt{-g}\left[f(\chi) + f'(\chi)(R-\chi)\right] + \int \mathrm{d}^4x\mathcal{L}_M(g_{\mu\nu}, \Psi_M). \tag{2.23}$$

Variation with respect to χ gives

$$f''(\chi)\left(R - \chi\right) = 0, \tag{2.24}$$

which implies that $R = \chi$ if $f''(\chi) \neq 0$, proving that Eq. (2.23) is the on-shell equivalent of the original action. Redefining the auxiliary field χ by $\varphi = f'(\chi)$ and introducing the potential

$$U(\varphi) \equiv \frac{M_{pl}^2}{2}\left[\chi(\varphi)\varphi - f(\chi(\varphi))\right], \tag{2.25}$$

Eq. (2.23) reduces to

$$S_{\text{BD}} = \int \mathrm{d}^4x\sqrt{-g}\left[\frac{M_{pl}^2}{2}\varphi R - U(\varphi)\right] + \int \mathrm{d}^4x\mathcal{L}_M(g_{\mu\nu}, \Psi_M). \tag{2.26}$$

This is the Jordan-frame (JF) action of a Brans-Dicke theory with parameter $\omega_{\rm BD} = 0$ [108, 109]. Note that when f'' is not defined, or it vanishes, the equivalence between the two theories is not guaranteed. The scalar degree of freedom ϕ should not be interpreted as a matter field. For example, like all non-minimally coupled scalars, it can violate all of the energy conditions [110].

2.3.2 Conformal transformation: Einstein frame

To fully exploit the analogy of $f(R)$ theories with GR with a propagating scalar degree of freedom, we perform a conformal transformation, which is essentially a *local* change of scale. Distances are measured by the metric, thus conformal transformations are implemented by multiplying the metric tensor by a non-vanishing function of spacetime coordinates $x \equiv \{x^\mu\}$

$$\tilde{g}_{\mu\nu} = \Omega^2(x) g_{\mu\nu}. \tag{2.27}$$

Under a conformal transformation, the Ricci scalar transforms as [104, 12]

$$R = \Omega^2 \left(\tilde{R} + 6\tilde{\Box}\omega - 6\tilde{g}^{\mu\nu}\partial_\mu\omega\partial_\nu\omega \right), \tag{2.28}$$

where

$$\omega \equiv \ln\Omega, \qquad \partial_\mu\omega \equiv \frac{\partial\omega}{\partial\tilde{x}^\mu}, \qquad \tilde{\Box}\omega \equiv \frac{1}{\sqrt{-\tilde{g}}}\partial_\mu\left(\sqrt{-\tilde{g}}\,\tilde{g}^{\mu\nu}\partial_\nu\omega\right). \tag{2.29}$$

By writing the JF action as done in Eq. (2.26), evaluating it on shell, and using the result (2.28), we obtain the transformed action

$$S = \int \mathrm{d}^4x\sqrt{-\tilde{g}}\left[\frac{M_{pl}^2}{2}F\Omega^{-2}\left(\tilde{R} + 6\tilde{\Box}\omega - 6\tilde{g}^{\mu\nu}\partial_\mu\omega\partial_\nu\omega\right) - \Omega^{-4}U\right] + \int \mathrm{d}^4x\mathcal{L}_M\left(\Omega^{-2}\tilde{g}_{\mu\nu}, \Psi_M\right). \tag{2.30}$$

The Einstein-frame (EF) action is by definition linear in $\tilde{R}$. This is recovered for $\Omega^2 = F$, which sets the conformal transformation and requires $F > 0$ for consistency. The term proportional to $\tilde{\Box}\omega$ in Eq. (2.30) vanishes on account of Gauss theorem using Eq. (2.29). After introducing a scalar field ϕ defined as

$$\phi \equiv M_{pl}\sqrt{\frac{3}{2}}\ln F, \tag{2.31}$$

we find that the action (2.30) can be arranged as

$$S_E = \int \mathrm{d}^4x\sqrt{-\tilde{g}}\left[\frac{M_{pl}^2}{2}\tilde{R} - \frac{1}{2}\tilde{g}^{\mu\nu}\partial_\mu\phi\partial_\nu\phi - V(\phi)\right] + \int \mathrm{d}^4x\mathcal{L}_M\left(F^{-1}(\phi)\tilde{g}_{\mu\nu}, \Psi_M\right), \tag{2.32}$$

where

$$V(\phi) \equiv \frac{U}{F^2} = \frac{M_{pl}^2}{2}\left(\frac{FR - f}{F^2}\right). \tag{2.33}$$

It is thus manifest that $f(R)$ theories are conformally equivalent to GR with a minimally coupled scalar field ϕ.

After neglecting the matter term for simplicity, the equations of motion in a spatially flat FLRW background take the familiar form

$$\begin{aligned} 3\tilde{H}^2M_{pl}^2 &= \frac{1}{2}\left(\frac{\mathrm{d}\phi}{\mathrm{d}\tilde{t}}\right)^2 + V(\phi), \\ \frac{\mathrm{d}^2\phi}{\mathrm{d}\tilde{t}^2} &+ 3\tilde{H}\frac{\mathrm{d}\phi}{\mathrm{d}\tilde{t}} + V_{,\phi} = 0, \end{aligned} \tag{2.34}$$

where we stress that, at variance with Eqs. (1.16) and (1.17), time derivatives are performed with respect to the time in the EF, $\mathrm{d}\tilde{t} = \sqrt{F}\,\mathrm{d}t$, which is consistent with the above requirement $F > 0$.

Analogously, the scale factor is transformed as $\tilde{a} = \sqrt{F}\, a$. Note that the Hubble parameter is different in the EF, namely

$$\tilde{H} = \frac{1}{\sqrt{F}} \left(H + \frac{\dot{F}}{2F} \right). \tag{2.35}$$

Some important considerations are in order:

- As anticipated in Sec. 2.2, $f(R)$ theories do not display Ostrogradsky instabilities. This is manifest in the EF: the original fourth-order equations for $g_{\mu\nu}$ are reduced to second-order equations for $\tilde{g}_{\mu\nu}$ (and the scalar field ϕ).
- Concerning the stability of perturbations, since $f(R)$ gravity is formally equivalent to a scalar-tensor theory, it corresponds to a scalar degree of freedom propagating at the speed of light. Vector and tensor modes are unaffected by $f(R)$ corrections. One can show that $F > 0$ is required to avoid ghosts, and $f_{,RR} > 0$ to avoid tachyonic instabilities.
- In the EF, matter is now coupled to the rescaled metric $e^{-\sqrt{2/3}\phi/M_{pl}}\tilde{g}_{\mu\nu}$. As a consequence, the scalar field mediates a fifth force $\sim e^{-m_\phi r}$, where m_ϕ is the effective mass of ϕ[6] and sets the range of the force $\lambda = m_\phi^{-1}$. If m_ϕ is small, then the force is long-ranged and can affect local gravity constraints on Solar System scales. However, in such high-density regimes, screening mechanisms such as the chameleon mechanism [111, 112] can become important and suppress fifth-force effects. Some $f(R)$ theories might pass the weak-field limit tests and, at the same time, constitute an alternative to dark energy only if the chameleon mechanism is effective. This condition restricts the possible forms of the function $f(R)$.
- We should also require that a $f(R)$ theory approaches GR asymptotically: in cosmology, $f(R) \to R - 2\Lambda$ for $R \gg R_0$, where R_0 is the Ricci scalar at the present epoch.

At this level, the JF and the EF can be considered just as (two of the potentially infinite [113]) different representations of the same gravity theory. As long as they are handled carefully, field redefinitions and different representations are perfectly legitimate and can be useful tools for studying gravitational theories. The issue of discriminating between truly different theories and different representations (or dynamical equivalence) of the same theory is, however, complicated. In particular, the physical equivalence between JF and EF is still a subject of intense debate and misconceptions. We will elaborate more on this controversy in the following.

2.3.3 Jordan and Einstein frame

The conformal transformation (2.27) establishes a *mathematical equivalence* between the JF and the EF, i.e., the space of solutions in the JF is isomorphic to the one in the EF, which is typically mathematically convenient to study. The mathematical equivalence between the two frames, however, does imply nothing a priori on their *physical equivalence* [114–116]. In general, the reformulation of a theory in a new conformal frame leads to a different, physically nonequivalent theory. Instead of proposing the long-standing question of what frame is the physical one – and what we really mean by "physical" frame –, we will outline some important facts that must be accounted for when performing calculations and deriving physical conclusions in either one of the two frames.

- The JF covariant conservation equations $\nabla_\mu T^{\mu\nu} = 0$ is mapped into the EF equation

$$\tilde{\nabla}_\mu \tilde{T}^{\mu\nu} = -\tilde{T}\, \frac{\tilde{g}^{\mu\nu}\tilde{\nabla}_\mu \Omega}{\Omega}, \qquad \text{where} \qquad \tilde{T}^M_{\mu\nu} \equiv -\frac{2}{\sqrt{-\tilde{g}}} \frac{\delta \mathcal{L}_M}{\delta \tilde{g}^{\mu\nu}}, \tag{2.36}$$

[6] The effective mass of a scalar field is defined as the second derivative of the effective potential at the minimum.

which shows that the energy-momentum tensor of matter is not covariantly conserved in the EF, unless it describes conformally-invariant matter (radiation) with $\tilde{T} = 0$.

- Consider a dust fluid with $\tilde{T}_{\mu\nu} = \rho\, \tilde{u}_\mu \tilde{u}_\nu$. By projecting Eq. (2.36) into the 3-sphere orthogonal to $\tilde{u}^\mu$ with the operator $\tilde{h}^\mu_\nu$ defined as $\tilde{g}_{\mu\nu} = -\tilde{u}_\mu \tilde{u}_\nu + \tilde{h}_{\mu\nu}$ and satisfying $\tilde{h}^\mu_\nu \tilde{u}^\nu = 0$, we obtain

$$\tilde{a}^\gamma \equiv \tilde{h}^\gamma_\beta \tilde{u}^\alpha \tilde{\nabla}_\alpha \tilde{u}^\beta = \tilde{h}^{\gamma\alpha} \frac{\partial_\alpha \Omega(\phi)}{\Omega(\phi)}. \tag{2.37}$$

  Note that the right-hand side would be zero for a standard geodesic equation: massive particles in the EF are always subject to a force,[7] so $\tilde{g}^{\mu\nu}$ is not the metric whose geodesics coincide with free fall trajectories.

- The interpretation of the fields as matter or purely gravitational fields can also be misleading. For example, the field φ in the Brans-Dicke representation of the JF is non-minimally coupled to gravity, suggesting that it should be interpreted as a gravitational field. However, the field ϕ in the EF is minimally coupled to gravity and has canonical kinetic energy, so it should be interpreted as a matter field. We can further stress this issue by reporting the conformal transformation of the Ricci tensor

$$\tilde{R}_{\mu\nu} = R_{\mu\nu} - 2\nabla_\mu \nabla_\nu \ln\Omega - g_{\mu\nu} g^{\rho\sigma} \nabla_\rho \nabla_\sigma \ln\Omega + 2\nabla_\mu \ln\Omega \nabla_\nu \ln\Omega - 2 g_{\mu\nu} g^{\rho\sigma} \nabla_\rho \ln\Omega \nabla_\sigma \ln\Omega. \tag{2.38}$$

  This shows that a JF vacuum solution ($R_{\mu\nu} = 0$) is in general mapped into a non-vacuum solution ($\tilde{R}_{\mu\nu} \neq 0$) in the EF. To keep track of the gravitational nature of Ω, it is useful to remind that units of time, length, and mass are not constant in the EF, namely $\tilde{t}_u = \Omega\, t_u$, $\tilde{l}_u = \Omega\, l_u$, and $\tilde{m}_u = \Omega^{-1}\, m_u$, where t_u, l_u, m_u are the constant units in the JF [117]. Instead of a system of units rigidly attached to the spacetime manifold, the EF can be viewed as containing a system of units that change with spacetime location. In this perspective, the symmetry group of classical physics is enlarged to include conformal transformations with the appropriate rescaling of units. In practice, suppose we want to measure the mass of the proton m_p: in any experiment, what we really measure is the ratio between the mass of the proton and some reference unit of mass m_u, which is insensitive to a conformal transformation, that is $\tilde{m}_p/\tilde{m}_u = m_p/m_u$. The outcome of the experiment will be the same in the JF and in the EF [118].

- The correspondence between the JF and EF does not, in general, preserve the space of solutions, as the conformal transformation can break down in regions where the conformal factor vanishes. For example, in [119], it was shown that in scale-invariant gravity theories with an R^2 term, Ricci-flat solutions are present in the JF but are not consistently mapped into the EF, where they are lost. Most likely, this is ultimately linked to the fact that flat solutions in quadratic gravity have zero (ADM-like) energy [120], which are not mapped to zero-energy solutions in the EF.

- In the context of inflation, it has been shown that the gauge-invariant curvature perturbation $\mathcal{R}$ is conformally invariant up to all orders in single-field inflation [121]. As a consequence, the scalar spectral index is so. The result was extended to multiple fields non-minimally coupled to gravity in [122], where it is shown that conformal invariance of the spectral indices n_s, n_T is valid in the slow-roll approximation. Therefore, under these approximations, one can equally well compute the observables related to cosmological perturbations in the JF or in the EF.

[7] The force is proportional to the gradient of ϕ under the assumption that $\Omega = \Omega(\phi)$. Note that, as a consequence of Eq. (2.37), there are no freely falling frames in the EF. This fact also clarifies that the formulation of the Einstein equivalence principle cannot be applied in the EF, which is conceptually different from saying that the Einstein equivalence principle is violated in the EF.

The above observations should be sufficient for our purposes to avoid misinterpretations between Jordan- and Einstein-frame quantities.

2.3.4 Starobinsky model

Initially motivated by one-loop contributions of quantized matter fields in the EH action, as anticipated in Sec. 1.6, Starobinsky model [1] is a remarkable example of $f(R)$ gravity which admits a quasi-de Sitter inflationary solution and stands in strong agreement with CMB observations.[8] In this section, we revise the model and its predictions for inflation. Starobinsky model corresponds to a particular case of the $f(R)$ action in Eq. (2.14) with

$$f(R) = R + \frac{R^2}{6M^2}, \tag{2.39}$$

where M is the only free parameter of the model, dimensionally a mass. In the absence of matter, the JF equations of motion can be derived from the first Friedmann equation (2.22) and the trace equation (2.17)

$$\ddot{H} - \frac{\dot{H}^2}{2H} + \frac{1}{2}M^2 H = -3H\dot{H}, \tag{2.40}$$

$$\ddot{R} + 3H\dot{R} + M^2 R = 0. \tag{2.41}$$

In the slow-roll regime, the first two terms in Eq. (2.40) can be neglected, and we find the solutions

$$\begin{aligned} H &\simeq H_i - (M^2/6)(t - t_i), \\ a &\simeq a_i \exp\left[H_i(t - t_i) - (M^2/12)(t - t_i)^2)\right], \\ R &\simeq 12H^2 - M^2, \end{aligned} \tag{2.42}$$

where we have used the relation $R = 12H^2 + 6\dot{H}$, and subscript i denotes quantities evaluated at the onset of inflation. This inflationary solution corresponds to a transient attractor of the system [124], entirely driven by the R^2 term. Inflation is therefore a natural consequence of R^2 gravity. Accelerated expansion stops at time $t = t_f$ when $\epsilon = 1$, i.e., $H_f \simeq M/\sqrt{6}$. Ultimately, the system settles to the stable, Minkowski, fixed point with $R = 0 = H$, at which the cosmological constant automatically vanishes.

Einstein frame

The action in the EF corresponds to (2.32) with a scalar field ϕ defined as

$$\phi \equiv M_{pl}\sqrt{\frac{3}{2}}\ln\left(1 + \frac{R}{3M^2}\right), \tag{2.43}$$

and potential

$$V(\phi) \equiv \frac{3M^2 M_{pl}^2}{4}\left(1 - e^{-\sqrt{2/3}\phi/M_{pl}}\right)^2, \tag{2.44}$$

[8] Recent data from ACT, when combined with *Planck*, BICEP/*Keck*, CMB lensing and BAO data, show a preference for a slightly higher value of n_s, 0.974 ± 0.003, and disfavor Starobinsky model at $\sim 2\sigma$ for the range $50 < N_k < 60$ [123, 49]. This discrepancy, however, should be understood as a breaking of the degeneracy between the baryon density Ω_b and n_s, which have opposite correlations in the separate *Planck* and ACT datasets, and should be interpreted with caution.

see Figure 2.2. Inflation occurs in the large-field limit, $\phi/M_{pl} \gg 1$, where the potential displays a flat plateau, and proceeds as ϕ moves from right to left, down to the minimum. Considering the EF field equations (2.34) in the slow-roll approximation, namely $\dot{\phi}^2 \ll V(\phi)$ and $|\ddot{\phi}| \ll |H\dot{\phi}|$[9], the slow-roll parameters as defined in Eqs. (1.20)-(1.21) can be approximated as

$$\begin{aligned} \epsilon \simeq \epsilon_{\rm v} &= \frac{M_{pl}^2}{2}\left(\frac{V_{,\phi}}{V}\right)^2 = \frac{4}{3}\left(e^{\sqrt{2/3}\phi/M_{pl}} - 1\right)^{-2}, \\ \eta \simeq \eta_{\rm v} - \epsilon_{\rm v} &= -\epsilon + M_{pl}^2\frac{V_{,\phi\phi}}{V} = \frac{4}{3}\left(1 - e^{\sqrt{2/3}\phi/M_{pl}}\right)^{-1}, \end{aligned} \tag{2.45}$$

where we used the potential slow-roll parameters introduced in Eq. (1.22), restoring M_{pl}.

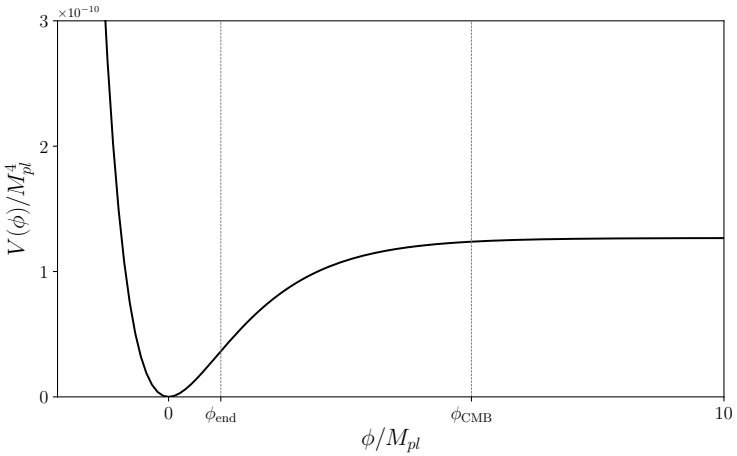

Figure 2.2: Scalar-field potential for Starobinsky model in the EF as defined in Eq. (2.44). The mass scale has been fixed from Eq. (2.50) to $M \simeq 1.5 \times 10^{-5}\, M_{pl}$, fixing A_s to the *Planck* 2018 best fit value, see Table 1.1, and choosing $N_k = 55$.

We introduce the e-folding number in the EF[10]

$$N = \int_{t_i}^{t_f} H{\rm d}t \simeq -\frac{1}{M_{pl}^2}\int_{\phi_i}^{\phi_f}\frac{V}{V_{,\phi}}{\rm d}\phi = -\frac{1}{M_{pl}}\int_{\phi_i}^{\phi_f}\frac{{\rm d}\phi}{\sqrt{2\epsilon}} \simeq \frac{3}{4}e^{\sqrt{2/3}\phi_i/M_{pl}}, \tag{2.46}$$

where the last equality holds in the large-field limit $\phi/M_{pl} \gg 1$. In this regime, the slow-roll parameters can be written entirely in terms of N. At leading order in N,

$$\epsilon \simeq \frac{3}{4N^2}, \qquad \eta \simeq -\frac{1}{N}. \tag{2.47}$$

The spectral properties can be derived from the known results of single-field slow-roll inflation, Eqs. (1.65) and (1.72)

$$n_s - 1 = 2\eta - 4\epsilon \simeq -\frac{2}{N}, \qquad r = 16\epsilon \simeq \frac{12}{N^2}, \tag{2.48}$$

resulting in the universal relation for Starobinsky inflation

$$n_s \simeq 1 - \sqrt{\frac{r}{3}}. \tag{2.49}$$

[9]Since it is clear that all quantities are understood to be in the EF, we omit the tilde here.

[10]It can be shown that in the slow-roll approximation the e-folding number in the JF and in the EF is the same [104].

Considering the pivot scale $k_* = 0.002\,\mathrm{Mpc}^{-1}$ adopted in the *Planck* analysis, which roughly exited the horizon $N_k = 55$ e-folds before the end of inflation, we have $n_s \simeq 0.9636$ and $r \simeq 0.004$, well within the bounds reported in Sec. 1.5. The free parameter M can be fixed from the amplitude of scalar perturbations, which is (see Eq. (1.64))

$$A_s \simeq \frac{V}{24\pi^2\epsilon M_{pl}^4} \simeq \frac{1}{6144\pi^2}\left(\frac{M}{M_{pl}}\right)^2 \frac{(3-4N_k)^4}{N_k^2}. \tag{2.50}$$

Setting the value of A_s to the observed one, see Table 1.1, gives $M \sim \mathcal{O}(10^{-5})M_{pl}$.

2.4 Scale-invariant gravity: motivations

The Starobinsky model represents one of the simplest realizations of inflation. Despite its minimal structure, it shows remarkable robustness to current observations and is therefore commonly adopted as a benchmark for assessing the potential of future CMB experiments. This empirical success naturally motivates the search for a deeper theoretical origin of the R^2 term, which appears to play a special role among higher-order curvature contributions.

One possible approach is provided by bottom-up reconstruction techniques, in which the form of $f(R)$ is inferred by requiring a slow-roll inflationary phase consistent with the observed values of the spectral indices (see, e.g., [125–133]). Remarkably, these analyses reveal a clear preference for an R^2 contribution, which systematically emerges as the large-curvature asymptotic limit of the reconstructed $f(R)$. This behavior is generic for slow-roll inflationary potentials and suggests that an R^2 term is an essential ingredient of any viable inflationary scenario based on modified gravity.

Beyond its phenomenological relevance, the R^2 term is also selected by theoretical considerations. It is the only higher-order curvature correction that leads to a ghost-free and one-loop renormalizable action, and it enjoys exact scale invariance. Although the original motivation for introducing the R^2 term stemmed from one-loop quantum corrections to the EH action, the above arguments point to a different interpretation. During inflation, the R^2 term dominates over the EH contribution in the Starobinsky model, effectively realizing scale invariance as an approximate symmetry of the inflationary phase.

From this perspective, one may speculate that gravity is fundamentally scale-invariant, with the EH term emerging only after the symmetry is broken. The success of the Starobinsky model could then be understood as a manifestation of its ability to capture this underlying property of gravity within its regime of validity.

The rationale for scale invariance as a fundamental symmetry is well grounded and is not limited to the context of inflation. After discussing its mathematical properties and distinctive features, we will review the primary theoretical motivations that have led to the proposal of scale invariance as a possible resolution to long-standing problems in cosmology, quantum field theory, and particle physics.

Part of this section has been written with the help of the contributions to the conference "Scale invariance in particle physics and cosmology" held at CERN from 28 January to 1 February 2019.

2.4.1 Properties

Scale invariance is ubiquitous in Nature: the coastline, snowflakes, lightning, and Romanesco broccoli all show scale invariance or fractal structure. The (discrete) scale invariance here is realized as self-similarity: the same system appears similar when viewed at different scales [134]. In statistical mechanics, scale invariance is a feature of phase transitions, where the correlation length becomes infinitely large and, with it, the system becomes totally insensitive to changes in scale [135]. In cosmology, as discussed in Chapter 1, the spectrum of primordial fluctuations is almost scale-invariant, hinting at a role of scale symmetry in the very early inflationary cosmology. In particle physics, the

SM is approximately scale-invariant at high energies, provided it can be extrapolated to energies much above the Fermi scale, since all particle masses are much smaller than that scale. Given the absence of new physics in the Large Hadron Collider (LHC) findings, such an extrapolation is increasingly accepted. The SM is then approximately scale-invariant already at TeV scales [4].

Scale transformations, sometimes called *dilatations*, are global spacetime transformations of the form

$$x^\mu \to x'^\mu = \ell^{-1} x^\mu, \tag{2.51}$$

with ℓ a real number. Considering the active transformation point of view, scale transformations are implemented on the fields as[11] [136, 137]

$$\phi(x) \to \phi'(x) = \ell^{\Delta_\phi} \phi(\ell x), \tag{2.52}$$

where Δ_ϕ represents the *scaling dimension* of the generic field ϕ (for example, $\Delta = 1$ for bosons and $\Delta = 3/2$ for fermions[12]). The metric tensor transforms as

$$g_{\mu\nu}(x) \to g'_{\mu\nu}(x) = g_{\mu\nu}(\ell x). \tag{2.53}$$

Sometimes global scale transformations are defined considering the coordinates as fixed, and acting on the metric tensor and the fields as[13] [138]

$$\phi \to \phi' = L^{\Delta_\phi} \phi, \qquad g_{\mu\nu} \to g'_{\mu\nu} = L^{-2} g_{\mu\nu}. \tag{2.54}$$

Whatever version of dilatation symmetry one takes, it should be clear that ℓ (L) is a constant. In this sense, scale transformations are different from conformal transformations as the type in Eq. (2.27), which are local ones. Conformal invariance is a stronger requirement than scale invariance. A Lorentz-invariant field theory that is invariant under a conformal transformation is also scale-invariant, while there is no corresponding theoretical reason for the converse to be true.[14]

We can easily convince ourselves that scale invariance always follows if no dimensional constants are present in the Lagrangian. This restricts the only operators allowed in 3+1 dimensions to be dimension-4 ones. While this is true at the classical level, quantum fluctuations may or may not preserve the symmetry. If not, the dilatation symmetry is anomalous and an intrinsic scale μ is introduced by quantization [138].

When no intrinsic mass or length scale is present in the quantum effective action, then we say that scale invariance is realized as a quantum symmetry [139]. It is the case for the fixed points of the renormalization group (RG) flow trajectories: at the fixed points, the couplings take a constant value g_*, and there is no running. As a consequence, no intrinsic mass scale is present at the fixed point. We talk about *quantum* scale symmetry since it occurs at fixed points *in the presence* of quantum fluctuations and *because* of quantum fluctuations, which should be seen as inducing the symmetry

[11] The inverse transformation appears in the argument because we are dealing with an active transformation in which the field is truly shifted.

[12] Note, however, that this is not a general rule. Gauge fields have scaling dimension $\Delta = 1$, but they are invariant under a scale transformation: $A'_\mu = A_\mu$

[13] To be precise, this should be regarded as a two-parameter (ℓ-L) abelian group of symmetries, with product symmetry corresponding to the usual diffeomorphism invariance for the choice $\ell = L^{-1}$. For this reason, if the action is invariant under the first transformation, then it is also invariant under the second, and vice versa; stated in another way, one cannot break one of the two symmetries without breaking also the other, unless diffeomorphism invariance is broken, too [5].

[14] Together with Lorentz transformations and translations, (special) conformal transformations and dilatations form a fifteen-parameter group, called *conformal group*, the group of transformations from the space to itself that preserves angles [136].

rather than destroying it [4]. In this sense, quantum scale symmetry does not require scale symmetry at the classical level. The classical action can involve some intrinsic mass or length scale, the memory of which is lost at the fixed points. It is the case of the well-known Ising model at the phase transition [140].

Unless otherwise stated, we will in general consider theories displaying *classical scale invariance*. The idea of scale invariance as a fundamental symmetry of Nature is, in essence, not far from the Copernican principle in cosmology, which states that no point in space is unique. Scale invariance then demands that no momentum scale is unique. As amply discussed in Chapter 1, the Universe does not appear isotropic and homogeneous on small scales, since quantum fluctuations have sourced inhomogeneities that give rise to structure formation. In complete analogy, particle interactions look different at different momentum scales because quantum fluctuations break tree-level scale invariance and lead to the running of couplings.

In the following, we will outline how scale-symmetry breaking can be realized in practice and associate it with the generation of the scales we observe.

2.4.2 Dynamical generation of scales and hierarchy problem

Most of the mass of the matter observed in the Universe has a dynamical origin. As an illustrative example, the proton mass receives only a few percent contribution from the bare quark masses, with the dominant part arising from strong interaction dynamics [141]. This observation motivates the search for mechanisms capable of dynamically generating all mass scales, providing a unified explanation for the origin of all dimensional quantities in Nature.

In this respect, scale-invariant theories – where no intrinsic mass scale is introduced by hand at the level of the action – offer a natural framework for dynamical mass generation, which occurs via scale symmetry breaking. Scale invariance may be broken in different ways, leading to two broad perspectives commonly discussed in the literature:

- The theory admits spontaneous symmetry breaking (SSB), for instance, when a scalar field ϕ settles at a nonzero value. In this case, mass scales are generated already at the classical level and are commonly referred to as *sliding scales*. As a consequence of SSB, the spectrum contains a massless Goldstone boson, the *dilaton*, whose interactions are purely derivative. It is important to note that scale invariance in this context does not imply that Nature looks the same at all scales. Such an interpretation is more appropriate in the context of critical phenomena in statistical physics, where scale invariance typically arises without SSB. This perspective is adopted, for example, in [142–150].

- The theory is classically scale invariant, but scale symmetry is broken by quantum corrections, leading to anomalous dilatation symmetry. In this case, mass scales are generated through dimensional transmutation, driven by the running of dimensionless couplings, and are referred to as *intrinsic scales*. The spectrum contains a pseudo-Goldstone boson with a non-vanishing mass, which in general does not couple purely derivatively. This perspective is adopted, for instance, in the "Agravity" framework [151], as well as in several other works (see, e.g., [4, 152–155]). The dynamics underlying dimensional transmutation may be either strongly or weakly coupled, corresponding to non-perturbative or perturbative approaches, respectively.

The possibility of dynamically generating mass scales via spontaneous scale symmetry breaking provided one of the earliest motivations for scale-invariant theories of gravity. In this spirit, Cooper and Venturi introduced in 1981 a model of induced gravity [156], following lines similar to those of the seminal work by Brans and Dicke in which the Newtonian gravitational constant becomes a

dynamical quantity [108]. The action of induced gravity formulated by Cooper and Venturi is

$$S = \int \mathrm{d}^4x\sqrt{-g}\left(\frac{\gamma}{2}\phi^2 R - \frac{\lambda}{4}\phi^4 - \frac{1}{2}g^{\mu\nu}\partial_\mu\phi\partial_\nu\phi\right), \tag{2.55}$$

where γ and λ are positive and dimensionless constants. When analyzed in a spatially flat FLRW background and neglecting the contribution of matter, the model admits a de Sitter solution with

$$\phi = \phi_0, \qquad R = \frac{\lambda}{\gamma}\phi_0^2. \tag{2.56}$$

The scalar field therefore acquires a nonzero vacuum expectation value, ϕ_0, thereby introducing an explicit mass scale into the theory. This spontaneous breaking of scale symmetry ultimately leads to the natural identification[15]

$$\gamma\phi_0^2 = M_{pl}^2, \tag{2.57}$$

so that the EH term with the Planck scale is generated dynamically. A similar formulation was also given in [157]. The model also leads to a nonzero cosmological constant

$$\Lambda = \frac{1}{4\gamma}\lambda\phi_0^2, \tag{2.58}$$

and was later on studied as a dark-energy model [158].

The dynamical generation of mass scales has also been proposed as a possible explanation of the hierarchy problem in particle physics, a perspective that was partly challenged by the absence of evidence for new physics at the LHC following the discovery of the Higgs boson [159, 160]. The conventional view of naturalness at the electroweak (EW) scale led to the expectation that the Higgs boson should be accompanied by new degrees of freedom at the weak scale, whose role would be to provide a cutoff for quadratically divergent quantum corrections to the Higgs mass squared. Although, on the one hand, the issue of quadratic divergences may be reinterpreted as an unphysical artifact of the renormalization scheme [161], it remains true that heavy particles coupled to the Higgs boson generically induce large radiative corrections to its mass. This results in a degree of fine-tuning that is, in principle, experimentally observable [162, 163]. For these reasons, many attempts have been made to explain the coexistence of two largely separated mass scales, namely the EW scale, $v = 246\,\mathrm{GeV}$, and the Planck scale, $M_{pl} = (8\pi G)^{-1/2} = 2.44 \times 10^{18}\,\mathrm{GeV}$. In one way or another, all these attempts invoke scale invariance [154, 161].

To address the naturalness problem at the EW scale, one must extend the scale-invariant framework to include the SM. This follows from the observation that the only intrinsic mass scale in the SM is the Higgs mass, m_H, which is explicitly forbidden in a scale-invariant theory. The purely gravitational action, taken in its minimal form (2.55), and possibly including quadratic curvature terms, must therefore be supplemented by an appropriate SM Lagrangian,

$$\mathcal{L}_{(4)}^{\mathrm{SM}} = -\frac{1}{4}F_{\mu\nu}F^{\mu\nu} + \bar{\psi}i\not{D}\psi + (\psi_i y_{ij}\psi_j H + \mathrm{h.c.}) - \lambda_H|H|^4 - \xi_H|H|^2 R, \tag{2.59}$$

where H is the Higgs doublet, h.c. stands for "Hermitian conjugate", and the subscript stresses that only operators with mass dimension four are allowed. The Higgs mass is then generated in full analogy with the Planck mass, including also a coupling $\lambda_{H\phi}$ between the same scalar field ϕ that is non-minimally coupled to gravity and the Higgs doublet

$$\mathcal{L}_{(4)}^{\mathrm{BSM}} = \lambda_{H\phi}\phi^2|H|^2. \tag{2.60}$$

[15] In the original paper [156] a slightly different expression is reported, resulting from a weak-field computation: $\gamma\phi_0^2(6\gamma + 1)/(8\gamma + 1) = M_{pl}^2$.

In addition to the condition for the dynamical generation of the Planck scale (2.57), we impose

$$\lambda_{H\phi}\phi_0^2 = m_H^2. \tag{2.61}$$

Scale invariance thus provides a universal mechanism for generating all scales. At the same time, however, the hierarchy between the Planck and the EW scale is just effectively translated into a hierarchy between dimensionless couplings, $\lambda_{H\phi} \ll \gamma$. This raises the question of whether scale invariance alone is sufficient to resolve the hierarchy problem. It is important to emphasize that the naturalness issue at the EW scale, also known as *gauge hierarchy problem*, is twofold. The first part concerns the unnaturally large difference between the Planck and Higgs scales. This problem is not addressed by scale invariance [145], as the observed values of the two scales still require a tuning of the couplings such that $\lambda_{H\phi} \ll \gamma$. The second part of the problem concerns the stability of the Higgs mass against radiative corrections from its coupling to heavier states. In the particular case where no intermediate mass scale exists between m_H and M_{pl}, the presence of radiative corrections depends on the UV completion of the theory. It has been shown [142, 149] that, by employing a renormalization scheme based on the assumption that the UV completion of the theory preserves scale invariance, the Higgs mass does not receive corrections proportional to M_{pl}. Under these conditions, scale invariance ensures the absence of this second part of the gauge hierarchy problem [145].

A different interpretation arises when the SM is treated as an effective field theory at energies well below the Planck scale, such that gravitational effects can be neglected. In this regime, as will be discussed in more detail in the following, the theory exhibits approximate scale invariance, since the EW vacuum phase transition is nearly second-order. Any second-order phase transition is associated with the presence of a fixed point in the quantum effective action, and exact scale invariance is realized at such fixed points.[16]

In this sense, the smallness of the dimensionless ratio $\epsilon = v^2/M_{pl}^2 = \mathcal{O}(10^{-32})$, where v is the Higgs vacuum expectation value, is *technically natural*[17] since, at the SM fixed point, the value $\epsilon = 0$ corresponds to an enhanced symmetry – precisely scale invariance. It follows that the small value of ϵ is protected against large radiative corrections as a consequence of the second-order nature of the SM fixed point.

One can further be convinced that this is indeed the case, considering the RG flow equations of the parameter δ, measuring – in units of mass squared – the distance to the EW phase transition,

$$\mu\frac{\partial}{\partial\mu}\delta = A\delta, \tag{2.62}$$

where A is the anomalous dimension, which can be computed in perturbation theory. The key observation is that the RG flow of δ is proportional to δ, thereby guaranteeing the stability of the critical surface.

Finally, it is important to stress that this argument does not address the origin of the smallness of ϵ, or, equivalently, the reason why we are sitting so close to the critical surface of the SM fixed point. Scale symmetry alone resolves only the second aspect of the gauge hierarchy problem. Overall, scale invariance can be regarded as a guideline for model building, and it can address the second part of the gauge hierarchy problem.[18]

[16] Scale invariance at the SM fixed point is often referred to as *particle scale symmetry*; see the discussion in Sec. 2.4.3.

[17] Here we adopt the notion of naturalness introduced by 't Hooft, according to which a parameter is allowed to be small only if setting it to zero enhances the symmetry of the theory [164].

[18] The only case in which scale invariance can also address the huge value of the gauge hierarchy is in the context of asymptotically safe quantum gravity. Depending on the details of the particle physics model, the parameter δ can be an irrelevant parameter of the theory, and thus it can be predicted, providing a natural explanation for why we are sitting so close to the critical trajectory [165]. Forthcoming quantum gravity calculations will clarify if this is indeed the case.

2.4.3 Cosmology

As discussed in Chapter 1, CMB observations indicate an almost scale-invariant spectrum of primordial curvature perturbations. This observational evidence suggests the presence of approximate scale symmetry in the physics of the early Universe. In the following, we discuss how scale symmetry has been proposed both as a mechanism for generating approximately flat inflationary potentials and as a possible approach to the cosmological constant problem.

Flat inflationary potentials

Current CMB observations favor Starobinsky-like inflationary models, which are typically formulated in terms of a scalar field ϕ non-minimally coupled to gravity through a term $f(\phi)R/2$ and endowed with a potential $V(\phi)$. In the EF, the potential is rescaled to $V_E = M_{pl}^4 V(\phi)/f^2(\phi)$. Such a potential must be sufficiently flat to allow for a phase of slow-roll inflation. One needs, therefore, to impose specific conditions like $V \propto f^2(\phi)$ for $\phi \gg M_{pl}$, which lead to predictions compatible with present observations but are nevertheless the result of a fine-tuning on the functions of the theory. An alternative interpretation is that the flattening of V_E at large field values, $\phi \gg M_{pl}$, may arise naturally if only dimensionless couplings are present [151].

As a concrete example, consider the simplest realization of scale-invariant inflation within the Cooper–Venturi model defined in Eq. (2.55). In this case, the EF potential reads

$$V_E = M_{pl}^4 \frac{\lambda\phi^4}{(\gamma\phi^2)^2} = M_{pl}^4 \frac{\lambda}{\gamma^2}, \tag{2.63}$$

and is exactly flat at tree level. Scale invariance, therefore, naturally leads to flat inflationary potentials without the need for fine-tuning. Clearly, for slow-roll inflation to end, a slight slope in the potential is required. In this simple setup, such a slope can be generated through the breaking of scale symmetry induced by the quantum running of the couplings λ and ξ, as discussed previously.

A tale of three scale-invariant fixed points

At this stage, it should be clear that scale symmetry plays a crucial role in many aspects of particle physics and cosmology. Following Wetterich, one can extend the discussion to quantum field theory to construct a unified framework connecting the different aspects of scale symmetry in particle physics, cosmology, and quantum gravity. We will mainly follow the dissertation presented in [4].

Quantum scale symmetry is directly linked to fixed points of the RG flow. Three main fixed points can be identified:

- UV fixed point, displaying *gravity scale symmetry*. This fixed point is associated with the combined theory of particle physics and quantum gravity and ensures the renormalizability of a quantum field theory description of gravity.

- SM fixed point, displaying *particle scale symmetry*. It is associated with the description of the SM treated as a low-energy effective field theory decoupled from gravity, valid below the Planck scale. The presence of the SM fixed point is closely related to the (approximately) second-order nature of the EW phase transition. It is a trivial fixed point, where all gauge and Yukawa couplings, as well as the fixed points in the Higgs sector, vanish. When the gauge couplings g_2 and g_3 become large, they induce a small minimal mass for the W and Z bosons. For this reason, the EW phase transition is only approximately second-order, and the SM fixed point cannot be reached exactly. Nevertheless, particle scale symmetry remains a reliable approximation for energies between the Fermi and Planck scales.

- IR fixed point, displaying *cosmic scale symmetry*. It is related to the description of the late-time Universe and to the cosmological constant problem.

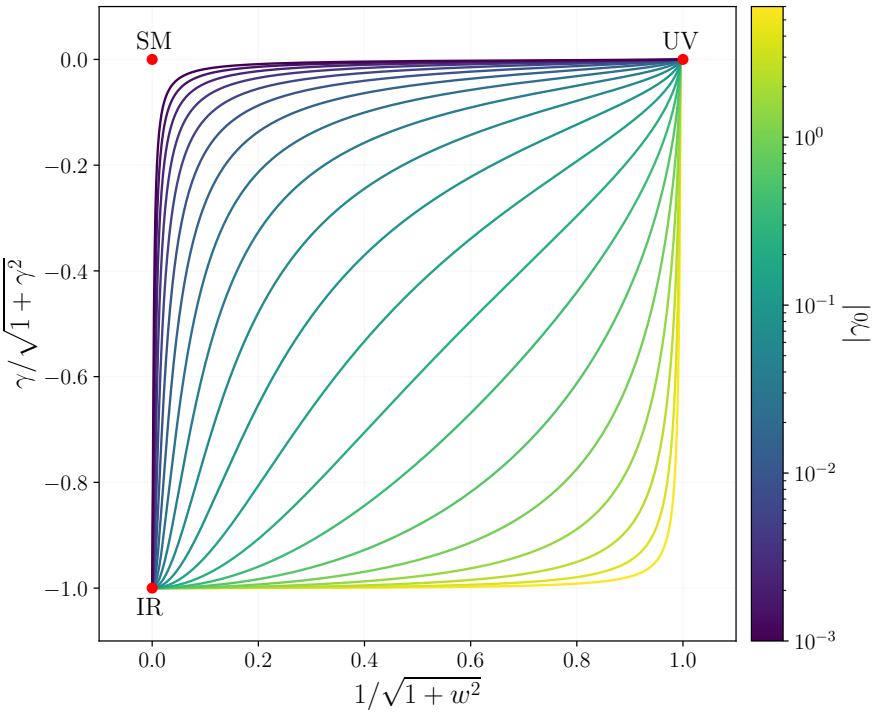

Figure 2.3: RG flow trajectories representing the crossover between the UV and the IR fixed point, from Eq. (2.66). For easier visualization, following [4], we plot on the x axis $f_w = 1/\sqrt{1+w^2}$, which approaches w^{-1} for large w – corresponding to weak gravity – and maps $w \to 0$ – strong gravity – to one. On the y axis, we plot $f_\gamma = \gamma/\sqrt{1+\gamma^2}$, mapping $\gamma \to \pm\infty$ to ± 1. We fix $b = c = 0.1$ and vary $\gamma_0 \in [-6, -10^{-3}]$. Typical RG trajectories start from $k \to \infty$ at the UV fixed point (*upper right corner*), where $\gamma = 0$ and $w > 0$. For sufficiently small $|\gamma_0|$, as k is lowered, trajectories come close to the SM fixed point (*upper left*), where $\gamma = w = 0$. Subsequently, they are attracted for $k \to 0$ towards the IR fixed point (*lower left*) at $\gamma \to -\infty$ and $w = 0$. The observed SM corresponds to a tiny $|\gamma_0|$.

In cosmology, the typical evolution of the Universe can be understood as following the RG trajectories: starting from the UV fixed point in the asymptotic past, passing near the SM fixed point, and ultimately approaching the IR fixed point in the asymptotic future. This *crossover trajectory* is represented in Figure 2.3 and can be analyzed from the flow equations. For simplicity, we restrict our discussion to two running parameters: a running squared Planck mass $M^2(k)$ – intuitively representing the relative strength of gravity – and a running deviation from the EW phase transition $\delta(k)$.

Introducing the dimensionless variables

$$\gamma \equiv \frac{\delta}{k^2}, \qquad w \equiv \frac{M^2}{2k^2}, \tag{2.64}$$

the flow equations take the form

$$\begin{aligned} \partial_t w &= -2w + 2c, \\ \partial_t \gamma &= \left(-2 + \frac{b}{w}\right)\gamma, \end{aligned} \tag{2.65}$$

with $\partial_t = k\,\partial_k$, and b and c being constants. The RG flow trajectories are then explicitly given by

$$\gamma = 2\gamma_0(w-c)\left(\frac{w}{(1+2c)(w-c)}\right)^{b/2c}, \tag{2.66}$$

where $\gamma_0 \equiv \gamma(k = M_{pl})$ and M_{pl} is the scale associated with the observed (constant) value of the Planck mass. Different trajectories in Figure 2.3 correspond to different negative values of γ_0, which indicate spontaneously broken EW symmetry.[19]

For small values of $|\gamma_0|$, the RG flow first follows a crossover trajectory from the UV fixed point to the vicinity of the SM fixed point, and then a second crossover trajectory ending at the IR fixed point. In the limit $|\gamma_0| \to 0$, the flow can approach the SM fixed point arbitrarily closely. In a cosmological context, inflation can be associated with the UV fixed point of quantum gravity, or its immediate neighborhood. As the flow evolves away from this point, scale symmetry becomes only approximate, leading to an almost scale-invariant quantum effective action Γ, and consequently, to nearly scale-invariant correlation functions and spectrum of primordial fluctuations.[20]

As the Universe evolves sufficiently away from the fixed point, scale symmetry is no longer a good approximation, and inflation ends. Since the observable cosmological fluctuations freeze long before the end of inflation, they retain the imprint of approximate scale symmetry.

At late times, the Universe approaches the IR fixed point, which is relevant for the dynamics of dark energy and the cosmological constant problem.

Cosmological constant problem: a possible solution

From the simple induced gravity model in Eq. (2.55), it is evident that SSB leads to a non-vanishing cosmological constant, given by the value of the EF potential at its minimum, see Eq. (2.58). Requiring that the residual cosmological constant vanishes is equivalent to the usual fine-tuning associated with the cosmological constant problem, which is therefore not addressed when scale invariance is exact.

The interesting scenario arises when quantum corrections break scale invariance, and some intrinsic scale μ is present in the non-minimal coupling and the potential. Consider the case of *cosmon inflation* [167, 168]

$$S = \int \mathrm{d}^4x\sqrt{-g}\left(\frac{C}{2}R^2 + \frac{f(\phi)}{2}R - \frac{1}{2}Kg^{\mu\nu}\partial_\mu\phi\partial_\nu\phi - V(\phi)\right), \tag{2.67}$$

where, compared to the Cooper-Venturi model (2.55), an additional quadratic term in the curvature is present and the kinetic term is allowed to be non-canonical. For $f(\phi) = \phi^2, V(\phi) = \lambda\phi^4$, and constant K the action is scale invariant. This action can, e.g., describe inflation near the UV fixed point. Quantum corrections may introduce a scale dependence in the functions $f(\phi)$ and $V(\phi)$ via an intrinsic mass scale $\bar{\mu}$, e.g., [4]

$$\begin{aligned} f(\phi,\bar{\mu}) &= \phi^2 + d\,\bar{\mu}^2, \\ V(\phi,\bar{\mu}) &= b\,\bar{\mu}^2\phi^2 + c\,\bar{\mu}^4, \end{aligned} \tag{2.68}$$

where b, c, d are constants. In the IR limit $\bar{\mu}^2/\phi^2 \to 0$ scale symmetry becomes exact provided K becomes $\bar{\mu}$-independent. This scale symmetry is associated with the IR fixed point.

If $\phi \to \infty$ in the asymptotic future, this limit is approached, giving rise to a pseudo-Goldstone boson with a small mass. In the context of (2.67), this field is called the *cosmon* and dynamically drives the cosmological constant toward zero. Indeed, the observable dimensionless ratio[21] $V/f^2 \to b\bar{\mu}^2/\phi^2$ vanishes as $\phi \to \infty$.

---

[19] Positive values of γ_0 correspond to unbroken EW symmetry and are not shown in Figure 2.3, which is symmetric under reflection about the axis $\gamma = 0$.

[20] The quantum effective action Γ encodes all the relevant information about the full propagators and vertices. Its first functional derivatives yield the field equations, while the second derivative $\Gamma^{(2)}$ corresponds to the inverse propagator. The spectrum of primordial fluctuations can be directly obtained from $\Gamma^{(2)}$ [166].

[21] Only dimensionless ratios of dimensionful quantities can be measured. Here, f^2 should be identified with M_{pl}^4.

Typical cosmological solutions evolve from the UV fixed point in the far past, where $\phi \to 0$, toward the IR fixed point in the far future, where $\phi \to \infty$ [169]. In this perspective, the vanishing of the cosmological constant is not intrinsic but rather a dynamical consequence of the fact that we live in a very old universe, and we are approaching the IR fixed point. In the model studied in [169], the existence of a second crossover leading to a growing neutrino-to-electron mass ratio can also address the coincidence problem (see Sec. 2.1).

2.4.4 Renormalizability

Scale invariance has been proposed by Wetterich in [139] as a general criterion beyond renormalizability. In the following, we discuss how a scale-invariant quantum field theory is renormalizable and exhibits significantly greater predictive power than a generic renormalizable theory.

Following [4], we define a *continuum renormalizable* quantum field theory as a theory that is well-defined in the continuum limit, i.e., it can be continued up to arbitrarily short distances. This definition goes beyond the concept of perturbative renormalizability, which only guarantees that a theory provides a valid low-energy effective description, without guaranteeing its consistency at arbitrarily short distances or high momenta.

This argument for renormalizability is based on the necessary presence of a UV fixed point. On one hand, the existence of a UV fixed point ensures that a theory can be consistently defined up to arbitrarily short distances or infinite momenta, making it a *sufficient* condition for a renormalizable quantum field theory. On the other hand, if the dimensionless couplings do not approach finite values as $\mu \to \infty$, they either diverge or enter a regime where the theory becomes inconsistent for other reasons. In this sense, the presence of a UV fixed point is also a *necessary* condition for renormalizability.

Two classes of UV fixed points can be adopted to define a renormalizable quantum field theory [170]

- UV fixed points with vanishing couplings, corresponding to a free quantum field theory. They define *asymptotic freedom*. Asymptotic free theories are perturbatively renormalizable, since one can perform a loop expansion for arbitrarily small couplings around the fixed point.

- UV fixed points with non-vanishing couplings, corresponding to an interacting quantum field theory. They define *asymptotic safety*. The theory is renormalizable, but typically not with a perturbative approach.

Quantum gravity is presumably not perturbatively renormalizable. A natural possibility is that it constitutes a renormalizable quantum field theory with diffeomorphisms as gauge symmetry, having an UV fixed point of the asymptotic safe type [171–173]. It is rather natural to associate the UV limit of quantum gravity with non-vanishing interactions, since gravity cannot be "switched off". This fact further motivates the general notion of renormalizability considered here.[22]

Since quantum scale symmetry is exact at any UV fixed point, scale invariance can be regarded as a guiding principle extending beyond renormalizability. Scale-invariant theories are renormalizable, but their predictive power goes even beyond general renormalizability. This is particularly evident when analyzing the flow of couplings near fixed points and the classification of relevant parameters.

Let's consider a theory with a finite number of dimensionless couplings g_i with fixed-point values g_{i*}. Their *beta*-functions specify the flow of couplings

$$\partial_t g_i = \mu \partial_\mu g_i \equiv \beta_i(g_j), \tag{2.69}$$

[22] Scale-invariant theories are clearly perturbatively renormalizable by power counting since all parameters are dimensionless. The discussion here aims to extend the concept of renormalizability beyond the perturbative regime.

whose zeros define the fixed points of the theory: $\beta_i(g_*) = 0$. Linearization around the fixed points gives the *stability matrix* T

$$\partial_t(g_i - g_{i*}) = \left.\frac{\partial \beta_i}{\partial g_j}\right|_{g_*} (g_j - g_{j*}) = -T_{ij}(g_j - g_{j*}). \tag{2.70}$$

The eigenvalues of T are the *critical exponents* θ_i.[23] The eigenvectors v_i associated with positive, negative, or zero θ_i correspond to *relevant*, *irrelevant*, or *marginal parameters*, respectively.

For an arbitrary scale Λ, the flow of the eigenvectors can be expressed as

$$v_i(\mu) = \left(\frac{\Lambda}{\mu}\right)^{\theta_i} v_i(\Lambda), \tag{2.71}$$

which shows that, for any finite $v_i(\Lambda)$, the irrelevant parameters vanish in the UV limit $\Lambda/\mu \to \infty$. All information carried by the irrelevant parameters is lost at the UV fixed point, and only the relevant parameters remain as the free parameters of the theory. The predictive power of a quantum field theory is therefore determined by the number of free parameters that must be specified at a given scale $\bar{\mu}$.

The crucial point for scale-invariant theories is that all the relevant parameters vanish at the UV fixed point, leaving no free parameters. In this sense, scale invariance has a much stronger predictive power than simple renormalizability and can be legitimately taken as a new theoretical construction principle for quantum field theories.

[23] While in asymptotic free theories the classification into relevant, irrelevant, and marginal parameters follows from simple dimensional analysis of the couplings, for an asymptotic safe theory one needs to explicitly compute the critical exponents to figure out the behavior near the fixed points.

2.5 Summary

In this chapter, we have explored modified gravity as a theoretically and phenomenologically motivated extension of GR. In Sec. 2.1, we outlined the main motivations for modifying the EH action, emphasizing both cosmological and fundamental aspects. On the cosmological side, we discussed the late-time accelerated expansion of the Universe, the cosmological constant problem, and the coincidence problem, highlighting how these challenges motivate alternatives to ΛCDM. On the theoretical side, we showed that once quantum effects of matter fields in curved spacetime are taken into account, higher-order curvature invariants such as R^2 and $R_{\mu\nu}R^{\mu\nu}$ naturally arise in the effective gravitational action. From an effective field theory perspective, such corrections are unavoidable in regimes of high curvature, thus providing a strong rationale for considering extensions of GR in the description of the very early Universe.

In Sec. 2.2, we addressed the mathematical consistency of modified gravity theories. In particular, we discussed Ostrogradsky instabilities in non-degenerate higher-derivative theories and clarified under what conditions they can be avoided. We further analyzed perturbative instabilities – tachyonic, gradient, and ghost instabilities – establishing the criteria required for the viability of a theory at the level of linear perturbations.

A central part of the chapter was devoted to $f(R)$ gravity as one of the simplest generalizations of GR. In Sec. 2.3, we derived the field equations in both the metric and Palatini formalisms, highlighting their inequivalence for nonlinear functions of R. Focusing on the metric formalism, we showed that $f(R)$ theories propagate an additional scalar degree of freedom and are dynamically equivalent to a Brans-Dicke theory with vanishing Brans-Dicke parameter. Through a conformal transformation, we established a connection between the JF and the EF, carefully discussing their physical interpretations and how to consistently map physical quantities from one frame to a conformally equivalent one.

As an illustrative example, we studied the Starobinsky model, $f(R) = R+R^2/6M^2$, which provides a phenomenologically successful realization of inflation within the gravitational sector. We derived its quasi-de Sitter solution in the JF and its scalar-field representation in the EF, computing the slow-roll parameters and the resulting spectral indices. Among higher-order curvature corrections, the R^2 contribution is uniquely singled out by the fact that it leads to a ghost-free and one-loop renormalizable gravitational action and enjoys exact scale invariance. In the inflationary regime of the Starobinsky model, the dynamics are dominated by the quadratic term, while the EH contribution is subleading, so that scale invariance is effectively an approximate symmetry of the inflationary phase. From this perspective, it is natural to speculate that scale invariance may represent a fundamental symmetry of gravity at high energies.

In Sec. 2.4, we motivated the study of scale-invariant extensions of gravity and their phenomenological implications in the early Universe, reviewing the main arguments that support scale invariance as a guiding principle in particle physics, cosmology, and quantum field theory.

Chapter 3

Scale-invariant inflation: background

The theoretical and phenomenological arguments discussed in Sec. 2.4 provide strong support for scale invariance as a guiding symmetry of a fundamental theory of Nature. In the context of inflation, the potential relevance of scale invariance is already hinted at by the underlying reasons for the success of the Starobinsky model. Indeed, Starobinsky inflation arises from a simple modification of the Einstein-Hilbert action through the inclusion of a term quadratic in the Ricci scalar, which effectively realizes an approximate scale invariance during the inflationary phase. Motivated by this observation, we push this idea further by exploring a framework in which the cosmological evolution during inflation is described by a classically scale-invariant theory. In this picture, scale invariance is subsequently broken through a mechanism of symmetry breaking, leading to the dynamical generation of the Planck scale.

In this chapter, we present the model introduced by Rinaldi and Vanzo in [5], which includes all relevant scale-invariant combinations of the Ricci scalar and a real scalar field. The results presented here build upon and extend a series of previous analyses in the literature (see, e.g., [5–9, 174–176]).

3.1 The model

Following [5], we consider a classically scale-invariant action in the Jordan frame (JF),

$$S_J = \int \mathrm{d}^4x\sqrt{-g}\left[\frac{\alpha}{36}R^2 + \frac{\xi}{6}\phi^2 R - \frac{1}{2}g^{\mu\nu}\partial_\mu\phi\partial_\nu\phi - \frac{\lambda}{4}\phi^4\right], \tag{3.1}$$

where $\phi(x)$ is a real scalar field and α, ξ, and λ are arbitrary dimensionless coupling constants, as required by scale invariance. Their values will be constrained by inflationary observables in the following analysis; for the time being, we assume they are strictly positive.

The action in Eq. (3.1) contains only operators of mass dimension four. It is invariant under the dilatation transformations defined in Eqs. (2.51)–(2.53), with scaling dimension $\Delta = 1$ for the scalar field. A detailed proof is provided in Appendix B.

In addition, the action is invariant under the rigid transformations given in Eq. (2.54). In this case, the transformation of the Ricci scalar follows directly from the general conformal transformation law (2.28), evaluated for a coordinate-independent conformal factor Ω.

We emphasize that the action in Eq. (3.1) is not conformally invariant. Conformal invariance would require the conditions $\alpha = 0$ and $\xi = -1/2$, as shown in Appendix B.[1] Moreover, the action should not be regarded as the most general scale-invariant theory quadratic in curvature invariants, since it

[1] The reason for restricting the analysis to positive values of ξ, despite the fact that the conformal limit is achieved for $\xi < 0$, is related to dynamical mass generation and will become clear in the following.

does not include a squared Weyl curvature term [81, 99]. The latter is defined as

$$C^2 \equiv W_{\mu\nu\rho\sigma}W^{\mu\nu\rho\sigma} = 2R_{\mu\nu}R^{\mu\nu} - \frac{2}{3}R^2 + \mathcal{G}, \qquad \mathcal{G} \equiv R^2 - 4R_{\mu\nu}R^{\mu\nu} + R_{\mu\nu\rho\sigma}R^{\mu\nu\rho\sigma}, \tag{3.2}$$

where $\mathcal{G}$ denotes the Gauss–Bonnet curvature invariant, a topological term that does not affect the equations of motion [96]. The absence of the Weyl-squared term is motivated by its conformal invariance. In a FLRW background, which is conformally flat, the Weyl tensor vanishes identically – as in Minkowski spacetime – and therefore does not affect the background dynamics. While this statement holds at the unperturbed level, the situation can change significantly once perturbations around the classical background are taken into account, even at the classical level.

In a recent work [177], the effects of a Weyl-squared term in the context of Starobinsky inflation were investigated. It was shown that the Weyl curvature induces a ghost degree of freedom coupled to the scalaron arising from the R^2 term, leading to a tachyonic instability. This instability manifests as exponential growth of the Bardeen potentials (see Eq. (1.30)), rendering the inflationary FLRW background unstable. Although a complete analysis of the action in Eq. (3.1) with a Weyl-squared term lies beyond the scope of this work, the results of [177] provide further motivation for neglecting this term in the construction of a viable inflationary model.

The classical effective potential for the scalar field ϕ can be identified with

$$V_{\text{eff}}(\phi) = -\frac{\xi}{6}\phi^2 R + \frac{\lambda}{4}\phi^4. \tag{3.3}$$

Its derivative with respect to ϕ, when R is fixed, vanishes at

$$\phi_0 = 0, \qquad \phi_0^2 = \frac{\xi R}{3\lambda}, \tag{3.4}$$

corresponding to a local maximum and a local minimum, respectively. This structure guarantees the presence of a symmetry-breaking mechanism in the model. Indeed, when an infinitely extended spacetime volume with constant curvature is considered, scale symmetry gets broken whenever the scalar field relaxes to the minimum, leading to dynamical mass generation along the same lines as what is described in Sec. 2.4.2, as we will show in the following.

3.2 Global evolution

In this section, we study the cosmological evolution of the scale-invariant model (3.1) on a spatially flat FLRW background. Once complemented with a detailed stability analysis, these results will clarify the role of the fixed points in Eq. (3.4) and the dynamical generation of mass scales. A parallel study will be performed in the Einstein frame (EF), ultimately leading to a minimal single-field description suitable for deriving the inflationary predictions.

3.2.1 Jordan frame

By varying the action (3.1) with respect to the metric tensor and taking the $(0,0)$ component, we obtain the equation of motion for the Hubble parameter H,

$$\alpha\left(2H\ddot{H} - \dot{H}^2 + 6H^2\dot{H}\right) - \frac{\dot{\phi}^2}{2} + 2\xi H\phi\dot{\phi} + \frac{\phi^2}{4}\left(4\xi H^2 - \lambda\phi^2\right) = 0. \tag{3.5}$$

The second equation of motion is the Klein-Gordon equation for the scalar field, obtained by varying the action with respect to ϕ,

$$\ddot{\phi} + 3H\dot{\phi} - 2\xi\phi\dot{H} - \phi\left(4\xi H^2 - \lambda\phi^2\right) = 0. \tag{3.6}$$

Together, Eqs. (3.5)–(3.6) determine the dynamics of the system in cosmic time t.

We now perform a dynamical system analysis to analytically investigate the stability properties of the system. This is conveniently done by casting the system of Eqs. (3.5)–(3.6) – a two-dimensional system of second-order differential equations – into a four-dimensional system of first-order equations. We further employ the e-folding time, as defined in Sec. 1.3. Denoting derivatives with respect to N with a prime, we introduce the new variables

$$x \equiv H(N), \quad y \equiv H'(N), \quad z \equiv \phi(N), \quad w \equiv \phi'(N). \tag{3.7}$$

When substituted in the equations of motion, they give the following equivalent system

$$\begin{aligned} &w' + \frac{yw}{x} + 3w - \frac{2\xi zy}{x} + \frac{\lambda z^3}{x^2} - 4\xi z = 0, \\ &y' + \frac{y^2}{2x} + 3y + \frac{\xi wz}{\alpha x} - \frac{\lambda z^4}{8\alpha x^3} + \frac{\xi z^2}{2\alpha x} - \frac{w^2}{4\alpha x} = 0, \\ &x' - y = 0, \\ &z' - w = 0. \end{aligned} \tag{3.8}$$

The fixed points of the dynamical system (3.8) are the ones solving the algebraic system $\{x' = y' = z' = w' = 0\}$. They turn out to be two distinct families, namely

$$P_1 : (x, y, z, w)_* = (x, 0, 0, 0)\,, \qquad P_2 : (x, y, z, w)_* = \left(x, 0, 2x\sqrt{\frac{\xi}{\lambda}}, 0\right), \tag{3.9}$$

for any value of $x = H(N) > 0$. Note that these fixed points coincide with the extrema of the potential derived in Eq. (3.4), since, when H is constant, $R \simeq 12H^2$. To determine whether they can also characterize a symmetry-breaking phase, we must perform a stability analysis of (3.8), which is done by linearizing the system about its fixed points. In matrix form,

$$\mathbf{x}' = \mathbf{J}_* \left(\mathbf{x} - \mathbf{x}_*\right), \tag{3.10}$$

where we adopted the compact notation for $\mathbf{x} \equiv (x, y, z, w)$ and $\mathbf{J}_*$, which stands for the Jacobian matrix evaluated at the fixed point $\mathbf{x}_* \equiv (x, y, z, w)_*$. An inspection of the eigenvalues of $\mathbf{J}_*$ shows that P_1 is a saddle (and therefore unstable) point. In contrast, no definitive conclusion can be drawn for P_2, due to the presence of vanishing eigenvalues. To unambiguously determine the nature of the fixed points, it is therefore necessary to compute the analytical solutions for $\phi(N)$ and $H(N)$ obtained from the linearized system (3.8) in the vicinity of P_1 and P_2. In the following, we summarize the results for each fixed point.

Unstable fixed point: P_1

The physical quantities of interest at the unstable saddle point are

$$H_{\rm unst} = \text{arbitrary}, \qquad H'_{\rm unst} = 0, \qquad \phi_{\rm unst} = \phi'_{\rm unst} = 0. \tag{3.11}$$

The solutions of the linearized system are readily obtained,

$$\begin{aligned} x = H(N) &= c_1 + c_2\, e^{-3N}, \\ z = \phi(N) &= c_3\, e^{\left(-\frac{3}{2}+\frac{1}{2}\sqrt{9+16\xi}\right)N} + c_4\, e^{\left(-\frac{3}{2}-\frac{1}{2}\sqrt{9+16\xi}\right)N}, \end{aligned} \tag{3.12}$$

where $c_i, i = 1, \ldots, 4$ are constants of integration. Since $\xi > 0$ by definition, $\phi(N)$ is a combination of growing and decaying modes, thus the saddle-point nature of P_1 follows. As the number of e-folds increases, the system is driven away from P_1: the Hubble parameter tends to a constant, while the scalar field grows towards larger values.

Stable fixed point: P_2

Here we have

$$H_{\rm st} = \text{arbitrary}, \qquad H'_{\rm st} = 0, \qquad \phi_{\rm st} = 2H_{\rm st}\sqrt{\frac{\xi}{\lambda}}, \qquad \phi'_{\rm st} = 0. \tag{3.13}$$

The solutions to the linearized system are

$$H(N) = c_1 + c_2 e^{-3N} + e^{-\frac{3}{2}N}\left[c_3 S(N) + c_4 C(N)\right], \tag{3.14}$$
$$\phi(N) = \sqrt{\frac{\xi}{\lambda}}\left[2c_1 + \frac{c_2}{2}e^{-3N} + \frac{\omega - \xi^2}{2\xi(1+2\xi)}e^{-\frac{3}{2}N}\Big((2Jc_4 - 5c_3)S(N) - (5c_4 + 2Jc_3)C(N)\Big)\right],$$

where Ω, not to be confused with the conformal factor, is defined as $\Omega \equiv \xi^2 + \alpha\lambda$ and

$$J \equiv \frac{1}{2}\sqrt{\frac{25\xi^2 + 32\xi\Omega - 9\Omega}{\Omega - \xi^2}}. \tag{3.15}$$

Furthermore, we have defined $S(N) \equiv \sin(JN)$ and $C(N) \equiv \cos(JN)$. These solutions clarify the nature of P_2 as a stable fixed point, which is reached through damped oscillations of both ϕ and H.

To assess the validity of the linearized solutions in Eq. (3.14), we compare them with the numerical results shown in Figure 3.1. The coefficients c_i are determined via a linear least-squares fit performed in the vicinity of P_2, yielding good agreement between the numerical evolution and the fitted solutions (see the inset of Figure 3.1).

We stress that the choice of model parameters and initial conditions is made to clearly illustrate the transition from the saddle point to the stable fixed point via damped oscillations over a few e-folds. These choices are not, in general, those required to obtain a phenomenologically viable inflationary phase, as will become apparent from the analysis presented in Sec. 3.3.

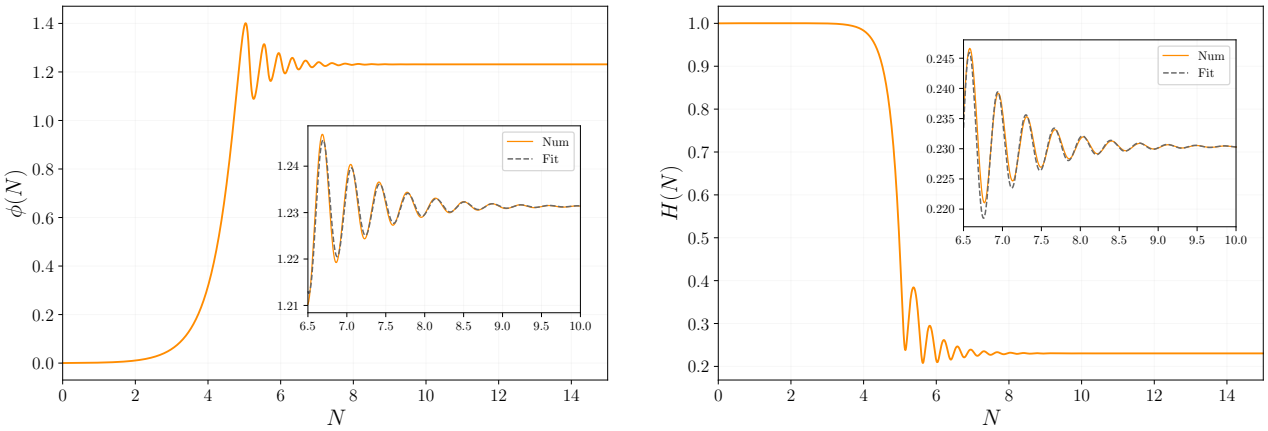

Figure 3.1: Numerical evolution of the scalar field ϕ (*left panel*) and the Hubble parameter (*right panel*) in the JF, obtained from the equations of motion (3.5)–(3.6) in e-folding time N, with $N = 0$ representing the beginning of the numerical integration and proceeding towards increasing positive values as the fields evolve. The insets show the comparison between the full numerical solution (orange solid line) and the linearized solution around P_2 given by Eq. (3.14), with c_i fixed via a linear least-squares fit (gray dashed line). The parameters are fixed to $\alpha = 1, \xi = 2, \Omega = 1.07\,\xi^2$, which are not, in general, the ones that yield a viable inflationary trajectory, but they help capture the oscillatory behavior visually. The initial conditions are set to: $\phi(0) = 10^{-5}, H(0) = 1, \phi'(0) = H'(0) = 0$.

It is also instructive to follow the evolution of the scalar field ϕ within the effective potential (3.3). In Figure 3.2, we show the effective potential $V_{\rm eff}(\phi)$ at different values of N, together with the

instantaneous position of the field ϕ, for the same dynamical evolution depicted in Figure 3.1. At early times, when the system lies close to the unstable fixed point, $V_{\rm eff}(\phi)$ exhibits a characteristic Mexican-hat shape, and the field rolls toward its minimum (see the first panel of Figure 3.2). As the evolution proceeds, the form of the effective potential is modified by the dynamics of the Ricci scalar R, and its minima at $\phi_0 \neq 0$ may disappear if R becomes negative (second panel of Figure 3.2). Eventually, the system approaches the stable attractor, with the field ϕ settling at the minimum of the effective potential (last panels of Figure 3.2).

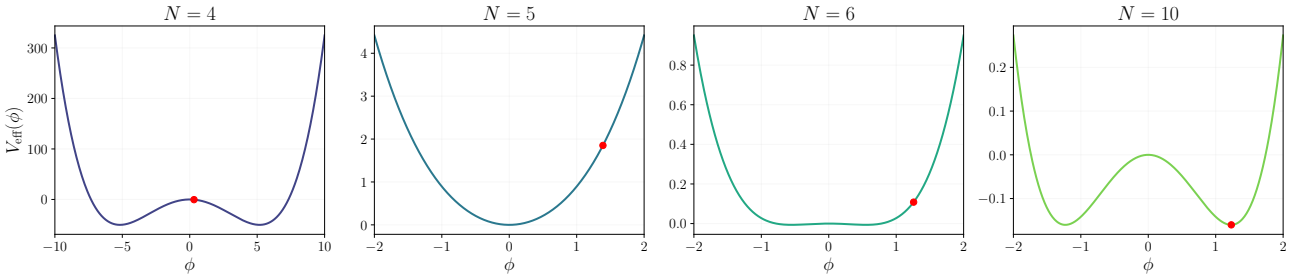

Figure 3.2: Effective potential as given in Eq. (3.2). Each panel shows the potential with R evaluated at a different e-folding time N, taken from the same cosmological evolution displayed in Figure 3.1. From left to right: $N = 4, 5, 6$, and 10. The red dot indicates the instantaneous value of the scalar field ϕ.

This evolution is consistent with a classical SSB mechanism, in which the scalar field ϕ acquires a non-vanishing expectation value, $\phi_{\rm st} \neq 0$, thereby dynamically introducing a mass scale into the system. The mechanism of dynamical mass generation described in Sec. 2.4.2 follows along the same lines as in the Cooper-Venturi model. Since, at late times, the term linear in the Ricci scalar in the action (3.1) is expected to dominate over the quadratic R^2 contribution, it is natural to make the identification

$$\frac{\xi}{6}\phi_{\rm st}^2 R = \frac{1}{2}M_{pl}^2 R, \tag{3.16}$$

which allows one to recover the EH term. This identification fixes the value of $\phi_{\rm st}$ and, consequently, that of $H_{\rm st}$ as

$$\phi_{\rm st} = M_{pl}\sqrt{\frac{3}{\xi}}, \qquad H_{\rm st} = M_{pl}\frac{\sqrt{3\lambda}}{2\xi}. \tag{3.17}$$

This identification clarifies our choice of restricting the analysis to positive values of ξ. Note that in the original and in some subsequent papers [5, 174, 175] the parameter α was fixed to $\alpha = \xi^2/\lambda$. With this choice, the R^2 term and the scalar self-interaction potential cancel at the stable fixed point, leaving only the EH contribution (3.16). As will be shown below, however, the condition $\alpha = \xi^2/\lambda$ is not compatible with a viable inflationary phase. For this reason, we treat α, ξ, and λ as independent parameters throughout our analysis. The identification in Eq. (3.16) nevertheless remains valid at late times, even in the presence of the quadratic curvature term.

Noether current

It is instructive to compute the Noether current associated with scale symmetry. While this will prove particularly useful in the EF, the calculation presented here will clarify the role of the current in the JF.

We consider an infinitesimal scale transformation defined in Eq. (2.54),

$$\phi \to e^{-\epsilon}\phi, \qquad g_{\mu\nu} \to e^{2\epsilon} g_{\mu\nu}, \tag{3.18}$$

where ϵ is an infinitesimal *constant*. A convenient method to compute the associated conserved current, commonly used in quantum field theory [178], consists in promoting the global symmetry to a local

one by allowing $\epsilon = \epsilon(x)$. In this case, the action is no longer invariant,[2] but the variation of the Lagrangian must take the form

$$\delta\mathcal{L} = (\partial_\mu \epsilon)\, h^\mu(\phi), \tag{3.19}$$

since $\delta\mathcal{L} = 0$ when ϵ is constant.

The corresponding variation of the action is then

$$\delta S = \int \mathrm{d}^4x\, \delta\mathcal{L} = -\int \mathrm{d}^4x\, \epsilon\, \partial_\mu h^\mu(\phi), \tag{3.20}$$

where we have integrated by parts and neglected boundary terms. Requiring $\delta S = 0$ on shell for arbitrary ϵ implies $\partial_\mu h^\mu = 0$, allowing us to identify h^μ as the conserved Noether current.

In a generic curved spacetime, this result can be written as

$$K^\mu \equiv \frac{1}{\sqrt{-g}} \frac{\delta S}{\delta \nabla_\mu \epsilon(x)}, \tag{3.21}$$

which makes explicit that only derivative terms in the action contribute to the current, while potential terms do not.

To proceed with the calculation for the action (3.1), it is convenient to write (3.1) as its on-shell equivalent, following the procedure outlined in [179] (see also [145] for an earlier application in the context of scale-invariant Higgs-dilaton cosmology)

$$S_J = \int \mathrm{d}^4x\sqrt{-g}\left[\left(\frac{\alpha\psi^2}{18} + \frac{\xi\phi^2}{6}\right) R - \frac{\alpha\psi^4}{36} - \frac{1}{2}\partial_\mu\phi\partial^\mu\phi - \frac{\lambda}{4}\phi^4\right]. \tag{3.22}$$

One can indeed verify that the equation of motion for the auxiliary field ψ implies $\psi^2 = R$, hence one recovers the original action (3.1). This transformation makes explicit that the R^2 term, which contains fourth-order derivatives, effectively introduces an additional scalar degree of freedom, identified with the field ψ in Eq. (3.22). As a result, the original fourth-order equations are reduced to second-order ones, significantly simplifying the analysis.

For this reason, the model is free from Ostrogradsky instabilities, as is the case for the simplest class of $f(R)$ theories. This feature will become even more transparent in the single-field description discussed below. Possible instabilities arising at the level of perturbations will instead be addressed in the next chapter.

Promoting the transformation (3.18) to a local one, we have the usual conformal transformation (see also Appendix B)

$$\begin{aligned} g_{\mu\nu} &\to e^{2\epsilon(x)} g_{\mu\nu}, \\ R &\to e^{-2\epsilon(x)}\left(R - 6\Box\epsilon(x) + \mathcal{O}\left(\epsilon^2, (\partial\epsilon)^2\right)\right), \\ \phi &\to e^{-\epsilon(x)}\phi, \\ \psi &\to e^{-\epsilon(x)}\psi. \end{aligned} \tag{3.23}$$

The conserved Noether current follows after applying the definition (3.21) with the action in Eq. (3.22) after the transformations (3.23),

$$K^\mu = (1+2\xi)\,\phi\partial^\mu\phi + \frac{2}{3}\alpha\,\psi\partial^\mu\psi. \tag{3.24}$$

We can further write

$$K^\mu = \partial^\mu K, \quad \text{with} \quad K = \frac{(1+2\xi)}{2}\phi^2 + \frac{\alpha}{3}\psi^2. \tag{3.25}$$

[2] In particular, this is not true for the action in Eq. (3.1), which would otherwise be conformally invariant.

The Noether current is covariantly conserved along the equations of motion, i.e. $\nabla_\mu K^\mu = 0$. In a spatially flat FLRW, this corresponds to

$$\ddot{K} + 3H\dot{K} = 0, \tag{3.26}$$

whose explicit solution is

$$K = c_1 + c_2 \int \frac{dt}{a^3(t)}, \tag{3.27}$$

with c_i constants of integration. This shows that in an exponentially expanding universe, $K(t)$ approaches exponentially fast a constant value, thereby breaking scale symmetry.

To gain further insight into the nature of this symmetry-breaking mechanism, it is instructive to consider Figure 3.3, which shows the numerical evolution of the system in the $(\phi, \sqrt{R})$ plane. The color scale indicates the e-folding time N associated with each point along the trajectory. The gray curve corresponds to the ellipse defined by

$$\frac{(1+2\xi)}{2}\phi^2 + \frac{\alpha}{3}(\sqrt{R})^2 = K(\phi_0, R_0), \tag{3.28}$$

where the constant value $K(\phi_0, R_0)$ is determined by the initial conditions. Note that Eq. (3.28) is precisely the asymptotic limit of the solution in Eq. (3.27), $K(t) \overset{t\to\infty}{=} c_1$, and we are considering the on-shell equivalence $\psi^2 = R$.

As can be seen from Figure 3.3, the quantity K rapidly approaches a constant value shortly after the onset of the evolution, thereby constraining the system's trajectory in the $(\phi, \sqrt{R})$ plane to lie on an ellipse. This behavior indicates that the scale symmetry breaking discussed here[3] possesses distinctive features compared to the SSB previously discussed in the context of dynamical mass generation. In particular:

- It is independent of the structure of the potential, as it is clear from the definition of the Noether current in Eq. (3.21). The shape of the ellipse is completely determined from the initial conditions (ϕ_0, R_0).
- It is realized all along the inflationary trajectory, even before the field settles at the minimum of the effective potential, corresponding to the yellow region in Figure 3.3 reached at late times.

Building on the results obtained for the JF, we now move to the EF analysis.

3.2.2 Einstein frame

In order to move to the EF, it is convenient to start from the on-shell equivalent action in Eq. (3.22). The conformal transformation then follows in a way similar to what was discussed in Sec. 2.3 for $f(R)$ theories. By writing the conformal transformation (2.27) as

$$\tilde{g}_{\mu\nu} = e^{2\omega(x)} g_{\mu\nu}, \tag{3.29}$$

and further choosing

$$\omega = \frac{1}{2} \ln \frac{2}{M^2} \left(\frac{\alpha\psi^2}{18} + \frac{\xi\phi^2}{6} \right), \tag{3.30}$$

[3] Ferreira *et al.* refer to this mechanism as *inertial symmetry breaking* [179].

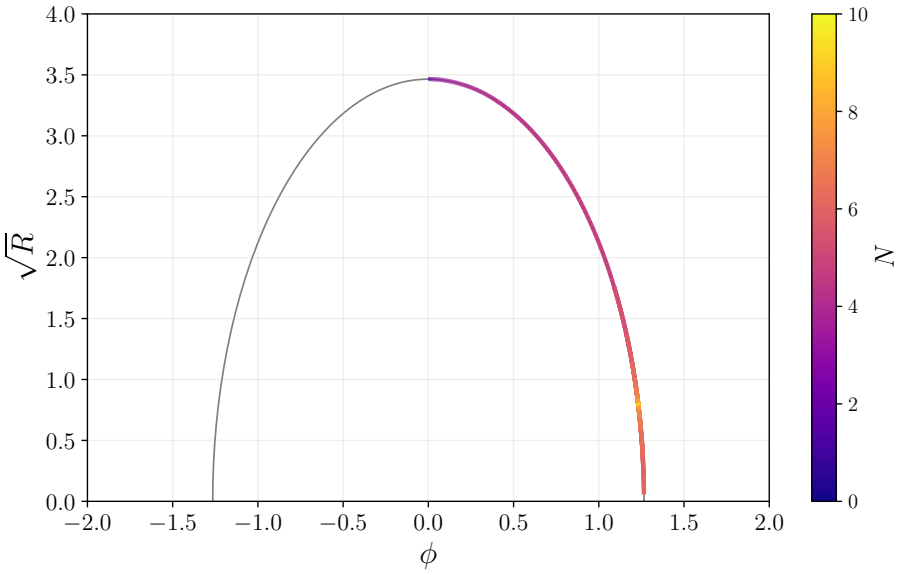

Figure 3.3: Noether current constraint in the JF. The gray curve shows the analytical ellipse given in Eq. (3.28), with R_0 and ϕ_0 fixed at the initial time of the numerical integration. The colored line traces the same numerical evolution shown in Figure 3.1, plotted parametrically here. Different colors correspond to different e-folding times N: the trajectory begins in the darker region and progresses toward the lighter shades, terminating at the yellow point marking the stable fixed point.

we obtain the EF action[4]

$$S_E = \int \mathrm{d}^4x\sqrt{-g}\left[\frac{M^2}{2}R - \frac{3M^2}{f^2}g^{\mu\nu}\partial_\mu f\partial_\nu f - \frac{f^2}{2M^2}g^{\mu\nu}\partial_\mu\phi\partial_\nu\phi - V(f,\phi)\right], \tag{3.31}$$

where

$$V(f,\phi) = -\frac{3\xi\phi^2 f^2}{2\alpha} + \frac{\Omega\phi^4 f^4}{4\alpha M^4} + \frac{9M^4}{4\alpha}, \tag{3.32}$$

We have introduced the scalar field $f \equiv Me^{-\omega(x)}$. Before moving to the dynamical analysis, some important considerations are in order:

- The EF action (3.31) makes explicit that the quadratic term $\propto R^2$ in the JF carries an additional scalar degree of freedom. Indeed, Eq. (3.31) has the form of an EH term with two propagating scalar fields, f and ϕ, subjected to a potential $V(f,\phi)$. Note that, compared to the intermediate JF action in Eq. (3.22), the additional degree of freedom has a kinetic term in the EF, resulting from the contribution $\propto g_{\mu\nu}\partial_\mu\omega\partial_\nu\omega$ in the conformal transformation of the Ricci scalar, as it is for the simpler $f(R)$ theories discussed in Sec. (2.3). At this stage, the theory therefore appears as a multifield model. Nevertheless, the two scalar fields enter the action only through the combination $f\phi$, suggesting that the effective dynamics may be reduced to a single-field description. This point will be examined in detail below.

- The mass parameter M has been introduced for dimensional consistency only, and should not be interpreted as a physical mass scale generated via SSB, such as that arising from dynamical mass generation in the JF. In particular, it was shown in [5] that M is a *redundant* parameter.

[4]We omit the tilde for EF quantities, as no ambiguity between the Jordan and the Einstein frame arises in this analysis.

Indeed, following the argument of [170], the variation of the action with respect to M vanishes upon use of the field equations. As a consequence, observable quantities computed in the EF do not, in general, depend on M, which can therefore be treated as an arbitrary parameter at this stage. We will return to this point later.

The Friedmann equations are

$$H^2 = \frac{\dot{f}^2}{f^2} + \frac{f^2\dot{\phi}^2}{6M^4} + \frac{3M^2}{4\alpha} - \frac{\xi f^2\phi^2}{2\alpha M^2} + \frac{\Omega f^4\phi^4}{12\alpha M^6}, \tag{3.33}$$

$$\dot{H} = -3\frac{\dot{f}^2}{f^2} - \frac{f^2\dot{\phi}^2}{2M^4}. \tag{3.34}$$

We then have two independent Klein-Gordon equations, obtained by varying the action (3.31) with respect to ϕ and f, respectively. They are

$$\ddot{\phi} + 3H\dot{\phi} + \frac{2\dot{\phi}\dot{f}}{f} - \frac{3\xi\phi M^2}{\alpha} + \frac{\Omega f^2\phi^3}{\alpha M^2} = 0, \tag{3.35}$$

$$\ddot{f} + 3H\dot{f} - \frac{\dot{f}^2}{f} - \frac{\dot{\phi}^2 f^3}{6M^4} - \frac{\xi\phi^2 f^3}{2\alpha M^2} + \frac{\Omega}{6\alpha}\frac{\phi^4 f^5}{M^6} = 0. \tag{3.36}$$

As further evidence that the parameter M is unrelated to the mass scale dynamically generated through scale symmetry breaking, one can verify that the equations of motion (3.33)–(3.36) are unaltered under the (active) dilatation transformations in Eqs. (2.51)–(2.53), which act as

$$H(t) \to \ell H(\ell t), \qquad \phi(t) \to \ell\phi(\ell t), \qquad f(t) \to \ell f(\ell t), \qquad M \to \ell M, \tag{3.37}$$

showing that scale invariance is preserved in the EF at the level of the equations of motion.

Analogously to the JF, we can perform a stability analysis of the EF equations of motion. Since this analysis closely parallels the one carried out previously, we restrict ourselves to summarizing the main results; see also [176] for a related discussion. It is worth noting that the dynamics are entirely determined by the second Friedmann equation and the Klein-Gordon equations, while the first Friedmann equation in (3.33) plays the role of a constraint, fixing the Hubble parameter in the EF.

We find that the EF system also admits two classes of fixed points, with the same qualitative nature as in the JF: a saddle point and a stable fixed point. In the following, we therefore limit ourselves to reporting the values of the relevant physical quantities at these fixed points, omitting the explicit form of the linearized solutions.

Unstable fixed point: P_1

The saddle point is defined by

$$f_{\rm unst} = \text{arbitrary}, \quad \dot{f}_{\rm unst} = \phi_{\rm unst} = \dot{\phi}_{\rm unst} = 0, \quad H_{\rm unst} = \frac{\sqrt{3}M}{2\sqrt{\alpha}}, \tag{3.38}$$

where we note that the arbitrariness of the Hubble parameter in the JF, see Eq. (3.11), has been entirely absorbed in the scalar field f entering the conformal transformation.

Stable fixed point: P_2

The stable attractor is defined by

$$f_{\rm st} = \sqrt{\frac{3\xi}{\Omega}}\frac{M^2}{\phi_{\rm st}}, \quad \phi_{\rm st} = \text{arbitrary}, \quad \dot{f}_{\rm st} = \dot{\phi}_{\rm st} = 0, \quad H_{\rm st} = \sqrt{\frac{\alpha\lambda}{\Omega}}H_{\rm unst} = \frac{\sqrt{3\lambda}M}{2\sqrt{\Omega}}. \tag{3.39}$$

Note that the ratio between the Hubble parameter at the stable and unstable fixed points is uniquely determined by the model parameters.

To gain insight into the relation between the mass parameter M and the Planck mass dynamically generated in the JF through Eq. (2.57), it is helpful to consider the relation between the Hubble parameters in the two frames. Generalizing Eq. (2.35) to an arbitrary conformal factor and evaluating it at the stable fixed point – where all time derivatives vanish – we obtain

$$\tilde{H}_{\rm st} = e^{-\omega} H_{\rm st} = \frac{\tilde{f}_{\rm st}}{M} H_{\rm st}, \tag{3.40}$$

where we have restored the notation with a tilde denoting EF quantities. Employing Eq. (3.39) to write $\tilde{H}_{\rm st}$ and $\tilde{f}_{\rm st}$ and Eq. (3.17) to write $H_{\rm st}$, we have

$$\frac{\sqrt{3\lambda}}{2\sqrt{\Omega}} M = \sqrt{\frac{3\xi}{\Omega}} \frac{M}{\tilde{\phi}_{\rm st}} M_{pl} \frac{\sqrt{3\lambda}}{2\xi} \longrightarrow \tilde{\phi}_{\rm st} = \sqrt{\frac{3}{\xi}} M_{pl} = \phi_{\rm st}, \tag{3.41}$$

Thus, the value of the scalar field at the stable fixed point is the same in both frames, as expected since the conformal transformation does not rescale ϕ. Therefore, the EF fields at the stable fixed point are fixed as

$$f_{\rm st} = \frac{\xi}{\sqrt{\Omega}} \frac{M^2}{M_{pl}}, \qquad \phi_{\rm st} = \sqrt{\frac{3}{\xi}} M_{pl}. \tag{3.42}$$

There are no means, at this level, to determine the value of M, which cancels out in Eq. (3.41).

A natural choice, given that M appears in the EH term of the action (3.31), is to identify it with the Planck mass. At first sight, this identification may appear puzzling, since an analogous identification was already made in the JF, where the Ricci scalar differs from its EF counterpart. We now show that no inconsistency arises by comparing the two identifications,

$$\text{JF}: \frac{\xi}{6}\phi_{\rm st}^2 R \longrightarrow \frac{M_{pl}^2}{2} R, \qquad \text{EF}: \frac{M^2}{2}\tilde{R} \longrightarrow \frac{M_{pl}^2}{2}\tilde{R}. \tag{3.43}$$

Since the identification in the JF is meaningful only at the stable fixed point, any comparison must be performed there. At this point, the Ricci scalars are related by $R = \Omega^2 \tilde{R}$. Consequently, the EH term in the JF is proportional to $M_{pl}^2 \Omega^2 \tilde{R}$, while in the EF it is proportional to $M_{pl}^2 \tilde{R}$. These expressions are fully consistent once one recalls, as discussed in Sec. 2.3.3, that mass units rescale when passing from the JF to the EF.

To make this explicit, suppose that we can measure the coefficient of the EH term. In the EF, what is physically accessible is the dimensionless ratio $M_{pl}^2/\tilde{m}_u^2$, where $\tilde{m}_u$ denotes a reference mass unit. In the JF, the corresponding measured quantity is $M_{pl}^2\Omega^2/m_u^2$. Since the mass units in the two frames are related by $\tilde{m}_u = \Omega^{-1} m_u$, the two measurements yield identical results. For this reason, we will henceforth identify

$$M = M_{pl}. \tag{3.44}$$

We represent in Figure 3.4 the numerical evolution of the fields and the Hubble parameter, as a function of the e-folding time. As done for the JF, the parameters and initial conditions are chosen to visually enhance the transition from the unstable to the stable fixed point through damped oscillations, and are not, in general, the ones that provide a viable inflationary phase.

Noether current and field redefinition

Similarly to what has been done in the JF, we compute the Noether current associated with scale symmetry. Acting with a local Weyl transformation on the EF metric and the fields, as in Eq. (3.23),

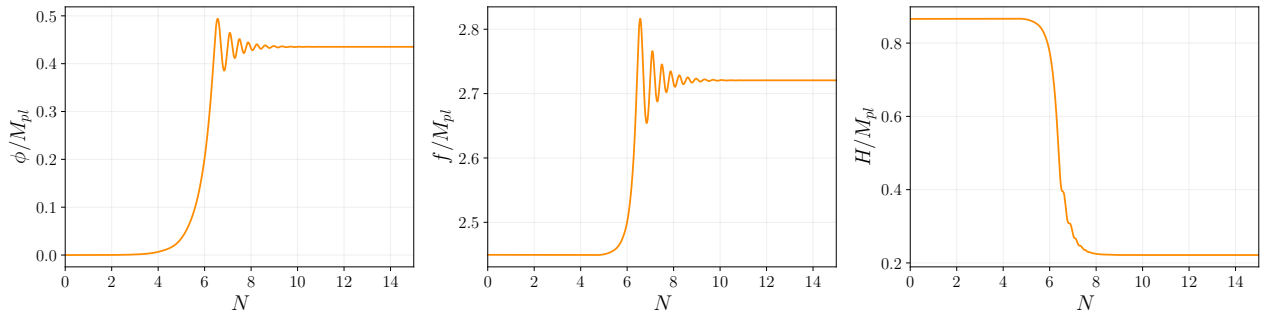

Figure 3.4: Numerical evolution of the scalar field ϕ (*left panel*), f (*central panel*), and the Hubble parameter (*right panel*) in the EF, obtained from the equations of motion (3.33)–(3.36) in e-folding time N. The parameters are fixed to $\alpha = 1, \xi = 2, \Omega = 1.07\,\xi^2$. The initial conditions are set to: $\phi(0) = 10^{-5}\,M_{pl}$, $f(0) = \sqrt{6}\,M_{pl}$, $H(0) = H_{\rm st}$, $\phi'(0) = f'(0) = 0$.

the conserved current can be computed from the definition (3.21). It reads

$$K^\mu = \phi\partial^\mu\phi - 6\frac{M^4}{f^3}\partial^\mu f, \tag{3.45}$$

which can be written as

$$K^\mu = \partial^\mu K, \quad \text{with} \quad K = \frac{M_{pl}^2}{2}\left(\frac{\phi^2}{M_{pl}^2} + \frac{6M_{pl}^2}{f^2}\right). \tag{3.46}$$

In complete analogy with the JF analysis, the Noether current is covariantly conserved along the equations of motion $\nabla_\mu K^\mu = 0$ and K approaches a constant value, thereby breaking scale symmetry. Eq. (3.45) makes it manifest that the conserved current is independent of the scalar potential, as its expression does not involve the parameters α, ξ, or λ.

As a further check that the dynamics are constrained after symmetry breaking, see Figure 3.5, where the gray line corresponds to the ellipse with equation

$$\frac{M_{pl}^2}{2}\left[\left(\frac{\phi}{M_{pl}}\right)^2 + 6M_{pl}^2(f^{-1})^2\right] = K(\phi_0, f_0), \tag{3.47}$$

and the colored line describes the same numerical evolution represented in Figure (3.4). As in the JF, the dynamics are constrained to an ellipse in the (ϕ, f^{-1}) plane, whose shape is uniquely fixed by the initial values of the fields.

The constraint imposed by the Noether current implies that, for any initial value of $K(\phi_0, f_0)$, the field f can be entirely expressed in terms of ϕ, and vice versa. This fact suggests that the dynamical content of the model in the EF can effectively be reduced to a single scalar degree of freedom. To further develop this idea, we make use of the constraint (3.46) to introduce two new fields, ρ and χ, defined as

$$\rho = \sqrt{6}M_{pl}\,\text{arcsinh}\left(\frac{\phi f}{\sqrt{6}M_{pl}^2}\right), \tag{3.48}$$

$$\chi = \frac{M_{pl}}{2}\ln\left(\frac{\phi^2}{2M_{pl}^2} + \frac{3M_{pl}^2}{f^2}\right), \tag{3.49}$$

where one can immediately notice that the argument of the logarithm in Eq. (3.49) carries the same dynamical content of K in Eq. (3.46).

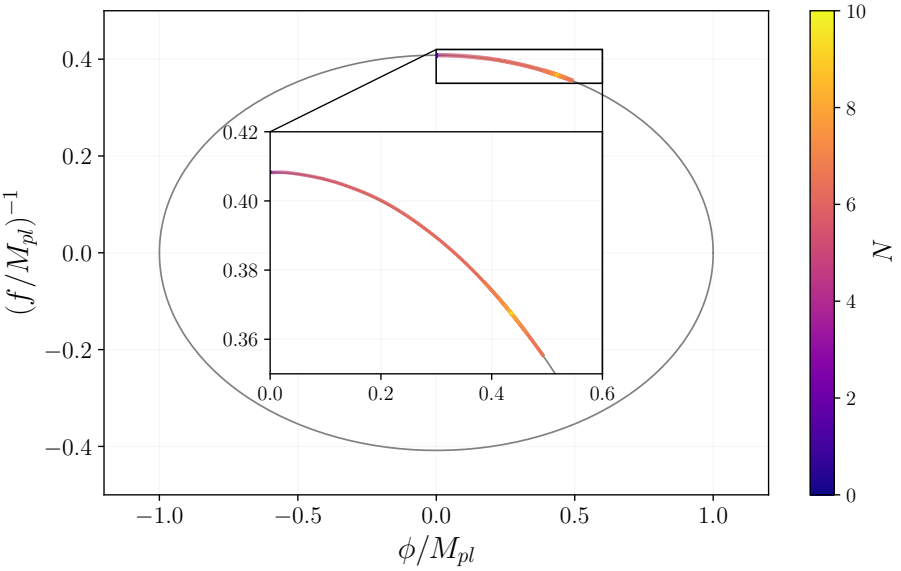

Figure 3.5: Noether current constraint in the EF. The gray curve shows the analytical ellipse given in Eq. (3.47), with ϕ_0 and f_0 fixed at the initial time of the numerical integration. The colored line traces the same numerical evolution shown in Figure 3.4, here plotted parametrically. Different colors correspond to different e-folding times N: the trajectory begins in the darker region and progresses toward the lighter shades, terminating at the yellow point marking the stable fixed point. The inset shows a zoom-in of the trajectory.

When written in terms of the new fields, the EF action (3.31) becomes

$$S_E = \int \mathrm{d}^4x\sqrt{-g}\left[\frac{M_{pl}^2}{2}R - \frac{1}{2}g^{\mu\nu}\partial_\mu\rho\partial_\nu\rho - 3\cosh^2\left(\frac{\rho}{\sqrt{6}M_{pl}}\right)g^{\mu\nu}\partial_\mu\chi\partial_\nu\chi - V(\rho)\right], \tag{3.50}$$

where the potential depends exclusively on ρ and is defined as

$$V(\rho) = \frac{9M_{pl}^4}{4\alpha}\left[1 - 4\xi\sinh^2\left(\frac{\rho}{\sqrt{6}M_{pl}}\right) + 4\Omega\sinh^4\left(\frac{\rho}{\sqrt{6}M_{pl}}\right)\right]. \tag{3.51}$$

An alternative way to identify the fields (ρ, χ) consists of requiring that scale transformations act on a single field only, namely ρ. Furthermore, ρ can always be defined so that scale transformations correspond to a shift symmetry of the form $\rho \to \rho + \sigma M_{pl}$, where σ is the infinitesimal transformation parameter. This construction has been adopted, for instance, in [145, 174].

Overall, it is clear that χ plays the role of the *Goldstone boson* of the theory, namely the massless mode associated with the flat directions of the potential [180]: when scale symmetry is broken, K approaches a constant value and, as a consequence, so does χ. The relevant degree of freedom governing the inflationary dynamics is therefore ρ, in agreement with the fact that the potential depends only on this field, $V = V(\rho)$.

As will be more clear and thoroughly tested in the following, the inflationary dynamics are effectively single-field, with ρ playing the role of the *inflaton*.

The potential in Eq. (3.51) admits stationary points at

$$\rho_{\max} = 0, \qquad \rho_{\min} = \pm\sqrt{6}M_{pl}\,\mathrm{arcsinh}\left(\sqrt{\frac{\xi}{2\Omega}}\right), \tag{3.52}$$

corresponding, respectively, to a local maximum and two symmetric minima, provided that $\xi/\alpha > 0$ and $\xi/\Omega > 0$. Hence, the single-field potential acquires a Mexican-hat profile, as displayed in Figure 3.6,

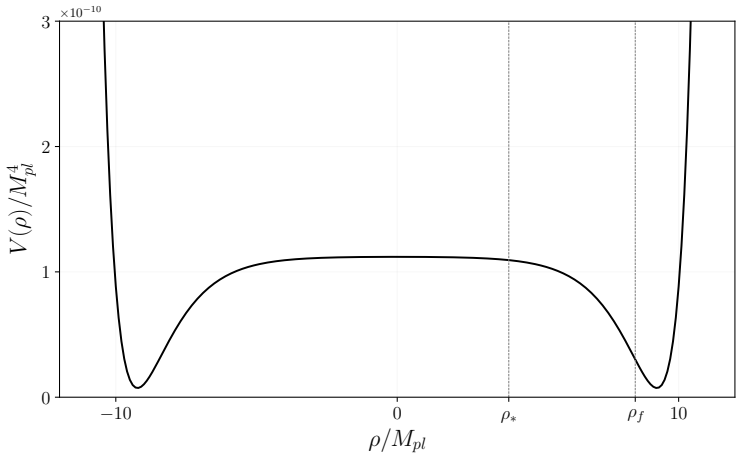

Figure 3.6: Single field potential $V(\rho)$ in the EF for the scale-invariant model (3.1), as defined in Eq. (3.51). The parameters are fixed to: $\xi = 10^{-3}, \Omega = 1.07\,\xi^2$, and $\alpha = 2 \times 10^{10}$, corresponding to a viable inflationary trajectory in agreement with the observational bounds, see Eqs. (3.80)–(3.81).

when α, ξ, and Ω share the same sign. Furthermore, since α controls the overall height of the potential, it must be positive to ensure a positive energy scale, in line with our initial assumption of positive model parameters. We remark, however, that λ may in principle take negative values, as long as it satisfies

$$\lambda > -\frac{\xi^2}{\alpha}. \tag{3.53}$$

Under the assumption of a positive λ, the minima shift towards larger values for smaller ξ. At the extrema, the potential takes the values

$$V_{\max} = \frac{9M_{pl}^4}{4\alpha}, \qquad V_{\min} = \frac{9\lambda M_{pl}^4}{4\Omega}. \tag{3.54}$$

We can thus draw some simple considerations:

- Under the assumption that α, λ, and ξ are positive, $V_{\min} > 0$;
- $V_{\min} \neq 0$, unless $\lambda = 0$;
- If $-\xi^2/\alpha < \lambda < 0$, the potential preserves a Mexican hat structure but now $V_{\min} < 0$.

As will become clearer in the following, this feature has important consequences for inflationary dynamics, the graceful exit into a radiation-dominated era, and the emergence of a residual cosmological constant.

In the (ρ, χ) representation, the Klein-Gordon equations for the two fields are

$$\ddot{\rho} + 3H\dot{\rho} - \frac{\sqrt{6}}{2M_{pl}} \sinh\left(\frac{2\rho}{\sqrt{6}M_{pl}}\right) \dot{\chi}^2 + \frac{\mathrm{d}V(\rho)}{\mathrm{d}\rho} = 0, \tag{3.55}$$

$$\ddot{\chi} + 3H\dot{\chi} + \frac{2}{\sqrt{6}M_{pl}} \tanh\left(\frac{\rho}{\sqrt{6}M_{pl}}\right) \dot{\chi}\dot{\rho} = 0. \tag{3.56}$$

The Friedmann equations are

$$H^2 = \frac{\dot{\rho}^2}{6M_{pl}^2} + \frac{1}{M_{pl}^2} \cosh^2\left(\frac{\rho}{\sqrt{6}M_{pl}}\right) \dot{\chi}^2 + \frac{V(\rho)}{3M_{pl}^2}, \tag{3.57}$$

$$\dot{H} = -\frac{\dot{\rho}^2}{2M_{pl}^2} - \frac{3}{M_{pl}^2} \cosh^2\left(\frac{\rho}{\sqrt{6}M_{pl}}\right) \dot{\chi}^2. \tag{3.58}$$

Since the transformation amounts to a simple field redefinition, the stability analysis remains unchanged with respect to the formulation in terms of the original fields (ϕ, f). Accordingly, the extrema of the potential correspond to an unstable fixed point at the local maximum $\rho_{\max}$ and to stable fixed points at the minima $\rho_{\min}$. From Eq. (3.56), one immediately observes that $\dot{\chi} = 0$ is a solution, implying that $\chi = \text{const.}$ throughout the cosmological evolution. It was shown in [176] via a full stability analysis that this constant-χ solution is, in fact, an attractor, stable under variations of the initial conditions. In an expanding FLRW spacetime, this behavior is fully consistent with the asymptotic solution for K given in Eq. (3.27).

In Figure (3.7), we represent the numerical evolution of the fields and the Hubble parameter as a function of the e-folding time. For a better comparison, the same parameters and initial conditions adopted in the (ϕ, f) representation in Figure 3.4 were considered. As expected, the evolution of the Hubble parameter is identical in the two descriptions. The field ρ exhibits a smooth evolution from the local maximum $\rho_{\max}$ toward the positive minimum $\rho_{\min}$, which is reached through damped oscillations, while the field χ remains exactly constant throughout the evolution. It is worth noting that the same result could equivalently be obtained directly from the numerical solutions in Figure 3.4 by applying the field redefinitions in Eqs. (3.48)–(3.49). In particular, the specific combination of ϕ and f entering the definition of χ leads to an exact cancellation of their oscillatory behavior, yielding the constant solution shown in Figure 3.7.

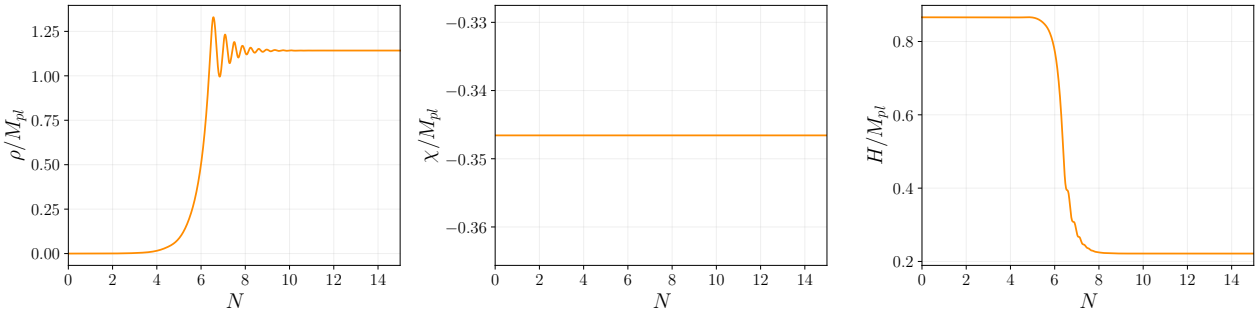

Figure 3.7: Numerical evolution of the scalar field ρ (*left panel*), χ (*central panel*), and the Hubble parameter (*right panel*) in the EF, obtained from the equations of motion (3.55), (3.56), and (1.5) in e-folding time N. The parameters are fixed to $\alpha = 1, \xi = 2, \Omega = 1.07\,\xi^2$. The initial conditions are set to: $\rho(0) = 2.5 \times 10^{-5}\ M_{pl}, \chi(0) = -0.35\,M_{pl}, H(0) = H_{\rm st}, \rho'(0) = \chi'(0) = 0$, in order to match the corresponding initial conditions in the (ϕ, f) representation displayed in Figure 3.4.

3.3 Slow-roll inflation

To study the inflationary dynamics, it is particularly convenient to work in the EF and in the effective single-field representation (ρ, χ). In this setting, the standard slow-roll formalism – introduced in Sec. 1.3.1, applied to the computation of spectral indices in Sec. 1.4.5, and discussed in the context of Starobinsky inflation in Sec. 2.3.4 – can be straightforwardly employed. At this stage, we restrict the analysis to the homogeneous background, while a complete treatment including perturbations will be presented in Chapter 4.[5]

[5]In practice, the application of the single-field results of Sec. 1.4.5 to the computation of the spectral indices in the present model implicitly assumes that the Goldstone mode is completely decoupled from the dynamics, including at the level of perturbations. Testing the validity of this assumption is therefore essential.

The relevant equations of motion in the slow-roll approximation $\dot{\rho}^2 \ll V(\rho), |\ddot{\rho}| \ll |H\dot{\rho}|$ reduce to

$$3H\dot{\rho} \simeq -\frac{\mathrm{d}V(\rho)}{\mathrm{d}\rho}, \qquad H^2 \simeq \frac{V(\rho)}{3M_{pl}^2}, \tag{3.59}$$

while the slow-roll parameters, see Eq. (2.45), are

$$\begin{aligned}
\epsilon &\simeq \frac{M_{pl}^2}{2}\left(\frac{V_{,\rho}}{V}\right)^2 = \frac{4\left[\xi+\Omega-\Omega\cosh\left(\sqrt{\frac{2}{3}}\frac{\rho}{M_{pl}}\right)\right]^2\sinh^2\left(\sqrt{\frac{2}{3}}\frac{\rho}{M_{pl}}\right)}{3\left[4\,\xi\sinh^2\left(\frac{\rho}{\sqrt{6}M_{pl}}\right)-4\,\Omega\sinh^4\left(\frac{\rho}{\sqrt{6}M_{pl}}\right)-1\right]^2}, \\
\eta &\simeq -\epsilon + M_{pl}^2\frac{V_{,\rho\rho}}{V} = -\epsilon + \frac{4\,(\xi+\Omega)\cosh\left(\sqrt{\frac{2}{3}}\frac{\rho}{M_{pl}}\right)-4\,\Omega\cosh\left(2\sqrt{\frac{2}{3}}\frac{\rho}{M_{pl}}\right)}{3\left[4\,\xi\sinh^2\left(\frac{\rho}{\sqrt{6}M_{pl}}\right)-4\,\Omega\sinh^4\left(\frac{\rho}{\sqrt{6}M_{pl}}\right)-1\right]}.
\end{aligned} \tag{3.60}$$

In the asymptotic limit $\rho/M_{pl} \to \infty$, they both approach the constant value

$$\lim_{\rho\to\infty}\epsilon(\rho) = \lim_{\rho\to\infty}\eta(\rho) = \frac{4}{3}, \tag{3.61}$$

which is greater than unity, suggesting that inflation cannot proceed as the field moves along the potential from right to left, as in some other single-field models [48]. Consistent with the nature of the fixed points, we consider the case in which ρ evolves from the unstable to the stable fixed point, and we investigate the conditions under which inflation can occur along this trajectory. Moreover,

$$\lim_{\rho\to 0}\epsilon(\rho) = 0, \qquad \lim_{\rho\to 0}\eta(\rho) = -\frac{4}{3}\xi, \tag{3.62}$$

therefore to have the slow-roll condition $\epsilon, |\eta| \ll 1$ satisfied close to $\rho_{\max}$, we must impose[6]

$$\boxed{\xi \ll \frac{3}{4}}. \tag{3.63}$$

As anticipated above, having a non-vanishing potential at the minima has crucial consequences for inflation. Since, by definition, $\epsilon(\rho_{\max}) = \epsilon(\rho_{\min}) = 0$, and ϵ is a semi-positive definite function, ϵ must have a local maximum $\bar{\rho}$ in the range $[0, \rho_{\min}]$. We further note that, with the definitions of ϵ and η adopted here, imposing the stationarity of ϵ we have $\epsilon(\bar{\rho}) = \eta(\bar{\rho})$. However, if $\epsilon(\bar{\rho}) < 1$, see the first panel in Figure 3.8, inflation does not end by violation of the slow-roll condition before the field ρ has settled to the minimum. Clearly, this is not possible, since the number of e-folds elapsed from horizon crossing is, see Eq. (2.46),

$$N = -\frac{1}{M_{pl}}\int_{\rho_i}^{\rho}\frac{\mathrm{d}\rho}{\sqrt{2\epsilon}}, \tag{3.64}$$

which diverges at $\epsilon(\rho_{\min}) = 0$. This means that any scenario in which $\epsilon(\bar{\rho}) < 1$ must be discarded, as physically unrealizable: inflation would never end, with the inflaton asymptotically approaching the minimum of the potential. In the following, we will sometimes refer to this case as *eternal inflation*.

This behavior is reminiscent of the Kähler Moduli Inflation I (KMII) scenario (see, e.g., [48]), as can be inferred from the qualitative form of the slow-roll parameter ϵ. However, unlike that case, in the present model, one must also discard a hypothetical inflationary phase in which the field rolls down the potential from right to left, as already discussed above.

We now aim to constrain the model's parameter space analytically by setting the conditions for which $\epsilon(\bar{\rho}) > 1$. Note that this fact was not considered in [5, 174].

[6] Note that this condition automatically excludes the parameter choice adopted in Figures 3.1, 3.4, and 3.7.

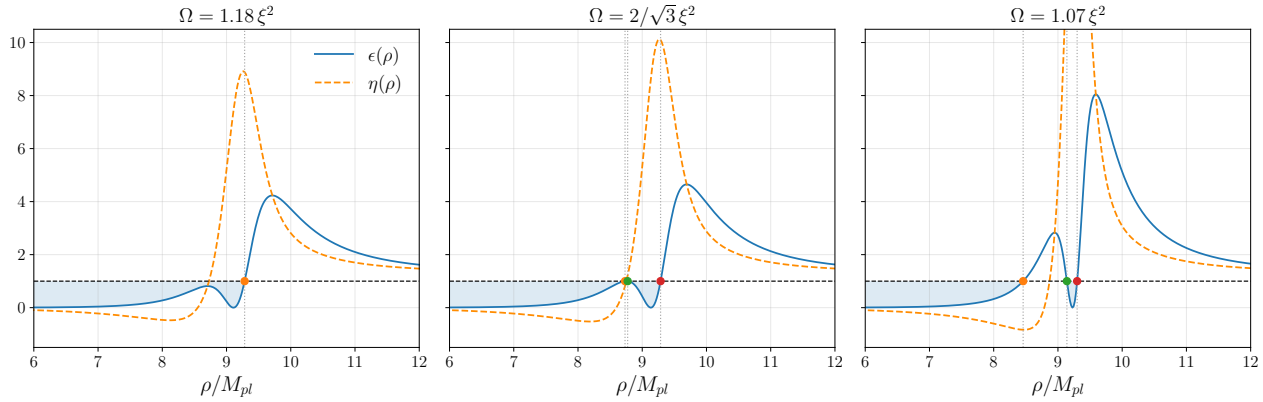

Figure 3.8: Slow-roll parameters ϵ and η for the inflaton ρ in the EF, as defined in (3.60) for $\xi = 10^{-3}$ and three different choices of Ω representing different scenarios. The orange, green, and red dots mark the first, second, and third positive roots of $\epsilon(\rho) = 1$, respectively. *Left panel:* $\Omega > 2/\sqrt{3}\,\xi^2$, corresponding to $\epsilon(\bar{\rho}) < 1$. Inflation does not stop by slow-roll violation and is eternal; *Central panel:* $\Omega = 2/\sqrt{3}\,\xi^2$, corresponding to $\epsilon(\bar{\rho}) \simeq 1$. The first two positive roots are approximately degenerate. Inflation ends at $\bar{\rho} < \rho_{\rm min}$; *Right panel:* $\Omega < 2/\sqrt{3}\,\xi^2$, corresponding to $\epsilon(\bar{\rho}) > 1$. Inflation stops at the first positive root, corresponding to the orange dot.

3.3.1 Approximate constraints

Computing $\epsilon(\bar{\rho})$ or solving the condition $\epsilon(\rho) = 1$ is analytically cumbersome, as it requires solving a fourth-order polynomial equation. To gain further analytical insight, we therefore resort to the large-field approximation $\rho/M_{pl} \gg 1$, which will turn out to be an excellent approximation within the regime of validity of the model.

At the level of the potential, taking the large-field approximation corresponds to replacing the hyperbolic sine with its dominant exponential term, $\sinh x \simeq e^x/2$ for $x \gg 1$,

$$V(\rho) \to \tilde{V}(\rho) = \frac{9M_{pl}^4}{4\alpha}\left[1 - \xi\,\exp\left(\sqrt{\frac{2}{3}}\frac{\rho}{M_{pl}}\right) + \frac{\Omega}{4}\exp\left(2\sqrt{\frac{2}{3}}\frac{\rho}{M_{pl}}\right)\right]. \tag{3.65}$$

Note that it is crucial to consider the $\rho/M_{pl} > 0$ branch of the potential at this level since the large-field approximation has led to the breaking of the parity invariance characterizing the original potential $V(\rho)$.

Figure 3.9 (right panel) compares the exact potential $V(\rho)$ with its large-field approximation $\tilde{V}(\rho)$. The approximation becomes increasingly accurate for smaller values of ξ, and, in view of the bound in Eq. (3.63), is fully reliable in our case.

The approximate form of the first slow-roll parameter can be computed by applying the usual definition (2.45) to the approximate potential $\tilde{V}(\rho)$. We obtain

$$\epsilon \simeq \frac{M_{pl}^2}{2}\left(\frac{\tilde{V}_{,\rho}}{\tilde{V}}\right)^2 = \frac{4x^2\,(\Omega x - 2\xi)^2}{3\,(4 - 4\xi x + \Omega x^2)^2}, \qquad x \equiv \exp\left(\sqrt{\frac{2}{3}}\frac{\rho}{M_{pl}}\right) \gg 1. \tag{3.66}$$

Solving for $\epsilon = 1$ we find four solutions,

$$\begin{aligned} x_{1,2} &= \frac{2\left(\sqrt{3}-1\right)\xi}{\Omega} \pm \frac{2}{\Omega}\sqrt{\left(3-2\sqrt{3}\right)\Omega - 2\left(\sqrt{3}-2\right)\xi^2}, \\ x_{3,4} &= -\frac{2\left(\sqrt{3}+1\right)\xi}{\Omega} \pm \frac{2}{\Omega}\sqrt{\left(3+2\sqrt{3}\right)\Omega + 2\left(\sqrt{3}+2\right)\xi^2}, \end{aligned} \tag{3.67}$$

corresponding to four real values – three positive and a negative one, due to the breaking of parity invariance – provided the square root appearing in $x_{1,2}$ is positive definite, that is

$$\Omega \lesssim \frac{2}{\sqrt{3}}\,\xi^2 \simeq 1.1547\,\xi^2, \tag{3.68}$$

where the equality applies to the case $x_1 = x_2$. This automatically implies a constraint on the allowed parameter space for viable slow-roll inflation. Together with the fact that we are considering $\alpha, \lambda > 0$, this condition restricts the allowed values of Ω to the rather narrow range

$$\boxed{\xi^2 < \Omega \lesssim \frac{2}{\sqrt{3}}\,\xi^2}. \tag{3.69}$$

Notably, the case $\Omega = 2\xi^2$ considered in [5, 174] is excluded.

From Figure 3.8, one observes that when $\Omega = 2/(\sqrt{3}\,\xi^2)$ the first two positive solutions become nearly degenerate, yielding $\epsilon(\bar{\rho}) \simeq 1$. In this case, viable inflation is realized only in the scenarios shown in the second and third panels of Figure 3.8.

Taken together, the bounds in Eqs. (3.63) and (3.69) represent approximate constraints required to achieve slow-roll inflation while avoiding eternal inflation. In this parameter regime, inflation ends at the first positive solution of Eq. (3.67), corresponding to

$$\rho_f = M_{pl}\sqrt{\frac{3}{2}}\ln\left[\frac{2\left(\sqrt{3}-1\right)\xi}{\Omega} - \frac{2}{\Omega}\sqrt{\left(3-2\sqrt{3}\right)\Omega - 2\left(\sqrt{3}-2\right)\xi^2}\right]. \tag{3.70}$$

The approximate bound derived in Eq. (3.69) suggests that, within the relevant parameter range, Ω scales approximately quadratically with ξ. This expectation is tested in Figure 3.9 (left panel), where the quadratic behavior is compared with the full numerical result and with a polynomial fit. In particular, fitting the bound up to fourth order in ξ, we find

$$\Omega = a_1\xi + a_2\xi^2 + a_3\xi^3 + a_4\xi^4, \tag{3.71}$$

with coefficients $a_1 = 2.5 \times 10^{-11}$, $a_2 = 1.15$, $a_3 = 0.36$, and $a_4 = 0.03$. This result confirms the reliability of the approximate bound and supports the validity of expanding $\Omega \simeq \beta\,\xi^2$, with $\beta > 1$, in the small-ξ regime.

3.3.2 Spectral indices

To correctly evaluate the slow-roll expressions for the spectral indices at the CMB scale, we must compute the number of e-folds from Eq. (3.64) and invert it to obtain $\rho(N)$. To this end, we again resort to the large-field approximation and employ the approximate potential introduced in Eq. (3.65). This yields

$$N(\rho) \simeq -\frac{1}{M^2}\int \frac{\tilde{V}}{\tilde{V}_{,\rho}}\,\mathrm{d}\rho \simeq \sqrt{\frac{3}{2}}\int \frac{\mathrm{d}x}{x\sqrt{2\epsilon(x)}} \simeq \frac{3}{2\xi x} + \frac{3}{4}\ln x, \tag{3.72}$$

where, in the final step, we have adopted the leading-order expansion $\Omega \to \xi^2$, in accordance with the considerations discussed above. By solving for $x(N)$ and restoring the field ρ, we find the convenient expression

$$\rho(\Delta N) \simeq \sqrt{\frac{3}{2}}M\ln\left[-\frac{2}{\xi}W_{-1}^{-1}\left[-\frac{2}{\xi x_f}\exp\left(-\frac{4}{3}\Delta N - \frac{2}{\xi x_f}\right)\right]\right], \tag{3.73}$$

where $\Delta N > 0$ counts the e-folding time elapsed from a given N – which could correspond to horizon crossing[7] – to the end of inflation, and W_{-1} is the lower branch of the W Lambert function, see [176]

[7] To clarify better the notational convention adopted here for the e-folding number, the value of ρ at horizon crossing would correspond to $\rho_* = \rho(\Delta N = 55)$.

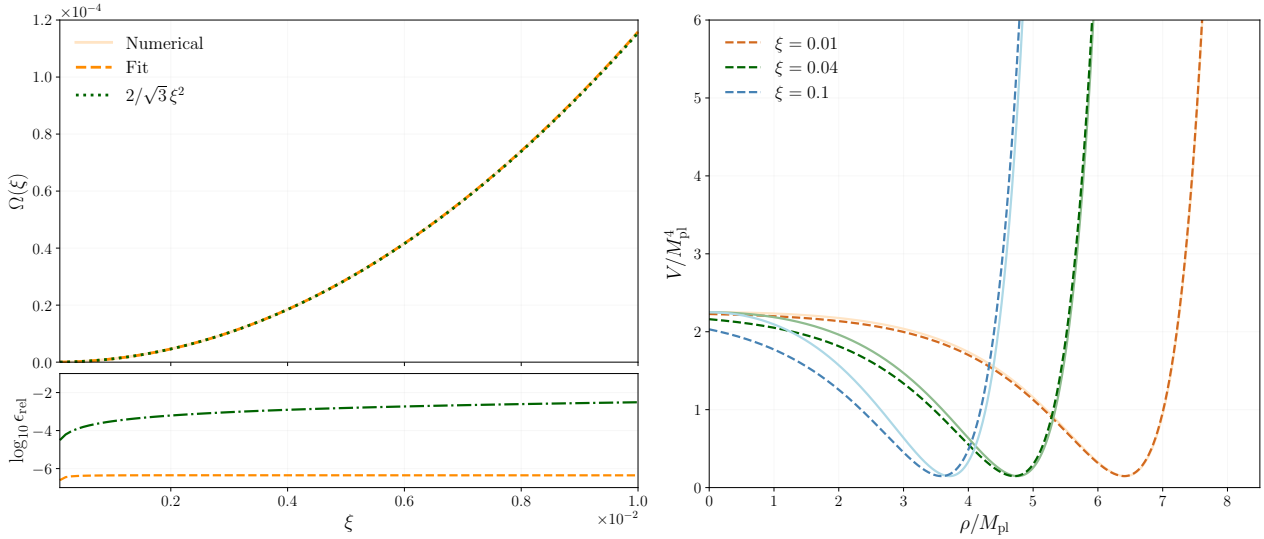

Figure 3.9: Validity tests of the large-field approximation. *Left panel*: comparison between the approximate bound on Ω reported in Eq. (3.69) (green dash-dotted line), the exact one obtained numerically (light orange solid line), and a polynomial fit to it (orange dashed line). The polynomial fit is obtained using the functional form in Eq. (3.71), restricted to the range $\xi \in [10^{-4}, 10^{-2}]$. The lower panel shows the logarithm of the relative error in the two approximations, defined as $\epsilon_{\rm rel} = |y - \bar{y}|/|\bar{y}|$, where $\bar{y}$ denotes the exact result and y the approximate one. *Right panel*: Comparison between the exact potential defined in Eq. (3.51) (light solid lines) and its large-field approximation in Eq. (3.65) (dark dashed lines), for different values of ξ and with Ω fixed to $\Omega = 1.07\,\xi^2$.

for more details.

If we use Eq. (3.73) to compute observables at horizon crossing, we implicitly assume that the large-field approximation is valid all the way up to the plateau of the potential. Another option to analytically compute the integral in Eq. (3.72) without explicitly relying on the large-field approximation is to consider the lowest order expansion of the first slow-roll parameter for $\xi \to 0$. In particular, we can take the exact expression for ϵ as defined in (3.60) and replace $\Omega \to \beta\xi^2$ for any $\beta > 1$, as motivated above. Expanding for $\xi \ll 1$, we have

$$\epsilon \simeq \frac{4}{3}\xi^2 \sinh^2\left(\sqrt{\frac{2}{3}}\frac{\rho}{M_{pl}}\right), \tag{3.74}$$

independent of β. The integral equation for the e-folding number now reduces to

$$N(\rho) \simeq \frac{1}{M_{pl}}\int \frac{\mathrm{d}\rho}{\sqrt{2\epsilon}} \simeq \frac{3}{4\xi}\ln\left(\tanh\left(\frac{\rho}{\sqrt{6}M_{pl}}\right)\right), \tag{3.75}$$

which is a monotonically increasing function. We obtain

$$\rho(\Delta N) = \sqrt{6}M_{pl}\,\mathrm{arctanh}\left(\exp\left(\frac{4}{3}\xi(N_f - \Delta N)\right)\right), \tag{3.76}$$

where $N_f \equiv N(\rho_f)$ is the number of e-folds from Eq. (3.75) evaluated at ρ_f in Eq. (3.70).

The spectral indices can be computed to leading order in the slow-roll approximation from the results of Eq. (2.48),

$$n_s - 1 = 2\eta - 4\epsilon, \qquad r = 16\epsilon, \tag{3.77}$$

and then evaluated at horizon crossing, fixing ΔN in Eq. (3.73) or (3.76).

In Figure 3.10, we plot the model's predictions in the same (n_s, r) plane of Figure 1.6, using the exact expressions for the slow-roll parameters in Eq. (3.60) and the approximate result obtained in the large-field approximation for ρ at horizon crossing and at the end of inflation. Since the bound on Ω derived in Eq. (3.69) is particularly stringent, we fix $\Omega = 1.07\,\xi^2$ and vary $\xi \in [10^{-3},\, 2\times 10^{-2}]$ (shown by the colored map) and $N_* \in [50,\, 60]$, with $N_* = 50$ and $N_* = 60$ corresponding to the upper and lower colored curves, respectively.

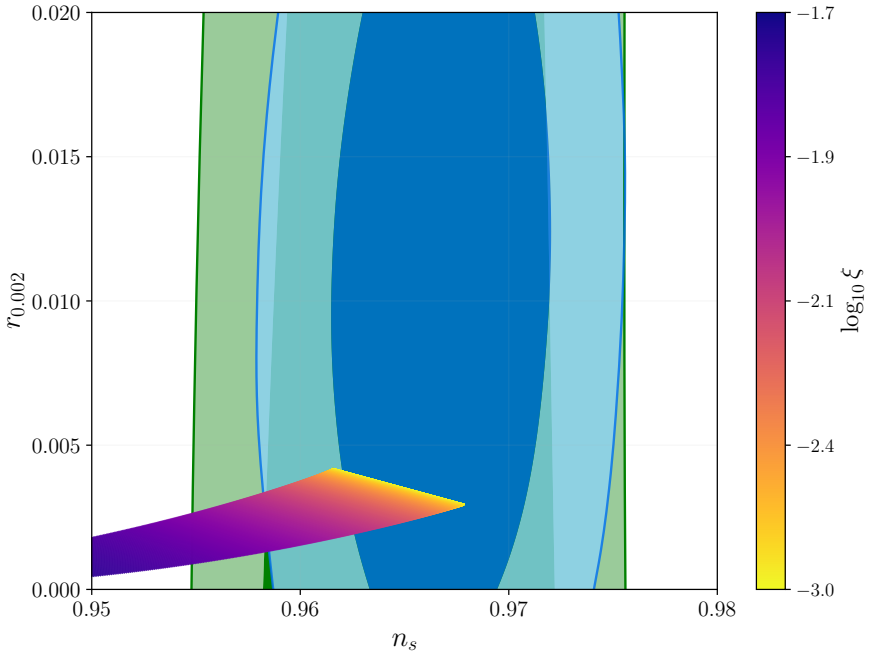

Figure 3.10: Comparison between the spectral indices predicted by the scale-invariant model in Eq. (3.1) and the observed ones. *Observational bounds*: marginalized joint 68% and 95% CL regions for n_s and r at $k = 0.002\,\mathrm{Mpc}^{-1}$ from the *Planck* 2018 baseline analysis (green contours) and in combination with BICEP/*Keck* data at the end of the 2018 season and BAO data (blue contours), obtained assuming $\alpha_s = 0$ [43]. *Model's predictions*: slow-roll calculations from Eq. (3.77) with the slow-roll parameters defined in Eq. (3.3) and the value of the inflaton at horizon crossing computed in the large-field approximation from Eq. (3.73). The parameter Ω is fixed to the reference value $\Omega = 1.07\,\xi^2$, and ξ is varied in $[10^{-3}, 2\times 10^{-2}]$ (colorbar). The number of e-folds elapsed from horizon crossing to the end of inflation is varied in $N_* \in [50,\, 60]$, with $N_* = 50$ and $N_* = 60$ corresponding to the upper and lower colored curves, respectively.

While observational constraints exclude larger values of ξ, smaller values with $\xi < 10^{-3}$ remain allowed; however, in this regime the spectral indices approach asymptotic values that are independent of ξ. Let's investigate this limit in more detail. Motivated by the quadratic fit shown in Figure 3.9, we write the spectral indices with $\Omega \to \beta\,\xi^2$, and we expand them for $\xi \ll 1$ up to $\mathcal{O}\left(\xi^2\right)$, which is the limit we want to investigate. The resulting expressions are

$$\begin{aligned} n_s &\simeq 1 - \frac{8}{3}\xi\cosh\left(\sqrt{\frac{2}{3}}\frac{\rho}{M_p}\right) \simeq 1 - \frac{2}{N_*}, \\ r &\simeq \frac{64}{3}\xi^2\sinh^2\left(\sqrt{\frac{2}{3}}\frac{\rho}{M_p}\right) \simeq \frac{12}{N_*^2}, \end{aligned} \tag{3.78}$$

which are precisely the results found for Starobinsky inflation in Eq. (2.48) and can be combined to give the universal expression

$$n_s \simeq 1 - \sqrt{\frac{r}{3}}. \tag{3.79}$$

This relation explains why, in the $\xi \to 0$ limit, the spectral indices saturate to values that depend only on N. In this regime, the non-minimal coupling effectively vanishes, leading to the decoupling of the scalar field ϕ from the inflationary dynamics and thereby reproducing the predictions of Starobinsky inflation.

The parameter α, which directly controls the overall amplitude of the potential $V(\rho)$, cannot be constrained through the analysis of the spectral indices alone, since these primarily encode information about the shape of the potential. Instead, α is fixed by the amplitude of the primordial scalar and tensor power spectra.

By matching the slow-roll expression for the scalar power spectrum in Eq. (2.50) to its observed value, α can be determined for any given choice of (ξ, Ω, N_*). As a representative example, taking $\xi = 10^{-3}$, $\Omega = 1.07\,\xi^2$, and $N_* = 55$, we obtain

$$\rho_f \simeq 8.46\, M_{pl}, \qquad \rho_* \simeq 3.96\, M_{pl}, \qquad n_s \simeq 0.965, \qquad r \simeq 3 \times 10^{-2}, \tag{3.80}$$

while setting A_s to the central value of the bound reported in Table 1.1 implies the following values for α and, therefore, λ

$$\alpha \simeq 2 \times 10^{10} \longrightarrow \lambda \simeq 3 \times 10^{-18}. \tag{3.81}$$

It is also worth noting that the large value of α required by CMB constraints disfavors an interpretation in which the R^2 term is generated only through quantum matter contributions, as originally proposed by Starobinsky. Indeed, a single quantized matter field contributes only $\mathcal{O}(10^{-4})$ to the coefficient α in the one-loop effective action (see Eq. (2.3)). Reproducing the observationally required value of α would therefore necessitate an unrealistically large number of quantized matter fields, of order 10^{14}. This point was recently emphasized in [181].

In summary, the scale-invariant model discussed in this chapter, besides providing a mechanism of dynamical generation of the Planck mass, is fully capable of describing an arbitrarily long inflationary phase interpolating between an unstable and a stable de Sitter fixed point. The slow-roll conditions are satisfied for a number of e-folds N sufficiently large to account for the observed homogeneity of the Universe. This behavior is a direct consequence of the flat plateau emerging in the potential (see Figure 3.6). Importantly, the presence of this plateau is a generic feature of the model: it arises for any choice of parameters within the viable ranges and does not rely on severe fine-tuning, in agreement with the general expectations for scale-invariant theories (see Sec. 2.4.3).

Within the same region of parameter space, the model's predictions for the spectral indices are fully consistent with the latest CMB observations, making it potentially competitive with other benchmark scenarios, such as Starobinsky inflation. While a more comprehensive treatment of scalar perturbations and a complete numerical analysis are left to the next chapter, we now turn to the elephant in the room: the residual cosmological constant.

3.4 Residual cosmological constant

As already discussed above, the EF potential is non-vanishing at the minima, resulting in a classical cosmological constant generated as a leftover from inflation, which can be potentially large, unless $\lambda = 0$, meaning a vanishing quartic self-interaction of the scalar field in the JF. More specifically, the residual cosmological constant would be[8]

$$\Lambda = \frac{V_{\min}}{M_{pl}^2} = \frac{9\lambda M_{pl}^2}{4\Omega} \simeq 6.3 \times 10^{-12}\, M_{pl}^2, \tag{3.82}$$

[8] Again, note that for a meaningful comparison with the effective cosmological constant in the JF we need to compare observable quantities, i.e., dimensionless ratios: $\Lambda_{\rm meas} = \Lambda/\tilde{m}_u^2$, which is the same in the two frames after appropriate rescaling of the unit mass and evaluating the JF contribution as the value of the quartic potential at the fixed point.

for the benchmark values considered in Eqs. (3.80)–(3.81). This is clearly huge compared to the observed value $\Lambda \sim 10^{-122}\, M_{pl}^2$, which would anyway require an enormous amount of fine tuning on the ratio λ/Ω. Note, however, that the same issue was present in the Cooper-Venturi model, see the discussion in Sec. 2.4.3. Scale invariance only shifts the fine-tuning problem of the cosmological constant to an unnatural hierarchy between the model's parameters.

This scenario is consistent with the fact that the stable fixed point corresponds to a de Sitter universe, characterized by a constant and non-vanishing Hubble parameter, $H_{\rm st} = \text{const.} \neq 0$. As such, it is clearly incompatible with a subsequent radiation-dominated phase and therefore does not allow for a graceful exit into the standard Friedmann evolution.

In this section, we discuss the cosmological constant problem in the scale-invariant framework, with the broader goal of providing a unified description of all its scale-invariant generalizations.

We note that, in principle, one could envisage a mechanism of particle production that fills the Universe with massless particles, arising from the coupling of the inflaton field – or the scalar field ϕ – with the SM particles. In such scenarios, energy transfer from the inflationary to the Standard Model sector occurs via damped oscillations of the scalar field around its minimum. This possibility was explored in earlier works (see, e.g., [5, 174]); however, we do not pursue this approach further here.

3.4.1 One loop quantum corrections

As discussed in Sec. 2.4.3, a possible solution to the cosmological constant problem can arise in some scale-invariant models by accounting for the explicit symmetry breaking induced by quantum corrections. Even if our model is different from the cosmon inflation described in Sec. 2.4.3, it is helpful to account for the running of the model's parameters, and study the behavior of Λ upon varying the renormalization scale μ.

The authors of [175] computed one-loop quantum corrections to the classical scale-invariant action (3.1). Calculations are performed on a curved background, in which gravity is kept classical[9] and divergences are treated with dimensional regularization using the $\overline{\rm MS}$-scheme. While some conclusions drawn in [175] might be reviewed in light of the constraints on the model's parameters derived in this chapter, we report the results for the running of the parameters, obtained upon integration of the β functions:[10]

$$\begin{aligned}
\lambda(\mu) &= \frac{\lambda_0}{1-\frac{9\lambda_0}{8\pi^2}\ln\left(\frac{\mu}{\mu_0}\right)}\,, \\
2\xi(\mu)+1 &= (2\xi_0+1)\left(1-\frac{9\lambda_0}{8\pi^2}\ln\left(\frac{\mu}{\mu_0}\right)\right)^{-1/3}\,, \\
\alpha(\mu) &= \alpha_0 - \frac{(2\xi_0+1)^2}{12\lambda_0} + \frac{(2\xi_0+1)^2}{12\lambda_0}\left(1-\frac{9\lambda_0}{8\pi^2}\ln\left(\frac{\mu}{\mu_0}\right)\right)^{1/3}\,,
\end{aligned} \tag{3.83}$$

where λ_0, ξ_0, and α_0 are the constant values of the coupling at the reference scale μ_0. We will set them to the values of the model's parameters as constrained in Sec. 3.3. Note that the non-minimal coupling ξ approaches its conformal value $\xi = -1/2$ in the IR limit, see Appendix B.

All the scale dependence of the parameters roots in the logarithm, which is, however, multiplied by the small value of $\lambda_0 \sim 10^{-18}$, see Eq. (3.81). For this reason, the model's parameters do not change

[9] The semi-classical gravity framework is introduced in [79, 80].

[10] Note the typo in [175] in the expression for $\lambda(\mu)$ and, as a consequence, for $\xi(\mu)$ and $\alpha(\mu)$. The overall λ_0 factor in front of the logarithm strongly suppresses any scale dependence of the parameters.

sensibly around the scale μ, and the classical inflationary predictions are robust against quantum corrections. On the other hand, the running of the couplings does not help to address the cosmological constant problem.

3.4.2 Three-field extension

An intriguing possibility is to send the cosmological constant to zero dynamically, along the same lines as the idea discussed in Sec. 2.4.3, but without introducing explicit scale symmetry breaking terms. This approach was described in [182]: starting from a classically scale-invariant model with the same structure as ours, the authors suggest the inclusion of a second scalar field σ which drives the cosmological constant in the EF to zero.

By adapting the notation of [182] to our model, we have the following JF action

$$S_J = \int \mathrm{d}^4x\sqrt{-g}\left[\frac{\alpha}{36}R^2 + \frac{\xi}{6}\phi^2 R - \frac{1}{2}g^{\mu\nu}\partial_\mu\phi\partial_\nu\phi - \frac{1}{2}g^{\mu\nu}\partial_\mu\sigma\partial_\nu\sigma - \frac{\lambda}{4}\left(\phi^2-\sigma^2\right)^2\right], \tag{3.84}$$

where the additional scalar field σ is not directly coupled to gravity, but it couples to the scalar field ϕ through the potential term. Note that the classical scale invariance of the theory is preserved, and the number of dimensionless constants is unchanged. Moreover, the dynamical generation of the Planck mass occurs precisely in the same way as described in Sec. 3.2.1.

In the EF, the action reads

$$S_E = \int \mathrm{d}^4x\sqrt{-g}\left[\frac{M^2}{2}R - \frac{1}{2}g^{\mu\nu}\left(\partial_\mu\psi\partial_\nu\psi + e^{-\sqrt{\frac{2}{3}}\frac{\psi}{M}}\left(\partial_\mu\phi\partial_\nu\phi + \partial_\mu\sigma\partial_\nu\sigma\right)\right) - V(\psi,\phi,\sigma)\right], \tag{3.85}$$

where the three-field potential is

$$V(\psi,\phi,\sigma) = \frac{9M^4}{4\alpha}\left(1 - \frac{\xi}{3}\frac{\phi^2}{M^2}e^{-\sqrt{\frac{2}{3}}\frac{\psi}{M}}\right)^2 + \frac{\lambda}{4}\left(\phi^2-\sigma^2\right)^2 e^{-2\sqrt{\frac{2}{3}}\frac{\psi}{M}}. \tag{3.86}$$

We note that the parameter M again plays the role of a redundant quantity and can be safely identified with the Planck mass, M_{pl}. The potential admits a continuous set of minima located at

$$\sigma^2_{\min} = \phi^2_{\min}, \qquad e^{\sqrt{\frac{2}{3}}\frac{\psi_{\min}}{M_{pl}}} = \frac{\xi}{3}\frac{\sigma^2_{\min}}{M^2_{pl}}, \tag{3.87}$$

for which the potential vanishes, $V_{\min} = 0$. Since the system relaxes to the minimum of the potential at late times, no residual cosmological constant remains in this case.

To simplify the analysis, one may again exploit the constraint imposed by the conservation of the Noether current to recast the EF dynamics in terms of an effective two-field system. The resulting two-field potential features a flat plateau analogous to that of $V(\rho)$ shown in Figure 3.6, supplemented by an additional well associated with the field σ, which drives the potential energy to zero.

Even within the simplified two-field description, the model remains analytically more involved than the single-field scenario discussed above. While an initial numerical study was presented in [182], a more comprehensive analysis – including cosmological perturbations and a systematic numerical exploration of the parameter space – is left for future work. Nevertheless, we can still study the background dynamics numerically in the full three-field formulation and draw some general conclusions.

The Friedmann equations in a spatially flat FLRW background are

$$\begin{aligned} H^2 &= \frac{1}{3M^2_{pl}}\left[\frac{\dot\psi^2}{2} + \frac{1}{2}e^{-\sqrt{\frac{2}{3}}\frac{\psi}{M_{pl}}}\left(\dot\sigma^2+\dot\phi^2\right) + V\right], \\ \dot H &= -\frac{1}{2M^2_{pl}}\left[\dot\psi^2 + e^{-\sqrt{\frac{2}{3}}\frac{\psi}{M_{pl}}}\left(\dot\sigma^2+\dot\phi^2\right)\right], \end{aligned} \tag{3.88}$$

and the Klein-Gordon equations read

$$\begin{aligned}
\ddot{\psi} + 3H\dot{\psi} + V_{,\psi} &= -\frac{1}{2}\sqrt{\frac{2}{3}}\frac{e^{-\sqrt{\frac{2}{3}}\frac{\psi}{M_{pl}}}}{M_{pl}}\left(\dot{\sigma}^2 + \dot{\phi}^2\right), \\
\ddot{\phi} + 3H\dot{\phi} - \sqrt{\frac{2}{3}}\frac{\dot{\phi}\dot{\psi}}{M_{pl}} &= -V_{,\phi}e^{\sqrt{\frac{2}{3}}\frac{\psi}{M_{pl}}}, \\
\ddot{\sigma} + 3H\dot{\sigma} - \sqrt{\frac{2}{3}}\frac{\dot{\sigma}\dot{\psi}}{M_{pl}} &= -V_{,\sigma}e^{\sqrt{\frac{2}{3}}\frac{\psi}{M_{pl}}}.
\end{aligned} \tag{3.89}$$

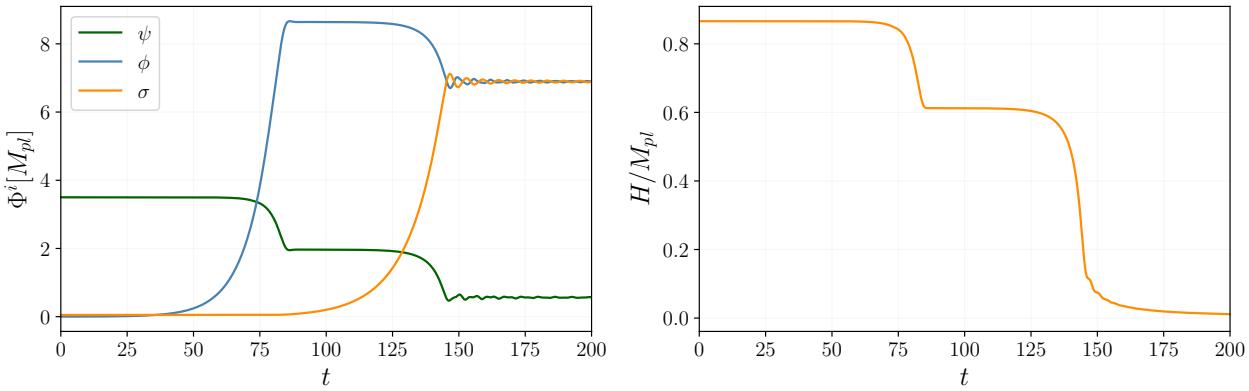

Figure 3.11: Numerical evolution of the scalar fields ψ, ϕ, and σ (*left*) and the Hubble parameter (*right*) for the three-field scale-invariant model in the EF. The results are obtained from the equations of motion (3.88) and (3.89) in cosmic time t. The parameters are fixed to $\alpha = 1, \xi = 10^{-1}, \lambda = 10^{-2}$. The initial conditions are set to: $\psi(0) = 3.5\, M_{pl}, \phi(0) = 10^{-3}\, M_{pl}, \sigma(0) = 5 \times 10^{-2}\, M_{pl}, \dot{\psi}(0) = \dot{\phi}(0) = \dot{\sigma}(0) = 0$.

In Figure 3.11, we show the numerical evolution of the equations of motion for a representative choice of parameters and initial conditions, selected to highlight the main features of the model. The dynamical evolution toward the stable minimum can be qualitatively described as follows:

- Initially, the field σ is effectively frozen, while ϕ and ψ, which are coupled to gravity, perform a slow-roll trajectory and settle in a local valley of the potential;
- As the evolution proceeds, the field σ is activated through its coupling to ϕ, triggering a second phase of slow-roll inflation involving ϕ and ψ. Eventually, all fields relax to the global minimum of the potential, where the Hubble parameter – and hence the effective cosmological constant – vanishes.

While this overall description depends on the initial conditions, the model presents some interesting features that deserve further investigation. In particular, the presence of two distinct slow-roll phases may imprint characteristic signatures on the primordial spectra, with potentially important phenomenological implications for the production of scalar-induced gravitational waves and, consequently, for primordial black hole formation [183, 184]. More broadly, this scenario opens the possibility of probing inflation across multiple scales, extending beyond the reach of CMB observations alone.

The scale-invariant extension of the model discussed here addresses the cosmological constant problem at the price of adding a new scalar degree of freedom. In the following, we aim to investigate the role of the residual cosmological constant in generalizations of the scale-invariant model (3.1) within the class of $f(R, \phi)$ theories.

3.5 Generalized scale invariance and cosmological constant

The model defined in Eq. (3.1) includes all scale-invariant combinations of R and ϕ that are at most quadratic in R and restricted to integer powers. One may nevertheless wish to generalize this framework by allowing for higher-order curvature terms or non-integer exponents. The most general scale-invariant scalar-tensor action in the JF can then be written as

$$S_J = \int \mathrm{d}^4x\sqrt{-g}\left[J\left(\frac{R}{\phi^2}\right)\phi^4 - \frac{1}{2}g^{\mu\nu}\partial_\mu\phi\partial_\nu\phi\right], \tag{3.90}$$

where J is a generic function with dimensionless argument $X \equiv R/\phi^2$. We only require J to be analytic in its argument, implying that we can expand it in a Taylor series around $R = 0$ for any $\phi \neq 0$.

In this section, we will not assume any specific form for J, and analyze the implications of the generalized scale-invariant model in Eq. (3.90) for the appearance of a residual cosmological constant, manifesting itself with a non-zero potential energy at the minima of the EF potential. Throughout the analysis, we explicitly keep track of the original JF variables even after performing the conformal transformation. This approach allows us to clearly distinguish genuine physical effects from potential artifacts of the conformal mapping.

It is instructive to write the trace of the Einstein equations in the JF,

$$\phi^4\left[2J(X) - XJ'(X)\right] = \frac{1}{2}\left(\partial\phi\right)^2, \tag{3.91}$$

where a prime denotes derivative with respect to X. The Klein-Gordon equation for ϕ is

$$\Box\phi^2 + 2\phi^3\left[2J(X) - XJ'(X)\right] = 0. \tag{3.92}$$

It is evident that fixed-point solutions, $X = X_*$, in the JF need to satisfy

$$2J(X_*) = X_*J'(X_*). \tag{3.93}$$

The most intuitive way to move to the EF without knowing the particular form of J is to introduce a Lagrange multiplier, in a way similar to what was done in Sec. 2.3.1 and also in Eq. (3.22). The action (3.90) can be written in the equivalent form

$$S_J \equiv \int \mathrm{d}^4x\sqrt{-g}\mathcal{L}_J = \int \mathrm{d}^4x\sqrt{-g}\left[J\left(\frac{\psi}{\phi^2}\right)\phi^4 + \chi\left(R-\psi\right) - \frac{1}{2}g^{\mu\nu}\partial_\mu\phi\partial_\nu\phi\right]. \tag{3.94}$$

One can indeed verify that, on shell,

$$\frac{\partial\mathcal{L}_J}{\partial\chi} = 0 \longrightarrow \psi = R, \tag{3.95}$$

thereby recovering the original action. The equation of motion for the auxiliary field ψ is

$$\frac{\partial\mathcal{L}_J}{\partial\psi} = 0 \longrightarrow \chi = J'\left(\frac{\psi}{\phi^2}\right)\phi^2, \tag{3.96}$$

which can also be considered as a definition for χ.

By performing a conformal transformation on the metric $\tilde{g}_{\mu\nu} = \Omega^2 g_{\mu\nu}$, and further choosing

$$\Omega^2 = \frac{2\chi}{M^2}, \tag{3.97}$$

where M plays the usual role of redundant mass parameter, we obtain the EF action

$$S_E = \int \mathrm{d}^4x\sqrt{-\tilde{g}}\left[\frac{M^2}{2}\tilde{R} - \frac{3M^2}{4\chi^2}\tilde{g}^{\mu\nu}\partial_\mu\chi\partial_\nu\chi - \frac{M^2}{4\chi^2}\tilde{g}^{\mu\nu}\partial_\mu\phi\partial_\nu\phi - V_E\right], \tag{3.98}$$

where the EF potential can be written in the compact form

$$V_E = \frac{M^4}{4}\frac{J'(X)X - J}{J'(X)^2}. \tag{3.99}$$

As already anticipated, this expression for the EF potential will allow us to keep track of the JF solutions step by step. In particular, we notice that the conformal mapping is well-defined provided

$$\Omega^2 \propto J'(X)\phi^2 > 0. \tag{3.100}$$

More specifically, if $J'(X)$ or ϕ vanishes at some point, the metric in the EF becomes degenerate and the EF ceases to be a suitable description for the model.

To investigate the conditions under which a residual cosmological constant is absent, we examine when the EF potential vanishes at a fixed point of the theory. Combining the JF fixed-point condition (3.93) with the definition of the EF potential, one finds that this can occur only if

$$\boxed{J(X_*) = 0}. \tag{3.101}$$

From Eq. (3.93), this requirement leads to two distinct possibilities:

- $X_* \neq 0$ and $J'(X_*) = 0$. In this case, the conformal transformation becomes ill-defined, as discussed above, and this pathology manifests itself in the Einstein frame through a divergent potential V_E.
- $X_* = 0$ and $J'(X_*) \neq 0$, corresponding to $R = 0$, as expected for a vanishing cosmological constant. Therefore, in order to obtain a fixed-point solution that is mapped to a vanishing cosmological constant in the EF, one must require $J(0) = 0, J'(0) \neq 0$. This condition is satisfied only if the quartic self-interaction of the scalar field ϕ vanishes identically, namely $\lambda\phi_*^4 = 0$.

Let us examine the second case in more detail. The condition $J(0) = 0$ may be realized either if $\lambda = 0$ or if $\phi_* = 0$. However, the option $\phi_* = 0$ with $J'(X_*) \neq 0$ once again renders the conformal transformation ill-defined.

Furthermore, as illustrated by the Noether-current constraint in the quadratic scale-invariant model (see Figure 3.3), there exists no nontrivial dynamical evolution when both $R_* = 0$ and $\phi_* = 0$. In this situation, the constraint reduces the phase-space trajectory to a single point, at least within a spatially flat FLRW cosmological setting.

We therefore conclude that, within the class of scale-invariant models defined by Eq. (3.90), the only viable way to obtain a vanishing residual cosmological constant is to set $\lambda = 0$.

We further stress that the two-field extension discussed above circumvents the problem in a natural way, since the quartic self-interaction is modified as

$$\frac{\lambda}{4}\phi^4 \longrightarrow \frac{\lambda}{4}\left(\phi^2 - \sigma^2\right)^2, \tag{3.102}$$

which vanishes for every $\phi_*^2 = \sigma_*^2$, which does not necessarily imply $\phi_* = 0$.

3.6 Summary

In this chapter, we studied a classically scale-invariant model of gravity devised in [5], in which the gravitational sector is extended by an R^2 term and a real scalar field, with all couplings dimensionless. See the action in Eq. (3.1). The model provides a concrete realization of inflation within a framework where scale invariance is implemented at the classical level and subsequently broken dynamically. The general features of the model are discussed in Sec. 3.1.

In Sec. 3.2, we analyzed the cosmological evolution of the model by performing a dynamical system analysis of the equations of motion. We identified two distinct families of fixed points: an unstable saddle point, corresponding to the symmetric configuration with vanishing scalar field, and a stable fixed point characterized by a non-zero scalar vacuum expectation value. We showed that the system naturally evolves away from the unstable fixed point and approaches the stable attractor through damped oscillations. At the stable fixed point, scale symmetry is spontaneously broken, and a mass scale is dynamically generated, allowing the EH term and the Planck mass to emerge from the underlying scale-invariant theory. We showed that in the EF the model is equivalent to the EH action with two scalar fields.

As a central aspect of our analysis, we investigated the role of the Noether current associated with scale invariance and its impact on the inflationary dynamics. We showed that, in an exponentially expanding spacetime, the conservation of the Noether current rapidly constrains the field-space trajectory to lie on an ellipse, independently of the detailed form of the potential. As a result, despite the model's apparent multifield structure, the dynamics effectively reduce to a single-field description. In the Einstein frame, this reduction becomes explicit through a suitable field redefinition: the Goldstone mode χ associated with scale symmetry quickly freezes to a constant value, while the inflationary evolution is entirely governed by a single scalar degree of freedom, ρ. The field ρ evolves in a Mexican-hat potential, which can exhibit an extended flat plateau around the origin and attains a non-vanishing value at its minima.

In Sec. 3.3, we analyzed the inflationary regime in the effective single-field formulation, in the slow-roll approximation. We established analytical, approximate constraints on the model's parameters required for a viable inflationary phase. In particular, we showed that arbitrarily long inflationary trajectories connecting the unstable and stable fixed points are possible, and that inflation must end by violation of the slow-roll conditions before the field reaches the minimum of the potential. Within the allowed parameter region, we computed the spectral indices and demonstrated that the model can reproduce values consistent with current observational bounds. Moreover, we have shown that in the limit $\xi \to 0$ the same predictions of Starobinsky inflation are recovered.

Finally, we analyzed the role of the non-vanishing vacuum energy at the stable fixed point, which generically gives rise to a residual cosmological constant after inflation. In Sec. 3.4, revisiting the results of [175], we showed that the running of the coupling parameters induced by quantum corrections does not substantially modify the value of the residual vacuum energy. We also outlined a three-field extension of the model, proposed in [182], in which the cosmological constant can be dynamically driven to zero.

In Sec. 3.5, we further clarified that the emergence of a residual cosmological constant is a generic feature of scale-invariant generalizations of the model that preserve the same field content, highlighting its structural origin within this class of theories.

Chapter 4

Scale-invariant inflation: perturbations

4.1 Theoretical framework

As discussed in Chapter 1, the simplest single-field slow-roll inflationary models predict an *adiabatic* primordial power spectrum whose amplitude can be characterized by the comoving curvature perturbation $\mathcal{R}$, which is conserved on super-Hubble scales.

As soon as we consider multiple scalar fields, perturbations are not necessarily adiabatic. Such non-adiabatic fluctuations can have important effects, both on the evolution of curvature perturbations and on seeding isocurvature (or entropy) perturbations, see, e.g., [31, 185–187]. This means that there is no spacetime slicing where each of the energy density fluctuations vanishes separately, even though there is always a spacetime slicing where the total energy density vanishes. As such, isocurvature fluctuations are related to the relative density between different matter components [188].

Since adiabatic and isocurvature perturbations lead to a different peak structure in the CMB fluctuations, CMB measurements can distinguish between the two and indeed constrain isocurvature fluctuations on scales larger than 10 Mpc to be less than 1–10 % of the total fluctuations [42].[1]

Theoretical predictions on the amplitude of the isocurvature power spectrum are strongly model-dependent: not only they depend on the particular multifield dynamics, but also on the details of the post-inflationary evolution, since isocurvature fluctuations require at least one field to decay into some particle species whose abundance cannot be determined by the thermal equilibrium at the end of inflation or by some conserved quantity [14]. For this reason, in this section we will outline some general techniques to tackle cosmological perturbation in multifield inflation, extending the formalism introduced in Chapter 1, and then focus on the scale-invariant model in Eq. (3.1) in the next section.

4.1.1 Perturbations in multifield inflation

Let's restrict to the class of actions that can be written in the form

$$S = \int \mathrm{d}^4x\sqrt{-g}\left[\frac{M_{pl}^2}{2}R - \frac{1}{2}\mathcal{G}_{IJ}g^{\mu\nu}\partial_\mu\phi^I\partial_\nu\phi^J - V(\phi^I)\right], \tag{4.1}$$

where we collectively indicate the scalar fields as ϕ^I and capital indices run over the number of fields. The field-space metric, $\mathcal{G}_{IJ}$, includes possible non-canonical kinetic terms. Note that the EF action of the scale-invariant model can be written in this form both in the (ϕ, f) representation, see Eq. (3.31), and in the (ρ, χ) representation, see Eq. (3.50).

[1] On much smaller scales, where CMB constraints no longer apply, the situation is different: for scales in the range 1 pc – 1 Mpc future CMB spectral distortions might be able to test isocurvature fluctuations [189, 190], while below the parsec scale the best probes would be primordial black holes and induced gravitational waves [188].

Considering linear perturbations about the homogeneous background fields, we can adopt the same notation as in Chapter 1 and write

$$\phi^I \to \phi^I(t) + \delta\phi^I(x^\mu). \tag{4.2}$$

The potential and its field derivative are transformed accordingly,

$$V \to V + V_{,I}\delta\phi^I, \qquad V_{,I} \to V_{,I} + V_{,IJ}\delta\phi^J. \tag{4.3}$$

We also consider scalar perturbations of the metric. In the longitudinal gauge, the line element can be written as

$$\mathrm{d}s^2 = -\left(1+2\Phi\right)\mathrm{d}t^2 + a^2\left(1-2\Phi\right)\delta_{ij}\mathrm{d}x^i\mathrm{d}x^j, \tag{4.4}$$

where, compared to Eq. (1.31), we have imposed the equivalence of the two Bardeen potentials, $\Psi = \Phi$, since the spatial part of the energy-momentum tensor is diagonal for all the actions of the form (4.1).[2]

The perturbed Einstein equations can be conveniently split into an unperturbed and a perturbed part as well

$$G^{(0)}_{\mu\nu} + \delta G_{\mu\nu} = \frac{1}{M_{pl}^2}\left(T^{(0)}_{\mu\nu} + \delta T_{\mu\nu}\right). \tag{4.5}$$

Practically, it is sufficient to compute the Einstein tensor starting from the line element (4.4) up to first order in perturbation theory and split it into a zeroth-order and a first-order part, see [192] for all the details. At the same time, the right-hand side of the Einstein equations can be computed from the usual definition:

$$T_{\mu\nu} = -\frac{2}{\sqrt{-g}}\frac{\delta\left(\sqrt{-g}\mathcal{L}\right)}{\delta g^{\mu\nu}} = \mathcal{G}_{IJ}\nabla_\mu\phi^I\nabla_\nu\phi^J - g_{\mu\nu}\left(\frac{1}{2}\mathcal{G}_{KL}g^{\lambda\sigma}\nabla_\lambda\phi^K\nabla_\sigma\phi^L + V\right). \tag{4.6}$$

To ease the continuity from Chapter 1, we follow the convention of labeling fluid quantities and the associated perturbations with the components of the energy-momentum tensor

$$\begin{aligned} T^0_0 &= -\left(\rho + \delta\rho\right), \\ T^0_i &= \partial_i\delta q, \\ T^i_j &= \delta^i_j\left(p + \delta p\right), \end{aligned} \tag{4.7}$$

where $\delta\rho$ is the density perturbation, δq is the momentum flow, δp is the isotropic pressure perturbation, and we have omitted the contribution from the anisotropic pressure since we are considering minimally-coupled scalar fields.

From the different components of the energy-momentum tensor computed from Eq. (4.6), we can identify[3]

$$\begin{aligned} \rho &= \frac{1}{2}\mathcal{G}_{IJ}\dot\phi^I\dot\phi^J + V, \\ \delta\rho &= \mathcal{G}_{IJ}\left(\dot\phi^I\dot{\delta\phi}^J - \dot\phi^I\dot\phi^J\Phi\right) + V_{,I}\delta\phi^I, \\ \delta q &= -\mathcal{G}_{IJ}\dot\phi^I\delta\phi^J, \\ p &= \frac{1}{2}\mathcal{G}_{IJ}\dot\phi^I\dot\phi^J - V, \\ \delta p &= \mathcal{G}_{IJ}\left(\dot\phi^I\dot{\delta\phi}^J - \dot\phi^I\dot\phi^J\Phi\right) - V_{,I}\delta\phi^I. \end{aligned} \tag{4.8}$$

[2] If we were to include a non-minimal coupling function $f(\phi^I)$, we would find the relation $\partial_i\partial_j(\Phi-\Psi) = -f^{-1}\partial_i\partial_j\delta f$, which implies that if at least one field is non-minimally coupled to gravity, the two Bardeen potentials will, in general, differ [191].

[3] Since now we are explicitly separating background quantities from perturbed quantities, ϕ^I should be interpreted as the background value.

Once the above equations are considered, we can adopt the standard definitions for the gauge-invariant quantities introduced in Sec. 1.4.1. In particular, the comoving curvature perturbation defined in Eq. (1.37) becomes

$$\mathcal{R} = \Phi + H\frac{\dot{\phi}_I \delta\phi^I}{\dot{\phi}_I \dot{\phi}^I}, \tag{4.9}$$

where field-space indices are raised and lowered with the field-space metric $\mathcal{G}_{IJ}$.

For completeness, we report the first-order perturbed Einstein equations [191]

$$\begin{aligned} 3H(\dot{\Psi} + H\Phi) - \frac{1}{a^2}\nabla^2\Psi &= -\frac{1}{2M_{pl}^2}\delta\rho, \\ \dot{\Psi} + H\Phi &= -\frac{1}{2M_{pl}^2}\delta q, \\ \ddot{\Psi} + 3H\dot{\Psi} + H\dot{\Phi} + \left(2\dot{H} + 3H^2\right)\Phi &= \frac{1}{2M_{pl}^2}\left(\delta p - \frac{2}{3}\nabla^2\Pi\right), \\ \frac{1}{a^2}\partial^i\partial_j\left(\Phi - \Psi\right) &= \frac{1}{M_{pl}^2}\partial^i\partial_j\Pi, \end{aligned} \tag{4.10}$$

derived from the $(0,0)$, $(0,i)$, $i=j$, and $i\neq j$ components of the Einstein field equations, respectively.

The background and first-order terms of the energy-momentum tensor are separately conserved, resulting in the following equations:

$$\begin{aligned} \dot{\rho} + 3H\left(\rho + p\right) &= 0, \\ \dot{\delta\rho} + 3H\left(\delta\rho + \delta p\right) &= -\frac{1}{a^2}\nabla^2\delta q + 3\left(\rho + p\right)\dot{\Psi}. \end{aligned} \tag{4.11}$$

Note that the anisotropic pressure, Π_{ij}, drops out of the conservation equations because it is traceless.

4.1.2 Decomposition into tangential and normal components

A very convenient formalism for understanding the role of adiabatic and entropy perturbations and their evolution was introduced by Gordon *et al.* [193] and amounts to decomposing scalar perturbations into components along and orthogonal to the background field trajectory. In the following, we present its extension to non-canonical kinetic terms, see, e.g., [194]. For the sake of simplicity, we restrict to the case of two fields, $\phi^I = (\psi, \chi)$, in which one of the two fields has a non-canonical kinetic term, corresponding to

$$\mathcal{G}_{IJ} = \begin{pmatrix} 1 & 0 \\ 0 & e^{2b(\psi,\chi)} \end{pmatrix}, \tag{4.12}$$

where b is a generic function of the two scalar fields. The Einstein equations take the form

$$\begin{aligned} H^2 &= \frac{1}{3M_{pl}^2}\left(\frac{1}{2}\dot{\psi}^2 + \frac{1}{2}e^{2b}\dot{\chi}^2 + V\right), \\ \dot{H} &= -\frac{1}{2M_{pl}^2}\left(\dot{\psi}^2 + e^{2b}\dot{\chi}^2\right), \end{aligned} \tag{4.13}$$

so the quantity $\dot{\sigma}^2 \equiv \mathcal{G}_{IJ}\dot{\phi}^I\dot{\phi}^J = \dot{\psi}^2 + e^{2b}\dot{\chi}^2$ can be naturally interpreted as (the square of) the rate of change of the scalar field vacuum expectation value along the trajectory followed by the background fields [195].

We may now introduce new fields σ and s by acting on the field space with a rotation such as to decompose it into tangential and orthogonal directions, such that

$$\begin{aligned} \mathrm{d}\sigma &= \cos\theta\,\mathrm{d}\psi + \sin\theta\, e^b \mathrm{d}\chi, \\ \mathrm{d}s &= -\sin\theta\,\mathrm{d}\psi + \cos\theta\, e^b \mathrm{d}\chi, \end{aligned} \tag{4.14}$$

where θ is the rotation angle with respect to the tangent of the background trajectory, and it satisfies

$$\cos\theta = \frac{\dot{\psi}}{\sqrt{\dot{\psi}^2 + e^{2b}\dot{\chi}^2}}, \qquad \sin\theta = \frac{e^b\dot{\chi}}{\sqrt{\dot{\psi}^2 + e^{2b}\dot{\chi}^2}}. \tag{4.15}$$

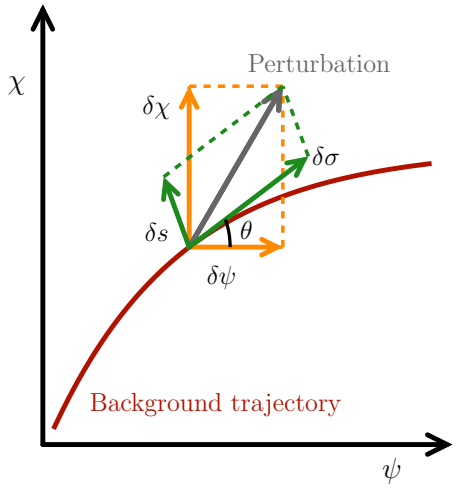

Figure 4.1: Illustrative example of the decomposition of an arbitrary perturbation (gray arrow) into adiabatic $\delta\sigma$ and entropy δs perturbations (green arrows) relative to the background field-space trajectory (red line). The decomposition in the usual field space (ψ, χ) is also represented (orange arrows). The angle θ represents the rotation between the two bases.

The *adiabatic field* σ measures the path length along the classical background trajectory in field space and corresponds to perturbations tangent to it, while the *entropy field* s describes perturbations orthogonal to the trajectory. This decomposition is illustrated in Figure 4.1.

It is convenient to define adiabatic and entropy unit vectors with components[4]

$$\mathbf{u}_\sigma^I = \left(\cos\theta, e^{-b}\sin\theta\right), \qquad \mathbf{u}_s^I = \left(-\sin\theta, e^{-b}\cos\theta\right), \tag{4.16}$$

which allow us to project field-space quantities into their adiabatic and entropy components, such as

$$\delta\sigma = \mathbf{u}_{\sigma I}\delta\phi^I, \qquad \delta s = \mathbf{u}_{sI}\delta\phi^I. \tag{4.17}$$

One can further check the orthonormality of the unit vectors, namely $\mathbf{u}_{\sigma I}\mathbf{u}_\sigma^I = \mathbf{u}_{sI}\mathbf{u}_s^I = 1$ and $\mathbf{u}_{\sigma I}\mathbf{u}_s^I = 0$.

It is easy to show that the entropy field is constant along the classical trajectory, $\dot{s} = \mathbf{u}_{sI}\dot{\phi}^I = 0$, thus entropy perturbations are automatically gauge-invariant.[5] Perturbations in $\delta\sigma$ with $\delta s = 0$ are entirely along the classical trajectory and describe adiabatic field perturbations, hence the name "adiabatic field". Adiabatic perturbations are locally indistinguishable from a time shift.

[4]Note that we are not making any statement about the matrix shape of the unit vectors, we are just listing their components.

[5]Under an infinitesimal time shift $t \to t + \delta t$, we have $\delta s \to \delta s - \dot{s}\delta t$, so $\delta s \to \delta s$ if $\dot{s} = 0$.

4.2 Perturbations in the Einstein frame

Although the analysis of perturbations may be performed equivalently in the Jordan frame (JF) or, for instance, within the frame-invariant formalism adopted in [179] for scale-invariant models, we restrict our study to the Einstein frame (EF). This choice allows us to directly employ the decomposition introduced above, thereby simplifying the numerical implementation, as will be illustrated in the following.

As shown in Chapter 3, the effective background dynamics are manifestly single-field. At the level of perturbations, however, the model must be treated as genuinely two-field to consistently evaluate the resulting isocurvature perturbations and assess their dependence on the initial conditions. In what follows, we therefore consider scalar perturbations of both the fields and the background metric in the (ρ, χ) representation introduced in Sec. 3.2.2.

The EF action in Eq. (3.50) can be written in the same form of Eq. (4.1) with $\phi^I = (\rho, \chi)$ and

$$\mathcal{G}_{IJ} = \begin{pmatrix} 1 & 0 \\ 0 & e^{2b(\rho)} \end{pmatrix}, \quad \text{where} \quad b(\rho) \equiv \frac{1}{2} \ln \left[6 \cosh^2 \left(\frac{\rho}{\sqrt{6} M_{pl}} \right) \right]. \tag{4.18}$$

At the background level, the Klein-Gordon equations for the two scalar fields are

$$\ddot{\rho} + 3H\dot{\rho} + V_{,\rho} = b_{,\rho}\, e^{2b(\rho)} \dot{\chi}^2, \tag{4.19}$$

$$\ddot{\chi} + 3H\dot{\chi} + 2b_{,\rho}\, \dot{\chi}\dot{\rho} = 0. \tag{4.20}$$

The Friedmann equations are

$$H^2 = \frac{1}{3M_{pl}^2} \left(\frac{\dot{\rho}^2}{2} + e^{2b(\rho)} \frac{\dot{\chi}^2}{2} + V(\rho) \right), \tag{4.21}$$

$$\dot{H} = -\frac{1}{2M_{pl}^2} \left(\dot{\rho}^2 + e^{2b(\rho)} \dot{\chi}^2 \right), \tag{4.22}$$

where we have simply cast Eqs. (3.55)–(3.58) in the compact notation adopted here.

In complete analogy to Sec. 4.1.2, we can identify $\dot{\sigma}^2 = \dot{\rho}^2 + e^{2b}\, \dot{\chi}^2$ and introduce the adiabatic and entropy fields via

$$d\sigma = \cos\theta\, d\rho + e^b \sin\theta\, d\chi, \tag{4.23}$$

$$ds = e^b \cos\theta\, d\chi - \sin\theta\, d\rho, \tag{4.24}$$

with the rotation angle satisfying

$$\cos\theta = \frac{\dot{\rho}}{\sqrt{\dot{\rho}^2 + e^{2b}\, \dot{\chi}^2}}, \qquad \sin\theta = \frac{e^b\, \dot{\chi}}{\sqrt{\dot{\rho}^2 + e^{2b}\, \dot{\chi}^2}}. \tag{4.25}$$

The components of the adiabatic and entropy unit vectors have the same structure as before

$$\mathbf{u}_\sigma^I = \left(\cos\theta, e^{-b} \sin\theta \right), \qquad \mathbf{u}_s^I = \left(-\sin\theta, e^{-b} \cos\theta \right). \tag{4.26}$$

The field-space trajectory, along with the adiabatic and entropy unit vectors, is represented in Figure 4.3, and is obviously a straight line, corresponding to a constant value of χ.

The Klein-Gordon equations (4.19)–(4.20) can be written entirely in terms of the rotated variables,

$$\ddot{\sigma} + 3H\dot{\sigma} + V_{,\sigma} = 0, \tag{4.27}$$

$$\dot{\theta} = -\frac{V_{,s}}{\dot{\sigma}} - b_{,\rho}\, \dot{\sigma} \sin\theta, \tag{4.28}$$

where we have introduced the convenient notation $V_{,\sigma} = \mathbf{u}^I_\sigma V_{,I}$ and $V_{,s} = \mathbf{u}^I_s V_{,I}$. From now on, we will adopt this notation to project quantities from the field space to the rotated frame.

Let's consider linear perturbations about the background homogeneous fields

$$\rho \to \rho(t) + \delta\rho(x^\mu), \qquad \chi \to \chi(t) + \delta\chi(x^\mu), \tag{4.29}$$

and scalar perturbations of the metric in the longitudinal gauge, corresponding to the line element in Eq. (4.4).

The evolution equations for the field perturbations in Fourier space, to linear order, are given by

$$\ddot{\delta\rho} + 3H\dot{\delta\rho} + \left(\frac{k^2}{a^2} + V_{,\rho\rho} - (b_{,\rho\rho} + 2b^2_{,\rho})\dot\chi^2 e^{2b}\right)\delta\rho - 2b_{,\rho}e^{2b}\dot\chi\dot{\delta\chi} = 4\dot\Phi\dot\rho - 2V_{,\rho}\Phi, \tag{4.30}$$

$$\ddot{\delta\chi} + 3H\dot{\delta\chi} + 2b_{,\rho}\left(\dot\chi\,\dot{\delta\rho} + \dot\rho\,\dot{\delta\chi}\right) + \frac{k^2}{a^2}\delta\chi + 2b_{,\rho\rho}\dot\chi\,\dot\rho\delta\rho = 4\dot\Phi\dot\chi. \tag{4.31}$$

The first-order contribution to the Einstein equations is

$$3H\left(\dot\Phi + H\Phi\right) + \dot H\Phi + \frac{k^2}{a^2}\Phi = -\frac{1}{2M^2_{pl}}\left(\dot\rho\dot{\delta\rho} + e^{2b}\dot\chi\dot{\delta\chi} + b_{,\rho}e^{2b}\dot\chi^2\delta\rho + V_{,\rho}\delta\rho\right), \tag{4.32}$$

$$\dot\Phi + H\Phi = \frac{1}{2M^2_{pl}}\left(\dot\rho\delta\rho + e^{2b}\dot\chi\delta\chi\right). \tag{4.33}$$

We can now consider the evolution of curvature perturbations. From the definition of comoving curvature perturbation $\mathcal{R}$ in Eq. (1.37), we can write[6]

$$\begin{aligned}\mathcal{R} &= \Phi - \frac{H}{\dot H}\left(\dot\Phi + H\Phi\right)\\ &= \Phi + H\left(\frac{\dot\rho\delta\rho + e^{2b}\dot\chi\delta\chi}{\dot\rho^2 + e^{2b}\dot\chi^2}\right),\\ &= \Phi + \frac{H}{\dot\sigma}\delta\sigma\end{aligned} \tag{4.34}$$

where, in the second-to-last equality, we have used the background equation (4.22) and the perturbed equation (4.33). The time evolution is

$$\begin{aligned}\dot{\mathcal{R}} &= \frac{k^2}{a^2}\frac{H}{\dot H}\Phi - 2H\left(\frac{V_{,\rho}e^{2b}\dot\rho\dot\chi^2}{\left(e^{2b}\dot\chi^2 + \dot\rho^2\right)^2}\right)\left(\frac{\delta\rho}{\dot\rho} - \frac{\delta\chi}{\dot\chi}\right)\\ &= \frac{k^2}{a^2}\frac{H}{\dot H}\Phi - 2\frac{V_{,s}}{\dot\sigma}\mathcal{S},\end{aligned} \tag{4.35}$$

where we have introduced the *isocurvature perturbation*, a dimensionless quantity measuring the total entropy fluctuations that inherits gauge invariance from $p_{\rm en}$ in Eq. (1.36), defined as

$$\boxed{\mathcal{S} \equiv \frac{H}{\dot\sigma}\delta s}, \tag{4.36}$$

and we have used the relation

$$\frac{\delta\rho}{\dot\rho} - \frac{\delta\chi}{\dot\chi} = -\frac{\dot\sigma e^{-b}}{\dot\rho\dot\chi}\delta s. \tag{4.37}$$

[6]Note that we are adapting the notation for the comoving curvature perturbation to the previous chapters. This is different from the one adopted in [7, 196, 197], where the comoving curvature perturbation is denoted by ζ instead of $\mathcal{R}$.

In the super-horizon limit $k \ll aH$, the first term on the right-hand side of Eq. (4.35) can be neglected, and we have

$$\dot{\mathcal{R}} \approx -2\frac{V_{,s}}{\dot{\sigma}}\mathcal{S}, \tag{4.38}$$

implying that in the presence of isocurvature perturbations, curvature perturbations are not conserved. As a consequence, in the presence of non-adiabatic fluctuations, it is necessary to follow the super-Hubble evolution of the field perturbations and to track their subsequent evolution during the expansion to determine the resulting large-scale curvature perturbations at late times.

Notably, as can be seen from Eq. (4.28), the coupling of isocurvature to adiabatic perturbations does not vanish on large scales even if $\dot{\theta} = 0$, due to the presence of the non-canonical kinetic term to the Goldstone boson, contributing with $b_{,\rho}\dot{\sigma}\sin\theta$, as first pointed out in [194].

The comoving density perturbation introduced in Eq. (1.34) can be written in terms of the new variables as

$$\delta\rho_m = \dot{\sigma}(\dot{\delta\sigma} - \dot{\sigma}\Phi) - \ddot{\sigma}\delta\sigma + 2V_{,s}\delta s = -2M_{pl}^2\frac{k^2}{a^2}\Phi, \tag{4.39}$$

where the last equality can be derived from the definition in Eq. (1.34) and the perturbed Einstein equations (4.10).

To derive the Klein-Gordon equations for the entropy field δs, we need to differentiate twice the definition given in Eq. (4.24) and further use the Klein-Gordon equations at background level (4.19)–(4.20) and at perturbed level (4.30)–(4.31) and Eq. (4.28). We get

$$\ddot{\delta s} + 3H\dot{\delta s} + \left(\frac{k^2}{a^2} + V_{,ss} - \dot{\theta}^2 - \dot{\sigma}^2 b_{,\rho\rho} + b_{,\rho}^2 g(t) + b_{,\rho} f(t)\right)\delta s = -2V_{,s}\Phi - \frac{2V_{,s}\ddot{\sigma}}{\dot{\sigma}^2}\delta\sigma + \frac{2V_{,s}}{\dot{\sigma}}\dot{\delta\sigma}, \tag{4.40}$$

where we have introduced the functions

$$\begin{aligned} g(t) &= -\dot{\sigma}^2(1 - \sin^2\theta), \\ f(t) &= V_{,\rho}(1 + \sin^2\theta) + 4V_{,s}\sin\theta. \end{aligned} \tag{4.41}$$

To cast Eq. (4.40) to a more compact form, we can use the homogeneous Friedmann equation (4.22) and the evolution equation for ζ (4.35), together with the result in Eq. (4.39). We obtain

$$\ddot{\delta s} + 3H\dot{\delta s} + \left(\frac{k^2}{a^2} + V_{,ss} + 3\dot{\theta}^2 - \dot{\sigma}^2 b_{,\rho\rho} + b_{,\rho}^2 g(t) + b_{,\rho} f(t) - 4\frac{V_{,s}^2}{\dot{\sigma}^2}\right)\delta s = \frac{2V_{,s}}{H}\dot{\mathcal{R}}, \tag{4.42}$$

where now

$$\begin{aligned} g(t) &= -\dot{\sigma}^2(1 + 3\sin^2\theta), \\ f(t) &= V_{,\rho}(1 + \sin^2\theta) - 4V_{,s}\sin\theta. \end{aligned} \tag{4.43}$$

Together, Eqs. (4.35) and (4.42) describe the coupling between the entropy and the adiabatic fluctuations. Eq. (4.35) determines how the entropy fluctuations source adiabatic modes, and Eq. (4.42) gives the growth of the entropy mode sourced by the adiabatic fluctuation component.

It is illuminating to cast the equation of motion (4.42) in an even simpler way, introducing the effective mass of entropy perturbations. Following the definition introduced in [198] and adopted in several subsequent works, we define the effective mass squared of entropy perturbations in terms of geometrical quantities as

$$m_{s(\mathrm{eff})}^2 = V_{;ss} + 3H^2\eta_\perp^2 + \epsilon H^2 M_{pl}^2 R_{\mathrm{fs}}, \tag{4.44}$$

where the dimensionless parameter $\eta_\perp \equiv -\mathbf{u}_s^I V_{,I}/(H\dot{\sigma})$ is a centrifugal term measuring the deviations of the background trajectory from a field-space geodesic [199, 200], $V_{;ss} = \mathbf{u}_s^I\mathbf{u}_s^J(V_{,IJ} - \Gamma_{IJ}^K V_{,K})$ is the

projection of the covariant second derivative of the potential along the entropic direction $\mathbf{u}_s^I$, with Γ^K_{IJ} denoting the Christoffel symbols in field space, and $R_{\rm fs}$ is the field-space Ricci scalar.

In our case, the Christoffel symbols associated with the field-space metric are

$$\begin{aligned} &\Gamma^\rho_{\rho\rho} = 0; \qquad \Gamma^\chi_{\chi\chi} = 0; \qquad \Gamma^\rho_{\chi\chi} = -b_{,\rho} e^{2b}; \\ &\Gamma^\chi_{\rho\rho} = 0; \qquad \Gamma^\rho_{\rho\chi} = \Gamma^\rho_{\chi\rho} = 0; \qquad \Gamma^\chi_{\chi\rho} = \Gamma^\chi_{\rho\chi} = b_{,\rho}. \end{aligned} \tag{4.45}$$

The Ricci scalar is thus

$$R_{\rm fs} = -2(b_{,\rho\rho} + b_{,\rho}^2) = -\frac{1}{3M_{pl}^2}, \tag{4.46}$$

which is clearly independent of the field representation we are considering and could be equivalently computed in the (ϕ, f) representation introduced in Sec. 3.2.2.

The other terms appearing in (4.44) are

$$V_{;ss} = V_{,ss} + b_{,\rho} V_{,\rho} \cos^2\theta, \tag{4.47}$$

$$\eta_\perp = \frac{\dot\theta}{H} + \frac{b_{,\rho}\dot\sigma \sin\theta}{H} = -\frac{1}{H}\frac{V_{,s}}{\dot\sigma}. \tag{4.48}$$

The final expression for the effective mass of entropy perturbations [196] reads

$$m^2_{s(\rm eff)} = V_{,ss} + 3\dot\theta^2 - \dot\sigma^2 b_{,\rho\rho} + b_{,\rho}^2 g(t) + b_{,\rho} f(t), \tag{4.49}$$

with $g(t)$ and $f(t)$ as in (4.43).

We can now write Eq. (4.42) as

$$\begin{aligned} \ddot{\delta s} + 3H\dot{\delta s} + \left(\frac{k^2}{a^2} + m^2_{s(\rm eff)}\right)\delta s &= \frac{2V_{,s}}{H}\left(\dot{\mathcal{R}} + \frac{2V_{,s}\delta s H}{\dot\sigma^2}\right) \\ &= 2V_{,s}\frac{k^2}{a^2}\frac{\Phi}{\dot H}, \end{aligned} \tag{4.50}$$

where, in the last equality, we have used Eqs. (4.35)–(4.36). On super-Hubble scales, the evolution equation reduces to

$$\ddot{\delta s} + 3H\dot{\delta s} + m^2_{s(\rm eff)}\delta s = 0, \tag{4.51}$$

suggesting that the evolution of entropy perturbations can be determined from the relative weight of the effective mass and the Hubble parameter. In the following, we will briefly outline the effect of the various contributions to the effective mass and the possible implications.

4.2.1 Entropy perturbations and tachyonic instabilities

The effects of field-space curvature on the mixing of adiabatic and entropy modes have been investigated in several works, revealing interesting phenomenological implications of multifield inflation. For example, when the inflationary trajectory displays sudden turns in field space, associated with a change in the sign of $\eta_\perp$, heavy modes with $m^2_{s(\rm eff)} \gg H^2$ could leave significant observational imprints on the curvature power spectrum, which displays oscillatory features. In addition, the interaction between curvature and isocurvature modes implies a change in the speed of sound for the curvature perturbations and, as a consequence, an enhancement in the level of non-Gaussianities in the equilateral configuration, see, e.g., [195, 198, 200–204].

At the same time, Renaux-Petel and Turzyński stressed in [205] that when $R_{\rm fs}$ is negative, corresponding to a hyperbolic geometry in field space, it acts in the direction of rendering the effective mass squared of entropy perturbations negative, leading to tachyonic instabilities.[7]

[7] See Sec. 2.2.2 for the general features of tachyonic instabilities.

In particular, from the generic definition in Eq. (4.44) we can see that this purely geometrical contribution cannot be neglected even when the static mass $V_{;ss}$ is large, since the first slow-roll parameter ϵ is positive and usually grows during inflation, reaching $\epsilon = 1$ at the end of inflation. In this regime, which precisely determines the end of inflation, entropy perturbations may turn tachyonic. It is important to stress that a negative $m^2_{s(\text{eff})}$ is not sufficient to trigger the growth of the tachyonic instability by itself, since Eq. (4.51) also displays the Hubble friction term.

The exponential growth of entropy perturbations affects all Fourier modes that crossed the Hubble radius before the onset of the tachyonic instability. After that, the cosmological evolution is determined by the backreaction of these fluctuations on the homogeneous background trajectory, which becomes unstable. Even in the most conservative scenario of inflation ending abruptly as soon as $m^2_{s(\text{eff})}$ turns negative, so that entropy perturbations do not have enough time to affect curvature perturbations, the observational consequences can be crucial: with a premature end of inflation and for a fixed number of e-folds from horizon crossing, the modes corresponding to CMB scales exited the horizon on a flatter part of the potential, bringing the predictions for the power spectra closer to scale invariance (i.e., n_s closer to one and r closer to zero).

Since we are precisely in the case of hyperbolic field-space geometry (from Eq. (4.46), $R_{\text{fs}} < 0$), it is important to understand the role of the effective mass in our model. First, in continuity with the background analysis performed in Chapter 3, we can safely set $\dot{\chi} = 0$, which trivially satisfies the Klein-Gordon equation (4.20). From Eq. (4.25), this also implies that $\sin\theta = 0$, which is expected as well, since in the (ρ, χ) representation the field-space trajectory is a line, see Figure 4.3. Let's inspect the contributions to $m^2_{s(\text{eff})}$ separately:

- **Static mass** $V_{;ss}$. From Eq. (4.47) we have

$$\begin{aligned} V_{;ss} &= \sin^2\theta\, V_{,\rho\rho} + \cos^2\theta\, b_{,\rho} V_{,\rho} \\ &= \frac{3M_{pl}^2}{\alpha}\cos^2\theta \sinh^2\left(\frac{\rho}{\sqrt{6}M_{pl}}\right)\left[2\Omega\sinh^2\left(\frac{\rho}{\sqrt{6}M_{pl}}\right) - \xi\right]. \end{aligned} \tag{4.52}$$

  Since we have shown that the large-field regime $\rho/M_{pl} \gg 1$ is a good approximation, and that $\Omega \sim \beta\,\xi^2$ with $\beta > 1$ and $\xi \ll 1$, the term in square brackets is negative throughout the inflationary stage, and thus the static mass is negative.

- **Centrifugal term** $3H^2\eta_\perp^2$. Given that the field-space trajectory is a straight line, $\eta_\perp = 0$. The centrifugal term does not contribute to the effective mass.

- **Geometric term** $\epsilon H^2 M_{pl}^2$. From Eq. (4.46) we have

$$\epsilon H^2 M_{pl}^2 R_{\text{fs}} = -\epsilon H^2/3, \tag{4.53}$$

  which is always negative.

We can easily conclude that $m^2_{s(\text{eff})}$ is always negative during inflation, as can also be checked from the numerical evolution displayed in Figure 4.2.

This result might suggest that entropy perturbations are driven towards a tachyonic instability before inflation ends. From the definition of the entropy field in Eq. (4.24), we have

$$\delta s = e^b\cos\theta\delta\chi - \sin\theta\delta\rho = e^b\cos\theta\delta\chi = e^b\delta\chi \simeq \sqrt{\frac{3}{2}}e^{\frac{\rho}{\sqrt{6}M_{pl}}}\delta\chi, \tag{4.54}$$

where the last equality comes after taking the large-field limit. On the other hand, from the first-order perturbed Klein-Gordon equation in field space (4.31), setting $\dot{\chi} = 0$, we have

$$\ddot{\delta\chi} + 3H\dot{\delta\chi} + 2b_{,\rho}\dot{\rho}\dot{\delta\chi} + \frac{k^2}{a^2}\delta\chi = 0. \tag{4.55}$$

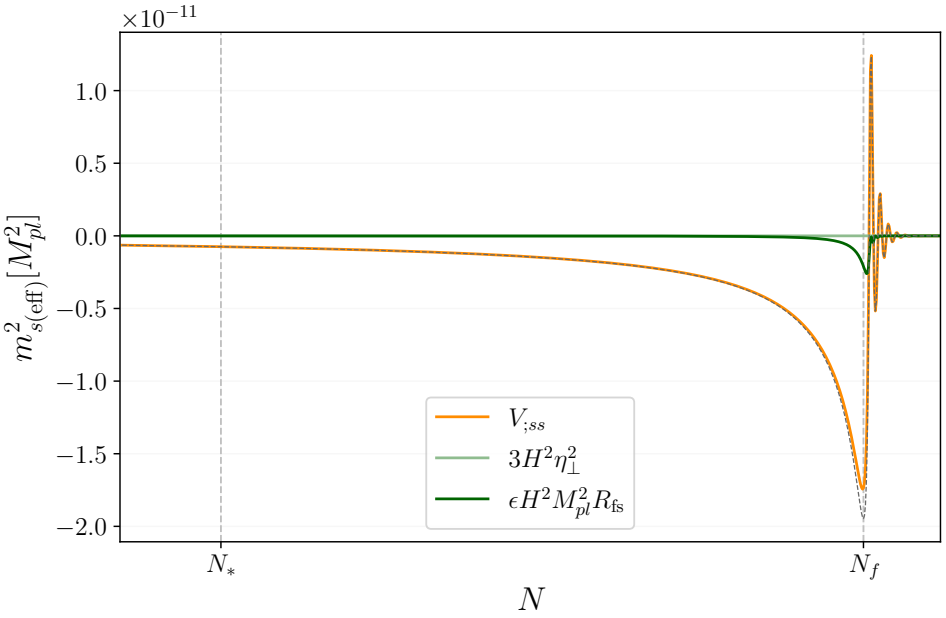

Figure 4.2: Evolution of the effective mass squared of entropy perturbations during inflation, obtained from the numerical integration of the equations of motion in the (ρ, χ) representation (4.19)–(4.22) in e-folding time N. Orange solid line: static mass term from Eq. (4.47); light green solid line: (vanishing) centrifugal term from Eq. (4.48); green solid line: geometrical term from Eq. (4.46); black dashed line: total $m^2_{s(\mathrm{eff})}$.

This implies that $\delta\chi$ becomes constant on super-horizon scales, signaling a potentially dangerous growth of δs from Eq. (4.54). This result is surprising, since the background dynamics should be effectively single-field, and we expect vanishing entropy perturbations as for any single-field, minimally coupled model.

To address this apparent ambiguity, it is illuminating to evaluate the entropy perturbations in the (ϕ, f) field representation. The EF action in Eq. (3.31) can be written in the same form of Eq. (4.1) with $\phi^I = (\phi, f)$ and

$$\mathcal{G}_{IJ} = \begin{pmatrix} e^{2b(f)} & 0 \\ 0 & 6\, e^{-2b(f)} \end{pmatrix}, \quad \text{where} \quad b(f) = \ln\left(\frac{f}{M_{pl}}\right). \tag{4.56}$$

In analogy with the (ρ, χ) representation, we introduce the quantity $\dot\sigma^2 = e^{2b}\dot\phi^2 + 6e^{-2b}\,\dot f^2$ and the adiabatic and entropy fields via

$$\mathrm{d}\sigma = e^b \cos\theta\, \mathrm{d}\phi + \sqrt{6}e^{-b} \sin\theta\, \mathrm{d}f, \tag{4.57}$$

$$\mathrm{d}s = \sqrt{6}e^{-b} \cos\theta\, \mathrm{d}f - e^b \sin\theta\, \mathrm{d}\phi, \tag{4.58}$$

where θ satisfies

$$\cos\theta = \frac{e^b\dot\phi}{\sqrt{e^{2b}\dot\phi^2 + 6e^{-2b}\,\dot f^2}}, \qquad \sin\theta = \frac{\sqrt{6}e^{-b}\,\dot f}{\sqrt{e^{2b}\dot\phi^2 + 6e^{-2b}\,\dot f^2}}. \tag{4.59}$$

The classical field-space trajectory, along with the decomposition into tangential and orthogonal components, is represented in Figure 4.3. In this field representation, the trajectory is clearly less trivial than the one presented above, even if the dynamical content is overall the same.

We can now employ the constraint imposed by Noether current conservation at the background level, Eq. (3.46), and fix $K = K_0$ since we have shown that K approaches a constant value very quickly.

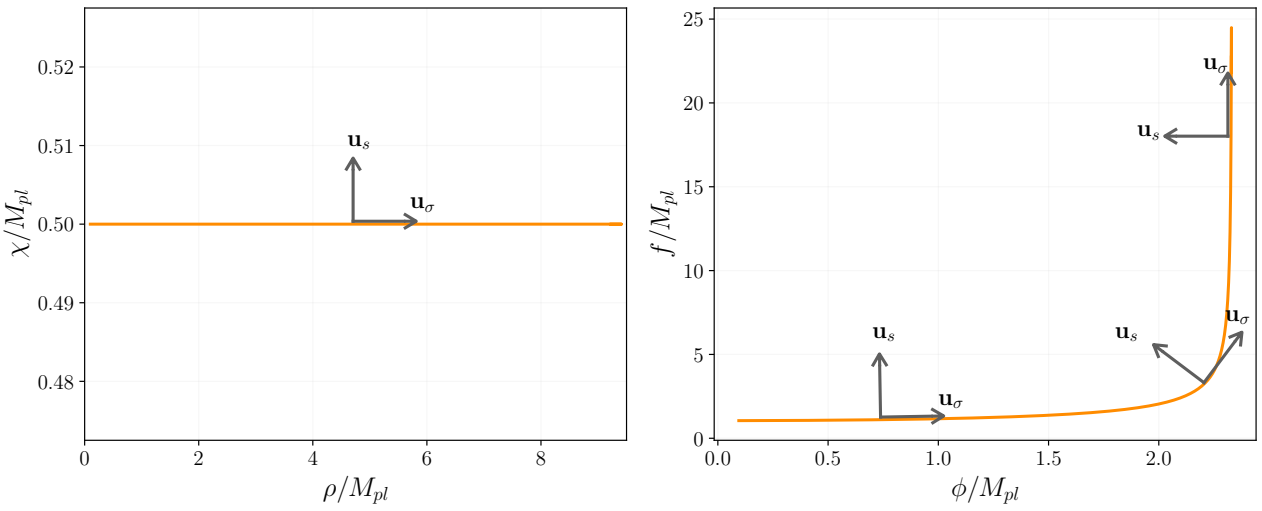

Figure 4.3: Field-space trajectory in the (ρ, χ) representation (*left panel*) and in the (ϕ, f) representation (*right panel*), obtained from numerical integration of the equations of motion (4.19)–(4.22), in e-folding time N. To give a realistic picture, the model parameters are set to values that are compatible with the inflationary bounds found in Chapter 3, namely $\xi = 10^{-3}, \Omega = 1.07\,\xi^2, \alpha = 2 \times 10^{10}$. The initial conditions are set to $\rho(0) = 0.1\ M_{pl}, \chi(0) = 0.5\ M_{pl}, \rho'(0) = 0, \chi'(0) = 0$. The dynamical evolution in the (ϕ, f) representation has been trivially obtained from inversion of the definitions for ρ and χ given in Eqs. (3.48)–(3.49). The black arrows represent the adiabatic and entropy unit vectors at different points of the trajectory.

It follows that the field f can be entirely expressed in terms of ϕ at each time t during inflation,

$$f(t) = \frac{\sqrt{6}M_{pl}^2}{\sqrt{2K_0 - \phi(t)^2}}. \tag{4.60}$$

As a consequence, the following relations hold

$$\begin{aligned} \delta f &= \frac{\mathrm{d}f}{\mathrm{d}\phi}\delta\phi = \frac{\sqrt{6}M_{pl}^2\phi}{(2K_0 - \phi^2)^{3/2}}\delta\phi, \\ \dot{f} &= \frac{\mathrm{d}f}{\mathrm{d}\phi}\dot{\phi} = \frac{\sqrt{6}M_{pl}^2\phi}{(2K_0 - \phi^2)^{3/2}}\dot{\phi}. \end{aligned} \tag{4.61}$$

The entropy perturbation δs from Eq. (4.58) can thus be written entirely in terms of ϕ

$$\begin{aligned} \delta s &= \sqrt{6}e^{-b}\cos\theta\delta f - e^b \sin\theta\delta\phi \\ &= \frac{\sqrt{6}}{\dot{\sigma}}\left(\dot{\phi}\delta f - \dot{f}\delta\phi\right) \\ &= \frac{\sqrt{6}}{\dot{\sigma}}\left(\frac{\sqrt{6}M_{pl}^2\phi}{(2K_0 - \phi^2)^{3/2}}\dot{\phi}\delta\phi - \frac{\sqrt{6}M_{pl}^2\phi}{(2K_0 - \phi^2)^{3/2}}\dot{\phi}\delta\phi\right) \\ &= 0. \end{aligned} \tag{4.62}$$

Consequently, the entropy perturbations vanish in the (ϕ, f) field representation. We can now draw the following conclusions:

- Moving from the field basis (ρ, χ) to the kinetic basis (σ, s), we found that the entropy perturbation δs is subjected to a potentially dangerous tachyonic instability, since the effective

mass squared of entropy perturbations is always negative (see Figure 4.2) and $\delta s \propto e^{\rho/M_{pl}}\delta\chi$, with $\delta\chi = $ const. on super-horizon scales.

- Moving from the field basis (ϕ, f) to the kinetic basis (σ, s), we found that the entropy perturbation δs is vanishing as a consequence of the constraint imposed by the Noether current conservation.
- As shown in Sec. 4.1.2, the entropy field δs is gauge-invariant.

Clearly, there is some intrinsic contradiction in the three points listed above. Moreover, since we recovered the (expected) single-field result $\delta s = 0$ starting with the field basis (ϕ, f), it is natural to conclude that the origin of the apparent geometrical instability leading to a tachyonic growth of δs is in the time evolution of the projector from the field basis (ρ, χ) to the kinetic basis (σ, s). Indeed, considering again $\theta = 0$, the unity vectors defined in Eq. (4.26) become

$$\mathbf{u}_{\sigma,I} = (1, 0)\,, \qquad \mathbf{u}_{s,I} = \left(0, e^b\right). \tag{4.63}$$

The growing factor imposed by orthonormality then leads to the apparent growth of δs. The pathology lies in the flat field-space trajectory and is absent in the less trivial trajectory in the (ϕ, f) representation. We conclude that this spurious effect is nonphysical and that entropy perturbations vanish as a mere consequence of the constraint imposed by scale symmetry.

A very similar effect was observed by Cicoli *et al.* in [206, 207] in the context of multifield non-linear sigma models and Fibre inflation with light kinetically coupled spectator fields. It was found that the effective mass squared of entropy perturbations becomes tachyonic, signaling exponential growth of isocurvature modes and a regime where perturbation theory breaks down. However, it was also shown that the background trajectory of these multifield models turns out to be fully stable.

This pathological effect was later explained by the same authors in [208] as a consequence of the fact that commonly used entropy variables like δs become ill-defined in these particular situations. One should instead adopt a modified version of the relative entropy variable, defined as

$$\hat{S}_{ij} \equiv -\frac{1}{6\dot{\rho}\dot{p}}\dot{\rho}_i\dot{\rho}_j\left(c_i^2 - c_j^2\right)S_{ij}, \quad \text{where} \quad S_{ij} = -3H\left(\frac{\delta\rho_i}{\dot{\rho}_i} - \frac{\delta\rho_j}{\dot{\rho}_j}\right), \tag{4.64}$$

and $c_i^2 \equiv \dot{p}_i/\dot{\rho}_i$. Clearly, $\hat{S}_{ij}$ remains finite even in the $\dot{\rho}_i \to 0$ limit.

In our case, since we have already proved that entropy perturbations are vanishing if we start from the (ϕ, f) representation, any concern about potential tachyonic instabilities is erased. At the same time, keeping this result in mind, we can continue adopting the decomposition into tangential and normal components presented above, which remains a very robust way to compute adiabatic and entropy perturbations numerically.

This analysis concludes that perturbations are purely adiabatic, meaning that the Goldstone boson does not contribute to the dynamics even at first order in perturbation theory. As we will see, the results for the power spectra and the level of non-Gaussianities are the same as those of single-field models. While this result seems rather natural in the (ρ, χ) representation, it is less immediate in the (ϕ, f) representation, where both scalar fields carry a non-trivial dynamical content.

Since perturbations are entirely along the direction tangential to the background trajectory, we can identify $\delta\sigma = \delta\rho$ from Eq. (4.23). The inflaton field is then interpreted as the only clock of the Universe:[8] it fixes the Hubble parameter, and its fluctuations are equivalent to a relative rescaling of the scale factor in different parts of the Universe.

[8]This interpretation is clear if we remind that adiabatic perturbations are locally indistinguishable from time shifts, as mentioned at the end of Sec. 4.1.2.

4.2.2 Slow-roll approximation

The results derived so far are exact up to linear order in perturbations. To make contact with the spectral indices, we now employ the slow-roll approximation. In a multifield scenario, requiring slow roll corresponds to imposing the following conditions

$$\begin{aligned}\epsilon &= -\frac{\dot{H}}{H^2} \ll 1 \longrightarrow \mathcal{G}_{IJ}\dot{\phi}^I\dot{\phi}^J \ll V(\phi^I),\\ \epsilon_1 &= \frac{\dot{\epsilon}}{H\epsilon} \ll 1 \longrightarrow 2\dot{\phi}^I\mathcal{D}_t\dot{\phi}^I \ll H\mathcal{G}_{IJ}\dot{\phi}^I\dot{\phi}^J,\end{aligned} \tag{4.65}$$

where $\mathcal{D}_t$ is the covariant time derivative in field space.

We remind that at the background level, the slow-roll approximation of the equations of motion is the same as found in Eq. (3.59), namely[9]

$$\dot{\rho} = \dot{\sigma}\cos\theta \simeq -\frac{V_{,\rho}}{3H}, \qquad \dot{\chi} = \dot{\sigma}\sin\theta e^{-b} \simeq 0, \qquad H^2 \simeq \frac{V(\rho)}{3M_{pl}^2}. \tag{4.66}$$

In terms of the quantities in the kinetic frame, Eqs. (4.27)–(4.28) become

$$\frac{\ddot{\sigma}}{H\dot{\sigma}} \simeq \epsilon - \frac{V_{,\rho\rho}}{3H^2}, \tag{4.67}$$

$$-\frac{\dot{\theta}}{H} \simeq 0, \tag{4.68}$$

which agrees with the fact that the background trajectory is flat, with the entropy field completely decoupled from the dynamics, which are entirely determined by the adiabatic one.

Under these conditions, the curvature power spectrum at horizon crossing reads

$$\mathcal{P}_{\mathcal{R}}(k) \simeq \left.\frac{H^2}{8\pi^2\,\epsilon}\right|_{k=k_*}, \tag{4.69}$$

which is consistent with the single-field result found in Eq. (1.64), once the correct units are restored.

The tensor power spectrum takes the familiar form derived in Eq. (1.71) as well, namely

$$\mathcal{P}_T(k) = \left.\frac{2}{\pi^2}\frac{H^2}{M_{pl}^2}\right|_{k=k_*}, \tag{4.70}$$

which is expected, since the result in Eq. (1.71) was obtained from the EH action and is independent of the matter content of the action, and thus is perfectly compatible with the EF formulation we are considering. See also [176] for the derivation of the tensor power spectrum.

From the definition of ϵ, inserting the two Friedmann equations (4.21)–(4.22) and further considering Eq. (4.67), we get

$$\dot{\epsilon} \simeq 2\epsilon H\left(2\epsilon - \frac{V_{,\rho\rho}}{3H^2}\right). \tag{4.71}$$

In this way, we can compute the scalar spectral index at horizon crossing ($k = k_*$)[10]

$$n_s - 1 \equiv \left.\frac{\mathrm{d}\ln\mathcal{P}_{\mathcal{R}}}{\mathrm{d}\ln k}\right|_{k_*} = \left.\frac{\mathrm{d}\ln\mathcal{P}_{\mathcal{R}}}{H\,\mathrm{d}t}\right|_{k_*} \simeq -6\epsilon_* + \frac{2V_{,\rho\rho}(\rho_*)}{3H_*^2}, \tag{4.72}$$

[9] Here and in what follows, the symbol $\simeq$ indicates that we are within the slow-roll approximation.

[10] Note the typo $n_s - 1 \to n_s$ in [7, 196, 197].

and its running $\alpha_s \equiv dn_s/d\ln k$[11]

$$\alpha_s \simeq -24\epsilon^2 + 16\epsilon\frac{V_{,\rho\rho}}{3H^2} + 2\sqrt{2\epsilon}\cos\theta\frac{V_{,\rho\rho\rho}}{3H^2}\,. \tag{4.73}$$

For completeness, even though it is not used in the later numerical analysis, we quote the expression for the running of the running of the scalar spectral index $\beta_s \equiv d\alpha_s/d\ln k$:

$$\beta_s \simeq -192\epsilon^3 + \frac{64\epsilon^2 V_{,\rho\rho}}{H^2} - \frac{32\epsilon V_{,\rho\rho}^2}{9H^4} + \frac{8\sqrt{2}\epsilon^{3/2}\cos\theta V_{,\rho\rho\rho}}{H^2} - \frac{2\sqrt{2\epsilon}\cos\theta V_{,\rho\rho}V_{,\rho\rho\rho}}{9H^4} + \frac{4\epsilon\cos^2\theta V_{,\rho\rho\rho\rho}}{3H^2}\,. \tag{4.74}$$

4.2.3 Transfer matrix formalism

To relate the initial curvature and entropy perturbations generated during inflation to the same quantities at much later cosmic times and to compare the latter with observations, we need to model their evolution on large, super-horizon scales. In our case, to prove that the effects of isocurvature modes on the adiabatic ones are absent on super-horizon scales, we employ the transfer matrix formalism first introduced by Wands *et al.* in [209].

Since, as already mentioned, purely adiabatic perturbations cannot source entropy perturbations on large scales, but entropy perturbations can affect curvature perturbation and also evolve by themselves, we can write the time evolution for curvature and isocurvature perturbations in the very general form [210]

$$\dot{\mathcal{R}} = AH\mathcal{S}, \qquad \dot{\mathcal{S}} = BH\mathcal{S}, \tag{4.75}$$

where A and B are in general time-dependent and dimensionless functions.

Integrating Eq. (4.75) over time, we can relate curvature and isocurvature perturbations generated during inflation and evaluated at horizon crossing ($t = t_*$) to the same quantities at some later time t. In matrix form,

$$\begin{pmatrix}\mathcal{R}\\ \mathcal{S}\end{pmatrix} = \begin{pmatrix}1 & T_{\mathcal{RS}}\\ 0 & T_{\mathcal{SS}}\end{pmatrix}\begin{pmatrix}\mathcal{R}\\ \mathcal{S}\end{pmatrix}_*, \tag{4.76}$$

where we introduced the transfer functions $T_{\mathcal{RS}}$ and $T_{\mathcal{SS}}$, defined as

$$\begin{aligned}\mathcal{T}_{\mathcal{RS}}(t_*,t) &= \int_{t_*}^{t} A(t')H(t')\mathcal{T}_{\mathcal{SS}}(t_*,t')dt',\\ \mathcal{T}_{\mathcal{SS}}(t_*,t') &= \exp\left(\int_{t_*}^{t'} B(t'')H(t'')dt''\right).\end{aligned} \tag{4.77}$$

The transfer functions are implicit functions of scale through their dependence on $t_*(k)$. More explicitly, their scale dependence reads

$$\begin{aligned}\frac{1}{H_*}\frac{\partial T_{\mathcal{RS}}}{\partial t_*} &= -A_* - B_* T_{\mathcal{RS}},\\ \frac{1}{H_*}\frac{\partial T_{\mathcal{SS}}}{\partial t_*} &= -B_* T_{\mathcal{SS}},\end{aligned} \tag{4.78}$$

so it is completely encoded into A and B evaluated at horizon crossing. To compute them, we can bring the evolution of curvature and isocurvature perturbations in the compact form (4.75). From the definition in Eq. (4.36) and the super-horizon result (4.38), we can write

$$\dot{\mathcal{R}} \approx -2\frac{V_{,s}}{\dot\sigma}\mathcal{S} = AH\mathcal{S}, \tag{4.79}$$

$$\dot{\mathcal{S}} = \frac{H}{\dot\sigma}\dot{\delta s} + \left(\frac{\dot H}{H^2} - \frac{\ddot\sigma}{H\dot\sigma}\right)\frac{H^2}{\dot\sigma}\delta s = BH\mathcal{S}. \tag{4.80}$$

[11] We omit the symbol $*$ for clarity, but all the variables are meant to be evaluated at horizon crossing.

To evaluate Eq. (4.80), we can use the slow-roll results (4.66)–(4.68), together with the evolution equation of entropy perturbations (4.42) and Eq. (4.35). We find

$$A = 2\xi_1 \sin\theta \simeq 0\,, \tag{4.81}$$

$$B = -2\epsilon + \xi_1 + \frac{\xi_1^2}{3} + \frac{\xi_2}{3} + \frac{V_{,\rho\rho}}{3H^2}\,, \tag{4.82}$$

with $\xi_1 \equiv \sqrt{2\epsilon}b_{,\rho}$ and $\xi_2 \equiv 2\epsilon b_{,\rho\rho}$. Applying the transfer matrix (4.76) to the initial scalar power spectrum at horizon crossing, computed in Eq. (4.69), we can obtain the resulting curvature and isocurvature power spectra at the start of the radiation domination era:

$$\begin{aligned}
\mathcal{P}_{\mathcal{R}} &= \left(1 + T_{\mathcal{RS}}^2\right) \mathcal{P}_{\mathcal{R}}|_*\,, \\
\mathcal{P}_{\mathcal{S}} &= T_{\mathcal{SS}}^2\, \mathcal{P}_{\mathcal{R}}|_*\,, \\
\mathcal{C}_{\mathcal{RS}} &= T_{\mathcal{RS}} T_{\mathcal{SS}}\, \mathcal{P}_{\mathcal{R}}|_*\,.
\end{aligned} \tag{4.83}$$

Hence, by means of Eq. (4.81) and the fact that $\theta \approx 0$, we see that isocurvature perturbations do not affect the evolution of the curvature power spectrum, as in any single-field slow-roll model of inflation.

4.3 Non-Gaussianities

The predictions for the power spectra (or, equivalently, for the two-point correlation functions) derived above fully characterize curvature perturbations provided that they are Gaussian. In this case, all odd n-point correlators vanish, while even n-point correlators can be expressed as sums of disconnected products of two-point functions via Wick's theorem [137].

From a statistical perspective, Gaussianity naturally arises as the limiting distribution when a large number of independent measurements are drawn from the same probability density function, as stated by the central limit theorem. Since observational data typically involve averages over many small-scale processes, assuming Gaussian statistics represents a well-motivated starting point for an unknown distribution. This expectation is particularly well justified for curvature perturbations, given their close analogy with the quantum harmonic oscillator, whose ground state is Gaussian. As an illustrative example, dividing the CMB sky into many small patches yields comparable numbers of hotter and colder regions relative to the mean temperature, resulting in a histogram consistent with a normal distribution [211].

Deviations from exact Gaussianity therefore carry important information about the inflationary dynamics and, as will be discussed below, may point toward extensions beyond single-field models. Since a Gaussian distribution is preserved under linear transformations but not under non-linear ones, perturbation theory naturally associates Gaussian perturbations with linear order, while non-Gaussian features arise from higher-order contributions. Furthermore, the intrinsic non-linearity of gravity tends to amplify departures from Gaussianity over time, so that even initially Gaussian perturbations generally evolve into non-Gaussian matter overdensities at late times.[12] This is why detecting non-Gaussianities is typically easier at CMB scales rather than from LSS [14].

The primary measure of non-Gaussianity is the three-point function,[13]

$$\langle \zeta(\mathbf{k}_1)\zeta(\mathbf{k}_2)\zeta(\mathbf{k}_3)\rangle = (2\pi)^3\, B_\zeta(k_1, k_2, k_3)\delta^{(3)}\left(\mathbf{k}_1 + \mathbf{k}_2 + \mathbf{k}_3\right), \tag{4.84}$$

[12] The non-Gaussianities arising from the non-linear gravitational evolution of an initially Gaussian perturbation are called *secondary non-Gaussianities* and are relevant only at late times [211].

[13] For consistency with the literature of non-Gaussianities, we use here the curvature perturbation ζ as defined in Eq. (1.35).

where we have introduced the *bispectrum* B_ζ, in continuity with the spectrum defined in Eq. (1.41). The delta function comes from assuming statistical homogeneity, while the assumption of statistical isotropy allows us to write the bispectrum as a function of the three amplitudes k_1, k_2 and k_3 only, with the only constraint imposed by momentum conservation, so that the three $\mathbf{k}_i$ form a triangle. Detecting non-Gaussianities is therefore observationally challenging, since there are many possible triangular shapes. On the other side of the coin, if detected, they could provide much information beyond that encoded in the power spectrum.

A simple model of non-Gaussianity is *local non-Gaussianity*, which is defined as a Taylor expansion of the curvature perturbation around its Gaussian part ζ_G [211]

$$\zeta(\mathbf{x}) = \zeta_G(\mathbf{x}) + \frac{3}{5} f_{\rm NL} \left(\zeta_G^2(\mathbf{x}) - \langle \zeta_G^2(\mathbf{x}) \rangle \right). \tag{4.85}$$

The name comes from the fact that it is defined locally in real space, i.e., $\zeta = \zeta(\mathbf{x})$. Note that the variance has been subtracted to have $\langle \zeta \rangle = 0$. In Fourier space, the quadratic term becomes a convolution, and we can write the bispectrum as

$$B_\zeta(k_1, k_2, k_3) = \frac{6}{5} f_{\rm NL} \left[P_\zeta(k_1) P_\zeta(k_2) + \text{c.p.} \right], \tag{4.86}$$

where c.p. denotes cyclic permutations of k_1, k_2, and k_3. In this way, observational constraints on non-Gaussianities are phrased in terms of $f_{\rm NL}$. Moreover, it can be shown that, for the local type of non-Gaussianities, the signal is concentrated in the *squeezed configuration* in Fourier space, corresponding to triangles with $k_3 \ll k_1, k_2$. This is also the shape LSS probes are more sensitive to, thus we will neglect other types of non-Gaussianities in the following.

A convenient method to compute $f_{\rm NL}$ for local non-Gaussianities is the δN formalism, see, e.g., [210, 212–215]. In the following, we review its main features. We will mainly follow the discussion presented in [216] for multifield inflation.

Let's consider a spatially flat FLRW metric where only scalar perturbations are present. The perturbed space part can be written as

$$g_{ij} = a(t)^2 e^{-2\psi(t,\mathbf{x})} \delta_{ij}, \tag{4.87}$$

which follows from the line element in Eq. (1.24). We can introduce an effective scale factor $\hat{a}$, defined as

$$\hat{a}(t, \mathbf{x}) \equiv a(t) e^{-\psi(t,\mathbf{x})}, \tag{4.88}$$

which allows us to define a local e-folding number

$$\hat{N} \equiv \ln \left(\frac{\hat{a}}{\hat{a}_*} \right) = -\psi + \psi_* + N. \tag{4.89}$$

For a spatially flat spacetime slice, $\psi = \psi_* = 0$, the local e-folding number $\hat{N}$ coincides with the background e-folding number N. The idea behind the δN formalism is that the curvature perturbation ζ on some final uniform density slice is given by the spatial fluctuations of the e-folding number between an initial spatially flat slice and the final uniform density slice. Indeed, replacing in Eq. (4.89) $\psi_* = 0$ for the initial slice and $\psi = -\zeta$ for the final uniform density slice, see the definition in Eq. (1.35), we have

$$\zeta(t, \mathbf{x}) = \hat{N}(t, \mathbf{x}) - N(t) \equiv \delta N. \tag{4.90}$$

We stress that it is not important when we consider the initial time t_* as long as $\psi_* = 0$ and t_* is after the time at which the scales under consideration have left the horizon. A convenient choice is to set t_* precisely as the horizon crossing time.

Since the scalar fields provide the only contribution to the energy density, we can equivalently write

$$\zeta(t,\mathbf{x}) = \hat{N}(\phi^I + \delta\phi^I) - N(\phi^I) \simeq N_{,I}(N,\phi_*^J)\delta\phi_*^I(\mathbf{x}) + \frac{1}{2}N_{,IJ}(\phi_*^K)\delta\phi_*^I(\mathbf{x})\delta\phi_*^J(\mathbf{x}) + \dots\,, \tag{4.91}$$

which is the δN expansion. Since the field perturbations, $\delta\phi_*^I(\mathbf{x}) \equiv \phi_*^I(\mathbf{x}) - \phi_*^I$, correspond to coordinate displacements, they do not transform covariantly in a curved spacetime. To make the δN expansion explicitly covariant, we follow the discussion of [216]. For sufficiently small $\delta\phi_*^I(\mathbf{x})$, the two points $\phi_*^I(\mathbf{x})$ and ϕ_*^I are connected by a unique geodesic that can be parametrized by λ. Choosing λ such that $\phi^I(\lambda=0) = \phi_*^I$ and $\phi^I(\lambda=1) = \phi_*^I(\mathbf{x})$, we can perform a Taylor expansion

$$\delta\phi^I = \phi^I(\lambda=1) - \phi^I(\lambda=0) \simeq \left.\frac{\mathrm{d}\phi^I}{\mathrm{d}\lambda}\right|_{\lambda=0} + \frac{1}{2}\left.\frac{\mathrm{d}^2\phi^I}{\mathrm{d}\lambda^2}\right|_{\lambda=0} + \dots\,. \tag{4.92}$$

The geodesic equation reads

$$\mathcal{D}_\lambda\frac{\mathrm{d}\phi^I}{\mathrm{d}\lambda} \equiv \frac{\mathrm{d}^2\phi^I}{\mathrm{d}\lambda^2} + \Gamma^I_{JK}\frac{\mathrm{d}\phi^J}{\mathrm{d}\lambda}\frac{\mathrm{d}\phi^K}{\mathrm{d}\lambda} = 0. \tag{4.93}$$

By introducing the quantity $\mathcal{Q}^I = d\phi^I/d\lambda|_{\lambda=0}$ which resides in the tangent space at $\phi^I(\lambda=0)$ and thus transforms covariantly [216, 217], we can express $\delta\phi^I$ in terms of $\mathcal{Q}^I$ as

$$\delta\phi^I = \mathcal{Q}^I - \frac{1}{2}\Gamma^I_{JK}\mathcal{Q}^J\mathcal{Q}^K + \dots\,, \tag{4.94}$$

where we inserted Eq. (4.93) into Eq. (4.92). We can now recast the δN expansion in Eq. (4.91) as follows:

$$\zeta(N,\mathbf{x}) = N_{,I}(N,\phi_*^J)\mathcal{Q}_*^I(\mathbf{x}) + \frac{1}{2}\mathcal{D}_I\mathcal{D}_J N(N,\phi_*^K)\mathcal{Q}_*^I(\mathbf{x})\mathcal{Q}_*^J(\mathbf{x}) + \dots\,, \tag{4.95}$$

which is now manifestly covariant. Starting from this expansion, we can compute the two-point correlator

$$\begin{aligned}\langle\zeta(\mathbf{k}_1)\zeta(\mathbf{k}_2)\rangle &= N_{,I}N_{,J}\langle\mathcal{Q}_*^I(\mathbf{k}_1)\mathcal{Q}_*^J(\mathbf{k}_2)\rangle \\ &= N_{,I}N_{,J}\mathcal{G}_*^{IJ}(2\pi)^3\delta^{(3)}\left(\mathbf{k}_1+\mathbf{k}_2\right)P_{\mathcal{Q},*}(k_1)\,,\end{aligned} \tag{4.96}$$

where, for brevity, we have dropped the arguments of N_I, and we have adopted the standard definition of the power spectrum, see Eq. (1.41). Since at linear order $\mathcal{Q}^I \simeq \delta\phi^I$, we can employ the result for the power spectrum for scalar field fluctuations

$$P_{\mathcal{Q},*}(k) = \frac{2\pi^2}{k^3}\mathcal{P}_{\mathcal{Q},*} = \frac{2\pi^2}{k^3}\left(\frac{H_*}{2\pi}\right)^2. \tag{4.97}$$

Note that we recover the power spectrum for curvature perturbations expected for single-field slow-roll inflation,

$$\mathcal{P}_\zeta(k) = \left(\frac{H_*}{2\pi}\right)^2\mathcal{G}_*^{IJ}N_{,I}N_{,J} = \left(\frac{H_*}{2\pi}\right)^2(N_{,\rho})^2\,, \tag{4.98}$$

where the last equality follows after considering the explicit field-space metric in the (ρ,χ) representation, see Eq. (4.18). Since then, from Eq. (3.64), $N \simeq -\int d\rho/(M_{pl}\sqrt{2\epsilon(\rho)})$, the result already found in Eq. (4.69) in terms of the slow-roll parameter ϵ is recovered.[14]

[14] In this particular case, we can safely identify $\mathcal{P}_\zeta = \mathcal{P}_\mathcal{R}$.

We can now compute the three-point function. Following [211], we have

$$\begin{aligned}\langle\zeta(\mathbf{k}_1)\zeta(\mathbf{k}_2)\zeta(\mathbf{k}_3)\rangle &= \frac{1}{2}N_{,I}N_{,J}N_{,KL}\langle\mathcal{Q}_*^I(\mathbf{k}_1)\mathcal{Q}_*^J(\mathbf{k}_2)\int\frac{\mathrm{d}^3q}{(2\pi)^3}\mathcal{Q}_*^K(\mathbf{q})\mathcal{Q}_*^L(\mathbf{k}_3-\mathbf{q})\rangle + \text{c.p.}\\ &= \frac{1}{2}N_{,I}N_{,J}N_{,KL}2\int\frac{\mathrm{d}^3q}{(2\pi)^3}\langle\mathcal{Q}_*^I(\mathbf{k}_1)\mathcal{Q}_*^K(\mathbf{q})\rangle\langle\mathcal{Q}_*^J(\mathbf{k}_2)\mathcal{Q}_*^L(\mathbf{k}_3-\mathbf{q})\rangle + \text{c.p.}\\ &= N_{,I}N_{,J}N_{,KL}\delta^{IK}\delta^{JL}P_{\mathcal{Q},*}(k_1)P_{\mathcal{Q},*}(k_2)\delta^{(3)}\left(\mathbf{k}_1+\mathbf{k}_2+\mathbf{k}_3\right),\end{aligned} \tag{4.99}$$

where, in the second equality, we have applied Wick's theorem to split the four-point function into the disconnected product of two two-point functions.

From the above expressions, we can appreciate the power of the δN formalism. Since the derivatives of N only depend on background quantities, we only need to know the statistical properties of the field perturbations at horizon crossing, which are encoded into $P_{\mathcal{Q},*}$, and compute the non-linear evolution of cosmological perturbations on large scales without the need to solve the full perturbed field equations.

After inverting Eq. (4.86), we can compute $f_{\rm NL}$

$$f_{\rm NL} = \frac{5}{6}\frac{\mathcal{G}_*^{IK}N_{,K}\mathcal{G}_*^{JL}N_{,L}\mathcal{D}_I N_{,J}}{(\mathcal{G}_*^{KH}N_{,H}N_{,K})^2} = \frac{5}{6}\frac{N_{,\rho}^2(N_{,\rho\rho}-\Gamma^\rho_{\rho\rho}N_{,\rho})}{N_{,\rho}^4} = \frac{5}{6}\frac{N_{,\rho\rho}}{N_{,\rho}^2} \simeq \frac{5}{3}M_{pl}\epsilon(\rho)\frac{\partial}{\partial\rho}\frac{1}{\sqrt{2\epsilon(\rho)}}\,. \tag{4.100}$$

The above expression is identical to the one obtained for single-field inflation models with canonical kinetic terms, see, e.g., Eq. (1.34) of [211]. This result is indeed consistent with the fact, already stressed earlier, that the inflationary dynamics within our model are effectively driven by the field ρ, whose kinetic term is canonical. The fact that χ has a non-canonical kinetic term is completely irrelevant.

Note that our result can be written in terms of the scalar spectral index as

$$f_{\rm NL} = \frac{5}{6}(\epsilon-\eta) = \frac{5}{12}\left(1-n_s-2\epsilon\right). \tag{4.101}$$

This result seems to be different from Maldacena's consistency relation [35], stating that in single-field inflation, the squeezed limit of the primordial bispectrum is uniquely fixed by the scalar spectral index as

$$\lim_{k_3\to0}\langle\zeta(\mathbf{k}_1)\zeta(\mathbf{k}_2)\zeta(\mathbf{k}_3)\rangle = (2\pi)^3\,\delta^{(3)}\left(\mathbf{k}_1+\mathbf{k}_2+\mathbf{k}_3\right)(n_s-1)\,P_\zeta(k_1)P_\zeta(k_3). \tag{4.102}$$

See also the proof of Maldacena's theorem by Creminelli and Zaldarriaga [218], which is independent of the inflationary dynamics and resides upon the sole assumption that the inflaton is the only dynamical field. The proof does not even assume the slow-roll approximation.

As shown in [219], the apparent inconsistency comes from considering the short-wavelength perturbations $\delta\phi^I$ to be independent of the long-wavelength ones. After correctly accounting for the long-wavelength modulation induced by the perturbation of the Hubble parameter, one can show that the $f_{\rm NL}$ parameter takes an additional contribution, namely

$$f_{\rm NL} = \frac{5}{6}\left(\frac{N_{,\rho\rho}}{N_{,\rho}^2}+\frac{1}{N_{,\rho}}\frac{V_{,\rho}}{2V}\right) = \frac{5}{12}\left(1-n_s\right), \tag{4.103}$$

therefore recovering Maldacena's consistency relation. The analysis presented in [219] also clarifies the role of the additional contribution as purely kinematical, rather than a genuinely intrinsic non-Gaussianity, as sometimes stated [220].

The result of Maldacena is a powerful way to probe single-field inflation. Since in the squeezed limit the three-point function is suppressed by $(1-n_s)$, which vanishes for a perfectly scale-invariant power

spectrum, a detection of primordial non-Gaussianity in the squeezed limit could rule out single-field inflation [14].
To give an example, for the benchmark point in the parameter space given in Eqs. (3.80)–(3.81), we have $f_{\rm NL} = -0.015$, well within the region allowed by present precision cosmological observations. As a reference, limits on the amplitude of the local bispectrum in the CMB measured by *Planck* give $f_{\rm NL}^{\rm local} = -0.9 \pm 5.1$ [221]. Constraints on $f_{\rm NL}^{\rm local}$ from LSS probes are weaker by at least an order of magnitude, see, for instance [222–226], which is consistent with the discussion made above on secondary non-Gaussianities.

4.4 Cosmological constraints

Thus far, we have studied the scale-invariant model primarily through analytical methods, supplementing the analysis of the homogeneous background with numerical integrations for a set of benchmark configurations. While this approach has allowed us to obtain robust results by treating the model within the standard multifield inflationary framework, our results are subject to the following limitations:

- Our analysis neglects any potential effect arising from variations of the initial conditions, i.e., the values of the fields and their velocity at the beginning of integration. Sampling over the initial conditions is a crucial aspect to assess the predictability of the model, in order to investigate whether inflation can occur for generic (or, conversely, fine-tuned) initial conditions. It is known that different initial conditions for the fields can lead to different trajectories in field space, which can produce slightly different observables [227]. In our case, since we have shown that the dynamics are effectively single-field, with a potential $V(\rho)$ with a sufficiently extended flat plateau, we expect only minor modifications to the values of the observables at horizon crossing for different initial conditions for ρ.

  On the other hand, we have seen that the constraint imposed by Noether current conservation, see Eq. (3.46), implies that the parameter K is composed of a constant term and a quickly decaying one as $\sim a^{-3}$, see Eq. (3.27). We have completely neglected the effect of the decaying mode, which discriminates between two-field and single-field dynamics. While this assumption is reasonable as a first approximation in an exponentially expanding universe, it must be checked upon variations of the initial conditions for the two fields.

- The analysis presented in Sec. 3.3 to constrain the model against observational data is rather qualitative, and is based on some benchmark points in parameter space, rather than performing a full sampling over α, ξ, and Ω. A more comprehensive analysis would instead require a sampling algorithm to set robust constraints on the model's parameter space against the latest observational data.

In this section, we present the numerical analysis carried out in [7], in which the full dynamical system of the model is solved numerically. This approach enables the computation of accurate predictions for a range of observable quantities beyond n_s and r, while also allowing for an efficient exploration of the dependence on the initial conditions.

4.4.1 Numerical methods

From the analysis presented in the previous sections, the scale-invariant model reduces to a scenario where two scalar fields coexist in a non-trivial field space $\mathcal{G}_{IJ}(\rho, \chi)$. In total, we are left with three free parameters: ξ, Ω, and α. Using Monte Carlo (MC) techniques, we aim to explore the model's 3D parameter space and compare its theoretical predictions with observational data.

To tackle the numerical analysis, we employ the code developed by Giarè *et al.* in [197], specifically designed to study generic multifield inflationary models where fields are minimally coupled to gravity and the field-space metric is allowed to be non-trivial.

The code uncovers some of the main limitations of numerical analyses for multifield inflation. Obtaining precise predictions from multifield inflation is much more involved than in single-field analyses, given the various factors that affect the dynamics, such as the initial conditions of the fields and the specific model assumed. For this reason, most tools employed in cosmological data analyses, such as typical Boltzmann integrator codes and samplers, are either unaware of the physics of inflation or assume single-field potentials. As a result, constraining the multifield landscape with current CMB data represents an ongoing challenge.

The algorithm is structured into three main parts:

1. Numerical integration of the field equations over the entire inflationary phase. On this basis, predictions for observable quantities are obtained, including the scalar power spectrum, primordial gravitational waves, and isocurvature perturbations. The transfer matrix formalism introduced in Sec. 4.2.3 is implemented to follow the evolution of adiabatic and isocurvature modes on super-horizon scales.

2. Interfacing the algorithm with Boltzmann solver codes to compute the subsequent cosmological evolution, including the CMB temperature anisotropy and polarization angular power spectra.

3. An efficient sampling procedure designed to explore a large region of the parameter space and to identify sub-regions in which the theoretical predictions are consistent with observational constraints.

Integration scheme

At each step of the MC, we randomly select initial conditions for the fields and values for the three free parameters of the model from the uniform prior ranges reported in the rightmost column of Table 4.1. This, therefore, also allows us to explore the impact of initial conditions on the fields.

We then integrate the equations of motion for the fields and track their evolution over the inflationary potential. Given the peculiarity of this model, where, depending on the parameter values, the field evolution can be characterized by a very prolonged slow-roll phase eventually leading to eternal inflation, see Sec. 3.3, the integration process is carried out for a (fairly large) maximum number of e-folds, set to $N_{\rm max} = 10^7$. During integration, we dynamically calculate the slow-roll parameter ϵ until $\epsilon = 1$. If this condition is not met within $N_{\rm max}$ e-folds, the model is classified as eternal inflation and rejected. Conversely, if the condition is satisfied during the integration, the point at which $\epsilon = 1$ in the parameter trajectory is considered as a possible end of inflation. To confirm that the point in question represents the actual end of inflation, we perform some tests detailed in [197]:

i) We check whether the fields remain sufficiently active to initiate a second stage of inflation. Specifically, this is done by testing whether the normalized field values, relative to their initial conditions, do not exceed a fixed threshold. If the field satisfies this condition, we can safely assume inflation is complete. In the opposite case, the integration continues until the fields fall below the specified threshold. If, during this additional stage of integration, inflation restarts (i.e., ϵ becomes smaller than one), the new end of inflation is determined by the joint conditions of $\epsilon = 1$ and the fields' values. Otherwise, the previously calculated end of inflation is kept as the definitive one.

ii) To ensure that the pathological cases examined in Sec. 3.3, corresponding to ϵ going to zero at the minimum of the potential before the condition $\epsilon = 1$ is met, we check that $\epsilon \neq 0$ throughout the full evolution.

iii) We check that inflation lasts for a total number of e-folds $\Delta N > 70$ to account for the observed homogeneity and isotropy of the Universe. If the total number of e-folds accumulated between the beginning and end of the integration is below the required threshold, we restart the integration with the same initial conditions and evolve the system backward in time to account for the missing e-folds. During this additional integration, we check the inflationary fields and parameters for any problematic behavior and verify that the model can indeed support the desired number of e-folds of expansion. Models that fail to satisfy these criteria are considered incompatible with observations and are therefore discarded.

After ensuring that the model satisfies all the above requirements, we reconstruct the full field dynamics during the entire inflationary phase, including how the slow-roll parameters and observables evolve as a function of N. By doing so, we can obtain the values of all slow-roll parameters at horizon crossing (set to $N_\star = 55$ e-folds before the end of inflation) including the amplitude of the primordial power spectrum of scalar perturbations (A_s), its spectral index (n_s), the running of the spectral index (α_s), and the amplitude of tensor perturbations (characterized by the tensor-to-scalar ratio $r \equiv A_T/A_s$).

Additionally, the code can account for super-horizon evolution and the transfer of entropy between isocurvature and scalar perturbations using the transfer matrix formalism described in Sec. 4.2.3. We find that the entropy transfer between isocurvature and scalar perturbations is consistent with zero also at the numerical level, confirming the theoretical result of Sec. 4.2.3.

For all selected models, we compute their full cosmology with `CAMB` [37, 38].

Sampling algorithm

By following this procedure, we generate a chain of points that is very similar to the output of typical Markov Chain MC (MCMC) methods. Each point of the chain is then assigned a likelihood based on how well it agrees with the latest CMB data.

In particular, our reference datasets include:

- The *Planck* 2018 temperature and polarization (TT, TE, EE) data, which also include low multipole data ($\ell < 30$) [15, 228, 229].
- The *Planck* 2018 lensing data, derived from measurements of the power spectrum of the lensing potential [230].
- The latest CMB B-modes power spectrum likelihood cleaned from the foreground contamination released by the *BICEP/Keck* collaboration, based on observations from the *BICEP2*, *Keck Array*, and *BICEP3* experiments up to and including the 2018 observation season [43].

We assign to each point in the chain a likelihood value obtained from an analytical multi-dimensional normal distribution:

$$\mathcal{L} \propto \exp\left(-\frac{1}{2}\left(\boldsymbol{x}-\boldsymbol{\mu}\right)^T \boldsymbol{\Sigma}^{-1}\left(\boldsymbol{x}-\boldsymbol{\mu}\right)\right), \tag{4.104}$$

where $\boldsymbol{\mu}$ and $\boldsymbol{\Sigma}$ represent the mean values and covariance matrix for the parameter vector $\boldsymbol{x} \equiv (A_s, n_s, \alpha_s, r)$ obtained from the above datasets, assuming an extension of the standard cosmological model which includes three additional parameters: r, α_s, and β_s, also referred to as ΛCDM+$n_s + \alpha_s + \beta_s$ [197].

The logical structure of the algorithm is schematized in the flowchart in Figure 4.4.

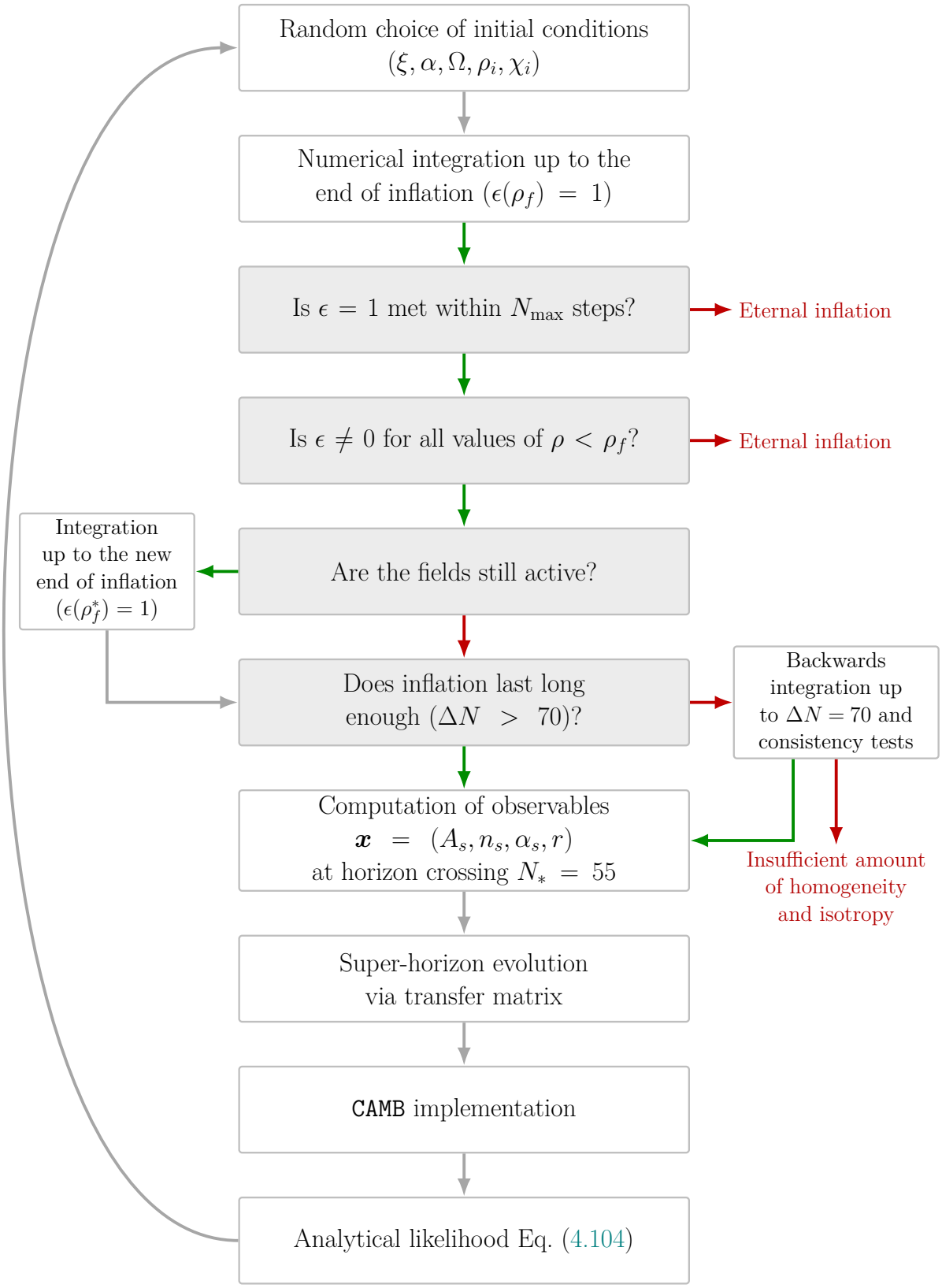

Figure 4.4: Flowchart of the numerical pipeline introduced in [197] and adapted to scale-invariant inflation, as described in Sec. 4.4.1. Gray boxes are node points representing questions for consistency checks. Green (red) arrows stand for positive (negative) answers.

This method was extensively validated in [197]. This was done by performing a full MCMC analysis using the publicly available sampler `Cobaya` [231] and the Boltzmann integrator `CAMB`. `Cobaya` explores the posterior distributions of the parameter space using the MCMC sampler developed for `CosmoMC` [232]. The results of the MCMC analysis were then used to construct the analytical likelihood in Eq. (4.104). To test that the analytical likelihood can reproduce the same constraints obtained from real experimental likelihoods, they considered the ΛCDM+$n_s + \alpha_s + \beta_s$ model again and performed a new run varying the inflationary parameters $(A_s, n_s, \alpha_s, \beta_s)$. The same prior ranges adopted in the MCMC analyses are used. They found that the resulting constraints agree with those obtained from the full MCMC analyses based on experimental likelihoods, demonstrating the equivalence of the two approaches. As a reference, see Figure 6 of [197] for the superposition of the posterior distributions obtained using `Cobaya` in combination with the full *Planck* 2018 and BK18 likelihoods, and the methodology outlined here.

Note that several other works have adopted and validated a similar compressed-likelihood approach to constrain fundamental parameters from inflation-related observables; see, for instance, [233, 234], used in the context of the stochastic gravitational wave background.

Using this method, we collect over 7×10^4 points within chains, each weighted by its own likelihood. This procedure enables us to constrain the model's free parameters and to analyze correlations both among these parameters and among observable quantities, including the spectral index and the amplitudes of the primordial scalar and tensor power spectra, which here are treated as *derived* parameters.

Differences from MCMC

We stress that, despite the similarity, our sampling method should *not* be considered an MCMC algorithm. For instance, the sampling is completely random, and there is no need to specify a proposal density or acceptance ratio (compare this to the widely used Metropolis-Hastings algorithm [235, 236]), thus the importance weight of each point in the chain is 1 by construction. For the same reason, there is no in-built notion of convergence (à la Gelman-Rubin [237]), but the level of convergence is assessed empirically from the stability of the resulting constraints against the addition of further samples.

As a further empirical test of convergence, we verified that by accumulating an increasing number of points in the chains and marginalizing to find the 1D posterior distributions, the tails corresponding to 5% C.L. actually contain approximately 5% of the total models. Such a result is exactly what is expected when marginalizing over the parameter space. It allows us to safely conclude that the tails of the distributions were well-sampled and adequately populated.

This methodology is intrinsically different from the standard approaches adopted to test inflationary models against observations, which is also the one we have employed in Figure 3.10. Instead of superimposing theoretical curves – typically at some fixed benchmark points in the parameter space – onto pre-obtained 2D marginalized probability contours in the (n_s, r) plane, here we can derive precise model-dependent predictions for inflationary parameters, such as the tensor-to-scalar ratio r and the running of the spectral index α_s. In this way, we have a more comprehensive view of the inter-relations among the model parameters and the inflationary observables.

4.4.2 Parameter Constraints

Constraints on the model parameters (including the initial conditions for the fields ρ and χ), as well as on the inflationary observables related to the primordial scalar and tensor power spectra, are reported in Table 4.1. For two-tailed bounds, we report 68% confidence level (C.L.) intervals, whereas 95% C.L. upper/lower limits are quoted for parameters whose distributions are not consistent with a "detection". In Figure 4.5, we instead show 2D joint and 1D marginalized posterior probability distributions for selected parameters, leaving out the distributions for the initial conditions.

Initial conditions	**Constraints**	**Uniform prior ranges**
ρ_i/M_{pl}	(*unconstrained*)	$\rho_i/M_{pl} \in [0.1,2]$
χ_i/M_{pl}	(*unconstrained*)	$\chi_i/M_{pl} \in [0.1,10]$
Model parameters	**Constraints**	**Uniform prior ranges**
ξ	< 0.00142	$\log_{10}(\xi) \in [-5,-1]$
α	$1.951^{+0.076}_{-0.11} \times 10^{10}$	$10^{-10} \times \alpha \in [1,3]$
Ω	$0.93^{+0.72}_{-2.8} \times 10^{-5}$	$\Omega \in [\xi^2,\, 2\xi^2]$
Primordial spectra parameters	**Constraints**	
A_s	$(\,2.112 \pm 0.033\,) \cdot 10^{-9}$	(*derived*)
n_s	$0.9638^{+0.0015}_{-0.0010}$	(*derived*)
α_s	$< 1.2 \times 10^{-4}$	(*derived*)
r	> 0.00332	(*derived*)

Table 4.1: External priors and observational constraints on the initial conditions of the fields ρ and χ (*first two rows*), the model parameters ξ (more precisely $\log_{10}\xi$), α, and Ω (*three intermediate rows*), and (derived) inflationary parameters controlling the primordial scalar and tensor power spectra A_s, n_s, α_s, and r (*lower four rows*). Concerning observational constraints, for two-tailed bounds we report 1σ (68% C.L.) intervals, whereas for all other cases we report 2σ (95% C.L.) upper/lower bounds.

As a first remarkable result, we find that even by varying the initial conditions for the fields ρ_i and χ_i within the flat priors reported in Table 4.1, these two parameters are entirely unconstrained. This emphasizes that our model is not (or at least only weakly) sensitive to the choice of initial conditions, suggesting that it does not rely on a fine-tuned choice of initial conditions and is physically robust.

In contrast, when focusing on the three free parameters of the model – α, ξ, and Ω (note that we impose a prior which is flat in $\log_{10}\xi$, rather than in ξ itself) – we observe that these are well constrained within the ranges set by our priors, with the bounds remaining well away from the upper and lower limits of the prior ranges. This indicates that the choice of prior ranges has no effect on our constraints, and that the latter are due to genuine physical effects of these parameters on observable quantities. In the following, we analyze the constraints on each parameter separately.

Parameter α

The parameter α, controlling the strength of the R^2 term in the JF action (3.1), is directly linked to the amplitude of the inflationary potential, since it only enters as an overall multiplicative factor in the expression for $V(\rho)$ in Eq. (3.51). It therefore affects the amplitudes of the primordial scalar and tensor power spectra. This connection is most evident if one observes the mutual correlations between α, A_s, and r in Figure 4.5. Given that data from *Planck* has been used to infer A_s to high accuracy, through its effect on the amplitude of the acoustic peaks in the temperature and polarization anisotropy power spectra, constraints on A_s usually impose stringent requirements on the amplitude of inflationary potentials, and therefore serve as calibrators for inflationary models. This holds in our scale-invariant inflationary model as well, for which matching the amplitude of the primordial scalar power spectrum $A_s = (2.112 \pm 0.033) \times 10^{-9}$, in excellent agreement with results in the literature,

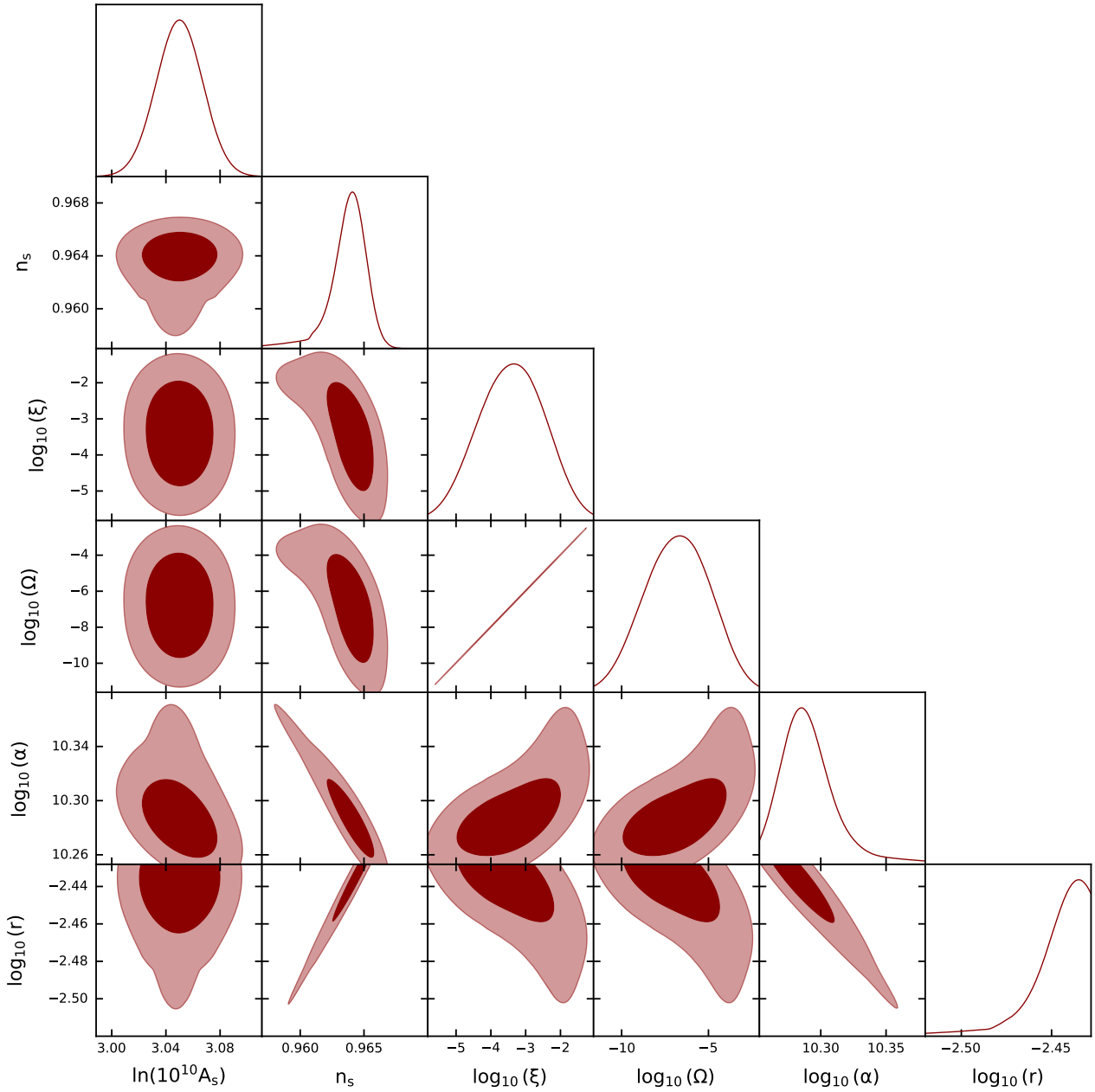

Figure 4.5: Triangular plot showing 2D joint and 1D marginalized posterior probability distributions obtained through the numerical method outlined in Sec. 4.4.1. A selection of parameters is represented: the (natural logarithm of the) amplitude of primordial scalar perturbations A_s, the scalar spectral index n_s, the (logarithm of the) coupling parameters ξ, Ω, and α, and the (logarithm of the) tensor-to-scalar ratio r.

leads to the constraint on α reported in Table 4.1. Note that the benchmark value found in Eq. (3.81) is compatible with the most robust constraint found with the present methodology.

Parameter ξ

The parameter ξ, controlling the strength of the non-minimal coupling $\phi^2 R$, significantly influences both the scalar tilt n_s and the amplitude of the primordial tensor power spectrum through the tensor-to-scalar ratio r.

The effect of ξ on the spectral indices is best represented in the scatter plot in Figure 4.6. We observe that values of $\xi \sim 10^{-2}$ lead to a shift towards smaller $n_s \sim 0.95$, while for $\xi \lesssim 10^{-3}$ we converge to a value around $n_s \sim 0.965$, consistent with the *Planck* results.[15] This behavior can equivalently be seen as the flat plateau in Figure 4.7 (left panel). Therefore, to maintain consistency with the derived value of n_s, excessively high values of ξ are not viable, as they would force us into a region of parameter space where n_s becomes too small to remain in good agreement with *Planck*. A similar behavior was observed in Figure 3.10. Note, however, that the band in Figure 3.10 represents different theoretical predictions varying the number of e-folds in $N_* \in [50, 60]$, while the spread of the points in Figure 4.6 reflects the posterior probability distributions obtained through the sampling algorithm for a fixed $N_* = 55$. Overall, these considerations translate into the upper limit

$$\boxed{\xi < 0.00142 \quad (95\%\ \text{C.L.})}. \tag{4.105}$$

This constraint is much more robust than the approximate one given in Eq. (3.63), namely $\xi \ll 3/4$.

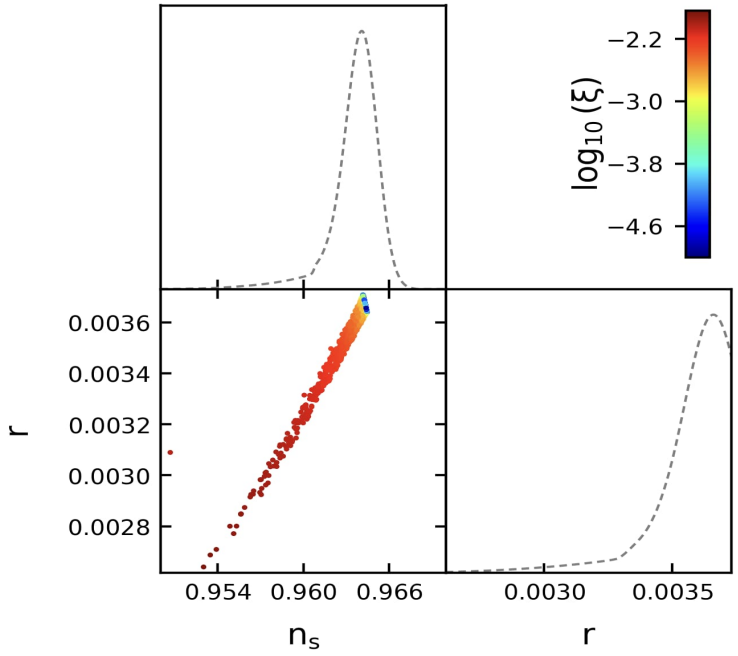

Figure 4.6: 2D scatter plot in the (n_s, r) plane colored by the value of the parameter ξ.

As a side remark, we note that the allowed values of ξ are much smaller than those required for the non-minimal coupling in Higgs inflation [238–240]. Therefore, our model does not suffer from the potential issues with unitarity violation raised in that context [239, 241–244]. Nevertheless, we stress that our inflaton field is not identified with the Higgs field, and a direct comparison between the two models should be considered just as a qualitative analogy.

[15] Note that the low-n_s tail is more extended than the heavier high-n_s tail. This leads to the somewhat peculiar shapes observed in the contours in Figure 4.5. As discussed in the text and evident from the figure, lower values of n_s are correlated with higher values of ξ, and vice versa. Therefore, the heavier high-n_s tail reflects the lower edge in $\log_{10}\xi$ prior (which we set at $\log_{10}\xi > -5$). Of course, the choice of this edge is somewhat arbitrary since we cannot sample all the way down to $\xi = 0$ once we choose to sample $\log_{10}\xi$. Nevertheless, as stressed above, our results are robust and converged, albeit not in the usual MCMC sense.

Parameter $\Omega \equiv \alpha\lambda + \xi^2$

The parameter Ω controls the strength of the $\sinh^4(\rho)$ term in the potential within the (ρ, χ) field representation, or, equivalently, the strength of the quartic self-interaction in the JF action (3.1) for fixed values of ξ and α. Guided by the analytical considerations presented in Sec. 3.3, we adopt the prior range $\Omega \in [\xi^2, 2\xi^2]$. This choice is deliberately broader than the tighter bound $\Omega \in [\xi^2, 1.15\xi^2]$ derived in Eq. (3.69), allowing us to test the validity of the approximate constraint numerically. We recall that the algorithm automatically discards models exhibiting eternal inflation. Consistently, we find that configurations with Ω outside the chosen interval are rejected, thereby providing numerical confirmation of the analytical results. This is visually captured by the very tight correlation between ξ and Ω in Figure 4.5, where the 2D marginalized posterior is effectively squeezed to a line.

That said, as with α and ξ, Ω also affects the inflationary potential and the associated observables. As a consequence, it exhibits strong correlations with the other parameters, including both model parameters and inflationary observables, as shown in Figure 4.5. In this case, we impose a two-tailed constraint of $\Omega = 0.93^{+0.72}_{-2.8} \times 10^{-5}$.

In light of the results presented above, we conclude with some remarks on the predictability of the method employed here, which allows us to derive the inflationary parameters as model-dependent predictions rather than assuming them a priori, and clarify their interrelations. In particular, this is manifest from the correlations in the three-dimensional parameter space spanned by n_s, r, and α_s shown in the right panel of Figure 4.7. We observe that, within our model, more negative values of α_s are only possible when $n_s \sim 0.965$ and $r \sim 0.0036$. This region of parameter space corresponds to the regime where the effects of the non-minimal coupling $\phi^2 R$ controlled by ξ are negligible, and we therefore approach the regime of Starobinsky inflation where the R^2 term dominates. Conversely, lower values of $n_s \lesssim 0.96$ imply smaller values of r and larger/less negative (thus smaller in absolute value) values of α_s, deviating significantly from the predictions of Starobinsky inflation.

Notice also that these correlations are obtained after marginalizing over all the free parameters of the model (ξ, α, and Ω, as well as initial conditions for the fields). Consequently, they offer a much more comprehensive overview of the interrelations between inflationary parameters within our specific scenario. This allows us to highlight the predictive power of scale-invariant inflation better.

For instance, we predict a non-zero value for the amplitude of primordial gravitational waves and the spectral index running

$$\boxed{r > 0.00332, \qquad \alpha_s < 1.2 \times 10^{-4} \quad (95\%\ \text{C.L.})}. \tag{4.106}$$

We further stress that these results represent *model-dependent* predictions which can be tested in light of future CMB experiments [51–55] to either validate or rule out the model. On the other hand, one might wonder whether – and to what extent – these predictions can help discriminate between this model and other competing models, such as Starobinsky inflation.

4.5 Comparison to Starobinsky inflation

In light of the theoretical affinity, discussed in the previous chapters, between the scale-invariant model and the Starobinsky model, we examine whether the predictive power of the scale-invariant framework identified here results in observational signatures that differ from those of the Starobinsky model, and assess the extent to which future data may allow one to discriminate between the two scenarios.

For completeness, we also extend the analysis to the broader class of α-attractor models, which provide a unifying framework encompassing Starobinsky inflation as a particular limit (see [245–249]). The action of α attractor models arises in the context of supergravity theories for specific forms of the

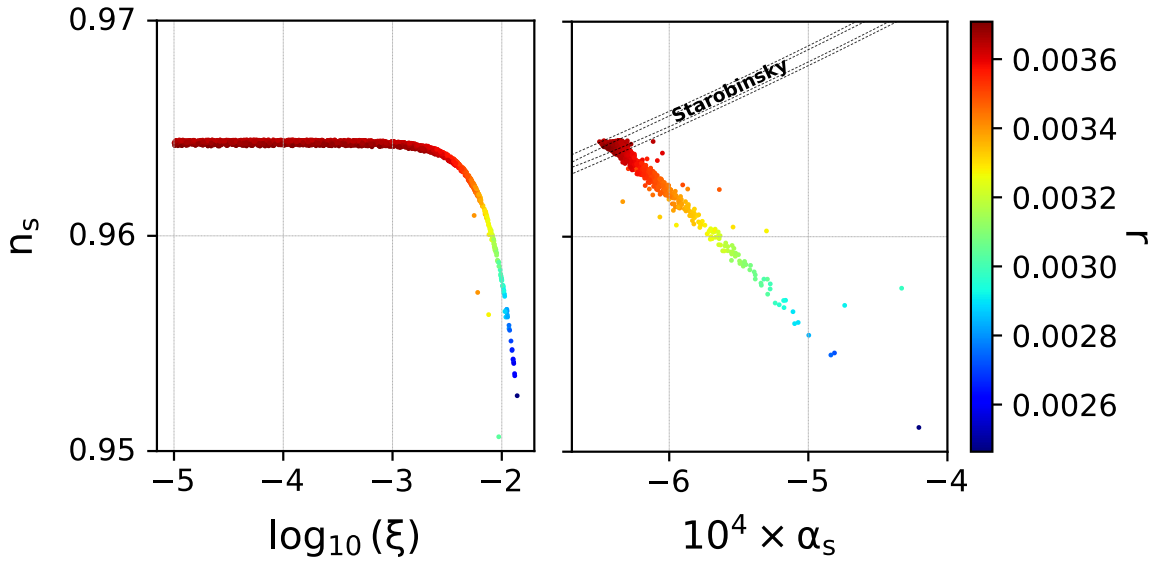

Figure 4.7: *Left panel:* 2D scatter plot in the $(\log_{10}\xi, n_s)$ plane colored by the value of the tensor-to-scalar ratio. *Right panel:* 2D scatter plot in the $(10^4\alpha_s, n_s)$ plane colored by the value of the tensor-to-scalar ratio. The predictions in the n_s-$10^4\alpha_s$ plane are compared to those from Starobinsky inflation (contours given by the dotted curves, not colored by r).

Kähler potential,

$$S = \int \mathrm{d}^4x\sqrt{-g}\left[\frac{M_{pl}^2}{2}R - \frac{1}{2}K(\phi)g^{\mu\nu}\partial_\mu\phi\partial_\nu\phi - V(\phi)\right], \quad \text{with} \quad K(\phi) = \left(1 - \frac{\phi^2}{6\alpha M_{pl}^2}\right)^{-2}, \tag{4.107}$$

where ϕ is the inflaton field and α the free parameter of the theory, related to the curvature of the Kähler manifold.

These models exhibit attractor behavior in their inflationary predictions, which is largely insensitive to the detailed form of the inflaton potential. In particular, they predict the following universal relation

$$n_s \simeq 1 - \sqrt{\frac{r}{3\alpha}} \tag{4.108}$$

with $\alpha = 1$ corresponding to Starobinsky inflation, see Eq. (2.49) for comparison. As such, α attractors provide a well-motivated framework to systematically explore departures from the Starobinsky predictions and their sensitivity to future observational data. For other works on α attractors, see also [250–259].

In Figure 4.8, we compare marginalized contours in the (n_s, r) and (α_s, r) plane for our scale-invariant inflationary model (red contours) against those obtained for Starobinsky inflation (green contours) and α-attractor inflation (light blue contours). In the latter two cases, the predictions are derived following the methodology outlined in [260], where the universal prediction in Eq. (4.108) is assumed in the cosmological model, and constraints are derived from the same dataset analyzed for the scale-invariant inflationary model studied here, for the comparison to be meaningful. Further details on this methodology, as well as information on the priors assumed for the different parameters, can be found in Sec. 3 of [260].

Let's first consider the (n_s, r) plane in the left panel of Figure 4.8. The red contours indicate a positive correlation between the amplitude of tensor modes and the scalar spectral index in the scale-invariant model of inflation. In other words, higher values of r are correlated with higher values of n_s. This is not the case in Starobinsky inflation, where these two parameters are related by Eq. (4.108)

with $\alpha = 1$, thereby leading to a behavior which is exactly the opposite. This relation clearly indicates a negative correlation: higher values of r correspond to lower values of n_s. Due to the different correlation between n_s and r in the two models, the respective marginalized probability contours are rotated relative to each other. A substantial portion of the parameter space falling within the 68% C.L. region in scale-invariant inflation would be excluded in Starobinsky inflation at a statistical level (largely) exceeding 95% C.L. (and vice versa).

Considering the more general α-attractor predictions, the correlation between n_s and r is basically lost due to marginalization upon the additional parameter α. Given that when n_s is fixed, α only affects the amplitude of tensor modes (interpolating vertically along the (n_s, r) plane between the predictions of Starobinsky inflation and those of the monomial $\propto \phi^2$ model), we are left with a substantial freedom to accommodate different values of r by appropriately changing α, which reflects in very broad contours once α is marginalized over. Similar conclusions can be drawn from the (α_s, r) plane in the right panel of Figure 4.8, where, however, the overlap between different predictions is larger and suggests that discriminating between the scale-invariant model and Starobinsky inflation becomes more challenging unless a complementary constraint on n_s is included.

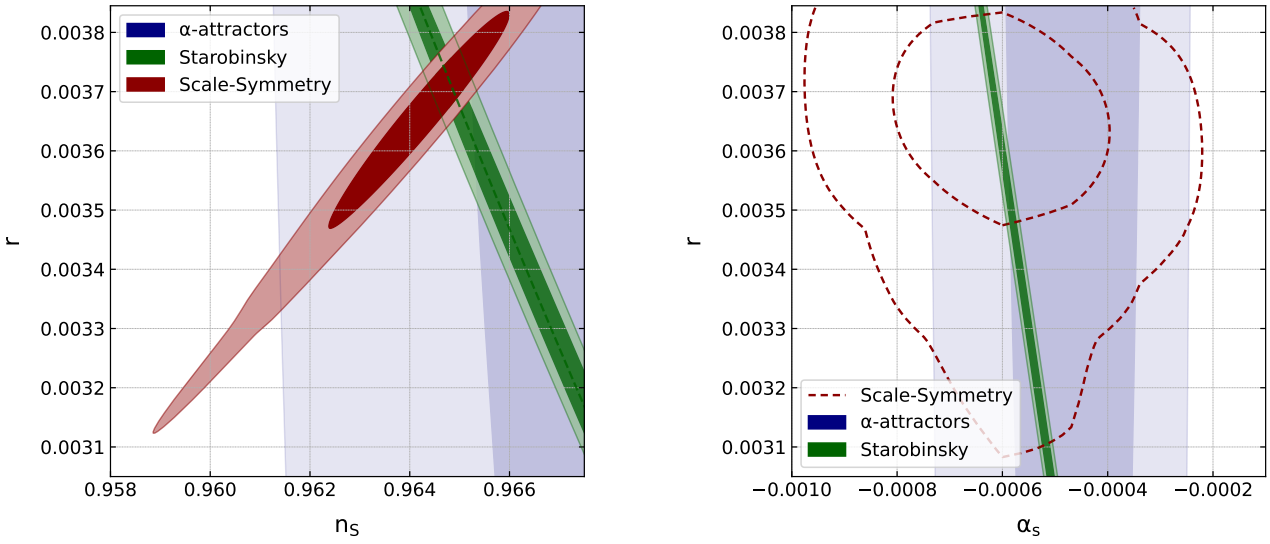

Figure 4.8: Comparison with Starobinsky and α-attractor models. 2D contours in the (n_s, r) (*left panel*) and (α_s, r) (*right panel*) plane for the scale-invariant model studied in this work (red contours), compared to those of Starobinsky inflation (green contours) and α-attractors (light blue contours), obtained in light of observations from the *Planck* 2018 legacy release and from the *BICEP/Keck* collaboration (*BICEP2*, *Keck Array* and *BICEP3* observations up to 2018) and sampling procedure described in Sec. 4.4.1.

Summing up, the increased freedom in α-attractor inflation complicates the discrimination between the models, given the much broader 2D probability contours obtained in this case. In contrast, the differences between scale-invariant inflation and Starobinsky inflation appear substantial enough to raise questions about *i)* the physical nature of the differences, and *ii)* conclusions one can draw about these models in light of forthcoming, more precise CMB observations, both satellite- and ground-based. Let's comment upon these two aspects:

i) We argued that ξ is the parameter that most prominently affects constraints in the (n_s, r) plane. This is manifest from Figure 4.6 and 4.7, stressing also that the predictions of the Starobinsky model are fully recovered in the limit $\xi \to 0$. In the regime of negligible ξ, we converge to the plateau described by $n_s \approx 0.965$ and $r \approx 0.0037$, which corresponds precisely to the region where the red and green contours in Figure 4.8 overlap. In contrast, as the value of ξ becomes sufficiently high, the shift towards lower values of the spectral index and tensor amplitude forces

us into a region of the (n_s, r) plane inaccessible to Starobinsky inflation. The analogy with Starobinsky inflation in the $\xi \to 0$ limit becomes particularly transparent when noting that, in this regime, the dynamics of the scale-invariant model are effectively dominated by the R^2 term. Moreover, as explicitly shown in Eqs. (3.78)–(3.79), the characteristic relation of Starobinsky inflation is recovered in the combined limit $\Omega \to \beta\,\xi^2$ and $\xi \ll 1$ of the scale-invariant model. This result implies that, for any fixed and sufficiently small value of ξ, the model predicts a negative correlation between n_s and r. Allowing ξ to vary, however, leads instead to the positively correlated posteriors shown in Figure 4.8.[16]

ii) Concerning future observations, we anticipate that the upcoming generation of CMB experiments, including the ground-based Simons Observatory (SO) [51, 52] and CMB-S4 [53, 54], and the LiteBIRD satellite [55], will significantly improve our ability to constrain the tensor amplitude, hopefully leading to a detection of primordial tensor modes. In some cases, these surveys are expected to reduce the observational uncertainties in the spectral index as well. To quote a few concrete values, assuming the usual power-law parametrization for primordial spectra, the official collaboration forecasts suggest that SO should achieve a sensitivity of $\sigma(r) \sim 0.003$ on tensor modes, along with an improvement in the constraining power on the scalar spectral index of up to $\sigma(n_s) \sim 0.003$. On the other hand, CMB-S4 is expected to reach $\sigma(r) \sim 0.001 - 0.007$ and $\sigma(n_s) \sim 0.002$. Additionally, LiteBIRD is also anticipated to have a similar sensitivity of $\sigma(r) \lesssim 0.001$, although its impact on the scalar spectral index is expected to be limited, which is not surprising, given that LiteBIRD is targeting the large angular scale CMB polarization signal.

The sensitivity forecasts anticipated from upcoming experiments quoted above could provide crucial insights into scale-invariant inflation. First and foremost, assuming that the model provides an accurate description of the inflationary Universe and based on current data, we *predict* the presence of a primordial gravitational wave background with an amplitude $r \gtrsim 0.003$. These values of the tensor amplitude are sufficiently large to be visible from all the above-mentioned experiments. For instance, CMB-S4 is expected to detect primordial gravitational waves with $r > 0.003$ at a statistical significance of up to 5σ or larger. In case of lack of detection, the same experiment should instead set an upper limit $r < 0.001$ at a 95% C.L.: it is therefore clear that, extrapolating the constraints from current data, failure to detect r (and therefore primordial tensor modes) by CMB-S4 would strongly contradict the predictions of scale-invariant inflation, essentially ruling out the model. Similar considerations can be drawn for SO and LiteBIRD.

[16] If we were to make a model comparison in the sense of determining which model, between the scale-invariant and Starobinsky one, best describes the observational data, then a careful analysis should account also for the Bayesian Information Criterion (BIC), a widely used tool for model comparison when models have different numbers of degrees of freedom. The BIC balances goodness of fit and model complexity by penalizing models with more free parameters, thereby reducing the risk of overfitting. For a model with maximum likelihood $\mathcal{L}_{\max}$, k free parameters, and N data points, the BIC is defined as $\mathrm{BIC} = -2\ln\mathcal{L}_{\max} + k\ln N$. Models with smaller BIC values are statistically preferred, and differences in BIC can be interpreted as evidence in favor of one model over another. Both models are consistent with current observational constraints; however, the scale-invariant model involves three free parameters (α, ξ, and λ – or, equivalently, Ω), whereas Starobinsky inflation depends on a single parameter, namely the mass scale M (see Eq. (2.39)). As a consequence, when evaluated on the same dataset, the BIC would generically penalize the scale-invariant scenario relative to Starobinsky inflation due to its higher-dimensional parameter space. The focus of the present work is nevertheless different: rather than performing a Bayesian model selection based on current data, we aim to assess whether future observations with improved experimental precision will have the discriminatory power to distinguish between the two models at the level of their predicted observables. From this perspective, the analysis presented here should be regarded as sufficient to address the question of prospective distinguishability, independent of a full BIC-based comparison.

That said, in the optimistic scenario where future experiments detect r, the question of whether a combined inference on n_s and r will be sufficient to discriminate between competing models remains open. On the one hand, we expect these experiments to significantly narrow down the region in the (n_s, r) plane where all inflationary models should lie compared to what we can currently infer from the analysis of *Planck* and *BICEP/Keck* data. Therefore, given the differences surrounding the predictions of the different models observed in Figure 4.8, one might be tempted to conclude that future data can eventually help discriminate between Starobinsky and scale-invariant inflation. While this is in part true, it is important to note that predictions in this plane crucially depend on the value of ξ. Assuming that large values of ξ are realized in Nature, we note that the differences in n_s between these two models can be at most as large as $\Delta n_s \sim 0.006$ when $r \sim 0.0032$. Although these differences could be significant when compared to the sensitivities to n_s mentioned above, it should be noted that in the more realistic case where ξ approaches small values, the differences become much smaller for higher values of the amplitude of tensor modes. In general, even within a very optimistic setup, these differences never exceed $2-3$ times the forecasted observational uncertainties. In light of these considerations, it appears quite unlikely that future data will provide conclusive evidence in favor of one model over the other at a high level of statistical significance.

4.6 Summary

In this chapter, we studied first-order cosmological perturbations of the scale-invariant model introduced in Chapter 3, with the primary goal of numerically constraining its parameter space using current observational data. To assess the role of the Goldstone boson χ associated with scale symmetry at the level of linear perturbations, we adopted a fully multifield approach to cosmological perturbation theory, which consistently captures effects that would be overlooked in a single-field description.

In Sec. 4.1, we introduced the general formalism for perturbations in multifield inflation and employed the decomposition of field perturbations into components tangential and orthogonal to the background trajectory. This decomposition provides a clear physical interpretation of adiabatic and entropy perturbations and allows one to transparently track their coupling and evolution.

In Sec. 4.2, we specialized the formalism to the EF description of the scale-invariant model, working in the (ρ, χ) field representation. We extended the set of gauge-invariant variables introduced in Chapter 1 to the multifield case by defining the isocurvature perturbation, Eq. (4.36), and explicitly relating it to the super-horizon evolution of the comoving curvature perturbation $\mathcal{R}$.

We then clarified the origin of an apparent tachyonic instability associated with entropy perturbations. We showed that, although the effective mass squared of the entropy mode is negative throughout inflation in the (ρ, χ) representation, this does not correspond to a physical instability. By comparing different field parametrizations and exploiting the constraint imposed by Noether current conservation, we demonstrated that entropy perturbations vanish once the dynamics are correctly restricted to the physical subspace. The apparent tachyonic growth is therefore a spurious, variable-dependent effect, and perturbations remain purely adiabatic, consistent with the effective single-field nature of the background evolution.

We subsequently investigated the observational implications of the perturbation dynamics, computing the scalar and tensor power spectra within the slow-roll approximation. By employing the transfer matrix formalism, we showed that isocurvature modes do not source curvature perturbations on super-horizon scales. As a further step, in Sec. 4.3 we analyzed primordial non-Gaussianities, focusing on the squeezed configuration, and found that the predictions coincide with those of single-field slow-roll inflation.

In Sec. 4.4, guided by the analytical results, we performed a full numerical analysis of the background and perturbation equations. Using the sampling algorithm introduced in [197], we explored a wide region of parameter space and identified the subset compatible with observations. We showed that the inflationary predictions are largely insensitive to the initial conditions of the scalar fields, reflecting the attractor nature of the inflationary trajectory and the predictive power of scale-invariant theories. Moreover, we identified a robust lower bound on the tensor-to-scalar ratio, $r > 0.00332$, which constitutes a characteristic prediction of the model and provides a potentially testable observational signature.

Finally, in Sec. 4.5, we compared the predictions of the scale-invariant model with those of Starobinsky inflation and α-attractor models. While a direct comparison with α-attractors is hindered by the broader posterior distributions resulting from marginalization over the parameter α, we showed that the Starobinsky predictions are smoothly recovered in the limit $\xi \to 0$. We concluded by discussing how future observations may discriminate between the two frameworks, which display an overall opposite correlation pattern in the (n_s, r) plane, as illustrated in Fig. 4.8 (left panel).

Chapter 5

Magnetic field generation in scale-invariant inflation

The Universe appears to be magnetized on all scales explored so far. Galaxies and galaxy clusters host magnetic fields of order μG, coherent over scales reaching up to tens of kiloparsecs. In addition, there exists compelling, albeit indirect, evidence for magnetic fields of order nG permeating cosmic voids and the intergalactic medium (IGM). A particularly intriguing possibility is that these observed fields are relics of the primordial Universe, generated during inflation. However, in an exponentially expanding spacetime, quantum vector perturbations cannot be amplified as long as electromagnetic (EM) conformal invariance is preserved. Consequently, successful inflationary magnetogenesis requires a mechanism that breaks this symmetry. One such possibility is to introduce a time-dependent coupling $I(t)$ into the EM action. As originally proposed by Ratra, this time dependence may naturally arise from the nontrivial dynamics of a scalar degree of freedom during inflation.

In this chapter, we investigate the generation of primordial magnetic fields (PMFs) within the scale-invariant inflationary framework introduced in the previous chapters.

5.1 Magnetic fields in the Universe: state of the art

The presence of magnetic fields in the Universe has been firmly established for more than a century, starting from the detection of Zeeman splitting in solar sunspots [261] and later extending to astrophysical systems well beyond the Milky Way. With the development of radio astronomy in the second half of the twentieth century, it became clear that magnetic fields are ubiquitous: the non-thermal radio emission observed in galaxies and clusters is a direct manifestation of synchrotron radiation from relativistic electrons spiralling in large-scale magnetic fields.

At galactic scales, magnetic fields are routinely measured through a combination of synchrotron emission, Faraday rotation of polarized radio sources, and, in limited cases, Zeeman splitting [262, 263]. Typical field strengths in spiral galaxies are of order a few to several μG, with ordered components extending over kiloparsec scales, comparable with the galactic size [264]. Active galaxies can eject jets of magnetized material into galaxy clusters, where similar magnetic field strengths are observed. It is therefore a common understanding that all the existing clusters are magnetized at the μG-level. For example, observations on a large number of Abell clusters have obtained a central magnetic field strength of $B_0 = 5.5\,\mu$G which decreases with increasing radius roughly following the gas density [265]. Interestingly, observations of galaxies and clusters at redshifts $z \gtrsim 1$ indicate that magnetic fields of comparable strength were already in place when the Universe was significantly younger [266, 267].

Despite this observational progress, measuring magnetic fields becomes increasingly challenging outside dense astrophysical environments. Most observational tracers rely on the presence of relativistic charged particles or thermal electrons, making them intrinsically biased toward galaxies and clusters.

In particular, both synchrotron emission and Faraday rotation depend on poorly constrained electron densities and path lengths, whereas Zeeman splitting becomes rapidly unobservable beyond the Milky Way due to the weakness of the signal. These limitations are most severe in the IGM, where magnetic fields are expected to be extremely weak – typically in the nG or sub-nG range – and relativistic particle densities are very low.

As a result, direct detections of intergalactic magnetic fields (IGMFs) are currently out of reach, and existing constraints are primarily statistical and model-dependent. Apart from very general considerations, their coherence length L_B has not been constrained by any analysis until very recently, when somewhat weak bounds were obtained based on observations of the neutrino-emitting blazar TXS 0506+056, $L_B \sim 10$ kpc – 300 Mpc [268].

Given the distance scales involved in typical IGM studies, only the large-scale distribution of magnetic fields is relevant. Clusters of galaxies fill $\lesssim 10^{-3}$ of the Universe's volume,[1] so their magnetic field is effectively negligible when we consider the propagation of particles over macroscopic scales. Cosmic filaments, whose magnetic fields are $B \sim 0.1$–10 nG [270, 271], compose the cosmic web and are believed to have filling factors of 10^{-3}–10^{-1}. On the other hand, cosmic voids, with a filling factor of $\gtrsim 10^{-1}$, are, to first order, the dominant component that determines how particles propagate over cosmological baselines [272].

According to a well-established paradigm, supported by numerical magnetohydrodynamics (MHD) simulations, magnetic fields up to galactic scales are the result of dynamo amplification of pre-existing seed fields and flux-conserving compression during gravitational collapse concurrent with structure formation [33, 273, 274]. On the other hand, an astrophysical process behind the magnetization of some clusters of galaxies could be, in principle, justified with an interplay between galactic dynamo and outflows [275]. However, all of these astrophysical mechanisms operating in the post-recombination epoch could hardly explain the observed magnetic fields in high z galaxies, which have undergone fewer turns than the oldest galaxies [275–277], or even potential magnetic fields in the cosmic voids. Even assuming that successful amplification can be achieved at all scales, the origin of the seed field, called *magnetogenesis*, remains a mystery that has sparked interest among the scientific community for over forty years [278]. For detailed reviews on magnetogenesis, see, e.g., [262, 274, 275, 279].

5.1.1 Origin of magnetic fields

We can broadly identify two classes of magnetogenesis scenarios: in *astrophysical scenarios*, weak seed magnetic fields emerge via local astrophysical processes, such as a battery effect, and are subsequently amplified by dynamo mechanisms. In *cosmological scenarios*, strong seed magnetic fields were created during the early Universe and later decayed to their present state.

In the following, we will outline – without any claim to completeness – possible mechanisms belonging to each class. Although this classification is convenient for presentation purposes, realistic scenarios likely involve a combination of both astrophysical and cosmological processes. Our focus will be on the generation of the initial seed fields rather than on their subsequent amplification. The dynamo mechanism is assumed to operate efficiently, whereby turbulent motions and large-scale shear exponentially amplify pre-existing magnetic fields and sustain them against dissipative effects; see, for instance, [273].

Astrophysical origin

Biermann battery: Originally proposed by Biermann to explain stellar magnetic fields [280], the battery effect has long been considered a natural mechanism for generating primordial magnetic seeds in the

[1] We refer to the volume filling factor of different components of the IGM [269].

late Universe, later amplified by dynamo processes. Cosmic battery mechanisms rely on the fact that electrons and ions respond differently to forces in an ionized, charge-neutral plasma, thereby generating electric fields in the presence of pressure gradients. When density and temperature gradients are misaligned, these electric fields cannot maintain electrostatic equilibrium and source magnetic fields by Faraday's induction law [281]. Before reionization, this process produces exceedingly weak fields in the intergalactic space $B \lesssim 10^{-15}$ nG [282]. In protogalaxies, these fields can reach $B \sim 10^{-13}$–10^{-8} nG [262].

Galaxy outflows: Galaxies themselves are a plausible source of IGMFs, as they release matter and energy into intergalactic space via galactic outflows. Such outflows are typically attributed to stellar processes, notably magnetized winds and cosmic rays [283–285].

Cosmic-rays return currents: Cosmic rays escaping from galaxies can also induce a charge imbalance resulting in electric fields and, in a second stage, return currents. These return currents can seed magnetic fields on sufficiently large scales [286].

Photoionization during reionization: During the reionization era, high-energy photons escaping from Population III stars, protogalaxies, and quasars propagate into the initially neutral IGM. The resulting photoionization generates radial currents and electric fields, which induce magnetic fields with strengths $B \sim 10^{-16}$–10^{-11} nG on scales between 1 kpc and 10 Mpc [287].

Primordial origin

First-order phase transitions: During a first-order phase transition, the order parameter may initially become trapped in a false vacuum expectation value corresponding to the symmetric phase [288]. Subsequently, vacuum or thermal fluctuations can locally trigger the transition to the true vacuum in the broken phase, leading to the nucleation of small bubbles. The vacuum energy released in this process drives the expansion of these bubbles, which grow and eventually collide until the new phase fills the entire volume [289, 290].

Magnetic fields can be generated during the highly nonlinear dynamics associated with bubble expansion and collisions. In particular, an initial seed field may arise via a battery mechanism, in which charge separation near shock fronts generates electric fields. This seed field can then be further amplified by a turbulent small-scale dynamo. Bubble collisions naturally provide the required turbulence, as the free energy released during the transition from the false to the true vacuum is converted into turbulent kinetic energy [274].

Assuming that a first-order phase transition takes place in the early Universe,[2] the coherence length of the generated magnetic field, L_B, is expected to be of the same order as the largest bubble size before collision. This scale can be parametrized as a fraction f_c of the Hubble radius d_H at the time of the transition. During radiation domination [295],

$$H^{-1} = 2t = \frac{4.8}{g_*^{1/2}} \left(\frac{T}{\mathrm{MeV}}\right)^{-2} \mathrm{s} \tag{5.1}$$

[2]In the SM, the EW phase transition is not first order for the experimentally measured Higgs mass; instead, it is a smooth crossover. However, many theories beyond the SM can accommodate a first-order EW phase transition, see, e.g., [291]. Also, the quantum chromodynamics (QCD) phase transition in the early Universe is believed to be a crossover: lattice calculations have shown that this is the case for large temperatures and low values of the baryon chemical potential μ_{B} [292], which are the conditions one expects in the early Universe. However, if the lepton chemical potential (say in neutrinos) is sufficiently large, but within cosmologically allowed values, the QCD phase could in principle be first order [293]. Note, however, that more recent results [294] place an upper bound on μ_{B} in the presence of flavor asymmetric lepton asymmetries, essentially ruling out the possibility of a first-order QCD phase transition.

with g_* the number of effective relativistic degrees of freedom. For the EW phase transition ($g_* \sim 100, T \sim 100\,\mathrm{GeV}$) and the QCD phase transition ($g_* \sim 60, T \sim 150\,\mathrm{MeV}$), the corresponding comoving coherence scale is

$$L_c^{\mathrm{EW}} = L_B/a \sim 6 \times 10^{-4}\, f_c\,\mathrm{pc}, \qquad L_c^{\mathrm{QCD}} \sim 0.3 f_c\,\mathrm{pc}, \tag{5.2}$$

respectively. In both scenarios, the resulting coherence scales are much smaller than typical coherence scales observed in galaxies and clusters of galaxies. Exceptions can arise when helicity is generated as well: in this case, dynamical mechanisms such as an inverse cascade can increase the field's coherence length [296]. Under suitable conditions, fields with strengths of 10^{-10} G can be generated over scales of $\sim 10\,\mathrm{kpc}$ [274].

Higgs field gradients: Magnetic fields may also be generated during second-order phase transitions, which proceed smoothly in the order parameter. In the EW case, spatial variations in the Higgs vacuum expectation value lead to the formation of domains with SU(2) and $\mathrm{U(1)_Y}$ phase gradients, which directly source magnetic fields, as proposed by Vachaspati in [297]. The field strength can be estimated at the Ginzburg temperature T_G, below which vacuum domains become stable; for the EW transition $T_G \simeq T_{\mathrm{EW}}$ [275]. This yields $B(\ell_b) \sim 10^{22}\,\mathrm{G}$ on the domain scale $\ell_b \sim 0.3\,\mathrm{cm}$, which, after averaging over uncorrelated domains, corresponds to a present-day field $B_0(1\,\mathrm{Mpc}) \sim 10^{-21}\,\mathrm{G}$ [274].

Inflationary production: Unlike phase transitions, inflation can naturally provide macroscopically large coherence lengths for the generated magnetic fields: as in the case of primordial scalar and tensor perturbations, quantum vacuum fluctuations of the gauge field could have been amplified and converted into observable EM fields. However, as anticipated in Chapter 1, EM conformal invariance prevents the magnetic fields from amplification in a conformally flat gravitational field (like a spatially flat FLRW background), washing out its amplitude as $B \sim a^{-2}$ [298].

Therefore, inflationary magnetogenesis requires a breaking of conformal symmetry in the EM sector [299].[3] Since mechanisms that violate gauge invariance are known to bring ghost instabilities [305], most of the attention has been devoted to gauge-invariant models of magnetogenesis. After the pioneering work of Turner and Widrow [299], many authors investigated different possibilities to break EM conformal invariance, see, e.g., [277, 279, 306–312]. Schematically, the various contributions to the modified EM action can be written as

$$S = \int \mathrm{d}^4x\sqrt{-g}\, b(t) \left[-\frac{f^2(\phi, R)}{16\pi} F_{\mu\nu}F^{\mu\nu} + g\theta F_{\mu\nu}\tilde{F}^{\mu\nu} - \nabla_\mu\psi\,(\nabla^\mu\psi)^* \right], \tag{5.3}$$

including coupling of the EM action to a scalar field ϕ (like the inflaton or the dilaton), to curvature invariants, to the evolution of an extra-dimensional scale factor $b(t)$, coupling to a pseudo-scalar field θ (like the axion), having charged scalar fields ψ and so on.

Once EM conformal invariance is broken, EM vacuum fluctuations are amplified from sub-Hubble to super-Hubble scales; after the end of inflation, the Universe reheats, leading to the production of charged particles and increasing plasma conductivity. At this point, the electric field $\mathbf{E}$ is shorted out, while the magnetic field $\mathbf{B}$ of the EM wave gets frozen in. Since during inflation the scale factor increases (almost) exponentially, any generated magnetic field scaling, for instance, as $B \sim 1/a^\epsilon$, is exponentially sensitive to any parameter of the model which affects ϵ. For this reason, even in the simplest models, the resulting field-strength estimates range from 10^{-65} to 10^{-9} G [312].

[3] As a remark, this conclusion holds only in a spatially flat FLRW Universe. When, instead, an open geometry is considered, the FLRW spacetime is conformally flat only locally, and it was argued [300, 301] that it could lead to a slowing down of the adiabatic decay rate of magnetic fields. However, as extensively discussed in [302–304], the resulting magnetic field amplitude is unlikely to be of astrophysical significance.

As a byproduct, the presence of PMFs could have important consequences in the physics of the early Universe, addressing some open issues of cosmology. For example, if helical PMFs are generated before the EW crossover, they could automatically generate the observed matter-antimatter asymmetry, without the need to invoke any physics beyond the SM [313–315]. We will explore this possibility in Sec. 5.3.3. Moreover, it was shown that PMFs present in the primordial plasma before recombination could relieve the Hubble tension [316, 317]. Notably, the magnetic field strength necessary to alleviate the Hubble tension is of the same order as that needed to explain cluster magnetic fields without dynamo amplification. The presence of PMFs also affects BBN, and could potentially address the cosmological lithium problem [318].

5.1.2 Statistical observables

Stochastic magnetic fields can be characterized by many observable quantities corresponding to different statistical averages. In this section, we clarify their definitions and the corresponding observational interpretation. In the previous sections, we have often referred to the magnetic field strength B, which should be interpreted as the *average* magnetic field strength. It is important not to confuse this with the mean of B, since on cosmological scales $\langle B_i \rangle = 0$ for each component i, in particular for a Gaussian distribution, see Sec. 4.3. The important quantity in physical space is then the *root mean square* of the magnetic field [272],

$$B^2(t) \equiv \frac{1}{V} \int_V \mathrm{d}^3x \, B_i(t, \mathbf{x}) B^i(t, \mathbf{x}), \tag{5.4}$$

where V is the considered volume. Another important quantity is the *magnetic helicity*, defined as

$$H_B(t) = \int_V \mathrm{d}^3x \, A^i(t, \mathbf{x}) B_i(t, \mathbf{x}), \tag{5.5}$$

where $A^i(t, \mathbf{x})$ is the vector potential. Magnetic helicity is directly related to the magnetic field's topology, specifically whether it is on average left- or right-handed. Note that H_B as defined above is well-defined, since it is gauge-invariant for a vanishing normal magnetic field component everywhere at the boundary of V. Magnetic helicity is conserved in ideal MHD and plays a crucial role in the evolution of the magnetic field, as we discuss below. In passing, it is well possible that PMF are helical, as first considered by Vachaspati in [319].

In close analogy with the definitions introduced in Chapter 1, we introduce the spectral properties of the magnetic field. Introducing its Fourier transform $B^i(t, \mathbf{k})$ following the standard convention introduced in Eq. (1.40), we define its equal-time two-point correlation function as

$$\langle B_i(t, \mathbf{k}) B_j(t, \mathbf{k}') \rangle \equiv (2\pi)^3 \left(\delta_{ij} - \hat{k}_i \hat{k}_j \right) \delta^3(\mathbf{k} + \mathbf{k}') P_B(t, k), \tag{5.6}$$

where we have assumed statistical homogeneity and isotropy. In complete analogy to the notations introduced for cosmological perturbations in Sec. 1.4.4, we define the power spectrum as

$$\mathcal{P}_B(t, k) \equiv \frac{2\pi^2}{k^3} P_B(t, k). \tag{5.7}$$

In the following section, we will adapt this notation to the general formalism of electrodynamics in curved spacetime and explicitly link the two-point correlation function with the magnetic energy density. We can parametrize the power spectrum by a power law as done for the scalar and tensor power spectra, $\mathcal{P}_B \propto k^{n_B}$. It is typically assumed that small-scale (large k) IGMFs have a red-tilted power spectrum: common choices based on dimensional considerations are a Kolmogorov spectrum ($n_B = -2/3$) or an Iroshnikov/Kraichnan spectrum ($n_B = -1/2$). On the other hand, at large scales one expects a Batchelor spectrum ($n_B = 5$) if the magnetic field is generated by a causal process [320]

after horizon entry – for example, a phase transition – and a flat spectrum ($n_B = 0$) if the magnetic field is generated during inflation [321].

To conclude, we introduce the *correlation length* as

$$L_c \equiv \frac{2\pi \int \mathrm{d}\ln k\, \mathcal{P}_B(k)/k}{\int \mathrm{d}\ln k\, \mathcal{P}_B(k)}, \tag{5.8}$$

which characterizes the typical *comoving* scale over which the magnetic field is correlated, or, once nonlinear MHD effects become important, the average size of the eddies of the magnetic field [272].

5.1.3 Observational constraints on intergalactic magnetic fields

The considerable relevance of PMFs for addressing key open problems across multiple research communities has motivated extensive ongoing efforts to detect them. However, the only environments in the present-day Universe where such fields are expected to retain their primordial characteristics are the voids of the LSS. In other regions, the imprint of PMFs is likely to be significantly altered by late-time astrophysical processes, such as cosmic dynamo amplification. These highly nonlinear plasma processes make it effectively impossible to reconstruct the initial magnetic field conditions before structure formation, thereby leaving magnetic fields in cosmic voids as the only pristine probe of cosmic magnetogenesis.

In the following, we summarize the main observational probes for IGMFs and the associated constraints on the *physical* magnetic field strength B and correlation length L_B.

- **Hubble radius** There is no formal upper limit on the possible correlation length of IGMFs. If generated during inflation, it might be even coherent on scales larger than the size of the visible part of the Universe. However, we can never observe correlations on scales larger than the present Hubble scale. In Figure 5.1, we indicate the bound corresponding to $L_B < H_0^{-1}$. A field with correlations scale larger than the present Hubble scale would be perceived as a constant field throughout the Universe [279].

- **Magnetic diffusion** Since IGMFs decay due to magnetic diffusion, there is a lower bound on L_B given by the length scale associated with their decay time, $L_B > \lambda_{\rm diff} \sim 2 \times 10^{13}\,\mathrm{cm}$ [322].

- **Zeeman splitting** An upper bound on the magnetic field can be found from the measurements of Zeeman splitting of the 21 cm absorption line in the spectra of distant quasars, which are used to infer galactic magnetic fields. Measurements of $\sim \mu$G galactic magnetic fields via the Zeeman splitting technique rule out the possibility of stronger IGMFs [322].

- **Faraday rotation** Faraday rotation is the wavelength-dependent rotation of the polarization plane of EM radiation as it propagates through a magnetized plasma. The rotation measure observed from the polarized radio emission from quasars and other extragalactic sources receives contributions from the source environment, the IGM, and the Milky Way. By performing a statistical analysis of the rotation-measure data and disentangling these components, one can isolate the contribution of the IGM and thus infer upper limits on B, which generally depend on L_B. In Figure 5.1, we adopt the bound reported in [322].

Since we will focus on mechanisms of primordial magnetogenesis, there are some additional bounds derived by assuming the presence of PMFs, namely

- **MHD turbulence** A theoretical approach is to consider a given magnetogenesis model and derive the corresponding limits on the initial B and L_B, and then calculate their time evolution via freely-decaying MHD turbulence up to the present day. In this way, we can identify a region in the (L_B, B) plane where turbulence erases the field. We consider the bound derived in [279].

- **CMB anisotropies** Since a PMF contributes to the energy-momentum tensor of the cosmic plasma, it would act as an additional source of scalar, vector, and tensor perturbations. Assuming, for example, a homogeneous PMF throughout the Universe, we can compute the corresponding CMB anisotropies and compare them against observations. In Figure 5.1, we plot the *Planck* 2015 bound for a scale-invariant magnetic power spectrum ($n_B = 0$), which is independent of the coherence length [323]. Jedamzik and Saveliev derived the strongest bound on IGMFs from CMB observations in [324], considering the change in the recombination process via PMF-induced density fluctuations: these induced inhomogeneities lead to an inhomogeneous recombination process that alters the peak structure of the CMB spectrum. In this way, the stringent bound $B \lesssim 50\,\mathrm{pG}$ for $n_B = 0$ is derived.

Recent advances in gamma-ray astronomy have opened a promising avenue for probing extremely weak magnetic fields in the IGM. This observational constraint is, to date, the main motivation for primordial magnetogenesis.

- **Gamma ray observations** Very high energy gamma rays in the TeV range emitted by distant sources (such as blazars) can interact with low-energy photons of the extragalactic background light, producing highly relativistic electron-positron pairs. These pairs subsequently inverse-Compton scatter CMB photons, generating secondary gamma rays in the GeV energy range. In the absence of magnetic fields, this cascade emission would be expected to appear as a GeV counterpart spatially associated with the original TeV source. However, in several cases where TeV emission is observed, the corresponding GeV cascade is not detected. As first proposed by Neronov and Vovk [325], this discrepancy can be explained by the presence of weak IGMFs, which deflect the electron-positron pairs. As a result, the surface brightness of the cascade emission may fall below the detection threshold of gamma-ray telescopes. The absence of a detectable GeV cascade has therefore been used to place lower limits on the strength of IGMFs. See also [279] for a review.

  The first constraint derived in [325] uses observations by Fermi-LAT and IACTs of three blazars, suggesting $B \gtrsim 10^{-16.5}\,\mathrm{G}$ for $L_B \gtrsim 1\,\mathrm{Mpc}$ and $BL_B^{1/2} \gtrsim 10^{-16.5}\,\mathrm{G\,Mpc}^{1/2}$ for $L_B \ll 1\,\mathrm{Mpc}$. Following this seminal work, which was the first to firmly exclude $B = 0$, much attention has been devoted to this topic, new objects were used in the analyses, and other observables were introduced. The Fermi-LAT collaboration [326] compiled a catalog of sources and performed a detailed analysis, including the time variability of the source. In Figure 5.1 we quote one of the tightest lower bounds derived in this work, assuming a source stability over 10^7 yrs.[4] See [272] for a recent review on the observational bounds on the gamma-ray window.

  As a final remark, non-vanishing parity-odd correlators of gamma ray arrival directions observed by Fermi-LAT suggest that IGMFs are helical [327–329].

Following the most recent bounds derived from gamma-ray observations, it is a common understanding that cosmic voids are magnetized at the level of at least $10^{-17}\,\mathrm{G}$ on Mpc scales. In light of the discussion of astrophysical and cosmological mechanisms of magnetogenesis presented in Sec. 5.1.1, we can argue that astrophysical mechanisms that inject magnetic energy via galaxies and active galactic nuclei typically result in a more patchy, source-dependent distribution of the IGMF, as opposed to primordial scenarios. This fact was further confirmed through extensive MHD simulations comparing the two families of models, finding also that primordial seeding tends to produce larger filling fractions than late, purely astrophysical seeding.

[4] We consider the more conservative bound obtained after removing the sources 1ES 0229-200 and 1ES 1218+304, since there are indications that they could be variable, see [272] for a detailed analysis.

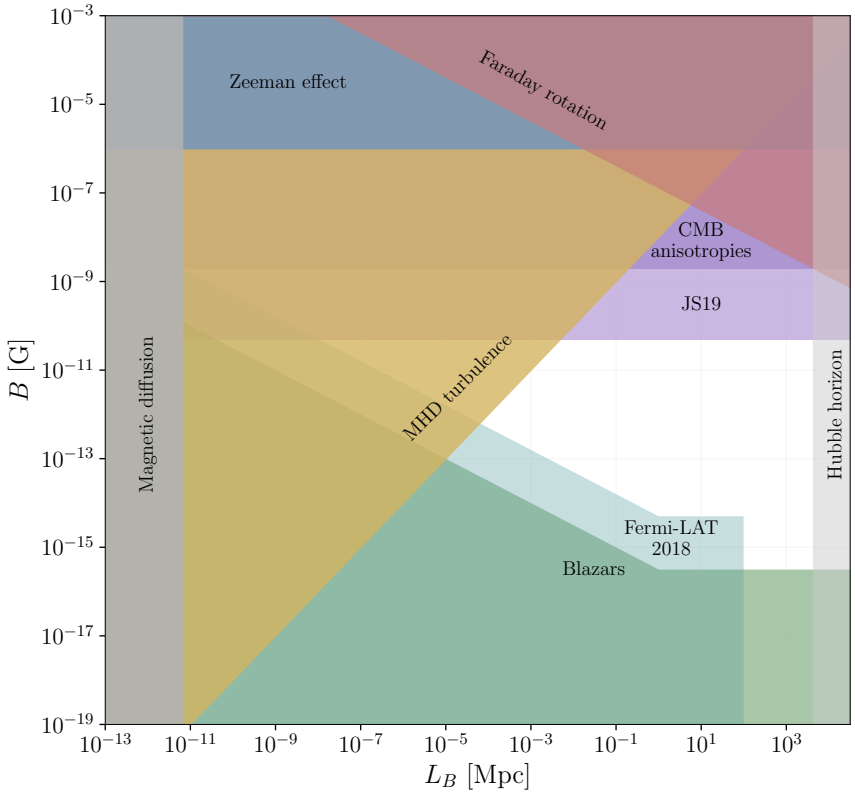

Figure 5.1: Schematic overview of the main observational constraints on the amplitude and correlation length of IGMFs, as discussed in Sec. 5.1.3. Colored regions are excluded by different observables. The lower and upper bounds on L_B arise from magnetic diffusion and the Hubble radius, respectively [322]. Upper limits on the magnetic field amplitude are set by Zeeman splitting and Faraday rotation measurements of extragalactic sources [322, 279]. The yellow region is excluded by freely decaying MHD turbulence in the early Universe; we adopt the bound presented in [279]. Additional cosmological constraints are provided by CMB observations: we show the *Planck* 2015 bound for scale-invariant magnetic fields from [323], together with the currently strongest limit from recombination derived by Jedamzik and Saveliev [324], labeled as JS19. Finally, lower bounds on the magnetic field amplitude are inferred from the non-observation of secondary GeV gamma-ray emission from TeV blazars. We indicate in green the first bound derived in [325], as well as one of the most stringent constraints obtained by the Fermi-LAT collaboration [326].

A recent analysis presented in [330] has shown that the ensemble of galactic magnetic dipole – assuming a quadrupolar dynamo field within galaxies that transitions to a dipolar configuration in their halos – can by itself generate space-filling magnetic fields in cosmic voids at the pG level. Remarkably, these fields are sufficient to account for the blazar observations, even in the absence of galactic outflows or turbulent processes. This result would downplay the motivation for searching for primordial generation mechanisms; however, it has been later shown in [331] that, once the assumption that the IGM can be modeled as a vacuum with a static superposition of galactic dipoles is corrected, the diffusion process is too slow to account for the observed magnetic fields. The authors of [331] therefore conclude that a primordial origin remains the most natural explanation for the space-filling weak fields in voids.

A clear proof of the existence of void fields would be the observation of GeV halos around TeV blazars, which would allow for a direct measurement of the void field strength, and simultaneously rule out alternative interpretations of the missing GeV observations [332]. Complementary to gamma-ray observations, a promising venue to firmly establish the presence of PMFs is the Silk-damping tail of CMB anisotropies, where there are likely differences between ΛCDM and bΛCDM, the latter including

the effect of PMF-enhanced recombination, see [317]. In addition, constraints may come from future direct measurements of H_0 and BAO surveys. If PMFs originate during inflation, their effect on small scales could be present in the Lyman-α forest, as detailed in [333]. Another potential observational signature of PMFs is the gravitational waves they source in the early Universe. As shown in [334], the stochastic background of gravitational waves observed by pulsar timing arrays [335–339] could be interpreted in terms of non-helical PMFs at the QCD energy scale.

5.2 Helical magnetic fields from a broken-power-law coupling

Following the work of Ratra [306], a common way to break conformal invariance in the EM sector is to introduce a coupling $\propto I^2(\phi)F_{\mu\nu}F^{\mu\nu}$, with ϕ evolving during inflation. However, this class of models suffers from significant drawbacks, in particular:

- The amplification mechanism required to generate sizable primordial magnetic fields typically leads to a rapid growth of the EM energy density during inflation. If this energy density becomes comparable to, or larger than, the inflationary energy density driving the expansion of the Universe, it can significantly alter the background dynamics, spoil slow-roll conditions, or even prematurely end inflation [340]. This is commonly referred to as *backreaction problem* and, broadly speaking, arises when the coupling function I monotonically decreases with the scale factor.

  As a remark, the backreaction problem is often associated with the IR divergence of the electric energy density, rather than the magnetic one.

- As pointed out in [340], a potential theoretical issue arises from the interpretation of the coupling function $I(\phi)$ as an *inverse coupling* "constant" for the vector field. If I becomes small during inflation, the effective coupling of the EM field grows large, potentially driving the theory into an uncontrollable strong-coupling regime. To avoid this *strong-coupling problem*, it is therefore typically required that $I(\phi) \gg 1$ throughout the inflationary phase.

  If one further demands that EM conformal invariance be restored at the end of inflation, such that $I_f = 1$, the strong-coupling problem can be directly associated with any monotonically increasing behavior of I during inflation.

- As mentioned previously, the EM fields generated during inflation source additional scalar, vector, and tensor perturbations. One should be concerned that the newly sourced perturbations are consistent with CMB bounds.

Motivated by the above reasons, many extensions to the Ratra model have been considered. Ferreira *et al.* proposed in [341, 342] to introduce the onset of the evolution of $I(\phi)$ during observable inflation, which acts as an IR cutoff to the electric energy density. Other works have proposed extending the evolution of $I(\phi)$ beyond the end of inflation, resulting in further amplification of the magnetic field [343]. In these scenarios, a present-day magnetic field strength of $B_0 \sim 10^{-15}$ G can be attained. It is worth noting that when magnetogenesis is extended beyond inflation, the effect of electric conductivity σ_c can no longer be neglected: if σ_c is large, as it happens after reheating, the electric field vanishes, and the magnetic field is frozen, thus it becomes difficult to produce sizable EM fields [321].

Another possible venue is to model I as a non-monotonic function of the scale factor, which seems the only way to avoid both the backreaction and strong coupling problems at the same time. In general, this comes at the price of significantly lowering the energy scale of inflation or the reheating temperature, depending on the model, resulting in lower magnetic field amplitudes [344, 345].

Moreover, in all the above cases non-helical magnetic fields are generated, which seem to be in tension with the Fermi-LAT observations outlined in Sec. 5.1.3. This motivation brings to another

possible scenario of magnetogenesis, first considered by Anber and Sorbo in [346] and motivated by axion inflation. Considering a Lagrangian density of the form $\mathcal{L} \propto -F_{\mu\nu}F^{\mu\nu} - g_{\phi\gamma}\phi F_{\mu\nu}\tilde{F}^{\mu\nu}$, with ϕ a pseudoscalar field evolving during inflation and $g_{\phi\gamma}$ its coupling to photons, the Chern–Simons interaction term $\phi F_{\mu\nu}\tilde{F}^{\mu\nu}$ breaks parity and CP invariance and leads to a tachyonic instability that selectively amplifies one circular polarization of the gauge field. As a consequence, the produced EM field acquires a net helicity. Even though numerical analyses indicate that the value of B_0 that can be attained during axion inflation is too small to explain the IGMF bounds [347], we should mention a remarkable feature of helical magnetic fields. Once the thermal plasma is formed during reheating, helical magnetic fields undergo a turbulent process called inverse cascade, which shifts their peak correlation scales from smaller to larger scales [348–350]. In this way, larger coherence scales compatible with IGM bounds could be obtained. We will detail the inverse cascade evolution in Sec. 5.2.4.

These results have motivated the study of a mixed axion-Ratra model of magnetogenesis, first presented by Caprini and Sorbo in [351], further investigated in [352], and generalized in [353]. This hybrid model contains both couplings, i.e. $\propto I^2(t)F_{\mu\nu}F^{\mu\nu}$ and $\propto I^2(t)F_{\mu\nu}\tilde{F}^{\mu\nu}$, where I is a monotonic decreasing function during inflation. It can generate a blue-tilted magnetic field with $B_0 \lesssim 10^{-21}\,\mathrm{G}$ at Mpc scales, provided the energy scale of inflation is significantly lowered from its upper bound derived from *Planck*.

In the following, we present and critically revisit the model originally introduced in [9], extending and refining the analysis in light of a more careful treatment of several theoretical and computational aspects. The model generalizes the hybrid axion-Ratra framework by allowing for a non-monotonic coupling function $I(t)$ featuring a sharp transition during inflation.

The function I is modeled as a (broken) power law of the scale factor, which represents the most natural and analytically tractable choice. In this setup, $I \neq 1$ only during inflation, so that EM conformal invariance is broken exclusively in this phase. The strong-coupling problem is avoided by imposing $I > 1$ throughout inflation. At the same time, the characteristic broken-power-law behavior of I generally alleviates the backreaction problem. As a result, efficient magnetogenesis can occur even at intermediate and high inflationary energy scales, leading to larger magnetic field amplitudes. Furthermore, the model predicts macroscopic correlation lengths, since the inverse cascade mechanism plays a significant role in the post-inflationary evolution of fully helical magnetic fields.

Other works studied the generation of helical magnetic fields with a non-monotonic coupling I [321, 354], but, to our knowledge, this has been done only in the context of a mixed inflation-reheating magnetogenesis. The results presented in this section consider a purely inflationary mechanism of magnetogenesis, and are derived without assuming a particular inflationary model. In Sec. 5.3, we will apply the model to the scale-invariant inflationary background described in the previous chapters.

5.2.1 Setup of the model

We consider the following action

$$S = -\frac{1}{16\pi}\int \mathrm{d}^4x\sqrt{-g}\, I^2(\phi)\left(F_{\mu\nu}F^{\mu\nu} - \gamma F_{\mu\nu}\tilde{F}^{\mu\nu}\right) + \int \mathrm{d}^4x\sqrt{-g}\,\mathcal{L}_\phi, \tag{5.9}$$

where the time dependence of the Ratra-like coupling $I^2(t)$ is assumed to originate from the inflationary evolution of ϕ, which is treated here as a generic scalar field. Moreover, $F_{\mu\nu} = \partial_\mu A_\nu - \partial_\nu A_\mu$ is the field strength of a U(1) gauge field and $\tilde{F}^{\mu\nu} = (1/2)\epsilon^{\mu\nu\alpha\beta}F_{\alpha\beta}$ is its dual with the totally antisymmetric tensor $\epsilon^{\mu\nu\alpha\beta}$ defined as $\epsilon^{\mu\nu\alpha\beta} = 1/\sqrt{-g}\,\eta^{\mu\nu\alpha\beta}$; $\eta^{\mu\nu\alpha\beta}$ is the Levi-Civita symbol with values ±1, and γ is a positive dimensionless constant.

Note that we have not included a source term of the form $j^\mu A_\mu$, since the density of free electric charges during inflation is assumed to be negligible. This assumption is well justified, as the inflationary expansion exponentially dilutes any pre-existing charged particles, and no significant charge production is expected during this phase.

Importantly, the gauge field is treated as a *test field*, so that its energy density and stress-energy tensor are assumed not to affect either the scalar field dynamics or the background spacetime geometry. This assumption, which considerably simplifies the analytical treatment of the model, will be explicitly checked a posteriori through a detailed backreaction analysis in Sec. 5.3, under the assumption that inflation is well described by the scale-invariant framework developed in the previous chapters.[5]

For the purposes of the present section, we do not impose any specific assumption on the evolution of the scalar field encoded in $\mathcal{L}_\phi$, and hence on the detailed inflationary dynamics.[6] The derivation of the EM spectra therefore follows the standard treatment of electrodynamics in curved spacetime, and we shall limit ourselves to reporting the key results relevant for our analysis (see [274, 312] for comprehensive reviews).

To generalize electrodynamics to an FLRW background, we introduce a family of fundamental observers identified by their four-velocity

$$u^\mu = \left(\frac{1}{a}, 0, 0, 0\right), \qquad u_\mu u^\mu = -1, \tag{5.10}$$

who measure the EM field. The physical components of the EM field are described relative to a locally inertial frame around the fundamental observer. It is therefore customary to introduce a set of four orthonormal vectors $\mathbf{e}_{(a)}$ $(a = 0, 1, 2, 3)$ (tetrad) which identify such a frame: $g_{\mu\nu} e^\mu_{(a)} e^\nu_{(b)} = \eta_{ab}$. One possible choice is

$$e^\mu_{(0)} = \delta^\mu_0, \qquad e^\mu_i = \frac{1}{a}\delta^\mu_i, \; i = 1, 2, 3. \tag{5.11}$$

It can be verified that the tetrad (5.11) is parallel-transported by the fundamental observer along its own geodesics: $u^\mu e^\alpha_{(a);\mu} = 0$. Laboratory measurements of the EM field are thus naturally interpreted as the ones referred to this coordinate system. For this reason, we will refer to the *physical* magnetic field components as the following projections along the tetrad

$$\bar{B}^a = B^\mu e^{(a)}_\mu \longrightarrow \bar{B}^0 = 0, \quad \bar{B}^i = a(t) B^i \; (i = 1, 2, 3). \tag{5.12}$$

We define the spatial components of the electric and magnetic fields (their time component is vanishing since they are purely spatial vectors for the fundamental observer) in terms of the vector potential as

$$E_i = -\frac{1}{a} A_i', \qquad B_i = \frac{1}{a} \epsilon_{ijk} \partial_j A_k, \tag{5.13}$$

where a prime denotes derivative with respect to conformal time τ, defined in Eq. (1.2). Unless otherwise stated, we will adopt the conformal time in this analysis.

To proceed with EM field quantization, we fix the gauge freedom by adopting the Coulomb gauge, $A_0 = \partial_i A^i = 0$, and then impose canonical commutation relations between the gauge field A_i and its conjugate momentum. Moving to Fourier space, we can decompose the vector potential in terms of creation and annihilation operators, $b^\dagger_\lambda(\mathbf{k})$ and $b_\lambda(\mathbf{k})$, as

$$A^i(\tau, \mathbf{x}) = \sqrt{4\pi} \int \frac{d^3k}{(2\pi)^3} \sum_{\lambda=\pm} \varepsilon^i_\lambda(\mathbf{k}) \left[b_\lambda(\mathbf{k}) A_\lambda(\tau, k) e^{i\mathbf{k}\cdot\mathbf{x}} + b^\dagger_\lambda(\mathbf{k}) A^*_\lambda(\tau, k) e^{-i\mathbf{k}\cdot\mathbf{x}} \right], \tag{5.14}$$

where $\mathbf{k}$ as the comoving wave vector, related as $\mathbf{k} = a\mathbf{k}_{ph}$ to the physical wave vector $\mathbf{k}_{ph}$. ε^i_λ is the helicity vector associated to the helicity state $\lambda = \pm$ [351, 352]. The creation and annihilation operators obey the usual commutation relations, $\left[b_\lambda(\mathbf{k}), b^\dagger_\sigma(\mathbf{k}') \right] = (2\pi)^3 \delta(\mathbf{k} - \mathbf{k}') \delta_{\lambda\sigma}$.

[5] Given that the dynamics effectively reduce to a single-field inflationary description, as shown in Chapter 3 and Chapter 4, this assumption can be regarded as conservative.

[6] We only assume the rather general condition of an approximately de Sitter expansion.

Variations of (5.9) with respect to A_μ lead to the Maxwell equations in a spatially flat FLRW spacetime with the coupling $I(\tau)$. In Fourier space, these are

$$\mathcal{A}_\pm''(\tau,k)+\left(k^2\pm 2\gamma k\frac{I'}{I}-\frac{I''}{I}\right)\mathcal{A}_\pm(\tau,k)=0, \tag{5.15}$$

where we have introduced the *canonically normalized field* $\mathcal{A}\equiv I(\tau)A(\tau,k)$. From now on, we will refer to the positive (negative) helicity state as the one corresponding to the upper (lower) sign in Eq. (5.15). The non-helical case is recovered by setting $\gamma=0$. Solutions to (5.15) can be found under specific assumptions on the coupling function $I(\tau)$. A monotonic coupling of the scale factor $I(\tau)\sim a^n$ was considered in [351], showing that with $\gamma\sim\mathcal{O}(10)$ magnetic fields compatible with IGM lower bounds could be generated without strong coupling or backreaction problems. This scenario is possible provided inflation occurs at an energy scale between 10^5 and 10^{10} GeV.

We instead consider a broken-power-law coupling function of the scale factor, featuring a sharp transition at $\tau=\tau_\star$, and we parametrize it as[7]

$$I(\tau)=\begin{cases}\mathcal{C}\left(\dfrac{a(\tau)}{a(\tau_\star)}\right)^{\nu_1} & \tau_i<\tau<\tau_\star\\ \mathcal{C}\left(\dfrac{a(\tau)}{a(\tau_\star)}\right)^{-\nu_2} & \tau_\star<\tau<\tau_f\end{cases} \tag{5.16}$$

where ν_i are positive numbers. In the following, we will refer to $\tau_i<\tau<\tau_\star$ as *first stage* and $\tau_\star<\tau<\tau_f$ as *second stage* of inflation. The constant $\mathcal{C}$ and the scale factor at transition $a_\star$ are found by imposing $I(\tau_i)=I(\tau_f)=1$; in this way, EM conformal invariance is broken only during inflation. This choice has a clear physical interpretation once the time evolution of I is tied to that of the inflaton field ϕ, as will be discussed in Sec. 5.3. Before the onset of inflation, ϕ is not yet rolling and no mechanism modifies the EM coupling, so the action reduces to the standard Maxwell form, naturally corresponding to $I=1$. Symmetrically, once inflation ends and ϕ approaches its final configuration, standard electromagnetism is recovered and EM conformal invariance is restored, again giving $I=1$. The condition $I(\tau_i)=I(\tau_f)$ is therefore not an artificial tuning, but simply reflects the fact that the EM sector is modified only during inflation. Furthermore, due to the broken-power-law profile of $I(\tau)$, the above boundary conditions are compatible with the additional requirement $I(\tau)\gtrsim 1$ throughout inflation, which is imposed to avoid the strong coupling problem [340].

5.2.2 Dynamics of the EM field

We can solve Eq. (5.15) for three regimes: in the sub-horizon limit (vacuum solutions), during the first stage, and during the second stage. In the following, we examine the three cases separately.

Vacuum solutions

The initial conditions are specified for each mode (or wavenumber k) in the short-wavelength/sub-horizon limit, $|k\tau|\gg 1$, where equation (5.15) reduces to the usual wave equation:

$$\mathcal{A}_\pm''(\tau,k)+k^2\mathcal{A}_\pm(\tau,k)=0, \tag{5.17}$$

and clearly $\mathcal{A}_+=\mathcal{A}_-$. Being deep within the Hubble sphere, the modes $\mathcal{A}$ are not amplified, thus we can solve (5.17) with the Bunch-Davies vacuum conditions given in Eq. (1.61), namely

$$\mathcal{A}_\pm^{\rm BD}(\tau,k)=\frac{1}{\sqrt{2k}}e^{-ik(\tau-\tau_i)}, \tag{5.18}$$

where the constant phase $e^{ik\tau_i}$ is added for later convenience.

[7] The same coupling function was referred to as "sawtooth coupling" in [9], with a reference to its shape in log-log.

First stage

When conformal invariance is explicitly broken by the coupling $I(\tau)$ in the first stage of inflation, Eq. (5.15) becomes

$$\mathcal{A}_{\pm}''(\tau,k)+\left(k^2\mp 2k\frac{\xi_1}{\tau}-\frac{\nu_1(\nu_1+1)}{\tau^2}\right)\mathcal{A}_{\pm}(\tau,k)=0, \qquad \xi_1\equiv\gamma\nu_1, \tag{5.19}$$

where we have considered a purely de Sitter expansion, $\tau=-1/aH$. As we will see, the parameter ξ_1 quantifies the enhancement of the magnetic field amplitude [351]. The general solutions can be written as a linear combination of the Whittaker functions $M_{\alpha,\beta}(z)$ and $W_{\alpha,\beta}(z)$ [355],

$$\mathcal{A}_{\pm}^{\rm I}(\tau,k)=\frac{1}{\sqrt{2k}}\left[C_1^{\pm}M_{\pm i\xi_1,\nu_1+\frac{1}{2}}(2ik\tau)+C_2^{\pm}W_{\pm i\xi_1,\nu_1+\frac{1}{2}}(2ik\tau)\right]. \tag{5.20}$$

The integration constants $C_i^{\pm}$ are found by imposing the following junction conditions at the beginning of inflation [341]:

$$\frac{\mathcal{A}_{\pm}^{\rm BD}(\tau_i,k)}{I(\tau_i)}=\frac{\mathcal{A}_{\pm}^{\rm I}(\tau_i,k)}{I(\tau_i)}, \qquad \frac{\partial}{\partial\tau}\left(\frac{\mathcal{A}_{\pm}^{\rm BD}(\tau,k)}{I(\tau)}\right)\bigg|_{\tau=\tau_i}=\frac{\partial}{\partial\tau}\left(\frac{\mathcal{A}_{\pm}^{\rm I}(\tau,k)}{I(\tau)}\right)\bigg|_{\tau=\tau_i}. \tag{5.21}$$

Note that the factor $I(\tau_i)=1$ in the denominator of the first equation has been written to stress that we require the continuity of the physical vector potential $A_{\pm}(\tau,k)$, not of the canonically normalized one. The system can be solved exactly to give[8]

$$C_1^{\pm}(k)=\frac{\Gamma(\nu_1+1\mp i\xi_1)}{2ik\tau_i\Gamma(2\nu_1+2)}\left[W_{1\pm i\xi_1,\nu_1+\frac{1}{2}}(2ik\tau_i)-(2ik\tau_i+\nu_1\mp i\xi_1)\,W_{\pm i\xi_1,\nu_1+\frac{1}{2}}(2ik\tau_i)\right], \tag{5.22}$$

$$C_2^{\pm}(k)=\frac{\Gamma(\nu_1+1\mp i\xi_1)}{2ik\tau_i\Gamma(2\nu_1+2)}\left[(2ik\tau_i+\nu_1\mp i\xi_1)\,M_{\pm i\xi_1,\nu_1+\frac{1}{2}}(2ik\tau_i)+(1+\nu_1\pm i\xi_1)\,M_{1\pm i\xi_1,\nu_1+\frac{1}{2}}(2ik\tau_i)\right].$$

For later convenience, we stress that, in the sub-horizon limit $|k\tau_i|\gg 1$, $C_1^{\pm}\to 0$ as $|k\tau_i|^{-1}$, while $C_2^{\pm}\simeq e^{\mp\frac{\pi}{2}\xi_1}$, reflecting the effect of the parity-violating term introduced in the action (5.9). In other words, only the negative helicity state ($\propto C_2^{-}$) is amplified, while the positive one is exponentially suppressed.[9]

Second stage

After transition, Eq. (5.15) becomes

$$\mathcal{A}_{\pm}''(\tau,k)+\left(k^2\pm 2k\frac{\xi_2}{\tau}-\frac{\nu_2(\nu_2-1)}{\tau^2}\right)\mathcal{A}_{\pm}(\tau,k)=0, \qquad \xi_2\equiv\gamma\nu_2, \tag{5.23}$$

with a general solution of the form

$$\mathcal{A}_{\pm}^{\rm II}(\tau,k)=\frac{1}{\sqrt{2k}}\left[D_1^{\pm}M_{\mp i\xi_2,\nu_2-\frac{1}{2}}(2ik\tau)+D_2^{\pm}W_{\mp i\xi_2,\nu_2-\frac{1}{2}}(2ik\tau)\right]. \tag{5.24}$$

[8] We employed the identity: $M_{\alpha,\beta}(z)\partial_z W_{\alpha,\beta}(z)-W_{\alpha,\beta}(z)\partial_z M_{\alpha,\beta}(z)=-\Gamma(2\beta+1)/\Gamma(\beta-\alpha+1/2)$

[9] Note the typo in [9]. This feature can be observed directly from Eq. (5.19): since $\tau<0$, the second term in brackets can be written as $\pm 2k\xi_1/|\tau|$, signaling a tachyonic growth for the negative helicity state. For comparison, in [321] the positive helicity state is amplified, since they consider a monotonic decreasing function of the scale factor in the first stage.

Note that the positive and negative helicity states inverted their roles compared to stage I, due to the opposite sign of $I'(\tau)$. The junction conditions are now imposed at the moment of transition $\tau = \tau_\star$:

$$\frac{\mathcal{A}_\pm^{\rm I}(\tau_\star,k)}{I(\tau_\star)} = \frac{\mathcal{A}_\pm^{\rm II}(\tau_\star,k)}{I(\tau_\star)}, \qquad \frac{\partial}{\partial\tau}\left(\frac{\mathcal{A}_\pm^{\rm I}(\tau,k)}{I(\tau)}\right)\bigg|_{\tau=\tau_\star} = \frac{\partial}{\partial\tau}\left(\frac{\mathcal{A}_\pm^{\rm II}(\tau,k)}{I(\tau)}\right)\bigg|_{\tau=\tau_\star}. \tag{5.25}$$

The expressions for $D_i^\pm$ are rather lengthy; therefore, extending the strategy outlined in [321], we use approximate expressions in two different regimes:

- Super-Hubble limit $|k\tau_\star| \ll 1$ for all the modes that exited the horizon during the first stage, $a_i H < k < a_\star H$,[10] whose evolution and spectral shape could be, in principle, affected by the coupling $I(\tau)$ during the second stage. We will label quantities referred to these modes as $\mathrm{I}\to\mathrm{II}$
- Sub-Hubble limit $|k\tau_\star| \gg 1$ for all the modes that exit the horizon during the second stage, $a_\star H < k < a_f H$.

With this important distinction, which was absent in [9], it will be possible to properly track the evolution of the power spectra for all the modes of interest and throughout inflation. We obtain the following results:

$$\begin{aligned}
&D^\pm_{1,\mathrm{I}\to\mathrm{II}}(k) \simeq C_2^\pm \frac{\Gamma(1+2\nu_1)}{\Gamma(1+\nu_1\mp i\xi_1)}(-2ik\tau_\star)^{-\nu_1-\nu_2},\\
&D^\pm_{2,\mathrm{I}\to\mathrm{II}}(k) \simeq C_2^\pm \frac{\Gamma(2\nu_1-1)}{\Gamma(\nu_1+1\pm i\xi_1)}\frac{\Gamma(2\nu_2\pm i\xi_2)}{\Gamma(2\nu_2)}\frac{\nu_1(\nu_1+\nu_2)}{(2\nu_2+1)}(1+\gamma^2)(-2ik\tau_\star)^{1-\nu_1+\nu_2},\\
&D_1^\pm(k) \simeq 0,\\
&D_2^\pm(k) \simeq C_2^\pm e^{\pm\frac{\pi}{2}(\xi_1+\xi_2)}2^{\pm i(\xi_1+\xi_2)}(-k\tau_\star)^{\pm i(\xi_1+\xi_2)}.
\end{aligned} \tag{5.26}$$

Since the coefficient $C_2^\pm$ is evaluated at τ_i, we can safely adopt its sub-horizon limit, $C_2^\pm \simeq e^{\mp\frac{\pi}{2}\xi_1}$. From the expression of $D_2^\pm(k)$ it is clear that the the two helicities exchange their roles: $D_2^\pm \simeq e^{\pm\frac{\pi}{2}\xi_2}$, thus the positive helicity is now amplified.

5.2.3 Power spectra

Once the analytical expressions for $\mathcal{A}_\pm^{\rm I,II}$ are known, we can compute the EM power spectra and their evolution in time. To this aim, it is instructive to evaluate the EM energy-momentum tensor by varying the EM part of the action (5.9) with respect to the metric tensor,

$$T_{\mu\nu} \equiv -\frac{2}{\sqrt{-g}}\frac{\delta\left[\sqrt{-g}\mathcal{L}_{EM}\right]}{\delta g^{\mu\nu}} = \frac{I^2}{4\pi}\left[g^{\gamma\beta}F_{\mu\gamma}F_{\nu\beta} - \frac{1}{4}g_{\mu\nu}F_{\alpha\beta}F^{\alpha\beta}\right]. \tag{5.27}$$

Note that the Chern–Simons term $F_{\mu\nu}\tilde{F}^{\mu\nu}$, being a topological (metric-independent) density, does not contribute to the energy-momentum tensor. The result in Eq. (5.27) is equivalent to the non-helical one, see [274].

By computing the EM energy density $T_{\mu\nu}u^\mu u^\nu$, the electric and magnetic contributions can be separated using the definitions in Eq. (5.13)

$$\begin{aligned}
T_{\mu\nu}u^\mu u^\nu &= \frac{I^2}{16\pi}\left[A_{m,i}-A_{i,m}\right]\left[A_{l,j}-A_{j,l}\right]g^{ij}g^{ml} + \frac{I^2}{8\pi}\left[A_i'A_j'\right]g^{ij}\\
&= I^2\frac{B_iB^i}{8\pi} + I^2\frac{E_iE^i}{8\pi}.
\end{aligned} \tag{5.28}$$

The vacuum[11] expectation value of the two contributions in (5.28) gives the corresponding spectral

[10] For our purposes, it will be sufficient to consider $H =$ const. throughout inflation.

[11] The vacuum state $|0\rangle$ is defined as one which is annihilated by $b_\lambda(\mathbf{k})$: $b_\lambda(\mathbf{k})\,|0\rangle = 0$.

energy density

$$\rho_B(\tau) \equiv \langle 0|\, T^B_{\mu\nu} u^\mu u^\nu \,|0\rangle = \sum_{\pm} \frac{1}{2\pi^2} \int \frac{\mathrm{d}k}{k} k^5 \frac{1}{a^4(\tau)} \left|\mathcal{A}_\pm(\tau,\mathbf{k})\right|^2 \tag{5.29}$$

where we have explicitly accounted for the sum over helicity states, and the integral is performed within some relevant interval of k. As detailed below, we will consider the modes that exited the horizon during inflation. Similarly, the electric field energy density reads

$$\rho_E(\tau) \equiv \langle 0|\, T^E_{\mu\nu} u^\mu u^\nu \,|0\rangle = \sum_{\pm} \frac{I^2}{2\pi^2 a^4(\tau)} \int \mathrm{d}k\, k^2 \left| \left[\frac{\mathcal{A}_\pm(\tau,\mathbf{k})}{I}\right]' \right|^2 . \tag{5.30}$$

To make contact with the EM spectra in the spirit of the definition given in Eqs. (5.6)–(5.7), we can write

$$\rho_B(\tau) = \sum_{\pm} \int \frac{\mathrm{d}k}{k} \frac{\mathrm{d}\rho^\pm_B(\tau,k)}{\mathrm{d}\ln k} = \sum_{\pm} \int \frac{\mathrm{d}k}{k} \frac{k^3}{2\pi^2} P^\pm_B(\tau,k) = \sum_{\pm} \int \frac{\mathrm{d}k}{k} \mathcal{P}^\pm_B(\tau,k), \tag{5.31}$$

and similarly for the electric part. We can thus identify the generic expressions for the electric and magnetic power spectra as

$$\mathcal{P}^\pm_B(\tau,k) = \frac{1}{2\pi^2}\left(\frac{k}{a}\right)^4 k \left|\mathcal{A}_\pm(\tau,k)\right|^2, \qquad \mathcal{P}^\pm_E(\tau,k) = \frac{I^2}{2\pi^2}\frac{k^3}{a^4}\left|\left[\frac{\mathcal{A}_\pm(\tau,k)}{I}\right]'\right|^2 . \tag{5.32}$$

By taking the asymptotic expansion of the Whittaker functions, we can compute the spectra in the super-Hubble limit $|k\tau| \ll 1$. The super-Hubble limit of the canonically-normalized field $\mathcal{A}_\pm$ and its conformal-time derivative is reported in Appendix C. In the first stage of inflation, we find

$$\mathcal{P}^\pm_{E,\mathrm{I}}(\tau,k) \simeq \mathcal{F}^\pm_{E,\mathrm{I}}(\nu_1) H^4 (-k\tau)^{4-2\nu_1}, \tag{5.33}$$

$$\mathcal{F}^\pm_{E,\mathrm{I}}(\nu_1) = e^{\mp\pi\xi_1} \frac{\xi_1^2}{2^{2\nu_1}\pi^2} \left|\frac{\Gamma(2\nu_1)}{\Gamma(1+\nu_1 \pm i\xi_1)}\right|^2,$$

$$\mathcal{P}^\pm_{B,\mathrm{I}}(\tau,k) \simeq \mathcal{F}^\pm_{B,\mathrm{I}}(\nu_1) H^4 (-k\tau)^{4-2\nu_1}, \tag{5.34}$$

$$\mathcal{F}^\pm_{B,\mathrm{I}}(\nu_1) = \gamma^{-2} \mathcal{F}^\pm_{E,\mathrm{I}}(\nu_1).$$

For the modes that exited the horizon during the first stage, the spectral evolution during the second stage follows a combination of different scalings, since the coefficients $D^\pm_{i,\mathrm{I}\to\mathrm{II}}$ derived in Eq. (5.26) carry an additional k-dependence. We find the following results:

$$\mathcal{P}^\pm_{E,\mathrm{I}\to\mathrm{II}}(\tau,k) \simeq H^4 \left[\mathcal{F}^\pm_{E,\mathrm{I}\to\mathrm{II}} (-k\tau)^{4-2\nu_1} \left(\frac{\tau_\star}{\tau}\right)^{-2\nu_1-2\nu_2} + \mathcal{G}^\pm_{E,\mathrm{I}\to\mathrm{II}} (-k\tau)^{6-2\nu_1} \left(\frac{\tau_\star}{\tau}\right)^{2-2\nu_1+2\nu_2}\right], \tag{5.35}$$

$$\mathcal{F}^\pm_{E,\mathrm{I}\to\mathrm{II}} = e^{\mp\pi\xi_1} \frac{\gamma^2}{\pi^2 2^{2+2\nu_1}} \left|\frac{\Gamma(2\nu_1+1)}{\Gamma(1+\nu_1\pm i\xi_1)}\right|^2,$$

$$\mathcal{G}^\pm_{E,\mathrm{I}\to\mathrm{II}} = e^{\mp\pi\xi_1} \frac{(1+\gamma^2)^2}{\pi^2 2^{2\nu_1-2}} \frac{\nu_1^2\,(\nu_1+\nu_2)^2}{(1+2\nu_2)^2} \left|\frac{\Gamma(2\nu_1-1)}{\Gamma(1+\nu_1\pm i\xi_1)}\right|^2,$$

$$\mathcal{P}^\pm_{B,\mathrm{I}\to\mathrm{II}}(\tau,k) \simeq H^4 \left[\mathcal{F}^\pm_{B,\mathrm{I}\to\mathrm{II}} (-k\tau)^{4-2\nu_1} \left(\frac{\tau_\star}{\tau}\right)^{-2(\nu_1+\nu_2)} + \mathcal{G}^\pm_{B,\mathrm{I}\to\mathrm{II}} (-k\tau)^{8-2\nu_1} \left(\frac{\tau_\star}{\tau}\right)^{2-2(\nu_1-\nu_2)} \right. \tag{5.36}$$

$$\left. + 2\mathcal{F}^\pm_{B,\mathrm{I}\to\mathrm{II}} \mathcal{G}^\pm_{B,\mathrm{I}\to\mathrm{II}} (-k\tau)^{6-2\nu_1} \left(\frac{\tau_\star}{\tau}\right)^{1-2\nu_1}\right],$$

$$\mathcal{F}^\pm_{B,\mathrm{I}\to\mathrm{II}} = e^{\mp\pi\xi_1} \frac{1}{\pi^2 2^{2\nu_1+2}} \left|\frac{\Gamma(2\nu_1+1)}{\Gamma(1+\nu_1\pm i\xi_1)}\right|^2,$$

$$\mathcal{G}^\pm_{B,\mathrm{I}\to\mathrm{II}} = e^{\mp\pi\xi_1} \frac{(1+\gamma^2)^2}{\pi^2 2^{2\nu_1-2}} \frac{\nu_1^2\,(\nu_1+\nu_2)^2}{(1+2\nu_2)^2} \left|\frac{\Gamma(2\nu_1-1)}{\Gamma(1+\nu_1\pm i\xi_1)}\right|^2 \left|\frac{\Gamma(2\nu_2-1)}{\Gamma(2\nu_2)}\right|^2 .$$

For the modes that exited the horizon during the second stage, we find

$$\mathcal{P}^{\pm}_{E,\mathrm{II}}(\tau,k) \simeq \mathcal{F}^{\pm}_{E,\mathrm{II}}(\nu_2) H^4 (-k\tau)^{4-2\nu_2}, \tag{5.37}$$

$$\mathcal{F}^{\pm}_{E,\mathrm{II}}(\nu_2) = e^{\pm\pi\xi_2} \frac{1}{\pi^2 2^{2\nu_2}} \left| \frac{\Gamma(2\nu_2)}{\Gamma(\nu_2 \pm i\xi_2)} \right|^2,$$

$$\mathcal{P}^{\pm}_{B,\mathrm{II}}(\tau,k) \simeq \mathcal{F}^{\pm}_{B,\mathrm{II}}(\nu_2) H^4 (-k\tau)^{6-2\nu_2}, \tag{5.38}$$

$$\mathcal{F}^{\pm}_{B,\mathrm{II}}(\nu_2) = e^{\pm\pi\xi_2} \frac{1}{\pi^2 2^{2\nu_2}} \left| \frac{\Gamma(2\nu_2 - 1)}{\Gamma(\nu_2 \pm i\xi_2)} \right|^2.$$

Note that we have employed the sub-horizon limit for the coefficients $C_2^{\pm}$. We now highlight some general remarks concerning the shape and properties of the power spectra:

- In the first stage of inflation, a scale-invariant magnetic power spectrum is attained for $\nu_1 = 2$. There, the property of scale invariance and having an τ-independent spectrum go together, as observed also in [274]. During the first stage, the negative helicity is amplified.
- In the first stage, the electric and magnetic power spectra share the same spectral tilt. This result is a consequence of having a monotonic increasing coupling $I(\tau)$, which in turn is only possible for a non-monotonic/broken-power-law coupling if we require $I(\tau) \geq 1$ and $I(\tau_f) = 1$, and having helicity. Indeed, this behavior does not occur in the non-helical case, as discussed in [344, 341].
- For modes that exit the horizon during the first stage, their subsequent evolution through the second stage is characterized by a combination of different scalings. At a fixed conformal time τ, modes with different wavenumbers k follow distinct power-law behaviors determined by both ν_1 and ν_2. Notably, the k- and τ-dependence are decoupled in this regime.
- The power spectra in stage I (II) for modes that exited the horizon during stage I (II) only depend on ν_1 (ν_2), in agreement with the intuitive expectation that they are sensitive solely to the dynamics responsible for their amplification.
- For modes amplified during stage II, the power spectra in Eqs. (5.37)–(5.38) display a behavior qualitatively similar to that of stage I, Eqs. (5.33)–(5.34), but with key differences. Owing to the opposite sign of $I'(\tau)$, the positive-helicity mode is now amplified, with a strength set by ξ_2. In addition, the electric and magnetic spectral tilts differ: for $\nu_2 = 2$, the electric spectrum is scale invariant, while the magnetic one is blue-tilted, $\mathcal{P}_{B,\mathrm{II}} \propto (-k\tau)^2$.

Although the shape of the EM power spectra is not directly constrained by observations, inflationary mechanisms are generally expected to produce nearly scale-invariant spectra, as is the case for scalar and tensor perturbations. Note, however, that achieving scale invariance during the first stage, corresponding to $\nu_1 = 2$, does not guarantee that modes exiting the horizon in this phase – those relevant for CMB observations – retain the same spectral tilt until the end of inflation. For this to occur, the leading power-law contribution $\propto (-k\tau)^{4-2\nu_1}$ in Eqs. (5.35)–(5.36) must dominate the spectra at $\tau = \tau_f$ over the relevant range of k. Whether this condition is satisfied depends on the relative values of ν_1 and ν_2, which control the factor $(\tau_\star/\tau_f)^{-2(\nu_1+\nu_2)}$. This issue will be addressed in Sec. 5.3. For the illustrative analysis presented here, we fix $\nu_1 = 2$.

We emphasize that, without the approximations adopted above, an analytical treatment of the power spectra would be prohibitively complicated. Nevertheless, the accuracy of these approximations can be assessed by direct comparison with the numerical results shown in Figures 5.2 and 5.3, which are obtained without approximations for $\nu_1 = 2$, $\nu_2 = 1$, and $\gamma = 3$. In particular, the stage-II spectra in Figure 5.3 are computed by numerically solving the equation of motion (5.23) with the junction conditions (5.25) at $\tau = \tau_\star$ for all relevant k modes at each time τ.

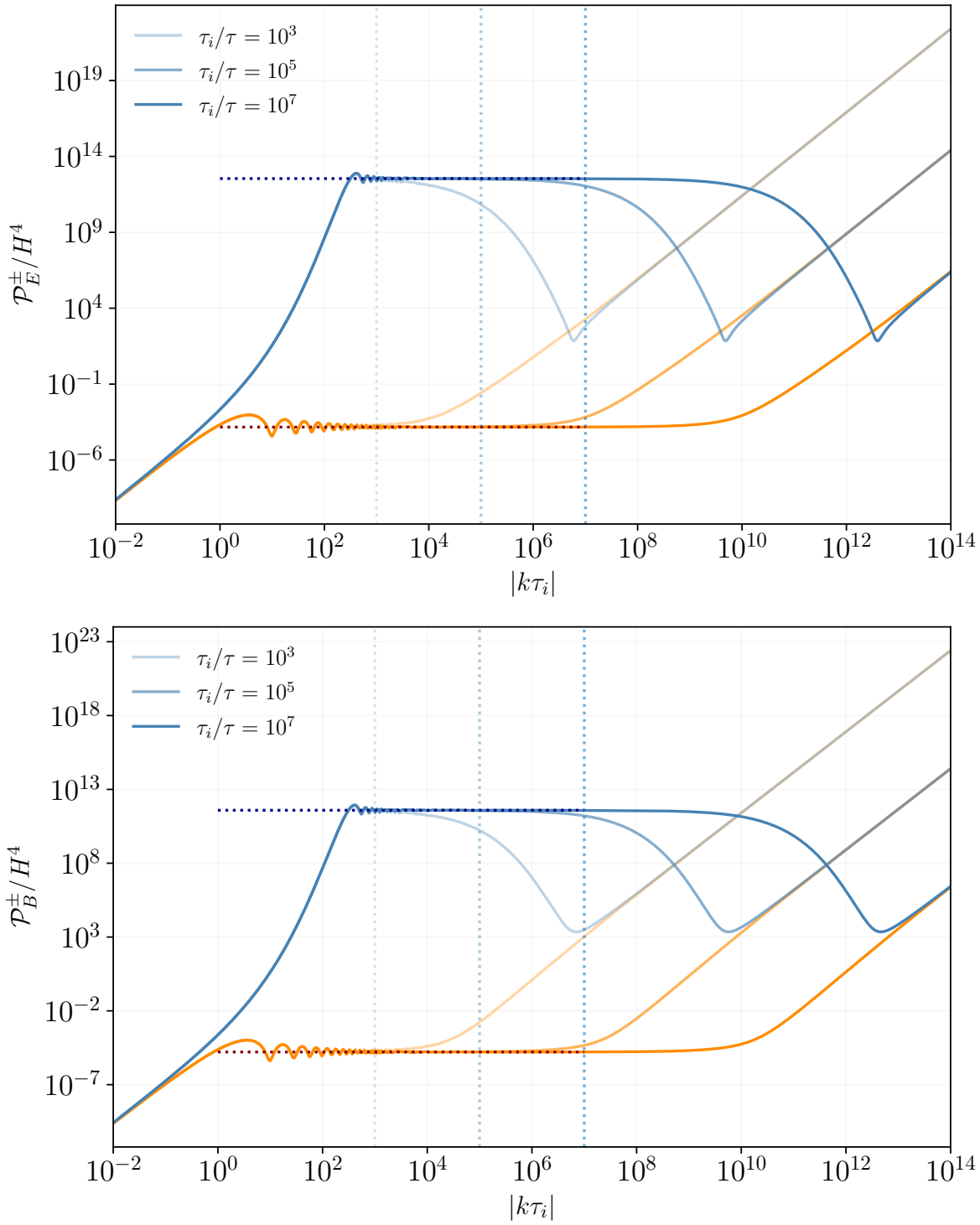

Figure 5.2: Electric (*upper panel*) and magnetic (*lower panel*) power spectra during the first stage of inflation, for positive (orange) and negative (blue) helicity. The time evolution is represented with progressively darker lines, corresponding to $\tau_i/\tau = 10^3, 10^5, 10^7$, respectively. Solid lines are exact solutions (see Eq. (5.20) with coefficients set as in Eq. (5.22)), and dotted lines are the super-Hubble approximations in Eqs. (5.33)–(5.34), with coefficients $C_i^{\pm}$ set to their sub-Hubble limit $|k\tau_i| \gg 1$. The approximate results are plotted only in their regime of validity, namely $|\tau_i^{-1}| \lesssim k \lesssim |\tau^{-1}|$, corresponding to the vertical dotted lines. The parameters of the magnetogenesis model are set to: $\nu_1 = 2, \nu_2 = 1, \gamma = 3$, and inflation is assumed to last for $N = 60$ e-folds, with no particular assumption but for de-Sitter evolution.

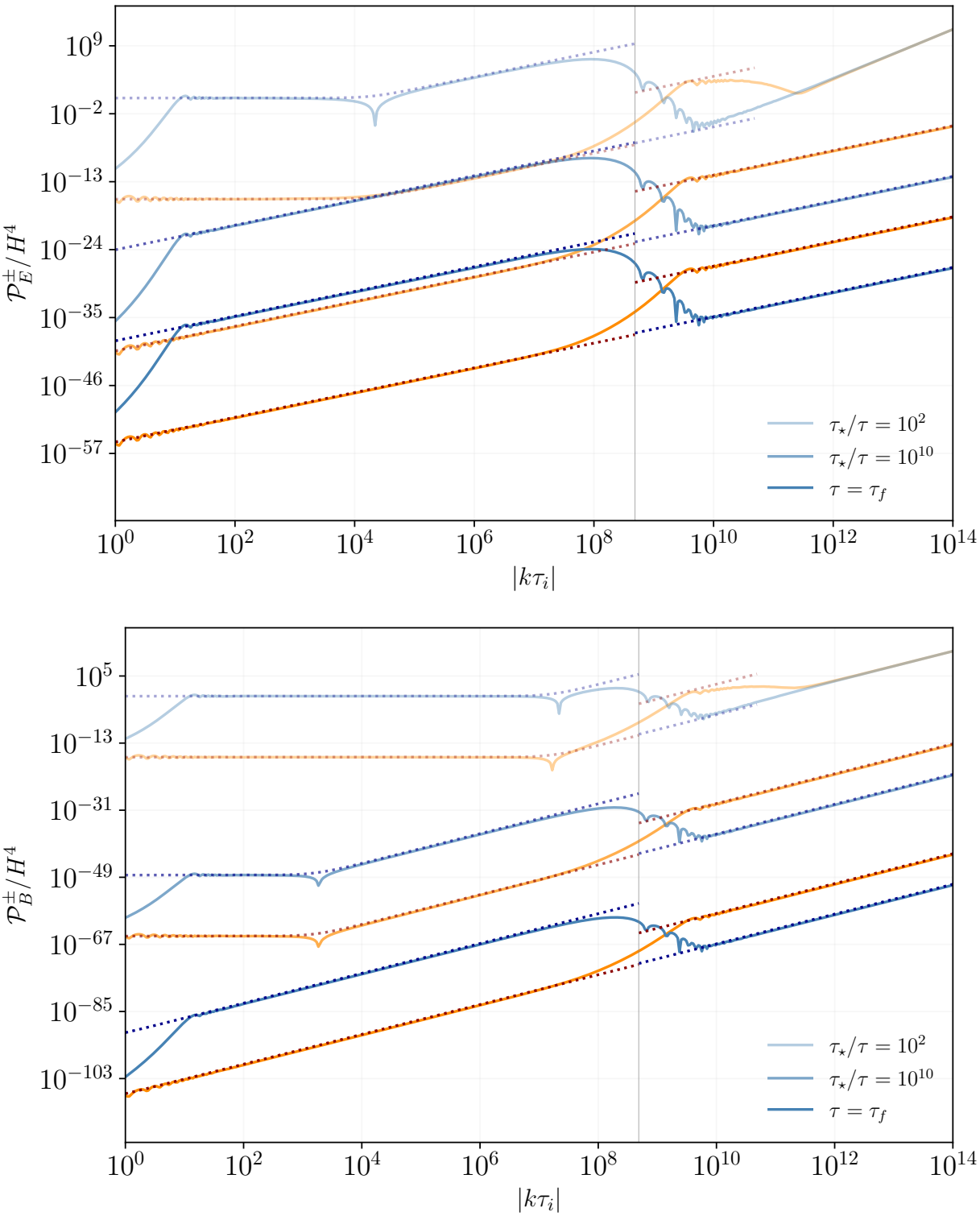

Figure 5.3: Same as Figure 5.2 for the second stage of inflation. The time evolution is represented by progressively darker lines, corresponding to $\tau_\star/\tau = 10^2, 10^{10}$ and $\tau = \tau_f$, respectively. Solid lines are exact solutions, obtained by solving the differential equation (5.23) along with the junction conditions in Eq. (5.25) numerically. Dotted lines are the super-Hubble approximations in Eqs. (5.35)–(5.38), with coefficients $D_i^{\pm}$ set to their super-Hubble (sub-Hubble) limit for modes that exited the horizon during stage I (II), corresponding to range of k values smaller (larger) than the vertical gray line, which marks the transition point. The scales relevant to inflation extend up to $|k\tau_i| \sim 10^{26}$.

From Figure 5.2, we can draw additional conclusions regarding the first stage of inflation:

- Modes that exit the horizon before the coupling $I(\tau)$ begins to vary, corresponding to $|k\tau_i| < 1$, are not amplified and exhibit very blue spectra.
- Modes that exit the horizon during stage I are instead amplified with scale-invariant electric and magnetic power spectra, since $\nu_1 = 2$. Consistent with the analytical results, only the negative-helicity modes (blue lines) are amplified at horizon crossing. Both spectra are also time independent, with curves at different τ differing only in the range of k over which they are defined.

Turning to the second stage, Figure 5.3 allows us to draw the following conclusions:

- Super-Hubble modes, corresponding to wave numbers smaller than the value indicated by the vertical gray line, continue to decay with time. Their spectral tilt is also modified: the initially flat spectra are gradually replaced by blue-tilted behaviors, $\mathcal{P}_E^{\pm} \sim k^2$ and $\mathcal{P}_B^{\pm} \sim k^4$, in agreement with Eqs. (5.35)–(5.36).
- For modes exiting the horizon during stage II, the positive-helicity component is amplified at horizon crossing. Both the spectral tilt and the time dependence are uniquely determined by the exponent ν_2, yielding $\mathcal{P}_E^{\pm} \sim (-k\tau)^2$ and $\mathcal{P}_B^{\pm} \sim (-k\tau)^4$, as shown in Eqs. (5.37)–(5.38).

5.2.4 Cosmological evolution after inflation

In the following, we summarize the main ingredients needed to compute the EM energy density during inflation and to track its evolution up to the present epoch. This will allow us, for any given model, to determine the present-day values of B and L_B, compare them with IGM constraints, and assess backreaction during inflation once a specific inflationary background is specified.

Following the definition in Eq. (5.31), the energy stored in the magnetic field for all the modes of interest at a given time τ during inflation can be computed as

$$\rho_B^{\pm}(\tau) = \begin{cases} \displaystyle\sum_{\pm} \int_{k_i=|1/\tau_i|}^{k=|1/\tau|} \frac{dk}{k} \mathcal{P}_{B,\mathrm{I}}^{\pm}(\tau,k), & \tau_i < \tau < \tau_\star \\ \displaystyle\sum_{\pm} \int_{k_i=|1/\tau_i|}^{k_\star=|1/\tau_\star|} \frac{dk}{k} \mathcal{P}_{B,\mathrm{I}\to\mathrm{II}}^{\pm}(\tau,k) + \sum_{\pm} \int_{k_\star=|1/\tau_\star|}^{k=|1/\tau|} \frac{dk}{k} \mathcal{P}_{B,\mathrm{II}}^{\pm}(\tau,k), & \tau_\star < \tau < \tau_f \end{cases} \tag{5.39}$$

where, at any moment τ, we are including the contribution of all the modes that exited the horizon from the beginning of inflation. Clearly, as long as we consider the approximate expressions for the power spectra, the energy density is not a continuous function of τ at the transition. Still, it is a reliable estimator for checking backreaction effects throughout inflation. In the same way, the integrals for the electric energy density and the comoving correlation length can be computed.

Once the magnetic energy density at a given time – for example, the end of inflation – is computed from Eq. (5.39), we can evaluate the amplitude of the magnetic field as

$$B(\tau) = \sqrt{\sum_{\pm} \frac{8\pi}{I^2(\tau)} \rho_B^{\pm}(\tau)}, \tag{5.40}$$

where the overall normalization follows from the form of the energy-momentum tensor in Eq. (5.28). Sometimes we refer to the *characteristic magnetic field strength at scale* λ as the quantity

$$B_\lambda(\tau) = \sqrt{\sum_{\pm} \frac{8\pi}{I^2(\tau)} \mathcal{P}_B^{\pm}(\tau,k)}\Bigg|_{k=2\pi/\lambda}. \tag{5.41}$$

Once the magnetic field amplitude and correlation length at the end of inflation are determined, their subsequent evolution up to the present epoch must be addressed. For simplicity, we assume instantaneous reheating at the end of inflation, so that the Universe is immediately filled with a relativistic plasma with very high electric conductivity. As a consequence, the electric field is rapidly damped and effectively shorted out.

The evolution of the magnetic field, instead, must be studied by accounting for the presence of the post-inflationary thermal plasma. In this regime, the appropriate description is provided by MHD. If the magnetic field is non-helical, its post-inflationary evolution is purely adiabatic, with the *comoving magnetic field amplitude* $B_c \equiv a^2 B$ and the comoving correlation length L_c remaining constant.[12]

The situation changes qualitatively in the presence of maximally helical magnetic fields. In this case, it has been shown both analytically and numerically [348–350, 356] that MHD turbulence during the radiation-dominated epoch drives an inverse-cascade process, leading to a significant deviation from purely adiabatic evolution.

In this turbulent MHD regime, the comoving magnetic correlation length L_c grows with time, while the comoving magnetic field amplitude B_c decreases. Energy is transferred from smaller to larger scales, whereas on scales larger than L the magnetic spectrum preserves its original slope, exhibiting a self-similar behavior,

$$B(\ell > L) = B \left(\frac{L}{\ell}\right)^{n_B/2} . \tag{5.42}$$

This turbulent evolution continues until viscous effects – first dominated by neutrino diffusion and later by photon diffusion – damp plasma motions. At that point, the inverse cascade effectively ceases, and the magnetic field subsequently undergoes adiabatic evolution. For a detailed illustration of the evolution of the comoving magnetic correlation length as a function of temperature, see Figure 2 of [351]. We can conservatively assume that L_c and B_c stay constant after recombination. Under these general assumptions, propagating the inverse-cascade evolution through the radiation era and matching to the subsequent adiabatic stage yields a relation between the present-day magnetic field amplitude and coherence length, namely

$$B_0 \simeq 10^{-8}\mathrm{G} \left(\frac{L_0}{\mathrm{Mpc}}\right) . \tag{5.43}$$

To determine the present-day values of B_0 and L_0, Eq. (5.43) must be supplemented by an additional relation. As discussed in [351], this relation is provided by the conservation of comoving magnetic helicity, whose physical-space definition is given in Eq. (5.5). For maximally helical magnetic fields, one finds $H_c \simeq B_c^2 L_c$. Imposing the conservation of H_c from the end of inflation to the present epoch then yields

$$B_0^2 L_0 = B_f^2 L_f \left(\frac{a_f}{a_0}\right)^3 , \tag{5.44}$$

which is expressed in terms of physical quantities and complements Eq. (5.43).

Note that in the scenario described here, due to the broken-power-law coupling function $I(\tau)$, one helicity is amplified during the first stage of inflation, while the opposite helicity dominates during the second stage. As a result, the magnetic field produced at the end of inflation is generally bi-helical, with contributions of opposite sign residing in different ranges of comoving wavenumber. This feature is clear from Figure 5.3. In this case, to access whether Eqs. (5.43)–(5.44) can be applied, we need to check if the magnetic field effectively behaves as helical during radiation domination. We thus

[12] In terms of physical quantities, the magnetic field amplitude defined in Eq. (5.40) scales as $B \sim 1/a$, while the physical correlation length $L = aL_c$ grows as $L \sim a$.

introduce a measure for the net comoving helicity,

$$H_c = \int \mathrm{d}^3x A^i B_{c,i} = \int \mathrm{d}\ln k \frac{k^4}{2\pi^2}\frac{1}{I^2}\left(|\mathcal{A}_+|^2 - |\mathcal{A}_-|^2\right), \tag{5.45}$$

where opposite-helicity contributions partially cancel in this integral, and can determine whether the magnetic field evolves toward a maximally helical configuration. In the cases that will be considered in Sec. 5.3, we have checked that at the end of inflation the following relation holds:

$$\frac{|H_c|}{B_c^2 L_c} = \mathcal{O}(1), \tag{5.46}$$

to consistently apply the inverse-cascade relations reported above.

As an additional remark, some care is required when applying Eq. (5.42), since in general the magnetic spectral index n_B is not unique over the range of wave numbers relevant for inflation. As discussed in Sec. 5.2.3 and illustrated in Figure 5.3, at the end of inflation the magnetic power spectrum takes the form

$$\mathcal{P}_B^{\pm}(\tau_f) \sim \begin{cases} k^{8-2\nu_1} \vee k^{4-2\nu_1}, & |\tau_i^{-1}| \lesssim k \lesssim |\tau_\star^{-1}| \\ k^{6-2\nu_2}, & |\tau_\star^{-1}| \lesssim k \lesssim |\tau_f^{-1}| \end{cases} \tag{5.47}$$

so that the appropriate spectral index must be chosen depending on the scale of interest, $k = 2\pi/\ell$.

All the results derived in this section are completely general and do not depend on the specific details of the inflationary dynamics. We emphasize that the generation of helical magnetic fields with a non-monotonic coupling has also been investigated in other works, see, e.g., [321, 354, 357]. However, to our knowledge, such analyses have been carried out only in scenarios of mixed inflation-reheating magnetogenesis. In this respect, the analytical results presented here are particularly useful, as they remain valid for arbitrary inflationary backgrounds.

In the next section, we will apply this general framework to the scale-invariant inflationary background introduced in the previous chapters.

5.3 Application to scale-invariant inflation

Applying the magnetogenesis model described above to a specific inflationary background is essential for a more realistic description of the PMF generation mechanism and for a consistent assessment of backreaction effects. A natural choice for the inflationary background is provided by the scale-invariant model introduced in the previous chapters.

In particular, we take the EM conformal-symmetry-breaking function $I(\tau)$ to depend on the inflaton field ρ in the effectively single-field representation discussed in Sec. 3.2.2, working in the Einstein frame. This choice is adopted for simplicity, since a coupling function of the form (5.16) can be straightforwardly mapped onto the evolution of $\rho(\tau)$. In principle, one could equivalently consider a coupling depending on a combination of fields in the (ϕ, f) representation, or on ϕ and R in the Jordan frame.

The dynamical evolution of the scale-invariant model naturally accommodates the asymptotic values imposed on the coupling function, namely $I_i = I_f = 1$. While, in the generic setup discussed in Sec. 5.2, there is no compelling reason for the coupling to remain constant either before the onset of inflation or after its end, this behavior arises naturally when I is associated with the fixed points of the scale-invariant model. In particular, from the approximate solution $\rho(N)$ found in Eq. (3.76), we can consider a coupling to the EM sector of the form

$$I\left[\rho(a)\right] \sim \tanh\left(\frac{\rho(a)}{\sqrt{6}M_{pl}}\right)^{\pm\frac{3}{4\xi}\nu_i} \sim a^{\pm\nu_i}, \tag{5.48}$$

where we omitted the normalization factors. This functional form correctly reproduces the coupling $I(\tau)$ given in Eq. (5.16). Since the total number of e-folds between the onset of the dynamical evolution of $\rho(\tau)$ and the end of inflation depends sensitively on the initial conditions $\rho(0)$ and $\dot{\rho}(0)$, we impose $I_i \equiv I(\rho_i) = 1$ by fixing the duration of inflation to be $a_f/a_i = e^{\Delta N}$ for a chosen value of ΔN. Without loss of generality, we take $\Delta N = 60$.

On the other hand, we set $I(\rho_*) = 1$ at the stable fixed points, which is a more natural choice than imposing $I(\rho_f) = 1$. Within this framework, EM conformal invariance is restored once the inflaton field settles into the minimum of its potential.

5.3.1 Backreaction

The analysis carried out in Sec. 5.2 implicitly assumes that the EM field does not backreact on the inflationary dynamics. Only under this assumption can the EM sector be consistently decoupled from the inflaton dynamics, and the equations of motion for the gauge field can be solved independently. This is a nontrivial assumption that must be explicitly verified for each inflationary background. In the following, we derive the conditions under which gauge-field backreaction can be neglected within the framework of scale-invariant inflation.

The full action under consideration is

$$S = -\frac{1}{16\pi}\int d^4x\sqrt{-g}\, I^2[\rho(a)]\left(F_{\mu\nu}F^{\mu\nu} - \gamma F_{\mu\nu}\tilde{F}^{\mu\nu}\right) + S_E(\rho,\chi), \tag{5.49}$$

with S_E as defined in Eq. (3.50). When the full action is considered, the first Friedmann equation, see Eq. (3.57), is corrected as

$$3H^2M_{pl}^2 = \frac{1}{2}\dot{\rho}^2 + 3\cosh^2\left(\frac{\rho}{\sqrt{6}M_{pl}}\right)\dot{\chi}^2 + V(\rho) + \rho_{EM}, \tag{5.50}$$

with $\rho_{EM} = \sum_{\pm}(\rho_E^{\pm} + \rho_B^{\pm})$ the total energy density of the EM field, consistent with the definitions in Sec. 5.2. The Klein-Gordon equation for the inflaton, Eq. (3.55), becomes

$$\ddot{\rho} + 3H\dot{\rho} - \frac{\sqrt{6}}{2M_{pl}}\sinh\left(\frac{2\rho}{\sqrt{6}M_{pl}}\right)\dot{\chi}^2 + \frac{\mathrm{d}V(\rho)}{\mathrm{d}\rho} = \mathcal{S}_{EM} \tag{5.51}$$

where we have defined

$$\mathcal{S}_{EM} \equiv \frac{1}{8\pi}I\frac{\mathrm{d}I}{\mathrm{d}\rho}\left(F_{\mu\nu}F^{\mu\nu} - \gamma F_{\mu\nu}\tilde{F}^{\mu\nu}\right). \tag{5.52}$$

From Eqs. (5.51)–(5.52), we conclude that EM backreaction is avoided provided the following conditions hold throughout inflation:

$$\rho_{EM} \ll 3H^2M_{pl}^2, \qquad |\mathcal{S}_{EM}| \ll 3H\dot{\rho}, \tag{5.53}$$

where we have assumed the validity of the slow-roll approximation. Note that, parametrically, the EM energy density scales as $\rho_{\rm EM} \sim H^4$, while the inflationary energy density scales as H^2 in Planck units. As a consequence, many magnetogenesis models must lower the inflationary energy scale, and hence H, to avoid backreaction effects; see, e.g., [311, 341, 351, 354]. In contrast, in our framework, the inflationary dynamics – including the energy scale – are completely fixed by the scale-invariant model discussed in the previous chapters.

In the following, we explicitly verify that the above backreaction conditions are satisfied for all the cases considered. We also note in passing that the second condition is stronger than the first by a slow-roll factor ϵ, and therefore typically provides the most stringent constraint on backreaction [358].

To facilitate the calculation, we can write $\mathcal{S}_{EM}$ in terms of the canonically normalized gauge field $\mathcal{A}_\pm$ as [359, 358]

$$\begin{aligned}\mathcal{S}_{EM} &= \frac{1}{4\pi} I \frac{\mathrm{d}I}{\mathrm{d}\rho} \left(B_i B_i - E_i E_i \mp 2 E_i B_i\right), \\ &= \frac{1}{a^5 \dot{\rho}} \frac{I'}{I} \sum_{\pm} \int \frac{\mathrm{d}^3 k}{(2\pi)^3} \left[k^2 \left|\mathcal{A}_\pm(\tau, k)\right|^2 - \left| I \left(\frac{\mathcal{A}_\pm(\tau, k)}{I(\tau)} \right)' \right|^2 \pm 2\gamma k \,\mathrm{Re}\left(\mathcal{A}_\pm(\tau, k) I \left(\frac{\mathcal{A}_\pm(\tau, k)}{I(\tau)} \right)' \right) \right],\end{aligned} \tag{5.54}$$

where a dot (prime) denotes derivative with respect to cosmic (conformal) time. The integral in Eq. (5.54) can be evaluated along the same lines as the EM energy density and the other integrals, see Eq. (5.39). We will use the asymptotic expressions for the canonically normalized gauge field and its conformal time derivative reported in Appendix C.

5.3.2 Tensor perturbations sourced by gauge fields

The amplification of gauge fields required for magnetogenesis inevitably sources additional cosmological perturbations beyond the standard vacuum fluctuations. In particular, the main by-products of gauge-field production during inflation can be summarized as follows:

- **Sourced curvature perturbations**: The gauge field contributes to scalar fluctuations both through its stress-energy tensor and via the inflaton-gauge coupling $I(\rho)$. This induces a sourced component of the curvature perturbation ζ, which may compete with – or remain subdominant to – the vacuum contribution, depending on the strength and time dependence of the gauge-field amplification.

- **Sourced tensor perturbations**: Similarly, the anisotropic stress of the gauge field sources tensor modes during inflation, providing an additional contribution to primordial gravitational waves. Moreover, if only one gauge-field polarization is amplified due to parity violation – as in the present case – the resulting tensor modes are chiral [360], offering a potentially distinctive observational signature of gauge-field-sourced gravitational waves.

- **Non-Gaussianities**: Since the source term is quadratic in A_μ, the induced scalar and tensor perturbations are generically non-Gaussian. The resulting bispectrum can therefore impose strong constraints whenever sourcing is efficient on CMB scales, once current bounds on $f_{\rm NL}$ are taken into account.

- **Induced spectral features**: For the broken-power-law coupling considered above, the electric and magnetic spectra can become strongly tilted. This may, in turn, generate localized features or bumps in the scalar and tensor power spectra. While CMB observations tightly constrain the spectra to be nearly scale-invariant on large scales, features at smaller scales may lead to interesting observational consequences. In particular, a small-scale enhancement of the curvature power spectrum can trigger primordial black hole formation upon horizon re-entry and simultaneously source second-order gravitational waves.

While a fully comprehensive analysis of magnetogenesis would require accounting for all the effects listed above to ensure consistency with CMB constraints, in the following, we restrict ourselves to estimating the contribution of tensor perturbations sourced by gauge fields. This channel typically provides the most stringent bound, as is the case, for instance, in pure axion magnetogenesis [361].

We emphasize that the magnetogenesis model discussed in Sec. 5.2 possesses a particularly interesting feature: owing to the broken-power-law coupling and the nontrivial evolution of modes amplified during stage I after the transition, the magnetic power spectrum at the end of inflation generally exhibits different spectral tilts across different scales. In particular, it is possible to

realize a nearly scale-invariant spectrum on CMB scales while simultaneously obtaining a strongly blue-tilted spectrum at smaller scales. Such a scenario allows, in principle, for the generation of phenomenologically interesting small-scale features without overproducing gravitational waves or curvature perturbations at CMB scales. For this reason, we defer a detailed investigation of induced spectral features to future work.

To compute the tensor power spectrum sourced by gauge fields during inflation, we follow the analysis of Caprini and Sorbo [351], which builds upon the earlier work of [360]. Although these results were originally derived for a monotonic coupling function rather than a broken-power-law profile, they still provide a reliable approximation over the limited range of scales relevant for CMB observations, where constraints on gravitational-wave production are the strongest.

The equation of motion for the helicity-λ tensor mode h_λ reads

$$h_\lambda'' + 2\frac{a'}{a}h_\lambda' + k^2 h_\lambda = \frac{2}{M_{pl}^2}\Pi_\lambda^{ij}(\mathbf{k})T_{ij}^{EM}(\mathbf{k}), \tag{5.55}$$

where we have introduced the polarization tensors $\Pi_\lambda^{ij} \equiv (\varepsilon^i_{-\lambda}\varepsilon^j_{-\lambda})/\sqrt{2}$ and T_{ij}^{EM} is the spatial part of the EM energy-momentum tensor.

It can be shown [351] that for a generic monotonic coupling $I(\tau) = a^n(\tau)$ with $n < 0$, the induced tensor power spectrum reads

$$\mathcal{P}_T = p_T(n)\frac{H^4}{M_{pl}^4}\frac{e^{4\pi\xi}}{\xi^6}, \tag{5.56}$$

where $\xi \equiv -\gamma n$ plays the same role as our $\xi_i \equiv \gamma\nu_i$, and only the helicity mode that is amplified is considered. The function $p_T(n)$ can be evaluated numerically and is plotted in Figure 1 of [351]. Introducing the tensor-to-scalar ratio r defined in Eq. (1.49), Eq. (5.56) becomes

$$\frac{H}{M_{pl}}\frac{e^{\pi\xi}}{\xi^{3/2}} = \left(\frac{r\mathcal{P}_\mathcal{R}}{p_T(n)}\right)^{1/4}, \tag{5.57}$$

from which we can evaluate the contribution to the tensor-to-scalar ratio r from gravitational waves sourced by the gauge field. Note that in the regime where a helicity-selective instability drives gauge-field amplification, the amplitude of the tensor spectrum sourced by gauge fields is primarily controlled by the instability parameter ξ, which is assumed $\xi \gtrsim \mathcal{O}(1)$ in this derivation. Since we ultimately want to constrain the value of r to CMB observations, which are sensitive to the low-k tail of the power spectrum, we can set $\xi = \gamma\nu_1$.

Fixing the amplitude of the curvature power spectrum to the observed one, see Table 1.1, and the Hubble parameter from the typical inflationary background considered in our analysis, we find

$$r \simeq 4 \times 10^{-5}, \tag{5.58}$$

where we have considered $\gamma = 1$ and $\nu_1 \simeq 2$.[13] For the parameters considered above, tensor perturbations sourced by vacuum fluctuations dominate, since we have shown in Chapter 4 that the scale-invariant inflationary background predicts $r > 0.00332$. However, the sourced contribution in Eq. (5.57) depends exponentially on ξ. As a result, if one requires a nearly scale-invariant magnetic power spectrum on CMB scales, corresponding to $\nu_1 \simeq 2$, the parameter γ cannot be significantly larger than unity, otherwise the tensor-to-scalar ratio r would exceed current observational bounds.

Larger values of γ become viable for smaller ν_1, since $p_T(n)$ decreases to $\mathcal{O}(10^{-6}$–$10^{-7})$ for smaller n, and/or for lower inflationary energy scales, corresponding to smaller values of the Hubble parameter. The latter situation is precisely the one realized in models of (helical) inflationary magnetogenesis with a monotonic coupling function I, where a low inflationary scale is required to generate sizable PMFs while avoiding the overproduction of gravitational waves on CMB scales [351, 352].

[13] Note that the function $p_T(n)$ diverges as $n \to -2$, thus we will limit to values of ν_1 smaller than 2.

5.3.3 Baryogenesis from helical magnetic fields

One of the fundamental open problems in cosmology and particle physics is the origin of the baryon asymmetry of the Universe (BAU), quantified by the observed excess of matter over antimatter. Measurements of the CMB and of primordial light element abundances indicate a baryon number-to-entropy ratio of order $n_B/s \sim 10^{-10}$, which cannot be explained by thermal equilibrium processes alone. To generate a baryon asymmetry from an initially matter-antimatter symmetric Universe, the system must contain processes that violate baryon number. More generally, as formulated by Sakharov, any successful baryogenesis mechanism must satisfy three conditions: baryon number violation, violation of CP symmetry, and a departure from thermal equilibrium [362]. While many proposed scenarios rely on physics beyond the SM, it has been shown that primordial hypermagnetic fields may provide an alternative explanation within the SM itself.

If helical magnetic fields are generated before the EW crossover, they can naturally explain the observed matter-antimatter asymmetry without invoking physics beyond the SM. This possibility has been extensively studied in the literature, see, e.g., [313–315]. In this context, primordial hypermagnetic fields carrying non-vanishing helicity play a central role. During EW symmetry breaking, the hypermagnetic field is partially converted into the ordinary EM field, leading to the decay of hypermagnetic helicity. Through the SM chiral anomaly [363], this decay sources a net $(B + L)$ asymmetry in the plasma. As shown in [314], the generated baryon asymmetry is efficiently transferred to fermionic degrees of freedom via Yukawa interactions and, crucially, is not erased by sphaleron processes. Moreover, the sign of the baryon asymmetry is directly correlated with the sign of the hypermagnetic helicity, establishing a direct connection between PMFs and baryogenesis.

Quantitatively, the observed BAU can be reproduced for hypermagnetic fields corresponding today to IGMFs with amplitude $B_0 \sim 10^{-7\text{–}8}\,\mathrm{nG}$, coherence length $L_0 \sim 10^{-2\text{–}3}\,\mathrm{pc}$, and positive helicity.

As already noted in [314], these values are in tension with blazar observations (see Figure 5.1). Larger values of B_0 would instead lead to an overproduction of the baryon number. Nevertheless, because the self-similar inverse-cascade scaling described by Eq. (5.42) is operative in this case, it is in principle possible to obtain magnetic fields compatible with baryogenesis constraints that are not strongly suppressed on scales larger than their correlation length. Such fields can also be sufficiently large to seed the galactic dynamo mechanism and account for the observed μG magnetic fields in galaxies. This requires a present-day magnetic field amplitude on megaparsec scales in the range [273, 351]

$$10^{-14}\,\mathrm{nG} \lesssim B_0(\ell = 1\,\mathrm{Mpc}) \lesssim 10^{-12}\,\mathrm{nG}. \tag{5.59}$$

In the following, we will investigate whether such predictions can be recovered for the magnetogenesis mechanism described above.

5.3.4 Results

To apply the model of magnetogenesis introduced above to the scale-invariant inflationary background, we proceed as follows. First, we set the inflationary parameters consistently with the analysis performed in Chapters 3–4, to guarantee that its predictions are consistent with observational constraints at CMB scales. Without any loss of generality, we will fix the model parameters α, ξ, and Ω to the benchmark values in Eqs. (3.80)–(3.81).

We also fix the duration of the magnetogenesis mechanism to $\Delta N = 60$ e-folds. More specifically, this means that the coupling $I(\rho)$ starts varying 60 e-folds before the inflaton has reached the stable fixed point, which in turn occurs a few e-folds after the end of inflation. In this way, the coupling $I(\rho)$ stops varying as ρ stops evolving.

We then fix the parameters of the inflationary model as follows. For any choice of (ν_1, ν_2), we determine the normalization of the coupling function $\mathcal{C}$ and the transition time $\tau_\star$ (see Eq. (5.16)) by imposing the boundary conditions $I(\tau_i) = I(\tau_f) = 1$. This requirement is crucial for two reasons. First,

it ensures that standard electromagnetism is recovered once the inflaton has settled at its potential minimum. Second, it maximizes the magnetic field amplitude at the end of inflation. Indeed, Eq. (5.40) shows that large values of I lead to a suppression of the magnetic field amplitude. Since avoiding the strong-coupling problem requires $I(\tau) \geq 1$, and since $I(\tau)$ typically evolves as a power law of the scale factor, this suppression could in general be very large.

Finally, we fix the parameter γ. We then compute the power spectra using the analytical expressions given in Eqs. (5.33)–(5.38) and consistently integrate them to determine the evolution of the electric and magnetic energy densities during inflation, following the general procedure outlined in Eq. (5.39). At the same time, we evaluate the background energy density $\rho = 3H^2 M_{pl}^2$, the quantity $3H\dot{\rho}$, and the source term $\mathcal{S}_{EM}$ using Eq. (5.54). This allows us to verify that the two backreaction constraints in Eq. (5.53) are satisfied throughout the inflationary phase.

For all the cases considered, we evaluate the magnetic spectral index n_B at *i*) CMB scales, to identify possible departures from scale invariance, and *ii*) at the scale corresponding to $\ell = 1\,\mathrm{Mpc}$, to correctly apply Eq. (5.42) when the correlation length is smaller than ℓ. We then compute the present-day values of the magnetic field amplitude and coherence scale (B_0, L_0), as well as $B_0(\ell = 1\,\mathrm{Mpc})$.

A representative result is shown in Figure 5.4, corresponding to $\nu_1 \simeq 2$, $\nu_2 = 0.6$, and $\gamma = 1$.[14]

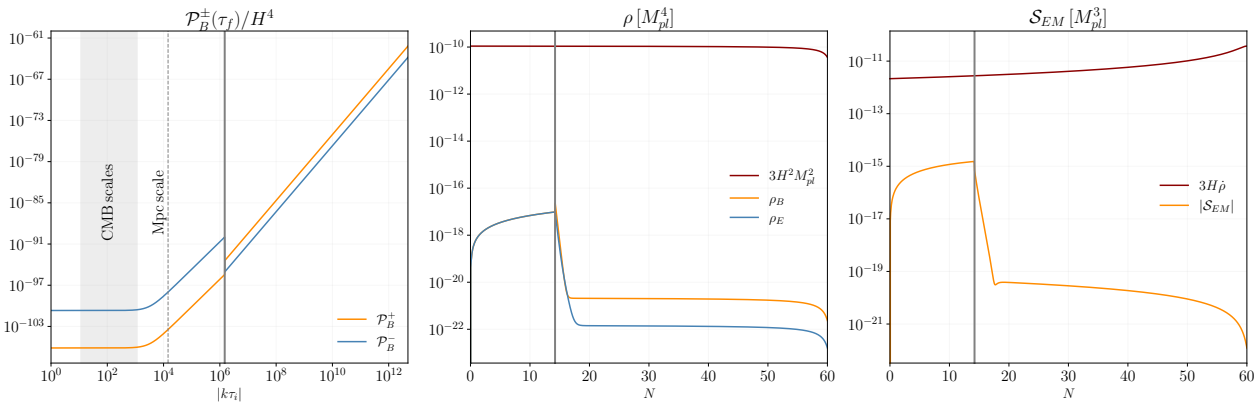

Figure 5.4: Representative result for the application of the magnetogenesis model detailed in Sec. 5.2 to scale-invariant inflation, obtained for $\nu_1 \simeq 2, \nu_2 = 0.6$, and $\gamma = 1$ (see also first line of Table 5.1 and orange dots in Figure 5.5). *Left panel*: magnetic field power spectrum derived from Eqs. (5.36) and (5.38), evaluated at the end of inflation, for the positive (orange) and negative (blue) helicity states. The solid vertical line marks the transition between the first and the second stage: smaller (larger) wavevectors k exited the horizon during stage I (II). Note that the modes relevant to inflation extend up to $|k\tau_i| = 6 \times 10^{25}$, since the second stage lasts longer than the first for this choice of parameters. Scales relevant to CMB observations, $k_*^{\mathrm{CMB}} \in [5 \times 10^{-3}, 5 \times 10^{-1}]\,\mathrm{Mpc}^{-1}$, are highlighted with a gray shaded band, and the wavevector corresponding to $\ell = 1\,\mathrm{Mpc}$ is indicated with a vertical dotted line. *Central panel*: first backreaction constraint in Eq. (5.53), with electric (magnetic) contribution to the EM energy density in blue (orange). *Right panel*: second backreaction constraint in Eq. (5.53).

In this case, as discussed in Sec. 5.2.3, the electric and magnetic power spectra are scale-invariant during the first stage. However, in contrast to the results shown in Figure 5.3, the magnetic power spectrum at the end of inflation retains a residual scale invariance over the range of wavenumbers relevant for CMB observations, as shown in the left panel of Figure 5.4. As a consequence, no significant spectral features are expected in the curvature and tensor power spectra at those scales. Note, however, that already at the scale corresponding to $\ell = 1\,\mathrm{Mpc}$ the spectral tilt is $n_B = 8 - 2\nu_1 \simeq 4$, implying that

[14] To avoid encountering poles of the Gamma functions or special values of the integrals entering the EM energy density, we avoid integer values of ν_i in practice, hence the use of the symbol $\simeq$. This choice is made solely for numerical convenience.

the inverse-cascade process is efficient at this scale and that Eq. (5.42) can be applied. At even larger values of k, the magnetic power spectrum becomes strongly blue-tilted, with $n_B = 6 - 2\nu_2 = 4.8$ for all modes that exited the horizon during the second stage of inflation. From the middle and right panels of Figure 5.4, we verify that the backreaction constraints are satisfied throughout the inflationary evolution.

The corresponding values of (B_0, L_0) are shown as an orange dot in Figure 5.5, which is graphically connected to a second point representing the magnetic field amplitude evaluated at megaparsec scales. These results are consistent with existing IGMF bounds, although they exhibit some tension with the most stringent lower limit inferred from the Fermi-LAT 2018 data, which, however, relies on very specific assumptions regarding the stability of the sources.

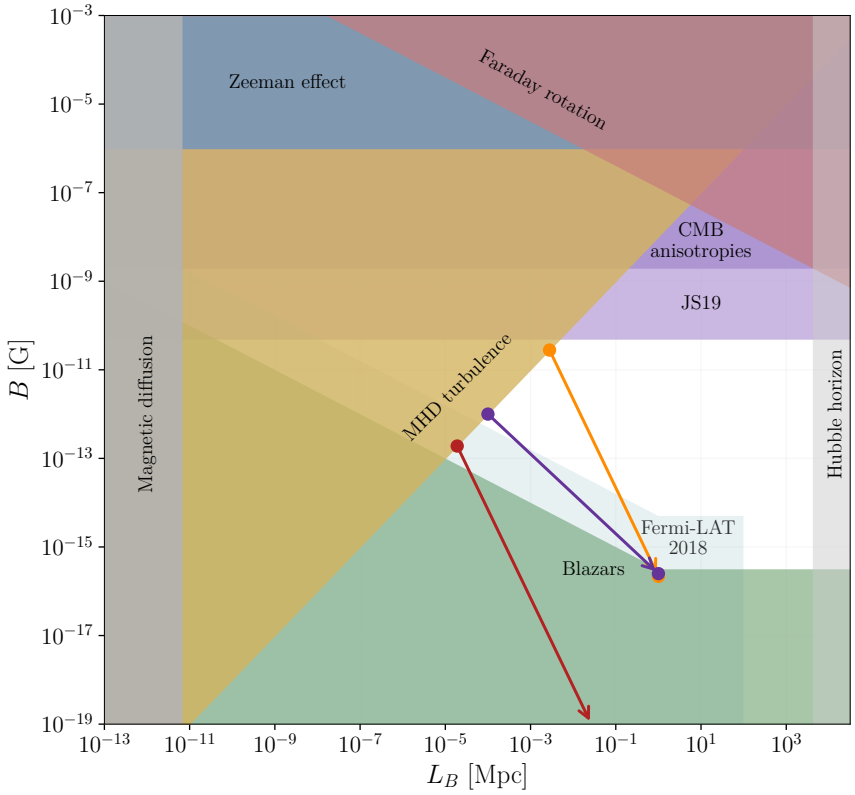

Figure 5.5: Bounds on IGMFs are shown as in Figure 5.1, together with benchmark predictions obtained from the magnetogenesis model described in Sec. 5.2 and applied to scale-invariant inflation. The dots lying close to the boundary of the yellow region correspond to the (L_0, B_0) values reported in Table 5.1: orange, red, and purple denote the first, second, and third rows, respectively. Each point is graphically connected to the corresponding value of $B_0(\ell = 1\,\mathrm{Mpc})$, computed using Eq. (5.42). Note that the second red point lies outside the plotted region, which is largely excluded by blazar observations. The strongest constraint derived from Fermi-LAT 2018 data is shown more transparently than in Figure 5.1, since it relies on stringent assumptions about the source stability time and should therefore be interpreted with caution.

Complementary to the magnetic field predictions shown in Figure 5.5, we report a set of representative benchmark values in Table 5.1, where we also list the magnetic spectral tilt evaluated at CMB scales and at $\ell = 1\,\mathrm{Mpc}$. In the lower part of Table 5.1, we present benchmark configurations that yield IGMFs consistent with those required for successful baryogenesis, as discussed in Sec. 5.3.3. We note that the second benchmark point also predicts magnetic field amplitudes at $\ell = 1\,\mathrm{Mpc}$ within the range (5.59) required to seed the galactic dynamo.

In conclusion, our analysis shows that the magnetogenesis mechanism considered here can

ν_1	ν_2	γ	L_0 [Mpc]	$B_0(L_0)$ [nG]	$B_0(\ell = 1\,\mathrm{Mpc})$ [nG]	n_B^{CMB}	n_B^{Mpc}
2	0.6	1	3×10^{-3}	3×10^{-2}	2×10^{-7}	$4 - 2\nu_1$	$8 - 2\nu_1$
2	2	1	2×10^{-5}	2×10^{-4}	7×10^{-14}	$8 - 2\nu_1$	$8 - 2\nu_1$
1.1	1.7	2.4	1×10^{-4}	1×10^{-3}	2.5×10^{-7}	$4 - 2\nu_1$	$4 - 2\nu_1$
0.5	2	1	4×10^{-8}	4×10^{-7}	4×10^{-18}	$4 - 2\nu_1$	$4 - 2\nu_1$
1.05	1.95	0.1	7×10^{-8}	7×10^{-7}	1×10^{-13}	$4 - 2\nu_1$	$4 - 2\nu_1$

Table 5.1: Present-day values of the magnetic field amplitude and coherence length for different choices of the parameters ν_1, ν_2, and γ in the magnetogenesis model described in Sec. 5.2, together with the magnetic spectral indices on CMB scales and on the scale $\ell = 1\,\mathrm{Mpc}$. The results are obtained following the procedure outlined in Sec. 5.3.4 and using Eqs. (5.43)–(5.44), which assume an inverse-cascade evolution for fully helical magnetic fields during radiation domination. Since $L_0 < \ell = 1\,\mathrm{Mpc}$ for all cases considered, the value of $B_0(\ell)$ reported in the sixth column is computed from Eq. (5.42), using the spectral index n_B^{Mpc} given in the last column and the corresponding (L_0, B_0) values from the fourth and fifth columns. The last two rows correspond to (L_0, B_0) values consistent with the baryogenesis mechanism from decaying helicity discussed in Sec. 5.3.3.

successfully operate within a well-constrained scale-invariant inflationary background, while simultaneously avoiding both the strong-coupling and backreaction problems. The broken-power-law shape of the coupling function ensures that $I(\tau) \geq 1$ at all times and remains bounded throughout inflation, thereby preventing excessive suppression of the magnetic field amplitude at the end of inflation, avoiding the strong coupling problem, and guaranteeing the recovery of standard electromagnetism at late times. At the same time, backreaction constraints are consistently satisfied for all the viable configurations explored.

A key ingredient of the scenario is the generation of fully helical magnetic fields, which subsequently undergo an efficient inverse-cascade process. As a result, the magnetic field amplitude is not strongly suppressed on large scales, allowing for sizable present-day fields at megaparsec scales that are compatible with IGMF bounds. Importantly, this mechanism operates without lowering the energy scale of inflation or modifying its dynamics, in contrast to many alternative magnetogenesis scenarios. The inflationary background is independently constrained by CMB observations, ensuring the internal consistency of the framework. Moreover, while the magnetic power spectrum remains nearly scale-invariant on CMB scales, the model naturally allows for nontrivial spectral features at smaller scales, offering a rich phenomenology that could be probed by future observations.

5.4 Summary

In this chapter, we investigated the generation of PMFs within the context of inflation, with particular emphasis on a magnetogenesis mechanism compatible with the scale-invariant inflationary dynamics. The chapter is organized around three main parts: a comprehensive overview of the current observational and theoretical status of cosmic magnetic fields (Sec. 5.1), a general analysis of an inflationary magnetogenesis model based on a broken-power-law coupling and a Chern-Simons term (Sec. 5.2), and its application to the scale-invariant inflationary framework developed in the previous chapters (Sec. 5.3).

In Sec. 5.1, we first provided a broad overview of the state of the art on cosmic magnetic fields, summarizing observational evidence across galactic, cluster, and intergalactic scales, as well as the main astrophysical and cosmological scenarios proposed for their origin. We reviewed the observational constraints on IGMFs, with particular emphasis on the lower bounds derived from gamma-ray observations of blazars. This discussion motivates the study of primordial magnetogenesis as a natural explanation for large-scale, space-filling magnetic fields, especially in cosmic voids, and highlights inflation as a privileged epoch for generating magnetic fields with large coherence lengths.

In Sec. 5.2, we introduced and critically revisited a model of inflationary magnetogenesis based on a time-dependent coupling function between the EM field and the inflationary sector modeled as a broken power law of the scale factor. This coupling breaks EM conformal invariance, thereby enabling the amplification of gauge-field fluctuations. The EM sector is further supplemented by a Chern-Simons term, which induces parity violation and generates helical magnetic fields. These fields subsequently undergo inverse-cascade evolution during the radiation-dominated era. Our analysis was formulated independently of any specific inflationary model, assuming only an approximately de Sitter evolution. By consistently employing the sub-Hubble and super-Hubble approximations, we derived analytical solutions for the gauge-field mode functions in the different stages of inflation and explicitly tested their validity by comparing them with full numerical solutions of the EM power spectra. This allowed us to substantially extend and refine the analysis presented in [9], clarifying the role of the transition in the coupling function and providing a consistent description of the evolution of electric and magnetic spectra throughout inflation.

Finally, in Sec. 5.3, we applied the magnetogenesis mechanism to the scale-invariant inflationary background developed in the previous chapters. We showed that scale-invariant inflation provides a natural framework for this scenario, as EM conformal invariance is restored when the system approaches the stable fixed point after the end of inflation. Within this setup, we analyzed the resulting magnetic field amplitudes and correlation lengths, verified the absence of backreaction on the inflationary dynamics, and provided a rough estimate of the gauge-field contribution to the tensor power spectrum. Finally, we discussed the phenomenological viability of the model in light of current observational constraints, concluding that scale-invariant inflation can simultaneously address the origin of cosmological perturbations and PMFs within a unified theoretical framework. As an interesting application, we showed that the model is compatible with the mechanism of baryogenesis from decaying magnetic helicity introduced in [313], with magnetic field amplitudes sufficient to seed the galactic dynamo.

Conclusions

Understanding the physical principles governing the very early Universe and the origin of fundamental mass scales remains one of the central challenges of modern cosmology. In this context, scale invariance represents a well-motivated guiding principle. Approximate scale invariance appears in several regimes of Nature: the Standard Model is nearly scale invariant at energies well above the electroweak scale, the observed spectrum of primordial cosmological perturbations is nearly scale invariant, and successful inflationary models – such as Starobinsky inflation – are characterized by dynamics that effectively approach a scale-invariant regime.

These observations naturally point toward a broader picture in which scale invariance is realized as an exact symmetry at the fixed points of the renormalization group (RG) flow, while physical mass scales emerge dynamically along the RG trajectories through symmetry breaking. From this perspective, scale invariance may be regarded as a fundamental symmetry of Nature at high energies, with the observed scales arising as low-energy manifestations of a more symmetric underlying theory. These considerations strongly motivate the investigation of scale-invariant extensions of gravity as viable descriptions of the early Universe.

In this thesis, we studied the cosmological implications of scale-invariant gravity during inflation. We considered the classically scale-invariant model introduced in [5], in which gravity is extended by an R^2 term and coupled to a scalar field through dimensionless parameters only. The model realizes inflation without introducing any explicit fundamental mass scale. Scale invariance is instead broken dynamically during cosmic evolution: the Universe undergoes inflation as it evolves away from its symmetric configuration – an unstable fixed point – towards a stable attractor, where the Planck mass is generated.

Despite its apparent multifield structure, the model exhibits remarkably simple inflationary dynamics. Owing to the conservation of the Noether current associated with scale invariance, the system rapidly settles onto a constrained trajectory in field space. As a consequence, the inflationary evolution effectively reduces to a single-field description, with the Goldstone mode associated with scale symmetry freezing out. The model therefore reproduces the phenomenology of single-field slow-roll inflation with a canonical kinetic term, while retaining a solid theoretical motivation rooted in scale invariance.

The inflationary predictions of the model are in excellent agreement with current observational data. In Chapter 3, we derived analytical constraints on the model parameters under suitable approximations of the homogeneous background dynamics. In Chapter 4, we carried out a comprehensive analysis of cosmological perturbations using a fully multifield formalism, confirming that single-field predictions are consistently recovered. In particular, we showed that any apparent tachyonic behavior of entropy perturbations is a spurious artifact of the choice of variables, that curvature perturbations evolve adiabatically, and that the resulting non-Gaussianities coincide with those expected in the simplest single-field slow-roll scenarios. These analytical results were further supported by a full numerical analysis aimed at constraining the model's parameter space with current data. We demonstrated the stability of the inflationary trajectory against variations in the initial conditions and identified a robust lower bound on the tensor-to-scalar ratio, providing a potentially

testable observational signature of the scale-invariant framework.

While the model successfully accounts for inflation and its observational signatures, it also highlights important limitations. In its minimal realization, the stable fixed point is generically associated with a non-vanishing vacuum energy. As a consequence, the model does not naturally provide a smooth transition to a radiation-dominated Universe after inflation, and it can be regarded only as an effective description of a viable inflationary stage. This feature reflects a more general issue: models built from scale-invariant combinations of the Ricci scalar R and a real scalar field ϕ generically exhibit a non-vanishing residual cosmological constant, unless the scalar self-interaction is tuned to vanish exactly. Our analysis indicates that addressing this issue requires the introduction of additional dynamical degrees of freedom, which can enable the vacuum energy to be dynamically relaxed to zero. In this sense, scale invariance remains a powerful organizing principle, but its successful implementation in a fully realistic cosmological model likely necessitates an extension of the minimal setup considered in this thesis.

In Chapter 5, we explored the implications of scale-invariant inflation for the generation of primordial magnetic fields. Cosmic magnetism constitutes a major open problem in cosmology, particularly in light of the increasing observational evidence for weak, space-filling magnetic fields in the voids of the large-scale structure. Inflation provides a privileged epoch for generating magnetic fields with super-Hubble coherence lengths, provided electromagnetic (EM) conformal invariance is broken, thereby enabling the amplification of gauge-field fluctuations, in close analogy with the scalar and tensor sectors.

We studied a magnetogenesis mechanism based on a broken-power-law coupling between the scale factor and the EM action, supplemented by a Chern-Simons term. The latter induces parity violation and produces helical magnetic fields, which subsequently undergo inverse-cascade evolution. The non-monotonic form of the coupling function extends existing magnetogenesis models and allows one to evade their typical shortcomings, most notably the strong-coupling and backreaction problems. While the magnetic power spectrum remains nearly scale invariant on CMB scales – thus preserving the successful predictions of inflation – the model can generate non-trivial spectral features at smaller scales, giving rise to a rich phenomenology that may be accessible to future observations.

When embedded within a scale-invariant inflationary background, EM conformal invariance is naturally restored as the system approaches the fixed points of the dynamics, while being effectively broken during the inflationary phase. Our results demonstrate that scale-invariant inflation can consistently account for both the origin of primordial curvature perturbations and the generation of cosmic magnetic fields within a unified theoretical setting, in good agreement with current observational constraints across a wide range of scales.

In conclusion, this work has highlighted how scale-invariant gravity provides a rich and predictive setting for the physics of the early Universe. It naturally accounts for inflation, explains the dynamical origin of the Planck mass, and establishes novel connections to magnetogenesis. At the same time, it reveals fundamental challenges – most notably the residual vacuum energy – that point toward the need for extending the minimal framework. These results reinforce the view that scale invariance may play a fundamental organizing principle in high-energy cosmology and motivate further investigations into its implications for both early- and late-time physics of the Universe.

Acknowledgments

This work closes the circle of a journey that began with my master's thesis, *Primordial magnetic fields in scale-invariant inflation*, which marked my first, surprising encounter with cosmology – revealing to me the world of research, so often told through its successes, yet truly shaped just as much by error, an essential part of the process of understanding how things work.

I would like to thank my supervisor, Max, who has guided me since those early days, for always encouraging me to pursue curiosity-driven research, where not every path leads to the hoped-for results, and yet none of them is ever in vain. Thank you for placing your trust in me and for giving me the freedom to explore new directions of my own.

I am grateful to the Theoretical Gravitation and Cosmology group in Trento, including Samuele and Luciano, for the many discussions we have shared over the years. Physics is, above all, a collective endeavor, built on people and the exchange of ideas.

I also wish to thank Valerie Domcke, Gabriele Franciolini, and Mauro Pieroni for welcoming me into the CERN Theory department, for supporting my wish to explore a path that was, at the time, entirely uncharted for me, and for inspiring me with their contagious curiosity and intellectual sharpness.

This thesis concludes a chapter spanning ten years within the Department of Physics at the University of Trento – a journey that began with me arriving as a chaotic bundle of determination and instinct, driven toward a passion I had not yet fully discovered, and that has shaped me into the scientist I am today.

Thank you to those who walked this entire road alongside me, Emi and Mirco (giga), sharing each day of a path that was often uphill and celebrating each other's successes along the way. You have been my daily laughter.

Thank you to my mum and dad, who supported and encouraged me to follow my passions, even when that meant letting me go and watching me come home less frequently. Thank you to my sisters, because at some point you began to take care of me, in that reciprocal exchange of attention that has made the three of us a force – always.

Trento became home above all thanks to the people who made it so. Thank you, Pietro, for making these past three years more extraordinary than I could have imagined, and for giving me, every day, a reason to be happy that transcends whatever happens in academia. Thank you for your constant understanding, for always standing by my side, and for encouraging me to continue on my path, wherever it may lead. You are my home.

Appendix A

Ostrogradsky's theorem

In the following, we outline the derivation of Ostrogradsky's theorem. To get familiar with Ostrogradsky's construction, we first review Hamilton's construction for the usual stable first-order derivative Lagrangian case, and then analyze the second-order case. Extensions to higher-order derivatives can be found, e.g., in [93, 94].

First-order derivative Lagrangian

Consider a Lagrangian depending on some family of fields ϕ^I and up to first-order derivatives of them, with Lagrangian

$$\mathcal{L} = \mathcal{L}(t, \phi^I, \dot{\phi}^I) \tag{A.1}$$

where ϕ^I and $\dot{\phi}^I$ should be considered as independent Lagrangian coordinates, i.e., $\dot{\phi}^I$ is not $\mathrm{d}\phi^I/\mathrm{d}t$ at this level. The Euler-Lagrangian equations are

$$\frac{\mathrm{d}}{\mathrm{d}t}\frac{\partial \mathcal{L}}{\partial \dot{\phi}^I} - \frac{\partial \mathcal{L}}{\partial \phi^I} = 0. \tag{A.2}$$

After applying the chain rule to the first term, we have

$$\frac{\mathrm{d}\dot{\phi}^J}{\mathrm{d}t}\frac{\partial^2 \mathcal{L}}{\partial \dot{\phi}^I \partial \dot{\phi}^J} + \frac{\mathrm{d}\phi^J}{\mathrm{d}t}\frac{\partial^2 \mathcal{L}}{\partial \phi^J \partial \dot{\phi}^I} - \frac{\partial \mathcal{L}}{\partial \phi^I} = 0. \tag{A.3}$$

Solving for the accelerations $\ddot{\phi}^I$ demands the invertibility of the matrix $\partial^2\mathcal{L}/(\partial\dot{\phi}^I\partial\dot{\phi}^J)$, that is, the Lagrangian must satisfy the non-degeneracy condition

$$\det\left(\frac{\partial^2 \mathcal{L}}{\partial \dot{\phi}^I \partial \dot{\phi}^J}\right) \neq 0. \tag{A.4}$$

From Eq. (A.3) we can then isolate the accelerations

$$\ddot{\phi}^I = \mathcal{Q}(t, \phi^I, \dot{\phi}^I), \tag{A.5}$$

which is solved as a Cauchy problem for some given initial conditions for the fields ϕ^I_0 and their velocities $\dot{\phi}^I_0$, for a total of $2I$ initial conditions. The Hamiltonian construction follows the usual way. We introduce the canonical variables

$$q^I \equiv \phi^I, \qquad \pi_I \equiv \frac{\partial \mathcal{L}}{\partial \dot{\phi}^I}. \tag{A.6}$$

If the Lagrangian satisfies the non-degeneracy condition (A.4), we can express the velocities as a function of the momenta $\dot{q}^I = \mathcal{F}(t, q^I, \pi_I)$ and construct the Hamiltonian

$$\mathcal{H} = \pi_I \mathcal{F}(t, q^I, \pi_I) - \mathcal{L}\left(t, q^I, \mathcal{F}(t, q^I, \pi_I)\right). \tag{A.7}$$

The dynamics are determined by the Hamilton equations

$$\begin{cases} \dot{q}^I = \dfrac{\partial \mathcal{H}}{\partial \pi_I} \\ \dot{\pi}_I = -\dfrac{\partial \mathcal{H}}{\partial q^I}, \end{cases} \tag{A.8}$$

which is a first-order system of differential equations, requiring two initial conditions for each canonical variable.

Second-order derivative Lagrangian

Let's now consider a Lagrangian depending on some family of fields ϕ^I and up to second-order time derivatives of them

$$\mathcal{L} = \mathcal{L}(t, \phi^I, \dot{\phi}^I, \ddot{\phi}^I). \tag{A.9}$$

The Euler-Lagrange equations are

$$\frac{\mathrm{d}^2}{\mathrm{d}t^2}\frac{\partial \mathcal{L}}{\partial \ddot{\phi}^I} - \frac{\mathrm{d}}{\mathrm{d}t}\frac{\partial \mathcal{L}}{\partial \dot{\phi}^I} + \frac{\partial \mathcal{L}}{\partial \phi^I} = 0. \tag{A.10}$$

Applying the chain rule and imposing the non-degeneracy condition on the Lagrangian

$$\det\left(\frac{\partial^2 \mathcal{L}}{\partial \ddot{\phi}^I \partial \ddot{\phi}^J}\right) \neq 0, \tag{A.11}$$

we can write the equations of motion as

$$\phi^{(4)I} = \mathcal{Q}\left(t, \phi^I, \dot{\phi}^I, \ddot{\phi}^I, \phi^{(3)I}\right), \tag{A.12}$$

whose solutions are found after imposing four initial conditions for each field, for a total of $4I$ initial conditions. Accordingly, the canonical variables should be $4I$. These are derived following Ostrogradsky's prescription [92],

$$q_1^I \equiv \phi^I, \qquad q_2^I \equiv \dot{\phi}^I, \qquad \pi_{1,I} \equiv \frac{\partial \mathcal{L}}{\partial \dot{\phi}^I} - \frac{\mathrm{d}}{\mathrm{d}t}\frac{\partial \mathcal{L}}{\partial \ddot{\phi}^I}, \qquad \pi_{2,I} \equiv \frac{\partial \mathcal{L}}{\partial \ddot{\phi}^I}. \tag{A.13}$$

The non-degeneracy condition (A.11) implies that we can invert the phase-space transformations (A.13) to solve for $\ddot{\phi}^I \equiv \dot{q}_2^I$ in terms of $q_1^I, \pi_{1,I}$, and $\pi_{2,I}$. That is, there exist an acceleration $\mathcal{F}(t, q_1^I, q_2^I, \pi_{2,I})$ such that

$$\left.\frac{\partial \mathcal{L}}{\partial \ddot{\phi}^I}\right|_{\substack{\phi^I = q_1^I \\ \dot{\phi}^I = q_2^I \\ \ddot{\phi}^I = \mathcal{F}}} = \pi_{2,I}\,. \tag{A.14}$$

Ostrogradsky's Hamiltonian is obtained as the Legendre transformation of the Lagrangian with respect to the time derivatives of the canonical positions q_1^I and q_2^I,

$$\begin{aligned} \mathcal{H} &= \sum_k \pi_{k,I} \dot{q}_k^I - \mathcal{L} \\ &= \pi_{1,I}\, \dot{q}_1^I + \pi_{2,I}\, \dot{q}_2^I - \mathcal{L} \\ &= \pi_{1,I} q_2^I + \mathcal{F}\left(t, q_1^I, q_2^I, \pi_{2,I}\right) \pi_{2,I} - \mathcal{L}\left(t, q_1^I, q_2^I, \mathcal{F}\left(t, q_1^I, q_2^I, \pi_{2,I}\right)\right). \end{aligned} \tag{A.15}$$

The time evolution equations follow in analogy to Eq. (A.8)

$$\begin{cases} \dot{q}_i^I = \dfrac{\partial \mathcal{H}}{\partial \pi_{i,I}} \\ \dot{\pi}_{i,I} = -\dfrac{\partial \mathcal{H}}{\partial q_i^I}. \end{cases} \tag{A.16}$$

Employing the phase space transformations (A.13), the Hamilton equations become

$$\begin{cases} \dot{q}_1^I = q_2^I \\ \dot{q}_2^I = \mathcal{F}\left(t, q_1^I, q_2^I, \pi_{2,I}\right) \\ \dot{\pi}_{1,I} = \dfrac{\partial \mathcal{L}}{\partial q_1^I} \\ \dot{\pi}_{2,I} = -\pi_{1,I} + \dfrac{\partial \mathcal{L}}{\partial q_2^I}. \end{cases} \tag{A.17}$$

It is manifest that the Hamiltonian (A.15) generates time evolution. However, it is important to notice that Ostrogradsky's Hamiltonian (A.15) is linear in the canonical momentum π_1, and it is therefore unbounded from below in the direction of the phase space given by π_1. This is a particular case of the more general Ostrogradsky's theorem [92, 94, 364]

Ostrogradsky's theorem
Let a Lagrangian involve n-th-order finite time derivatives of variables. If $n \geq 2$ and the Lagrangian is non-degenerate with respect to the highest-order derivatives, the Hamiltonian of this system linearly depends on a canonical momentum.

As a consequence of Ostrogradsky's theorem, any higher-order theory whose Lagrangian is non-degenerate has ghosts (Ostrogradsky's ghost). Note that these instabilities arise at the background level and are therefore distinct from those associated with perturbations.

Appendix B

Scale and conformal transformations

In this appendix, we explicitly derive the transformation properties of the model defined in Eq. (3.1) under scale and conformal transformations. For a comprehensive discussion of the conceptual distinctions between scale and conformal invariance, we refer the reader to [134].

Scale transformations

We want to show that the action in Eq. (3.1) is invariant under a scale transformation as defined by the set of Eqs. (2.51)–(2.53).

From the metric transformation in Eq. (2.53), one finds

$$\sqrt{-g(x)} \to \sqrt{-g(\ell x)}, \tag{B.1}$$

and from the coordinate transformation in Eq. (2.52), it is clear that a derivative with respect to spacetime coordinates brings a factor ℓ. Therefore, we have

$$R(x) \to \ell^2 R(\ell x), \qquad \partial_\mu \phi(x) \to \ell^2 \partial_\mu \phi(\ell x). \tag{B.2}$$

Overall, the transformed action is

$$\begin{aligned} S'_J &= \int \mathrm{d}^4x \sqrt{-g(\ell x)} \left[\frac{\alpha}{36} \ell^4 R^2(\ell x) + \frac{\xi}{6} \ell^2 \phi^2(\ell x) \ell^2 R(\ell x) - \frac{1}{2} \ell^2 \partial_\mu \phi(\ell x) \ell^2 \partial^\mu \phi(\ell x) - \frac{\lambda}{4} \ell^4 \phi^4(\ell x) \right] \\ &= \int \mathrm{d}^4x \sqrt{-g(\ell x)}\, \ell^4 \left[\frac{\alpha}{36} R^2(\ell x) + \frac{\xi}{6} \phi^2(\ell x) R(\ell x) - \frac{1}{2} \partial_\mu \phi(\ell x) \partial^\mu \phi(\ell x) - \frac{\lambda}{4} \phi^4(\ell x) \right] \\ &= \int \mathrm{d}^4\bar{x} \sqrt{-g(\bar{x})} \left[\frac{\alpha}{36} R^2(\bar{x}) + \frac{\xi}{6} \phi^2(\bar{x}) R(\bar{x}) - \frac{1}{2} \partial_\mu \phi(\bar{x}) \partial^\mu \phi(\bar{x}) - \frac{\lambda}{4} \phi^4(\bar{x}) \right], \end{aligned} \tag{B.3}$$

which is equivalent to the original one (3.1) after a coordinate redefinition $\bar{x} \equiv \ell x$.

Conformal transformations

We now want to show that the action in Eq. (3.1) is conformally invariant for the choice of parameters $\alpha = 0, \xi = -1/2$. Following [12], we define an equation for a scalar field ϕ as a conformally invariant one if there exist a number $\Delta_\phi \in \mathbb{R}$ – called the *conformal weight* of the field – such that ϕ is a solution with metric $g_{\mu\nu}$ if and only if $\tilde{\phi} = \Omega^{-\Delta_\phi} \phi$ is a solution with metric $\tilde{g}_{\mu\nu} = \Omega^2 g_{\mu\nu}$. From dimensional analysis, we set $\Delta_\phi = 1$ in 4 spacetime dimensions. Overall, this amounts to equipping the conformal transformation acting on the metric, see Eq. (2.27), with a transformation on the scalar field. Note that this is precisely the local version of the Weyl transformation in Eq. (2.54), defining dilatations. We therefore adopt the following transformed quantities

$$\tilde{g}_{\mu\nu} = \Omega^2 g_{\mu\nu}, \qquad \tilde{\phi} = \Omega^{-1} \phi, \tag{B.4}$$

which implies $\sqrt{-\tilde{g}} = \Omega^4\sqrt{-g}$ and

$$\tilde{R} = \Omega^{-2}\left[R - 6g^{\mu\nu}\partial_\mu\partial_\nu\omega - 6g^{\mu\nu}\partial_\mu\omega\partial_\nu\omega\right], \tag{B.5}$$

where $\omega \equiv \ln\Omega$, following Eq. (2.28).

For a matter of convenience, we already set $\alpha = 0$ and consider the transformed action (3.1)

$$\tilde{S}_J = \int \mathrm{d}^4x\sqrt{-\tilde{g}}\left[\frac{\xi}{6}\tilde{\phi}^2\tilde{R} - \frac{1}{2}\tilde{g}^{\mu\nu}\partial_\mu\tilde{\phi}\partial_\nu\tilde{\phi} - \frac{\lambda}{4}\tilde{\phi}^4\right], \tag{B.6}$$

and consider its first two terms separately. It is manifest that the self-interaction term is conformally invariant. Using the intermediate result

$$\partial_\mu\tilde{\phi} = \Omega^{-1}\partial_\mu\phi - \phi\Omega^{-1}\partial_\mu\omega, \tag{B.7}$$

we obtain

$$\begin{aligned}
\tilde{\phi}^2\tilde{R} &= \Omega^{-4}\left[\phi^2 R - 6\phi^2 g^{\mu\nu}\partial_\mu\partial_\nu\omega - 6\phi^2 g^{\mu\nu}\partial_\mu\omega\partial_\nu\omega\right], \\
\tilde{g}^{\mu\nu}\partial_\mu\tilde{\phi}\partial_\nu\tilde{\phi} &= \Omega^{-4}\left[g^{\mu\nu}\partial_\mu\phi\partial_\nu\phi - 2\phi g^{\mu\nu}\partial_\mu\phi\partial_\nu\omega + \phi^2 g^{\mu\nu}\partial_\mu\omega\partial_\nu\omega\right].
\end{aligned} \tag{B.8}$$

After integrating by part the term $\propto \phi^2 g^{\mu\nu}\partial_\mu\partial_\nu\omega$ and collecting all the terms, we have

$$\tilde{S}_J = \int \mathrm{d}^4x\sqrt{-g}\left[\frac{\xi}{6}\phi^2 R - \frac{1}{2}\partial_\mu\phi\partial^\mu\phi - \frac{\lambda}{4}\phi^4 + (1+2\xi)\left(\phi g^{\mu\nu}\partial_\mu\phi\partial_\nu\omega - \frac{1}{2}\phi^2 g^{\mu\nu}\partial_\mu\omega\partial_\nu\omega\right)\right], \tag{B.9}$$

showing that the last terms cancel for the choice

$$\boxed{\xi = -\frac{1}{2}}, \tag{B.10}$$

thus realizing conformal invariance.[1]

[1] Note that this result differs from what reported in [5, 7].

Appendix C

Super-Hubble evolution of the gauge field

As a complement to the asymptotic expressions for the power spectra derived in Sec. (5.2.3), we provide here the super-Hubble limits of the gauge field and its conformal time derivative. These results are further employed in Sec. 5.53.

For later convenience, we report the asymptotic limit of the Whittaker functions $W_{\kappa,\mu}(z)$ and $M_{\kappa,\mu}(z)$ for $z \to 0$:

$$M_{\kappa,\mu}(z) \sim z^{\mu+\frac{1}{2}}\,(1+\mathcal{O}(z)) \qquad (z\to 0), \tag{C.1}$$

$$W_{\kappa,\mu}(z) \sim \frac{\Gamma(2\mu)}{\Gamma(\frac{1}{2}+\mu-\kappa)} z^{-\mu+\frac{1}{2}} + \frac{\Gamma(-2\mu)}{\Gamma(\frac{1}{2}-\mu-\kappa)} z^{\mu+\frac{1}{2}} + \mathcal{O}(z^{\frac{3}{2}-\mathrm{Re}(\mu)}) \qquad (z\to 0). \tag{C.2}$$

These expressions are valid for generic μ and κ. When $2\mu \in \mathbb{Z}$, the two Frobenius indices differ by an integer and the small-z expansion may involve logarithmic terms; similarly, when $\frac{1}{2} \pm \mu - \kappa \in \mathbb{Z}_{\leq 0}$, the above coefficients must be understood via analytic continuation of the Gamma functions. In the following, we restrict to parameter values for which these subtleties do not arise.

First stage

By taking the super-Hubble limit $|k\tau| \ll 1$ of the solution found in Eq. (5.20), we have

$$\begin{aligned} \mathcal{A}^{\mathrm{I}}_{\pm}(\tau,k) &\simeq \frac{e^{\mp\frac{\pi}{2}\xi_1}}{\sqrt{2k}} \frac{2\nu_1\Gamma(2\nu_1)}{\Gamma(1+\nu_1\mp i\xi_1)} (-2ik\tau)^{-\nu_1}\,, \\ \frac{\mathrm{d}}{\mathrm{d}\tau}\left(\frac{\mathcal{A}^{\mathrm{I}}_{\pm}(\tau,k)}{I^{\mathrm{I}}(\tau)}\right) &\simeq -\frac{\sqrt{2k}}{I^{\mathrm{I}}(\tau)} e^{\mp\frac{\pi}{2}\xi_1} \frac{\gamma\nu_1\Gamma(2\nu_1)}{\Gamma(1+\nu_1\mp i\xi_1)} (-2ik\tau)^{-\nu_1}\,. \end{aligned} \tag{C.3}$$

Note that we have employed the sub-Hubble limit of the coefficients $C_i^{\pm}$, namely $C_1^{\pm} \simeq 0, C_2^{\pm} \simeq e^{\mp\frac{\pi}{2}\xi_1}$, since they are evaluated at the onset of inflation, $\tau = \tau_i$, and we are only interested in the modes that exited the horizon during inflation, meaning $|k\tau_i| \gg 1$.

Second stage

As stressed in Sec. 5.2.3, to properly evaluate the asymptotic behavior of the gauge field in the second stage of inflation, we should distinguish between modes that have already exited the horizon at the transition and those that exit the horizon during the second stage.

Modes that exited the horizon during stage I

Stage-II solutions corresponding to the modes that exited the horizon during the first stage are found from the super-Hubble limit $|k\tau| \ll 1$ of the solutions found in Eq. (5.24), and employing the super-Hubble limit – corresponding to $|k\tau_\star| \ll 1$ – of the coefficients $D_i^\pm$ reported in Eq. (5.26). Since the asymptotic expressions for $D_i^\pm$ carry an additional k-dependence, it is important to consider also the – otherwise subleading – term coming from the expansion of $M_{\kappa,\mu}(z)$ given in Eq. (C.1). We obtain

$$\begin{aligned}
\mathcal{A}_\pm^{\mathrm{I}\to\mathrm{II}}(\tau,k) &\simeq \frac{e^{\mp\frac{\pi}{2}\xi_1}}{\sqrt{2k}}\left[\frac{\nu_1(\nu_1+\nu_2)(1+\gamma^2)}{4\nu_2^2-1}\frac{\Gamma(2\nu_1-1)}{\Gamma(1+\nu_1\mp i\xi_1)}\left(-2k\tau_\star\right)^{1-\nu_1+\nu_2}\left(-2k\tau\right)^{1-\nu_2}+\right.\\
&\left.+\frac{\Gamma(1+2\nu_1)}{\Gamma(1+\nu_1\mp i\xi_1)}\left(-2k\tau_\star\right)^{-\nu_1-\nu_2}\left(-2k\tau\right)^{\nu_2}\right],\\
\frac{\mathrm{d}}{\mathrm{d}\tau}\left(\frac{\mathcal{A}_\pm^{\mathrm{I}\to\mathrm{II}}(\tau,k)}{I^{\mathrm{II}}(\tau)}\right) &\simeq -i\frac{\sqrt{2k}}{I^{\mathrm{II}}(\tau)}e^{\mp\frac{\pi}{2}\xi_1}\left[\frac{\nu_1(\nu_1+\nu_2)(1+\gamma^2)}{1+2\nu_2}\frac{\Gamma(2\nu_1-1)}{\Gamma(1+\nu_1\mp i\xi_1)}\left(-2k\tau_\star\right)^{1-\nu_1+\nu_2}\left(-2k\tau\right)^{-\nu_2}+\right.\\
&\left.+i\frac{\gamma}{2}\frac{\Gamma(1+2\nu_1)}{\Gamma(1+\nu_1\mp i\xi_1)}\left(-2k\tau_\star\right)^{-\nu_1-\nu_2}\left(-2k\tau\right)^{\nu_2}\right].
\end{aligned} \tag{C.4}$$

These approximate solutions will be applied to all $|\tau_i^{-1}| \lesssim k \lesssim |\tau_\star^{-1}|$. Whether one or the other power laws in the above expressions dominate depends on the values of ν_i and the ratio $\tau/\tau_\star$.

Modes that exited the horizon during stage II

If we instead consider the sub-Hubble limit $|k\tau_\star| \gg 1$ of the coefficients $D_i^\pm$ reported in Eq. (5.26), we obtain the asymptotic solutions corresponding to modes that exit the horizon during the second stage, namely

$$\begin{aligned}
\mathcal{A}_\pm^{\mathrm{II}}(\tau,k) &\simeq \frac{e^{\pm\frac{\pi}{2}\xi_2}}{\sqrt{2k}}\frac{\Gamma(2\nu_2-1)}{\Gamma(\nu_2\pm i\xi_2)}\left(-2k\tau\right)^{1-\nu_2},\\
\frac{\mathrm{d}}{\mathrm{d}\tau}\left(\frac{\mathcal{A}_\pm^{\mathrm{II}}(\tau,k)}{I^{\mathrm{II}}(\tau)}\right) &\simeq -i\frac{\sqrt{2k}}{I^{\mathrm{II}}(\tau)}e^{\pm\frac{\pi}{2}\xi_2}\frac{\Gamma(2\nu_2)}{\Gamma(\nu_2\pm i\xi_2)}\left(-2k\tau\right)^{-\nu_2}.
\end{aligned} \tag{C.5}$$

These approximate solutions will be applied to all $|\tau_\star^{-1}| \lesssim k \lesssim |\tau_f^{-1}|$. Since those modes are genuinely amplified by stage-II dynamics, the asymptotic expressions in Eq. (C.5) only depend on ν_2 (and not on ν_1).

Bibliography

[1] A. A. Starobinsky, *A New Type of Isotropic Cosmological Models Without Singularity*, *Phys. Lett. B* **91** (1980) 99.

[2] A. H. Guth, *The Inflationary Universe: A Possible Solution to the Horizon and Flatness Problems*, *Phys. Rev. D* **23** (1981) 347.

[3] A. D. Linde, *A New Inflationary Universe Scenario: A Possible Solution of the Horizon, Flatness, Homogeneity, Isotropy and Primordial Monopole Problems*, *Phys. Lett. B* **108** (1982) 389.

[4] C. Wetterich, *Quantum scale symmetry*, 1901.04741.

[5] M. Rinaldi and L. Vanzo, *Inflation and reheating in theories with spontaneous scale invariance symmetry breaking*, *Phys. Rev. D* **94** (2016) 024009 [1512.07186].

[6] M. De Angelis, C. Cecchini and M. Rinaldi, *Tracing cosmic stretch marks: probing scale invariance in the early Universe*, in *17th Marcel Grossmann Meeting: On Recent Developments in Theoretical and Experimental General Relativity, Gravitation, and Relativistic Field Theories*, 10, 2024, 2410.05977.

[7] C. Cecchini, M. De Angelis, W. Giarè, M. Rinaldi and S. Vagnozzi, *Testing scale-invariant inflation against cosmological data*, *JCAP* **07** (2024) 058 [2403.04316].

[8] M. Rinaldi, C. Cecchini, A. Ghoshal and D. Mukherjee, *Scale-invariant inflation*, *J. Phys. Conf. Ser.* **2531** (2023) 012012 [2303.16107].

[9] C. Cecchini and M. Rinaldi, *Inflationary helical magnetic fields with a sawtooth coupling*, *Phys. Dark Univ.* **40** (2023) 101212 [2301.07699].

[10] C. Cecchini, G. Franciolini and M. Pieroni, *Forecasting constraints on scalar-induced gravitational waves with future pulsar timing array observations*, *Phys. Rev. D* **111** (2025) 123536 [2503.10805].

[11] CosmoVerse Network collaboration, E. Di Valentino et al., *The CosmoVerse White Paper: Addressing observational tensions in cosmology with systematics and fundamental physics*, *Phys. Dark Univ.* **49** (2025) 101965 [2504.01669].

[12] R. M. Wald, *General Relativity*. Chicago Univ. Pr., Chicago, USA, 1984, 10.7208/chicago/9780226870373.001.0001.

[13] S. M. Carroll, *Spacetime and Geometry: An Introduction to General Relativity*. Cambridge University Press, 7, 2019, 10.1017/9781108770385.

[14] D. Baumann, *Inflation*, in *Theoretical Advanced Study Institute in Elementary Particle Physics: Physics of the Large and the Small*, pp. 523–686, 2011, 0907.5424, DOI.

[15] Planck collaboration, N. Aghanim et al., *Planck 2018 results. VI. Cosmological parameters*, *Astron. Astrophys.* **641** (2020) A6 [1807.06209].

[16] W. H. Kinney, *TASI Lectures on Inflation*, 0902.1529.

[17] A. Borde, A. H. Guth and A. Vilenkin, *Inflationary space-times are incomplete in past directions*, *Phys. Rev. Lett.* **90** (2003) 151301 [gr-qc/0110012].

[18] V. Mukhanov, *Physical Foundations of Cosmology*. Cambridge University Press, Oxford, 2005, 10.1017/CBO9780511790553.

[19] D. Baumann and L. McAllister, *Inflation and String Theory*, Cambridge Monographs on Mathematical Physics. Cambridge University Press, 5, 2015, 10.1017/CBO9781316105733, [1404.2601].

[20] S. Dodelson, *Modern Cosmology*. Academic Press, Amsterdam, 2003.

[21] A. D. Linde, *Inflationary Cosmology*, *Lect. Notes Phys.* **738** (2008) 1 [0705.0164].

[22] M. Pieroni, *Classification of inflationary models and constraints on fundamental physics*, Ph.D. thesis, APC, Paris, 2016. 1611.03732.

[23] A. D. Linde, *Hybrid inflation*, *Phys. Rev. D* **49** (1994) 748 [astro-ph/9307002].

[24] E. Silverstein and D. Tong, *Scalar speed limits and cosmology: Acceleration from D-cceleration*, *Phys. Rev. D* **70** (2004) 103505 [hep-th/0310221].

[25] G. W. Gibbons, *Cosmological evolution of the rolling tachyon*, *Phys. Lett. B* **537** (2002) 1 [hep-th/0204008].

[26] D. Bertacca, R. Jimenez, S. Matarrese and A. Ricciardone, *Inflation without an inflaton*, *Phys. Rev. Res.* **7** (2025) L032010 [2412.14265].

[27] V. Acquaviva, N. Bartolo, S. Matarrese and A. Riotto, *Second order cosmological perturbations from inflation*, *Nucl. Phys. B* **667** (2003) 119 [astro-ph/0209156].

[28] R. Durrer, *The Cosmic Microwave Background*. Cambridge University Press, Cambridge, 2008, 10.1017/CBO9780511817205.

[29] B. A. Bassett, S. Tsujikawa and D. Wands, *Inflation dynamics and reheating*, *Rev. Mod. Phys.* **78** (2006) 537 [astro-ph/0507632].

[30] J. M. Bardeen, *Gauge Invariant Cosmological Perturbations*, *Phys. Rev. D* **22** (1980) 1882.

[31] H. Kodama and M. Sasaki, *Cosmological Perturbation Theory*, *Prog. Theor. Phys. Suppl.* **78** (1984) 1.

[32] V. F. Mukhanov, H. A. Feldman and R. H. Brandenberger, *Theory of cosmological perturbations. Part 1. Classical perturbations. Part 2. Quantum theory of perturbations. Part 3. Extensions*, *Phys. Rept.* **215** (1992) 203.

[33] R. Durrer, *Gauge invariant cosmological perturbation theory: A General study and its application to the texture scenario of structure formation*, *Fund. Cosmic Phys.* **15** (1994) 209 [astro-ph/9311041].

[34] A. M. Green, *Pitfalls of a power-law parametrization of the primordial power spectrum for primordial black hole formation*, *Phys. Rev. D* **98** (2018) 023529 [1805.05178].

[35] J. M. Maldacena, *Non-Gaussian features of primordial fluctuations in single field inflationary models*, *JHEP* **05** (2003) 013 [astro-ph/0210603].

[36] T. S. Bunch and P. C. W. Davies, *Quantum Field Theory in de Sitter Space: Renormalization by Point Splitting*, *Proc. Roy. Soc. Lond. A* **360** (1978) 117.

[37] A. Lewis, A. Challinor and A. Lasenby, *Efficient computation of CMB anisotropies in closed FRW models*, *Astrophys. J.* **538** (2000) 473 [astro-ph/9911177].

[38] C. Howlett, A. Lewis, A. Hall and A. Challinor, *Cmb power spectrum parameter degeneracies in the era of precision cosmology*, *Journal of Cosmology and Astroparticle Physics* **2012** (2012) 027–027.

[39] D. Blas, J. Lesgourgues and T. Tram, *The cosmic linear anisotropy solving system (class). part ii: Approximation schemes*, *Journal of Cosmology and Astroparticle Physics* **2011** (2011) 034–034.

[40] M. J. Rees, *Polarization and Spectrum of the Primeval Radiation in an Anisotropic Universe*, *Astrophys. J. Lett.* **153** (1968) L1.

[41] eBOSS collaboration, S. Alam et al., *Completed SDSS-IV extended Baryon Oscillation Spectroscopic Survey: Cosmological implications from two decades of spectroscopic surveys at the Apache Point Observatory*, *Phys. Rev. D* **103** (2021) 083533 [2007.08991].

[42] Planck collaboration, Y. Akrami et al., *Planck 2018 results. X. Constraints on inflation*, *Astron. Astrophys.* **641** (2020) A10 [1807.06211].

[43] BICEP, Keck collaboration, P. A. R. Ade et al., *Improved Constraints on Primordial Gravitational Waves using Planck, WMAP, and BICEP/Keck Observations through the 2018 Observing Season*, *Phys. Rev. Lett.* **127** (2021) 151301 [2110.00483].

[44] D. Paoletti, F. Finelli, J. Valiviita and M. Hazumi, *Planck and BICEP/Keck Array 2018 constraints on primordial gravitational waves and perspectives for future B-mode polarization measurements*, *Phys. Rev. D* **106** (2022) 083528 [2208.10482].

[45] S. Dodelson, *Coherent phase argument for inflation*, *AIP Conf. Proc.* **689** (2003) 184 [hep-ph/0309057].

[46] A. D. Linde, *Chaotic Inflation*, *Phys. Lett. B* **129** (1983) 177.

[47] F. C. Adams, J. R. Bond, K. Freese, J. A. Frieman and A. V. Olinto, *Natural inflation: Particle physics models, power law spectra for large scale structure, and constraints from COBE*, *Phys. Rev. D* **47** (1993) 426 [hep-ph/9207245].

[48] J. Martin, C. Ringeval and V. Vennin, *Encyclopædia Inflationaris: Opiparous Edition*, *Phys. Dark Univ.* **5-6** (2014) 75 [1303.3787].

[49] Atacama Cosmology Telescope collaboration, E. Calabrese et al., *The Atacama Cosmology Telescope: DR6 constraints on extended cosmological models*, *JCAP* **11** (2025) 063 [2503.14454].

[50] SPT-3G collaboration, E. Camphuis et al., *SPT-3G D1: CMB temperature and polarization power spectra and cosmology from 2019 and 2020 observations of the SPT-3G Main field*, 2506.20707.

[51] Simons Observatory collaboration, P. Ade et al., *The Simons Observatory: Science goals and forecasts*, *JCAP* **02** (2019) 056 [1808.07445].

[52] Simons Observatory collaboration, M. H. Abitbol et al., *The Simons Observatory: Astro2020 Decadal Project Whitepaper*, *Bull. Am. Astron. Soc.* **51** (2019) 147 [1907.08284].

[53] CMB-S4 collaboration, K. N. Abazajian et al., *CMB-S4 Science Book, First Edition*, 1610.02743.

[54] CMB-S4 collaboration, K. Abazajian et al., *CMB-S4: Forecasting Constraints on Primordial Gravitational Waves*, *Astrophys. J.* **926** (2022) 54 [2008.12619].

[55] LiteBIRD collaboration, E. Allys et al., *Probing Cosmic Inflation with the LiteBIRD Cosmic Microwave Background Polarization Survey*, *PTEP* **2023** (2023) 042F01 [2202.02773].

[56] LiteBIRD collaboration, P. Campeti et al., *LiteBIRD science goals and forecasts. A case study of the origin of primordial gravitational waves using large-scale CMB polarization*, *JCAP* **06** (2024) 008 [2312.00717].

[57] S. W. Hawking and R. Penrose, *The Singularities of gravitational collapse and cosmology*, *Proc. Roy. Soc. Lond. A* **314** (1970) 529.

[58] D. S. Goldwirth and T. Piran, *Initial conditions for inflation*, *Phys. Rept.* **214** (1992) 223.

[59] R. Brandenberger, *Initial conditions for inflation — A short review*, *Int. J. Mod. Phys. D* **26** (2016) 1740002 [1601.01918].

[60] R. H. Brandenberger, *Challenges for inflationary cosmology*, in *10th International Symposium on Particles, Strings and Cosmology (PASCOS 04 and Pran Nath Fest)*, 11, 2004, astro-ph/0411671.

[61] R. Brandenberger and P. Peter, *Bouncing Cosmologies: Progress and Problems*, *Found. Phys.* **47** (2017) 797 [1603.05834].

[62] R. H. Brandenberger and C. Vafa, *Superstrings in the Early Universe*, *Nucl. Phys. B* **316** (1989) 391.

[63] G. F. R. Ellis and R. Maartens, *The emergent universe: Inflationary cosmology with no singularity*, *Class. Quant. Grav.* **21** (2004) 223 [gr-qc/0211082].

[64] A. S. Eddington, *The Mathematical Theory of Relativity*. Cambridge University Press, 1923.

[65] H. Weyl, *Gravitation and electricity*, *Sitzungsber. Preuss. Akad. Wiss. Berlin (Math. Phys.)* **1918** (1918) 465.

[66] T. Kaluza, *Zum Unitätsproblem der Physik*, *Sitzungsber. Preuss. Akad. Wiss. Berlin (Math. Phys.)* **1921** (1921) 966 [1803.08616].

[67] O. Klein, *Quantum Theory and Five-Dimensional Theory of Relativity. (In German and English)*, *Z. Phys.* **37** (1926) 895.

[68] Supernova Search Team collaboration, A. G. Riess et al., *Observational evidence from supernovae for an accelerating universe and a cosmological constant*, *Astron. J.* **116** (1998) 1009 [astro-ph/9805201].

[69] Supernova Cosmology Project collaboration, S. Perlmutter et al., *Measurements of Ω and Λ from 42 High Redshift Supernovae*, *Astrophys. J.* **517** (1999) 565 [astro-ph/9812133].

[70] D. Brout et al., *The Pantheon+ Analysis: Cosmological Constraints*, *Astrophys. J.* **938** (2022) 110 [2202.04077].

[71] A. Einstein, *Cosmological Considerations in the General Theory of Relativity*, *Sitzungsber. Preuss. Akad. Wiss. Berlin (Math. Phys.)* **1917** (1917) 142.

[72] L. Amendola and S. Tsujikawa, *Dark Energy: Theory and Observations*. Cambridge University Press, 1, 2015.

[73] DESI collaboration, K. Lodha et al., *Extended Dark Energy analysis using DESI DR2 BAO measurements*, 2503.14743.

[74] DESI collaboration, M. Abdul Karim et al., *DESI DR2 Results II: Measurements of Baryon Acoustic Oscillations and Cosmological Constraints*, 2503.14738.

[75] K.-i. Maeda, *Towards the Einstein-Hilbert Action via Conformal Transformation*, *Phys. Rev. D* **39** (1989) 3159.

[76] S. Gottlober, H. J. Schmidt and A. A. Starobinsky, *Sixth Order Gravity and Conformal Transformations*, *Class. Quant. Grav.* **7** (1990) 893.

[77] V. Faraoni and S. Capozziello, *Beyond Einstein Gravity: A Survey of Gravitational Theories for Cosmology and Astrophysics*. Springer, Dordrecht, 2011, 10.1007/978-94-007-0165-6.

[78] V. Mukhanov and S. Winitzki, *Introduction to quantum effects in gravity*. Cambridge University Press, 6, 2007.

[79] N. D. Birrell and P. C. W. Davies, *Quantum Fields in Curved Space*, Cambridge Monographs on Mathematical Physics. Cambridge University Press, Cambridge, UK, 1982, 10.1017/CBO9780511622632.

[80] L. E. Parker and D. Toms, *Quantum Field Theory in Curved Spacetime: Quantized Field and Gravity*, Cambridge Monographs on Mathematical Physics. Cambridge University Press, 8, 2009, 10.1017/CBO9780511813924.

[81] K. S. Stelle, *Renormalization of Higher Derivative Quantum Gravity*, *Phys. Rev. D* **16** (1977) 953.

[82] D. Anselmi, *On the quantum field theory of the gravitational interactions*, *JHEP* **06** (2017) 086 [1704.07728].

[83] J. F. Donoghue and G. Menezes, *Unitarity, stability and loops of unstable ghosts*, *Phys. Rev. D* **100** (2019) 105006 [1908.02416].

[84] A. Platania and C. Wetterich, *Non-perturbative unitarity and fictitious ghosts in quantum gravity*, *Phys. Lett. B* **811** (2020) 135911 [2009.06637].

[85] H. Lu, A. Perkins, C. N. Pope and K. S. Stelle, *Black Holes in Higher-Derivative Gravity*, *Phys. Rev. Lett.* **114** (2015) 171601 [1502.01028].

[86] H. Lü, A. Perkins, C. N. Pope and K. S. Stelle, *Spherically Symmetric Solutions in Higher-Derivative Gravity*, *Phys. Rev. D* **92** (2015) 124019 [1508.00010].

[87] J. Podolsky, R. Svarc, V. Pravda and A. Pravdova, *Explicit black hole solutions in higher-derivative gravity*, *Phys. Rev. D* **98** (2018) 021502 [1806.08209].

[88] J. Podolský, R. Švarc, V. Pravda and A. Pravdova, *Black holes and other exact spherical solutions in Quadratic Gravity*, *Phys. Rev. D* **101** (2020) 024027 [1907.00046].

[89] A. Bonanno and S. Silveravalle, *Characterizing black hole metrics in quadratic gravity*, *Phys. Rev. D* **99** (2019) 101501 [1903.08759].

[90] S. M. Silveravalle, *Isolated Objects in Quadratic Gravity: From Action Principles to Observations*, Ph.D. thesis, Trento U., 2024. 10.1007/978-3-031-48994-5.

[91] T. Baker, "The gravity landscape." T. Baker's personal webpage.

[92] M. Ostrogradsky, *Mémoires sur les équations différentielles, relatives au problème des isopérimètres*, *Mem. Acad. St. Petersbourg* **6** (1850) 385.

[93] R. P. Woodard, *Ostrogradsky's theorem on Hamiltonian instability*, *Scholarpedia* **10** (2015) 32243 [1506.02210].

[94] A. Delhom, A. Jiménez-Cano and F. J. Maldonado Torralba, *Instabilities in Field Theory: A Primer with Applications in Modified Gravity*, SpringerBriefs in Physics, Springer, 7, 2022, 2207.13431, DOI.

[95] R. P. Woodard, *Avoiding dark energy with 1/r modifications of gravity*, *Lect. Notes Phys.* **720** (2007) 403 [astro-ph/0601672].

[96] D. Lovelock, *The Einstein tensor and its generalizations*, *J. Math. Phys.* **12** (1971) 498.

[97] S. Nojiri, S. D. Odintsov and M. Sasaki, *Gauss-Bonnet dark energy*, *Phys. Rev. D* **71** (2005) 123509 [hep-th/0504052].

[98] G. Cognola, E. Elizalde, S. Nojiri, S. D. Odintsov and S. Zerbini, *Dark energy in modified Gauss-Bonnet gravity: Late-time acceleration and the hierarchy problem*, *Phys. Rev. D* **73** (2006) 084007 [hep-th/0601008].

[99] A. Salvio, *Quadratic Gravity*, *Front. in Phys.* **6** (2018) 77 [1804.09944].

[100] A. Salvio, *Metastability in Quadratic Gravity*, *Phys. Rev. D* **99** (2019) 103507 [1902.09557].

[101] A. Pais and G. E. Uhlenbeck, *On Field theories with nonlocalized action*, *Phys. Rev.* **79** (1950) 145.

[102] E. Pagani, G. Tecchiolli and S. Zerbini, *On the Problem of Stability for Higher Order Derivatives: Lagrangian Systems*, *Lett. Math. Phys.* **14** (1987) 311.

[103] V. A. Rubakov, *The Null Energy Condition and its violation*, *Phys. Usp.* **57** (2014) 128 [1401.4024].

[104] A. De Felice and S. Tsujikawa, *f(R) theories*, *Living Rev. Rel.* **13** (2010) 3 [1002.4928].

[105] T. P. Sotiriou and V. Faraoni, *f(R) Theories Of Gravity*, *Rev. Mod. Phys.* **82** (2010) 451 [0805.1726].

[106] C. W. Misner, K. S. Thorne and J. A. Wheeler, *Gravitation*. W. H. Freeman, San Francisco, 1973.

[107] T. P. Sotiriou and S. Liberati, *Metric-affine f(R) theories of gravity*, *Annals Phys.* **322** (2007) 935 [gr-qc/0604006].

[108] C. Brans and R. H. Dicke, *Mach's principle and a relativistic theory of gravitation*, *Phys. Rev.* **124** (1961) 925.

[109] J. O'Hanlon, *Intermediate-range gravity - a generally covariant model*, *Phys. Rev. Lett.* **29** (1972) 137.

[110] V. Faraoni, *Cosmology in scalar tensor gravity*. 2004, 10.1007/978-1-4020-1989-0.

[111] J. Khoury and A. Weltman, *Chameleon cosmology*, *Phys. Rev. D* **69** (2004) 044026 [astro-ph/0309411].

[112] J. Khoury and A. Weltman, *Chameleon fields: Awaiting surprises for tests of gravity in space*, *Phys. Rev. Lett.* **93** (2004) 171104 [astro-ph/0309300].

[113] E. E. Flanagan, *The Conformal frame freedom in theories of gravitation*, *Class. Quant. Grav.* **21** (2004) 3817 [gr-qc/0403063].

[114] C. H. Brans, *Nonlinear lagrangians and the significance of the metric*, *Classical and Quantum Gravity* **5** (1988) L197.

[115] S. Cotsakis, *Conformal transformations single out a unique measure of distance*, *Phys. Rev. D* **47** (1993) 1437.

[116] G. Magnano and L. M. Sokolowski, *On physical equivalence between nonlinear gravity theories and a general relativistic selfgravitating scalar field*, *Phys. Rev. D* **50** (1994) 5039 [gr-qc/9312008].

[117] R. H. Dicke, *Mach's principle and invariance under transformation of units*, *Phys. Rev.* **125** (1962) 2163.

[118] V. Faraoni and S. Nadeau, *The (pseudo)issue of the conformal frame revisited*, *Phys. Rev. D* **75** (2007) 023501 [gr-qc/0612075].

[119] M. Rinaldi, *On the equivalence of Jordan and Einstein frames in scale-invariant gravity*, *Eur. Phys. J. Plus* **133** (2018) 408 [1808.08154].

[120] D. G. Boulware, G. T. Horowitz and A. Strominger, *Zero Energy Theorem for Scale Invariant Gravity*, *Phys. Rev. Lett.* **50** (1983) 1726.

[121] J.-O. Gong, J.-c. Hwang, W.-I. Park, M. Sasaki and Y.-S. Song, *Conformal invariance of curvature perturbation*, *JCAP* **09** (2011) 023 [1107.1840].

[122] T. Chiba and M. Yamaguchi, *Extended Slow-Roll Conditions and Primordial Fluctuations: Multiple Scalar Fields and Generalized Gravity*, *JCAP* **01** (2009) 019 [0810.5387].

[123] Atacama Cosmology Telescope collaboration, T. Louis et al., *The Atacama Cosmology Telescope: DR6 power spectra, likelihoods and ΛCDM parameters*, *JCAP* **11** (2025) 062 [2503.14452].

[124] K.-i. Maeda, *Inflation as a Transient Attractor in R^2 Cosmology*, *Phys. Rev. D* **37** (1988) 858.

[125] M. Rinaldi, G. Cognola, L. Vanzo and S. Zerbini, *Reconstructing the inflationary $f(R)$ from observations*, *JCAP* **08** (2014) 015 [1406.1096].

[126] R. Myrzakulov, L. Sebastiani and S. Zerbini, *Reconstruction of Inflation Models*, *Eur. Phys. J. C* **75** (2015) 215 [1502.04432].

[127] L. Sebastiani and R. Myrzakulov, *F(R) gravity and inflation*, *Int. J. Geom. Meth. Mod. Phys.* **12** (2015) 1530003 [1506.05330].

[128] S. D. Odintsov and V. K. Oikonomou, *Reconstruction of Slow-roll $F(R)$ Gravity Inflation from the Observational Indices*, *Annals Phys.* **388** (2018) 267 [1710.01226].

[129] S. D. Odintsov and V. K. Oikonomou, *The reconstruction of $f(\phi)R$ and mimetic gravity from viable slow-roll inflation*, *Nucl. Phys. B* **929** (2018) 79 [1801.10529].

[130] T. Chiba, *Reconstructing $f(R)$ gravity from the spectral index*, *PTEP* **2018** (2018) 113E01 [1806.04297].

[131] S. Nojiri, S. D. Odintsov and V. K. Oikonomou, *k-essence $f(R)$ gravity inflation*, *Nucl. Phys. B* **941** (2019) 11 [1902.03669].

[132] S. D. Odintsov and V. K. Oikonomou, *R^2 inflation revisited and dark energy corrections*, *Phys. Rev. D* **104** (2021) 124065 [2112.06269].

[133] G. Giacomozzi and S. Zerbini, *Direct smooth reconstruction of inflationary models in f(R) gravity*, *Phys. Dark Univ.* **44** (2024) 101431 [2401.03796].

[134] Y. Nakayama, *Scale invariance vs conformal invariance*, *Phys. Rept.* **569** (2015) 1 [1302.0884].

[135] R. K. Pathria and P. D. Beale, *Statistical Mechanics*. Elsevier/Academic Press, Amsterdam ; Boston, 3rd ed ed., 2011.

[136] S. Coleman, *Aspects of Symmetry: Selected Erice Lectures*. Cambridge University Press, Cambridge, U.K., 1985, 10.1017/CBO9780511565045.

[137] M. E. Peskin and D. V. Schroeder, *An Introduction to quantum field theory*. Addison-Wesley, Reading, USA, 1995, 10.1201/9780429503559.

[138] C. Wetterich, *Cosmology and the Fate of Dilatation Symmetry*, *Nucl. Phys. B* **302** (1988) 668 [1711.03844].

[139] C. Wetterich, *Fundamental scale invariance*, *Nucl. Phys. B* **964** (2021) 115326 [2007.08805].

[140] E. Ising, *Contribution to the Theory of Ferromagnetism*, *Z. Phys.* **31** (1925) 253.

[141] Y.-B. Yang, J. Liang, Y.-J. Bi, Y. Chen, T. Draper, K.-F. Liu et al., *Proton Mass Decomposition from the QCD Energy Momentum Tensor*, *Phys. Rev. Lett.* **121** (2018) 212001 [1808.08677].

[142] M. Shaposhnikov and D. Zenhausern, *Quantum scale invariance, cosmological constant and hierarchy problem*, *Phys. Lett. B* **671** (2009) 162 [0809.3406].

[143] W. A. Bardeen, K. Higashijima and M. Moshe, *Spontaneous Breaking of Scale Invariance in a Supersymmetric Model*, *Nucl. Phys. B* **250** (1985) 437.

[144] F. Englert, C. Truffin and R. Gastmans, *Conformal Invariance in Quantum Gravity*, *Nucl. Phys. B* **117** (1976) 407.

[145] J. Garcia-Bellido, J. Rubio, M. Shaposhnikov and D. Zenhausern, *Higgs-Dilaton Cosmology: From the Early to the Late Universe*, *Phys. Rev. D* **84** (2011) 123504 [1107.2163].

[146] R. Armillis, A. Monin and M. Shaposhnikov, *Spontaneously Broken Conformal Symmetry: Dealing with the Trace Anomaly*, *JHEP* **10** (2013) 030 [1302.5619].

[147] F. Gretsch and A. Monin, *Perturbative conformal symmetry and dilaton*, *Phys. Rev. D* **92** (2015) 045036 [1308.3863].

[148] D. M. Ghilencea, *Manifestly scale-invariant regularization and quantum effective operators*, *Phys. Rev. D* **93** (2016) 105006 [1508.00595].

[149] P. G. Ferreira, C. T. Hill and G. G. Ross, *Scale-Independent Inflation and Hierarchy Generation*, *Phys. Lett. B* **763** (2016) 174 [1603.05983].

[150] D. M. Ghilencea, Z. Lalak and P. Olszewski, *Standard Model with spontaneously broken quantum scale invariance*, *Phys. Rev. D* **96** (2017) 055034 [1612.09120].

[151] A. Salvio and A. Strumia, *Agravity*, *JHEP* **06** (2014) 080 [1403.4226].

[152] L. Boyle, S. Farnsworth, J. Fitzgerald and M. Schade, *The Minimal Dimensionless Standard Model (MDSM) and its Cosmology*, 1111.0273.

[153] K. A. Meissner and H. Nicolai, *Conformal Symmetry and the Standard Model*, *Phys. Lett. B* **648** (2007) 312 [hep-th/0612165].

[154] K. Kannike, G. Hütsi, L. Pizza, A. Racioppi, M. Raidal, A. Salvio et al., *Dynamically Induced Planck Scale and Inflation*, *JHEP* **05** (2015) 065 [1502.01334].

[155] A. Salvio, *Dimensional Transmutation in Gravity and Cosmology*, *Int. J. Mod. Phys. A* **36** (2021) 2130006 [2012.11608].

[156] F. Cooper and G. Venturi, *Cosmology and Broken Scale Invariance*, *Phys. Rev. D* **24** (1981) 3338.

[157] Y. Fujii, *Origin of the Gravitational Constant and Particle Masses in Scale Invariant Scalar - Tensor Theory*, *Phys. Rev. D* **26** (1982) 2580.

[158] F. Finelli, A. Tronconi and G. Venturi, *Dark Energy, Induced Gravity and Broken Scale Invariance*, *Phys. Lett. B* **659** (2008) 466 [0710.2741].

[159] CMS collaboration, S. Chatrchyan et al., *Observation of a New Boson at a Mass of 125 GeV with the CMS Experiment at the LHC*, *Phys. Lett. B* **716** (2012) 30 [1207.7235].

[160] ATLAS collaboration, G. Aad et al., *Observation of a new particle in the search for the Standard Model Higgs boson with the ATLAS detector at the LHC*, *Phys. Lett. B* **716** (2012) 1 [1207.7214].

[161] M. Heikinheimo, A. Racioppi, M. Raidal, C. Spethmann and K. Tuominen, *Physical Naturalness and Dynamical Breaking of Classical Scale Invariance*, *Mod. Phys. Lett. A* **29** (2014) 1450077 [1304.7006].

[162] M. Farina, D. Pappadopulo and A. Strumia, *A modified naturalness principle and its experimental tests*, *JHEP* **08** (2013) 022 [1303.7244].

[163] A. de Gouvea, D. Hernandez and T. M. P. Tait, *Criteria for Natural Hierarchies*, *Phys. Rev. D* **89** (2014) 115005 [1402.2658].

[164] G. 't Hooft, *Naturalness, chiral symmetry, and spontaneous chiral symmetry breaking*, *NATO Sci. Ser. B* **59** (1980) 135.

[165] C. Wetterich and M. Yamada, *Gauge hierarchy problem in asymptotically safe gravity–the resurgence mechanism*, *Phys. Lett. B* **770** (2017) 268 [1612.03069].

[166] C. Wetterich, *Quantum correlations for the metric*, *Phys. Rev. D* **95** (2017) 123525 [1603.06504].

[167] C. Wetterich, *Cosmon inflation*, *Phys. Lett. B* **726** (2013) 15 [1303.4700].

[168] C. Wetterich, *Variable gravity Universe*, *Phys. Rev. D* **89** (2014) 024005 [1308.1019].

[169] J. Rubio and C. Wetterich, *Emergent scale symmetry: Connecting inflation and dark energy*, *Phys. Rev. D* **96** (2017) 063509 [1705.00552].

[170] S. Weinberg, *The Quantum theory of fields. Vol. 1: Foundations*. Cambridge University Press, 6, 2005, 10.1017/CBO9781139644167.

[171] S. Weinberg, *Ultraviolet divergences in quantum theories of gravitation*, pp. 790–831. Cambridge University Press, 1980.

[172] M. Reuter, *Nonperturbative evolution equation for quantum gravity*, *Phys. Rev. D* **57** (1998) 971 [hep-th/9605030].

[173] R. Percacci, *Asymptotic Safety*, 0709.3851.

[174] G. Tambalo and M. Rinaldi, *Inflation and reheating in scale-invariant scalar-tensor gravity*, *Gen. Rel. Grav.* **49** (2017) 52 [1610.06478].

[175] S. Vicentini, L. Vanzo and M. Rinaldi, *Scale-invariant inflation with one-loop quantum corrections*, *Phys. Rev. D* **99** (2019) 103516 [1902.04434].

[176] A. Ghoshal, D. Mukherjee and M. Rinaldi, *Inflation and primordial gravitational waves in scale-invariant quadratic gravity with Higgs*, *JHEP* **05** (2023) 023 [2205.06475].

[177] A. De Felice, R. Kawaguchi, K. Mizui and S. Tsujikawa, *Starobinsky inflation with a quadratic Weyl tensor*, *Phys. Rev. D* **108** (2023) 123524 [2309.01835].

[178] D. Tong, "Quantum field theory." https://www.damtp.cam.ac.uk/user/tong/qft.html, 2017.

[179] P. G. Ferreira, C. T. Hill, J. Noller and G. G. Ross, *Inflation in a scale invariant universe*, *Phys. Rev. D* **97** (2018) 123516 [1802.06069].

[180] S. Weinberg, *The quantum theory of fields. Vol. 2: Modern applications*. Cambridge University Press, 8, 2013, 10.1017/CBO9781139644174.

[181] S. V. Ketov, *On Legacy of Starobinsky Inflation*, 1, 2025, 2501.06451.

[182] C. van de Bruck and R. Daniel, *Inflation and scale-invariant R^2 gravity*, *Phys. Rev. D* **103** (2021) 123506 [2102.11719].

[183] G. Domènech, *Scalar Induced Gravitational Waves Review*, *Universe* **7** (2021) 398 [2109.01398].

[184] C. Byrnes, G. Franciolini, T. Harada, P. Pani and M. Sasaki, eds., *Primordial Black Holes*, Springer Series in Astrophysics and Cosmology. Springer, 2025, 10.1007/978-981-97-8887-3.

[185] H. Kodama and M. Sasaki, *Evolution of Isocurvature Perturbations. 1. Photon - Baryon Universe*, *Int. J. Mod. Phys. A* **1** (1986) 265.

[186] H. Kodama and M. Sasaki, *Evolution of Isocurvature Perturbations. 2. Radiation Dust Universe*, *Int. J. Mod. Phys. A* **2** (1987) 491.

[187] D. Langlois, *Isocurvature cosmological perturbations and the CMB*, *Comptes Rendus Physique* **4** (2003) 953.

[188] G. Domènech, *Cosmological gravitational waves from isocurvature fluctuations*, *AAPPS Bull.* **34** (2024) 4 [2311.02065].

[189] J. Chluba and D. Grin, *CMB spectral distortions from small-scale isocurvature fluctuations*, *Mon. Not. Roy. Astron. Soc.* **434** (2013) 1619 [1304.4596].

[190] J. Chluba et al., *Spectral Distortions of the CMB as a Probe of Inflation, Recombination, Structure Formation and Particle Physics: Astro2020 Science White Paper*, *Bull. Am. Astron. Soc.* **51** (2019) 184 [1903.04218].

[191] D. I. Kaiser and A. T. Todhunter, *Primordial Perturbations from Multifield Inflation with Nonminimal Couplings*, *Phys. Rev. D* **81** (2010) 124037 [1004.3805].

[192] T. Tapia and C. Rojas, *Scalar Cosmological Perturbations*, 2007.04423.

[193] C. Gordon, D. Wands, B. A. Bassett and R. Maartens, *Adiabatic and entropy perturbations from inflation*, *Phys. Rev. D* **63** (2000) 023506 [astro-ph/0009131].

[194] F. Di Marco, F. Finelli and R. Brandenberger, *Adiabatic and isocurvature perturbations for multifield generalized Einstein models*, *Phys. Rev. D* **67** (2003) 063512 [astro-ph/0211276].

[195] A. Achucarro, J.-O. Gong, S. Hardeman, G. A. Palma and S. P. Patil, *Features of heavy physics in the CMB power spectrum*, *JCAP* **01** (2011) 030 [1010.3693].

[196] M. De Angelis and C. van de Bruck, *Adiabatic and isocurvature perturbations in extended theories with kinetic couplings*, *JCAP* **10** (2023) 023 [2304.12364].

[197] W. Giarè, M. De Angelis, C. van de Bruck and E. Di Valentino, *Tracking the multifield dynamics with cosmological data: a Monte Carlo approach*, *JCAP* **12** (2023) 014 [2306.12414].

[198] S. Cespedes, V. Atal and G. A. Palma, *On the importance of heavy fields during inflation*, *JCAP* **05** (2012) 008 [1201.4848].

[199] S. Groot Nibbelink and B. J. W. van Tent, *Scalar perturbations during multiple field slow-roll inflation*, *Class. Quant. Grav.* **19** (2002) 613 [hep-ph/0107272].

[200] A. Achucarro, J.-O. Gong, S. Hardeman, G. A. Palma and S. P. Patil, *Mass hierarchies and non-decoupling in multi-scalar field dynamics*, *Phys. Rev. D* **84** (2011) 043502 [1005.3848].

[201] S. Cremonini, Z. Lalak and K. Turzynski, *Strongly Coupled Perturbations in Two-Field Inflationary Models*, *JCAP* **03** (2011) 016 [1010.3021].

[202] A. Achucarro, V. Atal, S. Cespedes, J.-O. Gong, G. A. Palma and S. P. Patil, *Heavy fields, reduced speeds of sound and decoupling during inflation*, *Phys. Rev. D* **86** (2012) 121301 [1205.0710].

[203] A. Achucarro, J.-O. Gong, S. Hardeman, G. A. Palma and S. P. Patil, *Effective theories of single field inflation when heavy fields matter*, *JHEP* **05** (2012) 066 [1201.6342].

[204] D. I. Kaiser and E. I. Sfakianakis, *Multifield Inflation after Planck: The Case for Nonminimal Couplings*, *Phys. Rev. Lett.* **112** (2014) 011302 [1304.0363].

[205] S. Renaux-Petel and K. Turzyński, *Geometrical Destabilization of Inflation*, *Phys. Rev. Lett.* **117** (2016) 141301 [1510.01281].

[206] M. Cicoli, V. Guidetti, F. G. Pedro and G. P. Vacca, *A geometrical instability for ultra-light fields during inflation?*, *JCAP* **12** (2018) 037 [1807.03818].

[207] M. Cicoli, V. Guidetti and F. G. Pedro, *Geometrical Destabilisation of Ultra-Light Axions in String Inflation*, *JCAP* **05** (2019) 046 [1903.01497].

[208] M. Cicoli, V. Guidetti, F. Muia, F. G. Pedro and G. P. Vacca, *On the choice of entropy variables in multifield inflation*, *Class. Quant. Grav.* **40** (2023) 025008 [2107.03391].

[209] D. Wands, N. Bartolo, S. Matarrese and A. Riotto, *An Observational test of two-field inflation*, *Phys. Rev. D* **66** (2002) 043520 [astro-ph/0205253].

[210] D. Wands, K. A. Malik, D. H. Lyth and A. R. Liddle, *A New approach to the evolution of cosmological perturbations on large scales*, *Phys. Rev. D* **62** (2000) 043527 [astro-ph/0003278].

[211] C. T. Byrnes, *Lecture notes on non-Gaussianity*, *Astrophys. Space Sci. Proc.* **45** (2016) 135 [1411.7002].

[212] M. Sasaki and E. D. Stewart, *A General analytic formula for the spectral index of the density perturbations produced during inflation*, *Prog. Theor. Phys.* **95** (1996) 71 [astro-ph/9507001].

[213] M. Sasaki and T. Tanaka, *Superhorizon scale dynamics of multiscalar inflation*, *Prog. Theor. Phys.* **99** (1998) 763 [gr-qc/9801017].

[214] D. H. Lyth, K. A. Malik and M. Sasaki, *A General proof of the conservation of the curvature perturbation*, *JCAP* **05** (2005) 004 [astro-ph/0411220].

[215] N. S. Sugiyama, E. Komatsu and T. Futamase, *δN formalism*, *Phys. Rev. D* **87** (2013) 023530 [1208.1073].

[216] T. Mori, K. Kohri and J. White, *Multi-field effects in a simple extension of R^2 inflation*, *JCAP* **10** (2017) 044 [1705.05638].

[217] J.-O. Gong and T. Tanaka, *A covariant approach to general field space metric in multi-field inflation*, *JCAP* **03** (2011) 015 [1101.4809].

[218] P. Creminelli and M. Zaldarriaga, *Single field consistency relation for the 3-point function*, *JCAP* **10** (2004) 006 [astro-ph/0407059].

[219] A. A. Abolhasani and M. Sasaki, *Single-field consistency relation and δN-formalism*, *JCAP* **08** (2018) 025 [1805.11298].

[220] D. Wands, *Local non-Gaussianity from inflation*, *Class. Quant. Grav.* **27** (2010) 124002 [1004.0818].

[221] Planck collaboration, Y. Akrami et al., *Planck 2018 results. IX. Constraints on primordial non-Gaussianity*, *Astron. Astrophys.* **641** (2020) A9 [1905.05697].

[222] G. Cabass, M. M. Ivanov, O. H. E. Philcox, M. Simonović and M. Zaldarriaga, *Constraints on Single-Field Inflation from the BOSS Galaxy Survey*, *Phys. Rev. Lett.* **129** (2022) 021301 [2201.07238].

[223] G. D'Amico, M. Lewandowski, L. Senatore and P. Zhang, *Limits on primordial non-Gaussianities from BOSS galaxy-clustering data*, *Phys. Rev. D* **111** (2025) 063514 [2201.11518].

[224] G. Cabass, M. M. Ivanov, O. H. E. Philcox, M. Simonović and M. Zaldarriaga, *Constraints on multifield inflation from the BOSS galaxy survey*, *Phys. Rev. D* **106** (2022) 043506 [2204.01781].

[225] A. Barreira, *Can we actually constrain f_{NL} using the scale-dependent bias effect? An illustration of the impact of galaxy bias uncertainties using the BOSS DR12 galaxy power spectrum*, *JCAP* **11** (2022) 013 [2205.05673].

[226] M. S. Cagliari, E. Castorina, M. Bonici and D. Bianchi, *Optimal constraints on Primordial non-Gaussianity with the eBOSS DR16 quasars in Fourier space*, *JCAP* **08** (2024) 036 [2309.15814].

[227] R. Easther, J. Frazer, H. V. Peiris and L. C. Price, *Simple predictions from multifield inflationary models*, *Phys. Rev. Lett.* **112** (2014) 161302 [1312.4035].

[228] Planck collaboration, N. Aghanim et al., *Planck 2018 results. V. CMB power spectra and likelihoods*, *Astron. Astrophys.* **641** (2020) A5 [1907.12875].

[229] Planck collaboration, N. Aghanim et al., *Planck 2018 results. I. Overview and the cosmological legacy of Planck*, *Astron. Astrophys.* **641** (2020) A1 [1807.06205].

[230] Planck collaboration, N. Aghanim et al., *Planck 2018 results. VIII. Gravitational lensing*, *Astron. Astrophys.* **641** (2020) A8 [1807.06210].

[231] J. Torrado and A. Lewis, *Cobaya: Code for Bayesian Analysis of hierarchical physical models*, *JCAP* **05** (2021) 057 [2005.05290].

[232] A. Lewis and S. Bridle, *Cosmological parameters from CMB and other data: A Monte Carlo approach*, *Phys. Rev. D* **66** (2002) 103511 [astro-ph/0205436].

[233] M. Benetti, L. L. Graef and S. Vagnozzi, *Primordial gravitational waves from NANOGrav: A broken power-law approach*, *Phys. Rev. D* **105** (2022) 043520 [2111.04758].

[234] S. Vagnozzi, *Inflationary interpretation of the stochastic gravitational wave background signal detected by pulsar timing array experiments*, *JHEAp* **39** (2023) 81 [2306.16912].

[235] N. Metropolis, A. W. Rosenbluth, M. N. Rosenbluth, A. H. Teller and E. Teller, *Equation of state calculations by fast computing machines*, *J. Chem. Phys.* **21** (1953) 1087.

[236] W. K. Hastings, *Monte Carlo Sampling Methods Using Markov Chains and Their Applications*, *Biometrika* **57** (1970) 97.

[237] A. Gelman and D. B. Rubin, *Inference from Iterative Simulation Using Multiple Sequences*, *Statist. Sci.* **7** (1992) 457.

[238] F. L. Bezrukov and M. Shaposhnikov, *The Standard Model Higgs boson as the inflaton*, *Phys. Lett. B* **659** (2008) 703 [0710.3755].

[239] F. Bezrukov, A. Magnin, M. Shaposhnikov and S. Sibiryakov, *Higgs inflation: consistency and generalisations*, *JHEP* **01** (2011) 016 [1008.5157].

[240] J. Rubio, *Higgs inflation*, *Front. Astron. Space Sci.* **5** (2019) 50 [1807.02376].

[241] J. L. F. Barbon and J. R. Espinosa, *On the Naturalness of Higgs Inflation*, *Phys. Rev. D* **79** (2009) 081302 [0903.0355].

[242] C. P. Burgess, H. M. Lee and M. Trott, *Comment on Higgs Inflation and Naturalness*, *JHEP* **07** (2010) 007 [1002.2730].

[243] X. Calmet and R. Casadio, *Self-healing of unitarity in Higgs inflation*, *Phys. Lett. B* **734** (2014) 17 [1310.7410].

[244] A. Salvio and A. Mazumdar, *Classical and Quantum Initial Conditions for Higgs Inflation*, *Phys. Lett. B* **750** (2015) 194 [1506.07520].

[245] R. Kallosh and A. Linde, *Universality Class in Conformal Inflation*, *JCAP* **07** (2013) 002 [1306.5220].

[246] R. Kallosh, A. Linde and D. Roest, *Superconformal Inflationary α-Attractors*, *JHEP* **11** (2013) 198 [1311.0472].

[247] M. Galante, R. Kallosh, A. Linde and D. Roest, *Unity of Cosmological Inflation Attractors*, *Phys. Rev. Lett.* **114** (2015) 141302 [1412.3797].

[248] R. Kallosh and A. Linde, *Planck, LHC, and α-attractors*, *Phys. Rev. D* **91** (2015) 083528 [1502.07733].

[249] R. Kallosh and A. Linde, *Polynomial α-attractors*, *JCAP* **04** (2022) 017 [2202.06492].

[250] D. Roest and M. Scalisi, *Cosmological attractors from α-scale supergravity*, *Phys. Rev. D* **92** (2015) 043525 [1503.07909].

[251] A. Linde, *Single-field α-attractors*, *JCAP* **05** (2015) 003 [1504.00663].

[252] E. V. Linder, *Dark Energy from α-Attractors*, *Phys. Rev. D* **91** (2015) 123012 [1505.00815].

[253] M. Scalisi, *Cosmological α-attractors and de Sitter landscape*, *JHEP* **12** (2015) 134 [1506.01368].

[254] S. D. Odintsov and V. K. Oikonomou, *Inflationary α-attractors from $F(R)$ gravity*, *Phys. Rev. D* **94** (2016) 124026 [1612.01126].

[255] M. Braglia, W. T. Emond, F. Finelli, A. E. Gumrukcuoglu and K. Koyama, *Unified framework for early dark energy from α-attractors*, *Phys. Rev. D* **102** (2020) 083513 [2005.14053].

[256] J. G. Rodrigues, S. Santos da Costa and J. S. Alcaniz, *Observational constraints on α -attractor inflationary models with a Higgs-like potential*, *Phys. Lett. B* **815** (2021) 136156 [2007.10763].

[257] R. Shojaee, K. Nozari and F. Darabi, *α-Attractors and reheating in a nonminimal inflationary model*, *Int. J. Mod. Phys. D* **29** (2020) 2050077 [2101.03981].

[258] S. Bhattacharya, K. Dutta, M. R. Gangopadhyay and A. Maharana, *α-attractor inflation: Models and predictions*, *Phys. Rev. D* **107** (2023) 103530 [2212.13363].

[259] L. Brissenden, K. Dimopoulos and S. Sánchez López, *Non-oscillating early dark energy and quintessence from α-attractors*, *Astropart. Phys.* **157** (2024) 102925 [2301.03572].

[260] W. Giarè, S. Pan, E. Di Valentino, W. Yang, J. de Haro and A. Melchiorri, *Inflationary potential as seen from different angles: model compatibility from multiple CMB missions*, *JCAP* **09** (2023) 019 [2305.15378].

[261] G. E. Hale, *On the probable existence of a magnetic field in sun-spots*, *Journal of Geophysical Research* **13** (1908) 159.

[262] L. M. Widrow, *Origin of galactic and extragalactic magnetic fields*, *Rev. Mod. Phys.* **74** (2002) 775 [astro-ph/0207240].

[263] J. P. Vallee, *Magnetic fields in the galactic Universe, as observed in supershells, galaxies, intergalactic and cosmic realms*, *New Astron. Rev.* **55** (2011) 91.

[264] R. Beck and R. Wielebinski, *Magnetic Fields in the Milky Way and in Galaxies*. 2, 2013. 1302.5663. 10.1007/978-94-007-5612-0_13.

[265] L. Feretti, G. Giovannini, F. Govoni and M. Murgia, *Clusters of galaxies: observational properties of the diffuse radio emission*, *The Astronomy and Astrophysics Review* **20** (2012) .

[266] M. L. Bernet, F. Miniati, S. J. Lilly, P. P. Kronberg and M. Dessauges-Zavadsky, *Strong magnetic fields in normal galaxies at high redshifts*, *Nature* **454** (2008) 302 [0807.3347].

[267] G. Di Gennaro et al., *Fast magnetic field amplification in distant galaxy clusters*, *Nature Astron.* **5** (2021) 268 [2011.01628].

[268] R. Alves Batista and A. Saveliev, *Multimessenger Constraints on Intergalactic Magnetic Fields from the Flare of TXS 0506+056*, *Astrophys. J. Lett.* **902** (2020) L11 [2009.12161].

[269] A. A. Meiksin, *The Physics of the Intergalactic Medium*, *Rev. Mod. Phys.* **81** (2009) 1405 [0711.3358].

[270] D. Ryu, D. R. G. Schleicher, R. A. Treumann, C. G. Tsagas and L. M. Widrow, *Magnetic fields in the large-scale structure of the universe*, *Space Science Reviews* **166** (2011) 1–35.

[271] F. Vazza, G. Brunetti, M. Brüggen and A. Bonafede, *Resolved magnetic dynamo action in the simulated intracluster medium*, *Mon. Not. Roy. Astron. Soc.* **474** (2018) 1672 [1711.02673].

[272] R. Alves Batista and A. Saveliev, *The Gamma-ray Window to Intergalactic Magnetism*, *Universe* **7** (2021) 223 [2105.12020].

[273] A. Brandenburg and K. Subramanian, *Astrophysical magnetic fields and nonlinear dynamo theory*, *Phys. Rept.* **417** (2005) 1 [astro-ph/0405052].

[274] K. Subramanian, *The origin, evolution and signatures of primordial magnetic fields*, *Rept. Prog. Phys.* **79** (2016) 076901 [1504.02311].

[275] D. Grasso and H. R. Rubinstein, *Magnetic fields in the early universe*, *Phys. Rept.* **348** (2001) 163 [astro-ph/0009061].

[276] L. M. Widrow, D. Ryu, D. R. G. Schleicher, K. Subramanian, C. G. Tsagas and R. A. Treumann, *The first magnetic fields*, *Space Science Reviews* **166** (2011) 37–70.

[277] A. Kandus, K. E. Kunze and C. G. Tsagas, *Primordial magnetogenesis*, *Phys. Rept.* **505** (2011) 1 [1007.3891].

[278] I. B. Zeldovich, A. A. Ruzmaikin and D. D. Sokolov, eds., *Magnetic fields in astrophysics*, vol. 3, Jan., 1983.

[279] R. Durrer and A. Neronov, *Cosmological Magnetic Fields: Their Generation, Evolution and Observation*, *Astron. Astrophys. Rev.* **21** (2013) 62 [1303.7121].

[280] L. Biermann, *Über den Ursprung der Magnetfelder auf Sternen und im interstellaren Raum (miteinem Anhang von A. Schlüter)*, *Zeitschrift Naturforschung Teil A* **5** (1950) 65.

[281] L. Biermann and A. Schlüter, *Cosmic radiation and cosmic magnetic fields. ii. origin of cosmic magnetic fields*, *Phys. Rev.* **82** (1951) 863.

[282] S. Naoz and R. Narayan, *Generation of Primordial Magnetic Fields on Linear Over-density Scales*, *Phys. Rev. Lett.* **111** (2013) 051303 [1304.5792].

[283] S. Bertone, C. Vogt and T. Ensslin, *Magnetic Field Seeding by Galactic Winds*, *Mon. Not. Roy. Astron. Soc.* **370** (2006) 319 [astro-ph/0604462].

[284] A. M. Beck, M. Hanasz, H. Lesch, R.-S. Remus and F. A. Stasyszyn, *On the magnetic fields in voids*, *Monthly Notices of the Royal Astronomical Society: Letters* **429** (2013) L60.

[285] S. Samui, K. Subramanian and R. Srianand, *Efficient cold outflows driven by cosmic rays in high redshift galaxies and their global effects on the IGM*, *Mon. Not. Roy. Astron. Soc.* **476** (2018) 1680 [1706.01890].

[286] F. Miniati and A. R. Bell, *Resistive magnetic field generation at cosmic dawn*, *The Astrophysical Journal* **729** (2011) 73.

[287] M. Langer and J.-B. Durrive, *Magnetizing the Cosmic Web during Reionization*, *Galaxies* **6** (2018) 124 [1811.09717].

[288] E. Witten, *Cosmic Separation of Phases*, *Phys. Rev. D* **30** (1984) 272.

[289] S. R. Coleman, *The Fate of the False Vacuum. 1. Semiclassical Theory*, *Phys. Rev. D* **15** (1977) 2929.

[290] P. J. Steinhardt, *Relativistic Detonation Waves and Bubble Growth in False Vacuum Decay*, *Phys. Rev. D* **25** (1982) 2074.

[291] C. Caprini et al., *Detecting gravitational waves from cosmological phase transitions with LISA: an update*, *JCAP* **03** (2020) 024 [1910.13125].

[292] S. Borsanyi, Z. Fodor, J. N. Guenther, R. Kara, S. D. Katz, P. Parotto et al., *QCD Crossover at Finite Chemical Potential from Lattice Simulations*, *Phys. Rev. Lett.* **125** (2020) 052001 [2002.02821].

[293] D. J. Schwarz and M. Stuke, *Lepton asymmetry and the cosmic QCD transition*, *JCAP* **11** (2009) 025 [0906.3434].

[294] F. Di Clemente, A. Drago, L. Formaggio, C. Ratti, V. Vovchenko and G. Yadav, *Upper Bound on the Cosmic Baryon Chemical Potential from Lepton-Flavor Asymmetry*, 2511.11995.

[295] A. De Angelis and M. Pimenta, *Introduction to Particle and Astroparticle Physics: Multimessenger Astronomy and its Particle Physics Foundations*, Undergraduate Lecture Notes in Physics. Springer Nature, Heidelberg, 2018, 10.1007/978-3-319-78181-5.

[296] U. Frisch, A. Pouquet, J. Leorat and A. Mazure, *Possibility of an inverse cascade of magnetic helicity in magnetohydrodynamic turbulence*, *Journal of Fluid Mechanics* **68** (1975) 769.

[297] T. Vachaspati, *Magnetic fields from cosmological phase transitions*, *Phys. Lett. B* **265** (1991) 258.

[298] L. Parker, *Particle creation in expanding universes*, *Phys. Rev. Lett.* **21** (1968) 562.

[299] M. S. Turner and L. M. Widrow, *Inflation Produced, Large Scale Magnetic Fields*, *Phys. Rev. D* **37** (1988) 2743.

[300] J. D. Barrow and C. G. Tsagas, *Cosmological magnetic field survival*, *Mon. Not. Roy. Astron. Soc.* **414** (2011) 512 [1101.2390].

[301] J. D. Barrow, C. G. Tsagas and K. Yamamoto, *Do Intergalactic Magnetic Fields Imply An Open Universe?*, *Phys. Rev. D* **86** (2012) 107302 [1210.1183].

[302] Y. Shtanov and V. Sahni, *Can a marginally open universe amplify magnetic fields?*, *JCAP* **01** (2013) 008 [1211.2168].

[303] J. Adamek, C. de Rham and R. Durrer, *Mode Spectrum of the Electromagnetic Field in Open Universe Models*, *Mon. Not. Roy. Astron. Soc.* **423** (2012) 2705 [1110.2019].

[304] D. Yamauchi, T. Fujita and S. Mukohyama, *Is there supercurvature mode of massive vector field in open inflation?*, *JCAP* **03** (2014) 031 [1402.2784].

[305] B. Himmetoglu, C. R. Contaldi and M. Peloso, *Ghost instabilities of cosmological models with vector fields nonminimally coupled to the curvature*, *Phys. Rev. D* **80** (2009) 123530 [0909.3524].

[306] B. Ratra, *Cosmological "Seed" Magnetic Field from Inflation*, *Astrophys. J. Lett.* **391** (1992) L1.

[307] A. Dolgov, *Breaking of conformal invariance and electromagnetic field generation in the universe*, *Phys. Rev. D* **48** (1993) 2499 [hep-ph/9301280].

[308] M. Gasperini, M. Giovannini and G. Veneziano, *Primordial magnetic fields from string cosmology*, *Phys. Rev. Lett.* **75** (1995) 3796 [hep-th/9504083].

[309] M. Giovannini, *Magnetogenesis and the dynamics of internal dimensions*, *Phys. Rev. D* **62** (2000) 123505 [hep-ph/0007163].

[310] M. Giovannini, *Magnetic fields, strings and cosmology*, *Lect. Notes Phys.* **737** (2008) 863 [astro-ph/0612378].

[311] J. Martin and J. Yokoyama, *Generation of Large-Scale Magnetic Fields in Single-Field Inflation*, *JCAP* **01** (2008) 025 [0711.4307].

[312] K. Subramanian, *Magnetic fields in the early universe*, *Astron. Nachr.* **331** (2010) 110 [0911.4771].

[313] T. Fujita and K. Kamada, *Large-scale magnetic fields can explain the baryon asymmetry of the Universe*, *Phys. Rev. D* **93** (2016) 083520 [1602.02109].

[314] K. Kamada and A. J. Long, *Baryogenesis from decaying magnetic helicity*, *Phys. Rev. D* **94** (2016) 063501 [1606.08891].

[315] K. Kamada and A. J. Long, *Evolution of the Baryon Asymmetry through the Electroweak Crossover in the Presence of a Helical Magnetic Field*, *Phys. Rev. D* **94** (2016) 123509 [1610.03074].

[316] K. Jedamzik and L. Pogosian, *Relieving the Hubble tension with primordial magnetic fields*, *Phys. Rev. Lett.* **125** (2020) 181302 [2004.09487].

[317] K. Jedamzik, L. Pogosian and T. Abel, *Hints of Primordial Magnetic Fields at Recombination and Implications for the Hubble Tension*, 2503.09599.

[318] D. G. Yamazaki, M. Kusakabe, T. Kajino, G. J. Mathews and M.-K. Cheoun, *Cosmological solutions to the Lithium problem: Big-bang nucleosynthesis with photon cooling, X-particle decay and a primordial magnetic field*, *Phys. Rev. D* **90** (2014) 023001 [1407.0021].

[319] T. Vachaspati, *Estimate of the primordial magnetic field helicity*, *Phys. Rev. Lett.* **87** (2001) 251302 [astro-ph/0101261].

[320] R. Durrer and C. Caprini, *Primordial magnetic fields and causality*, *JCAP* **11** (2003) 010 [astro-ph/0305059].

[321] T. Fujita and R. Durrer, *Scale-invariant Helical Magnetic Fields from Inflation*, *JCAP* **09** (2019) 008 [1904.11428].

[322] A. Neronov and D. V. Semikoz, *Sensitivity of gamma-ray telescopes for detection of magnetic fields in intergalactic medium*, *Physical Review D* **80** (2009) .

[323] Planck collaboration, P. A. R. Ade et al., *Planck 2015 results. XIX. Constraints on primordial magnetic fields*, *Astron. Astrophys.* **594** (2016) A19 [1502.01594].

[324] K. Jedamzik and A. Saveliev, *Stringent Limit on Primordial Magnetic Fields from the Cosmic Microwave Background Radiation*, *Phys. Rev. Lett.* **123** (2019) 021301 [1804.06115].

[325] A. Neronov and I. Vovk, *Evidence for strong extragalactic magnetic fields from fermi observations of tev blazars*, *Science* **328** (2010) 73–75.

[326] Fermi-LAT collaboration, M. Ackermann et al., *The Search for Spatial Extension in High-latitude Sources Detected by the Fermi Large Area Telescope*, *Astrophys. J. Suppl.* **237** (2018) 32 [1804.08035].

[327] H. Tashiro and T. Vachaspati, *Cosmological magnetic field correlators from blazar induced cascade*, *Phys. Rev. D* **87** (2013) 123527 [1305.0181].

[328] H. Tashiro, W. Chen, F. Ferrer and T. Vachaspati, *Search for CP Violating Signature of Intergalactic Magnetic Helicity in the Gamma Ray Sky*, *Mon. Not. Roy. Astron. Soc.* **445** (2014) L41 [1310.4826].

[329] W. Chen, B. D. Chowdhury, F. Ferrer, H. Tashiro and T. Vachaspati, *Intergalactic magnetic field spectra from diffuse gamma rays*, *Mon. Not. Roy. Astron. Soc.* **450** (2015) 3371 [1412.3171].

[330] D. Garg, R. Durrer and J. Schober, *Are magnetic fields in cosmic voids primordial?*, 2505.14774.

[331] O. Ghosh, A. Brandenburg, C. Caprini, A. Neronov and F. Vazza, *Can galactic magnetic fields diffuse into the voids?*, *Phys. Rev. D* **113** (2026) 023523 [2510.26918].

[332] A. E. Broderick, P. Tiede, P. Chang, A. Lamberts, C. Pfrommer, E. Puchwein et al., *Missing Gamma-ray Halos and the Need for New Physics in the Gamma-ray Sky*, *Astrophys. J.* **868** (2018) 87 [1808.02959].

[333] M. Pavičević, V. Iršič, M. Viel, J. S. Bolton, M. G. Haehnelt, S. Martin-Alvarez et al., *Constraints on Primordial Magnetic Fields from the Lyman-α Forest*, *Phys. Rev. Lett.* **135** (2025) 071001 [2501.06299].

[334] A. Roper Pol, C. Caprini, A. Neronov and D. Semikoz, *Gravitational wave signal from primordial magnetic fields in the Pulsar Timing Array frequency band*, *Phys. Rev. D* **105** (2022) 123502 [2201.05630].

[335] NANOGrav collaboration, G. Agazie et al., *The NANOGrav 15 yr Data Set: Evidence for a Gravitational-wave Background*, *Astrophys. J. Lett.* **951** (2023) L8 [2306.16213].

[336] EPTA, InPTA: collaboration, J. Antoniadis et al., *The second data release from the European Pulsar Timing Array - III. Search for gravitational wave signals*, *Astron. Astrophys.* **678** (2023) A50 [2306.16214].

[337] D. J. Reardon et al., *Search for an Isotropic Gravitational-wave Background with the Parkes Pulsar Timing Array*, *Astrophys. J. Lett.* **951** (2023) L6 [2306.16215].

[338] H. Xu et al., *Searching for the Nano-Hertz Stochastic Gravitational Wave Background with the Chinese Pulsar Timing Array Data Release I*, *Res. Astron. Astrophys.* **23** (2023) 075024 [2306.16216].

[339] M. T. Miles et al., *The MeerKAT Pulsar Timing Array: the first search for gravitational waves with the MeerKAT radio telescope*, *Mon. Not. Roy. Astron. Soc.* **536** (2024) 1489 [2412.01153].

[340] V. Demozzi, V. Mukhanov and H. Rubinstein, *Magnetic fields from inflation?*, *JCAP* **08** (2009) 025 [0907.1030].

[341] R. J. Z. Ferreira, R. K. Jain and M. S. Sloth, *Inflationary magnetogenesis without the strong coupling problem*, *JCAP* **10** (2013) 004 [1305.7151].

[342] R. J. Z. Ferreira, R. K. Jain and M. S. Sloth, *Inflationary Magnetogenesis without the Strong Coupling Problem II: Constraints from CMB anisotropies and B-modes*, *JCAP* **06** (2014) 053 [1403.5516].

[343] T. Kobayashi, *Primordial Magnetic Fields from the Post-Inflationary Universe*, *JCAP* **05** (2014) 040 [1403.5168].

[344] R. Sharma, S. Jagannathan, T. R. Seshadri and K. Subramanian, *Challenges in Inflationary Magnetogenesis: Constraints from Strong Coupling, Backreaction and the Schwinger Effect*, *Phys. Rev. D* **96** (2017) 083511 [1708.08119].

[345] D. Nandi, *Inflationary magnetogenesis: solving the strong coupling and its non-Gaussian signatures*, *JCAP* **08** (2021) 039 [2103.03159].

[346] M. M. Anber and L. Sorbo, *N-flationary magnetic fields*, *JCAP* **10** (2006) 018 [astro-ph/0606534].

[347] T. Fujita, R. Namba, Y. Tada, N. Takeda and H. Tashiro, *Consistent generation of magnetic fields in axion inflation models*, *JCAP* **05** (2015) 054 [1503.05802].

[348] D. T. Son, *Magnetohydrodynamics of the early universe and the evolution of primordial magnetic fields*, *Phys. Rev. D* **59** (1999) 063008 [hep-ph/9803412].

[349] G. B. Field and S. M. Carroll, *Cosmological magnetic fields from primordial helicity*, *Phys. Rev. D* **62** (2000) 103008 [astro-ph/9811206].

[350] M. Hindmarsh, M. Christensson and A. Brandenburg, *MHD inverse cascade in the early universe*, in *5th International Conference on Particle Physics and the Early Universe*, 1, 2002, astro-ph/0201466.

[351] C. Caprini and L. Sorbo, *Adding helicity to inflationary magnetogenesis*, *JCAP* **10** (2014) 056 [1407.2809].

[352] C. Caprini, M. C. Guzzetti and L. Sorbo, *Inflationary magnetogenesis with added helicity: constraints from non-gaussianities*, *Class. Quant. Grav.* **35** (2018) 124003 [1707.09750].

[353] K.-W. Ng, S.-L. Cheng and W. Lee, *Inflationary dilaton-axion magnetogenesis*, *Chin. J. Phys.* **53** (2015) 110105 [1409.2656].

[354] R. Sharma, K. Subramanian and T. R. Seshadri, *Generation of helical magnetic field in a viable scenario of inflationary magnetogenesis*, *Phys. Rev. D* **97** (2018) 083503 [1802.04847].

[355] M. Abramowitz, I. A. Stegun and R. H. Romer, *Handbook of mathematical functions with formulas, graphs, and mathematical tables*, *Am J Phys* **56** (1988) 958.

[356] M. Christensson, M. Hindmarsh and A. Brandenburg, *Inverse cascade in decaying 3-D magnetohydrodynamic turbulence*, *Phys. Rev. E* **64** (2001) 056405 [astro-ph/0011321].

[357] S. Maiti, *Magnetogenesis from a sawtooth coupling: Gravitational wave probe of reheating*, *Phys. Rev. D* **112** (2025) 043536 [2506.06183].

[358] A. Talebian, A. Nassiri-Rad and H. Firouzjahi, *Primordial helical magnetic fields from inflation?*, *Phys. Rev. D* **105** (2022) 023528 [2111.02147].

[359] B. Salehian, M. A. Gorji, H. Firouzjahi and S. Mukohyama, *Vector dark matter production from inflation with symmetry breaking*, *Phys. Rev. D* **103** (2021) 063526 [2010.04491].

[360] L. Sorbo, *Parity violation in the Cosmic Microwave Background from a pseudoscalar inflaton*, *JCAP* **06** (2011) 003 [1101.1525].

[361] N. Barnaby, J. Moxon, R. Namba, M. Peloso, G. Shiu and P. Zhou, *Gravity waves and non-Gaussian features from particle production in a sector gravitationally coupled to the inflaton*, *Phys. Rev. D* **86** (2012) 103508 [1206.6117].

[362] A. D. Sakharov, *Violation of CP Invariance, C asymmetry, and baryon asymmetry of the universe*, *Pisma Zh. Eksp. Teor. Fiz.* **5** (1967) 32.

[363] G. 't Hooft, *Symmetry Breaking Through Bell-Jackiw Anomalies*, *Phys. Rev. Lett.* **37** (1976) 8.

[364] K. Aoki and H. Motohashi, *Ghost from constraints: a generalization of Ostrogradsky theorem*, *JCAP* **08** (2020) 026 [2001.06756].